



**Jarol Ramon Miranda Andrades**

**Analytical methods for the determination of mercury species using cold vapour based spectrometry: application in challenging samples and use of nanoparticles as photocatalytic agents**

**Tese de Doutorado**

Thesis presented to the Programa de Pós-graduação em Química of PUC-Rio in partial fulfillment of the requirements for the degree of Doutor em Química.

Advisor: Prof. Ricardo Queiroz Aucélio

Co-Advisor: Prof. Sarzamin Khan

Rio de Janeiro

September 2019



**Jarol Ramon Miranda Andrades**

**Analytical methods for the determination of mercury species using cold vapour based spectrometry: application in challenging samples and use of nanoparticles as photocatalytic agents.**

The thesis presented to the Programa de Pós-graduação em Química of PUC-Rio in partial fulfillment of the requirements for the degree of Doctor in Chemistry. Approved by the Examination Committee.

**Prof. Ricardo Queiroz Aucélio**

Advisor

Departamento de Química - PUC-Rio

**Profa. Maria Luiza Bragança Tristão**

PUC-Rio

**Prof. Aderval Severino Luna**

UERJ

**Prof. Jose Marcus de Oliveira Godoy**

Departamento de Química - PUC-Rio

**Profa. Adriana Gioda**

Departamento de Química - PUC-Rio

**Prof. Fábio Grandis Lepri**

UFF

**Prof. Pedro Vitoriano de Oliveira**

USP

Rio de Janeiro, September 27, 2019

All rights reserved

## Jarol Ramon Miranda Andrades

Doctorate candidate in Chemistry of the Pontifical Catholic University of Rio de Janeiro (PUC-Rio). He holds a Master's degree in Chemistry from the Pontifical Catholic University of Rio de Janeiro (2015). He holds a degree in Chemistry from the University of the Atlantic in (2013). Has experience in Instrumental Analytical Chemistry.

### Bibliographic data

Miranda Andrades, Jarol Ramon

Analytical methods for the determination of mercury species using cold vapor based spectrometry : application in challenging samples and use of nanoparticles as photocatalytic agents / Jarol Ramon Miranda Andrades ; advisor: Ricardo Queiroz Aucélio ; co-advisor: Sarzamin Khan. – 2019.

181 f. : il. color. ; 30 cm

Tese (doutorado)–Pontifícia Universidade Católica do Rio de Janeiro, Departamento de Química, 2019.

Inclui bibliografia

1. Química – Teses. 2. Espécies de mercúrio. 3. Nanopartículas. 4. Águas produzidas. 5. Vapor frio. I. Aucélio, Ricardo Queiroz. II. Khan, Sarzamin. III. Pontifícia Universidade Católica do Rio de Janeiro. Departamento de Química. IV. Título.

CCD:540

## Acknowledgments

To God, for the strength of culminating this dream;

To Coordenação de Aperfeiçoamento de Pessoal de Nível Superior (CAPES, Brazil) for scholarship (Finance code 001).

To PUC-Rio (VRAC) for isenption of taxes.

To the Brazilian Agencies CNPq and FAPERJ for scientific grants;

To Dr. Ricardo Queiroz Aucélio, from PUC-Rio, for the confidence he had in accepting me in his research group, for always correct orientation, motivation in the most difficult moments of the research, friendship and also dedication;

To my co-advisor Dr. Sarzamin Khan for dedicated help, contribution to work and friendship;

To Dr<sup>a</sup>. Andrea Rosane for her immense support during my beginnings in graduate research

To the examining members, for their availability and for accepting the invitation.

To my parents and my brothers for their unconditional love and their support to fulfill this goal.

To all my family who has always been by my side in the most difficult moments;

My wife Joseane Alves, for your understanding and support, over these years, she was a motivation of my effort every day

To the friends and technicians of LEEA, Joseany, Ana, Cristiani, Juliana, Thais, Ana Paula, Sônia Gomes, Leila, Júnior, Claudiomar, Luis Maqueira, Larissa, Igor always willing to help me in the laboratory;

To my friends, Marlin Pedrozo, Jessica Rada, Lina Barranco, Rafael Celin, Stefany Ortiz, Wendy Sandoval, Oliver Everett, Maria F.Quijano, Mauricio Ceron and Jeferson Rodrigues;

Prof. Dr. Dunieskys and Prof. Dr. Eric for the support in the morphological and characterization analysis of the nanomaterials synthesized.

To the graduate Department of Chemistry at PUC-Rio, for the opportunity and the support of the research; and of course, to the professors of the department whose

teachings gave me significant academic growth, and especially to Fatima, who has always demonstrated personal and professional availability during this work;  
Finally, I thank all the people who have passed through my life and influenced me in some way, but, eventually, were not mentioned in here.

## Abstract

Miranda, Jarol Ramon Andrades; Aucélio, Ricardo Queiroz (Advisor); Khan, Sarzamin (Co-advisor). **Analytical methods for the determination of mercury species using cold vapour based spectrometry: application in challenging samples and use of nanoparticles as photocatalytic agentes.** Rio de Janeiro, 2019. 181p. Tese de doutorado - Departamento de Química, Pontifícia Universidade Católica do Rio de Janeiro.

The aim of the present work was to develop analytical methods capable of determining mercury species such as methylmercury ( $\text{CH}_3\text{Hg}$ ), ethylmercury ( $\text{CH}_3\text{CH}_2\text{Hg}$ ), inorganic mercury ( $\text{Hg}^{2+}$ ,  $\text{Hg}^0$ ), in produced water (PW) and urine, as well as thiomersal ( $\text{C}_9\text{H}_9\text{HgNaO}_2\text{S}$ ) in effluent from a pharmaceutical industry and in urine. Despite many methods for quantifying mercury species are reported, few studies address speciation in PW, sample known to have high oil and salt contents. Besides, the use of nanomaterials such as graphene quantum dots (GQDs) alone or decorating titanium dioxide nanoparticles (GQDs- $\text{TiO}_2$  NPs) were used as photocatalytic agents to produce the detected elemental mercury. The analytical techniques used for total mercury detection and mercury speciation were multipath cold vapor atomic absorption spectrometry (multipath-CV-AAS) and gas chromatography cold vapor atomic fluorescence spectrometry (GC-CV-AFS).

In the first work, the photo-degradation of thiomersal has been achieved using visible light and GQDs, obtained from hydro-exfoliation of citric acid and glutathione, as catalysts. The generated  $\text{Hg}^0$  (using adjusted experimental conditions) was detected by multipath-CV-AAS, enabling quantification of thiomersal at values as low as  $20 \text{ ng L}^{-1}$  even in complex samples as aqueous effluents from the pharmaceutical industry and in the urine. The reaction kinetic (pseudo-first-order with  $k = 0.11 \text{ min}^{-1}$ ) was determined.

The second work provided a speciation method for mercury in PW using multipath-CV-AAS. Under adjusted salt and oil contents (by dilution and centrifuging), a sample aliquot was treated with  $\text{SnCl}_2$ , leading to the  $\text{Hg}^0$  quantified as the original inorganic mercury. A second sample aliquot was exposed to UV (under optimized conditions) that promoted oxidation of  $\text{CH}_3\text{Hg}$  to  $\text{Hg}^{2+}$ , which was

then reduced, with  $\text{SnCl}_2$ , producing the  $\text{Hg}^0$  relative to the total mercury content in the sample. The  $\text{CH}_3\text{Hg}$  content was obtained by the difference in results achieved for both aliquots. Matrix effects imposed by oil and salt were studied, and although affecting the intensity of the mercury time profile, quantification was successfully achieved by matrix-matched standards containing NaCl and mineral oil.

Conductivimetric measurements (to estimate salt content) and turbidimetric measurements (to estimate oil content) were made for the PW samples in order to allow proper adjustment of sample to the matrix-matched standards (containing mineral oil at  $6 \text{ mg L}^{-1}$  and NaCl at  $6 \text{ g L}^{-1}$ ). Analyte addition was also used, and limit of quantification was  $12 \text{ ng L}^{-1}$ .

In the third work, a new method was developed for speciation of mercury in PW using a combination of extraction and distillation before propylation and determination by GC-CV-AFS. Ultrasonic assisted extraction (40 min) using the use of anionic surfactant (Triton X-114 at 0.5% w/v in solution at pH 3) improved recoveries of the distillation process used to separate mercury species from the interfering PW matrix. Recoveries achieved were: 92% ( $\text{Hg}^{2+}$ ), 87% ( $\text{CH}_3\text{Hg}$ ) and 86% ( $\text{CH}_3\text{CH}_2\text{Hg}$ ). Chemical derivatization (using propylation agent) was found to be efficient in the presence of salt and oil, enabling limits of 5.0, 8.0 and  $11.0 \text{ pg L}^{-1}$  respectively for  $\text{Hg}^{2+}$ ,  $\text{CH}_3\text{Hg}$ , and  $\text{CH}_3\text{CH}_2\text{Hg}$ . The accuracy of the method was guaranteed by matrix-matched standards (containing mineral oil at  $40 \text{ mg L}^{-1}$  and NaCl at  $30 \text{ g L}^{-1}$ ). The method was successfully applied in four different PW samples obtained from off-shore operations.

The fourth work presented a method for the speciation of mercury using a GQDs decorated  $\text{TiO}_2$  nanoparticles (GQDs- $\text{TiO}_2$  NPs) to mediate photolytic degradation that efficiently produced the  $\text{Hg}^0$  (without the need for chemical reduction agents) that was detected by CV-AAS. For the determination, 5 mL of sample solution (containing  $\text{Hg}^{2+}$ ,  $\text{CH}_3\text{CH}_2\text{Hg}$ , and  $\text{CH}_3\text{Hg}$  at the sub- $\mu\text{g L}^{-1}$ ) were placed in quartz tubes, inside a photochemical reactor, and directly adapted to the mercury-dedicated spectrometer. For photocatalytic degradation, a microliter aliquot of GQDs- $\text{TiO}_2$  NPs dispersion ( $0,6 \text{ mg L}^{-1}$  GQDs- $\text{TiO}_2$ ) was added to the sample solution, under adjusted conditions (pH 2.5,  $\text{H}_2\text{O}_2$  as oxidant agent and formic acid). Under such conditions, quantitative speciation was successfully achieved taking advantage of the differences in UV photodegradation kinetics:  $\text{Hg}^{2+}$  (5.0 min),  $\text{CH}_3\text{CH}_2\text{Hg}$  (9.0 min) and 12.0 min for  $\text{CH}_3\text{Hg}$ . The evaluation of the

photodegradation kinetics was also made by GC-CV-AFS, which confirmed the differentiated decreasing in concentration of  $\text{Hg}^{2+}$ ,  $\text{CH}_3\text{CH}_2\text{Hg}$  and  $\text{CH}_3\text{Hg}$  (detected after propylation) during photo-degradation. The limit of detection of the method was  $7 \text{ ng L}^{-1}$  for  $\text{Hg}^{2+}$  and  $\text{CH}_3\text{Hg}$  and  $10 \text{ ng L}^{-1}$  for the  $\text{CH}_3\text{CH}_2\text{Hg}$ . Quantification was performed in a urine sample with certified values for inorganic mercury, which was also fortified with  $\text{CH}_3\text{Hg}$  and  $\text{CH}_3\text{CH}_2\text{Hg}$ .

## **Keywords**

Mercury species; nanoparticles; Produced water; Atomic absorption, Atomic Fluorescence; Cold vapor.

## Resumo

Miranda, Jarol Ramon Andrades; Aucélio, Ricardo Queiroz; Khan, Sarzamin. **Métodos analíticos para a determinação de espécies de mercúrio utilizando espectrometria baseada na geração de vapor frio: Aplicação em amostras complexas e utilizando nanopartículas como agentes fotocatalíticos.** Rio de Janeiro, 2019. 181p. Tese de Doutorado - Departamento de Química, Pontifícia Universidade Católica do Rio de Janeiro.

O objetivo do trabalho foi desenvolver métodos analíticos capazes de especiar mercúrio, determinando metilmercúrio ( $\text{CH}_3\text{Hg}$ ), etilmercúrio ( $\text{CH}_3\text{CH}_2\text{Hg}$ ), mercúrio inorgânico ( $\text{Hg}^{2+}$ ,  $\text{Hg}^0$ ), em água de produção (AP), e tiomersal ( $\text{C}_9\text{H}_9\text{HgNaO}_2\text{S}$ ), em urina e em efluente de uma indústria farmacêutica. Apesar de existir muitos métodos para quantificar espécies de mercúrio, poucos estudos abordam a especiação em AP, amostras conhecidas por ter altos teores de óleo e sal. Além disso, o uso de nanomateriais, como pontos quânticos de grafeno (GQDs), sozinho ou dopados de nanopartículas de dióxido de titânio (GQDs-TiO<sub>2</sub> NPs), foram usados como agentes fotocatalíticos para produzir o mercúrio elementar detectado. As técnicas analíticas utilizadas para a detecção de mercúrio total e para especiação por mercúrio foram espectrometria de absorção atômica com vapor frio em cela multipasso (multipath-CV-AAS) e espectrometria de fluorescência atômica com vapor frio acoplado ao sistema de cromatografia gasosa (GC-CV-AFS).

No primeiro trabalho, a foto-degradação do tiomerosal foi alcançada utilizando luz visível e GQDs, obtidos a partir da hidroexfoliação de ácido cítrico e glutatona, como foto-catalisador. O  $\text{Hg}^0$  gerado (usando condições experimentais ajustadas) foi detectado por multipath-CV-AAS, permitindo a quantificação de tiomersal em concentrações equivalentes a 20 ng L<sup>-1</sup>, mesmo em amostras complexas como efluentes aquosos da indústria farmacêutica e em urina. A cinética de reação (pseudo-primeira ordem com  $k = 0,11 \text{ min}^{-1}$ ) foi determinada.

O segundo trabalho relata o método de especiação de mercúrio em AP usando o sistema CV-AAS. Sob condições ajustadas de concentrações de sal e óleo (por diluição e centrifugação), uma alíquota de amostra foi tratada com  $\text{SnCl}_2$ , levando

ao  $\text{Hg}^0$  quantificado como mercúrio inorgânico original. Uma segunda alíquota de amostra foi exposta a UV (sob condições otimizadas) que promoveu a oxidação de  $\text{CH}_3\text{Hg}$  a  $\text{Hg}^{2+}$ , formando  $\text{Hg}^{2+}$  que foi posteriormente reduzido, com  $\text{SnCl}_2$ , produzindo o  $\text{Hg}^0$  referente ao teor total de mercúrio na amostra. O teor de  $\text{CH}_3\text{Hg}$  foi obtido pela diferença nos resultados alcançados para as duas alíquotas. O efeito matriz imposto por óleo e sal foram estudados e, apesar de afetar a intensidade do perfil do tempo de mercúrio, a quantificação foi alcançada com sucesso com padrões ajustados (assemelhamento de matriz) combinando quantidades de  $\text{NaCl}$  e óleo mineral. As medições de condutividade (estimativa de teor de sal) e turbidimétrica (estimativa de teor de óleo) foram feitas para as amostras de PW, a fim de permitir o ajuste adequado da amostra aos padrões correspondentes (contendo óleo mineral a  $5 \text{ mg L}^{-1}$  e  $\text{NaCl}$  a  $5 \text{ g L}^{-1}$ ). O método de adição de analito também foi utilizada e o limite de quantificação foi de  $12 \text{ ng L}^{-1}$ .

No terceiro trabalho foi desenvolvido um método para especificação de mercúrio em AP usando uma combinação de extração e destilação antes da propilação e determinação por GC-CV-AFS. A extração assistida por ultrassom (40 min), usando o surfactante não iônico (Triton X-114 a 0,5% p/v em solução a pH 3), melhorou as recuperações do processo de destilação que separou as espécies de mercúrio da matriz de AP. As recuperações alcançadas foram elevadas: 92% ( $\text{Hg}^{2+}$ ), 87% ( $\text{CH}_3\text{Hg}$ ) e 86% ( $\text{CH}_3\text{CH}_2\text{Hg}$ ). Descobriu-se que a derivatização química (usando agente de propilação) era eficiente na presença de sal e óleo, permitindo limites de 5,0, 8,0 e  $11,0 \text{ pg L}^{-1}$ , respectivamente para  $\text{Hg}^{2+}$ ,  $\text{CH}_3\text{Hg}$  e  $\text{CH}_3\text{CH}_2\text{Hg}$ . A precisão do método foi garantida por padrões com matriz assemelhada (contendo óleo mineral a  $40 \text{ mg L}^{-1}$  e  $\text{NaCl}$  a  $30 \text{ g L}^{-1}$ ). O método foi aplicado com sucesso em quatro diferentes amostras de AP obtidas em operações *offshore*.

Finalmente, no quarto trabalho é apresentado um método para a especificação de mercúrio usando pontos quânticos de grafeno dopadas com nanopartículas de dióxido de titânio (GQDs- $\text{TiO}_2$  NPs) para mediar a eficiente na produção fotocatalítica de  $\text{Hg}^0$  (sem a necessidade de agentes de redução química) que foi detectada por multipath-CV-AAS. Para a determinação, 5 mL de solução de amostra (contendo  $\text{Hg}^{2+}$ ,  $\text{CH}_3\text{CH}_2\text{Hg}$  e  $\text{CH}_3\text{Hg}$  na afaixa de  $\text{sub-}\mu\text{g L}^{-1}$ ) foram colocados em tubos de quartzo, dentro de um reator fotoquímico, e adaptados diretamente ao sistema CV-AAS. Para a degradação fotocatalítica, uma alíquota de

alguns microlitros da dispersão de nanomaterial ( $0,6 \text{ mg L}^{-1}$  de GQDs-TiO<sub>2</sub> NPs) foi adicionada à solução sob condições ajustadas (pH 3.0, 2% v/v de ácido fórmico). Sob tais condições, a especiação quantitativa foi alcançada com sucesso, aproveitando as diferenças na cinética de fotodegradação UV: Hg<sup>2+</sup> (5.0 min), CH<sub>3</sub>CH<sub>2</sub>Hg (9.0 min) e 13.0 min para CH<sub>3</sub>Hg. A avaliação da cinética de fotodegradação também foi feita por GC-CV-AFS, que confirmou a diminuição diferenciada na concentração de Hg<sup>2+</sup>, CH<sub>3</sub>CH<sub>2</sub>Hg e CH<sub>3</sub>Hg (detectada após a propilação) durante a fotodegradação. O limite de detecção do método foi de  $7 \text{ ng L}^{-1}$  para Hg<sup>2+</sup> e CH<sub>3</sub>Hg, e  $10 \text{ ng L}^{-1}$  para as espécies CH<sub>3</sub>CH<sub>2</sub>Hg. A quantificação foi realizada em amostra certificada de urina que também foi fortificada com CH<sub>3</sub>Hg e CH<sub>3</sub>CH<sub>2</sub>Hg.

## Palavras-Chave

Espécies de mercúrio; Nanopartículas; Águas produzidas, Absorção atômica, Fluorescência atômica; Vapor frio.

## Table of contents

1 Introduction	28
1.1 Contextualization of work	28
1.2 Thesis structure	29
1.3 The objective of this work	30
2 Theoretical fundamentals	31
2.1 Mercury	31
2.2 Produced Waters	32
2.3 Hg determination methods	33
2.4 Thiomersal	39
2.5 Analytical methods for thiomersal determination	40
2.6 Graphene quantum dots (GQDs)	43
2.7 Titanium dioxide	45
2.8 Photo-catalytic applications of GQDs and GQDs associated with TiO <sub>2</sub> .	46
3. Experimental	47
3.1. Apparatus	47
3.2 Reagents and materials	49
3.3. Synthesis of nanomaterials	50
3.4 Characterization of nanomaterials	51
3.5 General procedures	57
3.6 Specific procedures used in “Thiomersal photo-degradation with visible light-mediated by graphene quantum dots: indirect quantification using optical multipath mercury cold-vapor absorption spectrophotometry”	59

3.7 Specific procedures in “Speciation and ultra-trace determination of mercury in produced waters from offshore drilling operations using portable instrumentation and matrix-matching calibration”	62
3.8 Specific procedures in “Mercury speciation in offshore petroleum produced waters by gas chromatography cold vapor atomic fluorescence spectrometry”	65
3.9 Specific procedures in “Photo-generation of cold mercury vapor mediated by GQDs-TiO <sub>2</sub> nanocomposite: on-line ultra-trace speciation of mercury and kinetic studies”	67
4. Results and discussion I. Speciation and ultra-trace determination of mercury in produced waters from offshore drilling operations using portable instrumentation and matrix-matching calibration	70
4.1 Abstract	70
4.2 Results and discussion.	71
4.3 Partial Conclusion	87
5. Results and discussion II. Combination of ultrasonic extraction in a surfactant-rich medium and distillation for mercury speciation in offshore petroleum produced waters by gas chromatography cold vapor atomic fluorescence spectrometry	88
5.1 Abstract	88
5.2 Results and discussion.	89
5.3 Partial conclusion	108
6. Results and discussion III. Thiomersal photo-degradation with visible light-mediated by graphene quantum dots: indirect quantification using optical multipath mercury cold-vapor absorption spectrophotometry	110
6.1 Abstract	110
6.2 Results and Discussion	111

6.3 Partial conclusion	122
7. Results and discussion IV. Photo-generation of mercury cold vapor mediated by graphene quantum dots decorated P <sub>25</sub> -TiO <sub>2</sub> nanoparticles: on-line ultra-trace speciation of mercury and kinetic studies	124
7.1 Abstract	124
7.2 Results and discussion	125
7.3 Partial Conclusion	152
8 General Conclusion	153
9. References	155
10 Attachment	177
A Published papers	177
B Participation in Congress	180

## List of figures

Figure 2. 1	Chemical structure of thiomersal	40
Figure 3. 1	A) Photoluminescence spectra of aqueous dispersions of (a) GQDs and (b) GQDs/TiO <sub>2</sub> ; B) UV–visible spectra of aqueous dispersions of (a) GQDs, (b) P <sub>25</sub> -TiO <sub>2</sub> and (c) nanomaterial prepared using GQDs and TiO <sub>2</sub> ; C) FTIR spectra of a dry film of (a) TiO <sub>2</sub> , (b) GQDs and (c) nanomaterial prepared using GQDs and TiO <sub>2</sub> .	52
Figure 3.2	STEM images of A) GQDs in dispersion; B) solid P <sub>25</sub> -TiO <sub>2</sub> and C) mixture of GQDs and TiO <sub>2</sub> dispersed in water.	54
Figure 3.3	XRD patterns of the GQDs/TiO <sub>2</sub> (a) and (b) pure P <sub>25</sub> -TiO <sub>2</sub> samples.	56
Figure 3.4	XRD pattern with Rietveld refined data for GQDs/TiO <sub>2</sub> . The dotted line represents the experimental points, red line the Rietveld refined data, and the grey line is the difference between experimental data and refined data.	56
Figure 4. 1	Graphical Abstract	71
Figure 4.2	Time profiles after chemical reduction of a Hg <sup>2+</sup> standard solution (50 µg L <sup>-1</sup> ): A) using 2 mL of SnCl <sub>2</sub> at a) 5%; b) 10%; c) 20%; d) 30%; e) 40% (w/w); B) using different volumes of SnCl <sub>2</sub> (20% w/w) solution: a) 0.5 mL; b) 1.0 mL; c) 1.5 mL; d) 2.0 mL; c) 3.0 mL; d) 4.0 mL.	72
Figure 4. 3	A) Effect of NaCl in the time profiles after chemical reduction of a Hg <sup>2+</sup> standard solution (50 µg L <sup>-1</sup> ) in the presence of NaCl at a) 0; b) 10; c) 100 g L <sup>-1</sup> . B) Mercury signal intensities (from a 50 ng L <sup>-1</sup> Hg <sup>2+</sup> standard solution) in function of the NaCl concentrations (0 - 100 g L <sup>-1</sup> ). C) Effect of NaCl in the time profiles after chemical reduction of a Hg <sup>2+</sup> standard solution (50 µg L <sup>-1</sup> ) in the presence of dispersed oil at:	

a) 0; b) 10; c) 20; d) 40; e) 60; f) 80; g) 100 g L<sup>-1</sup> oil.

D) Mercury signal intensities (from a 50 ng L<sup>-1</sup> Hg<sup>2+</sup> standard solution) in function of the dispersed oil (0-100 mg L<sup>-1</sup>).

See Table 4.1 for chemical reduction conditions.

73

Figure 4.4 Circumscribed experimental planning for the chemical reduction of Hg<sup>2+</sup>: A) Response surface for mercury vapor released in the presence of both NaCl and dispersed oil;

75

Figure 4.5 A) Effect of pH of the 50 ng L<sup>-1</sup> analyte solution on mercury signal intensities: a) Hg<sup>2+</sup>; b) CH<sub>3</sub>Hg. B) UV irradiation time for the quantitative conversion of CH<sub>3</sub>Hg (70 ng L<sup>-1</sup>) into Hg<sup>2+</sup> (to be measured as mercury vapor) Effect of UV irradiation time on the oxidation of 70 ng L<sup>-1</sup> solution of CH<sub>3</sub>Hg in the absence (a) and (b) in the presence of H<sub>2</sub>O<sub>2</sub>. C) Effect of H<sub>2</sub>O<sub>2</sub> on the photo-induced oxidation of CH<sub>3</sub>Hg (70 ng L<sup>-1</sup>).

See Table 4.1 for photo-induced oxidation and chemical reduction conditions.

77

Figure 4.6 A) Comparative interference imposed by the dispersed oil content (2 - 10 mg L<sup>-1</sup>) on the mercury signal: a) Solution of Hg<sup>2+</sup> (75 ng L<sup>-1</sup>); b) Solution of CH<sub>3</sub>Hg (75 ng L<sup>-1</sup>).

B) Comparative interference imposed by the NaCl content (2 - 10 g L<sup>-1</sup>) on the mercury signal: a) Solution of Hg<sup>2+</sup> (75 ng L<sup>-1</sup>); b) Solution of CH<sub>3</sub>Hg (75 ng L<sup>-1</sup>). See

Table 4.1 for photo-induced oxidation and chemical reduction conditions.

78

Figure 4.7 Circumscribed experimental planning for the UV photo-induced oxidation of CH<sub>3</sub>Hg (70 ng L<sup>-1</sup>) followed by chemical reduction of Hg<sup>2+</sup> to mercury vapor: A) Graphic of effects; B) Topographic plot for mercury signal in the presence of both NaCl and dispersed oil. See Table 1 for photo-induced oxidation and chemical reduction conditions.

79

Figure 4.8 A) Analytical curves: a) using a standard solution of  $\text{Hg}^{2+}$  and b) using standard solution of  $\text{Hg}^{2+}$  in the presence of  $5 \text{ g L}^{-1}$  NaCl. B) Analytical curves: a) using standard solution of  $\text{Hg}^{2+}$  and b) using standard solution of  $\text{Hg}^{2+}$  in the presence of  $5 \text{ mg L}^{-1}$  of dispersed mineral oil; C) Analytical curves: a) using standard solution of  $\text{Hg}^{2+}$  and b) using standard solution of  $\text{Hg}^{2+}$  in a solution containing  $5 \text{ g L}^{-1}$  NaCl and  $5 \text{ mg L}^{-1}$  of dispersed mineral oil.

83

Figure 5. 9 Determination of mercury species (at  $800 \text{ pg L}^{-1}$ ) using the chosen conditions for the US assisted extraction using Triton X114 (conditions in Table 5.2) in PW simulated samples containing dispersed oil in the range from 20 to  $100 \text{ mg L}^{-1}$  before distillation and GC-CV-AFS determination after propylation. Error bars (associated standard deviation of three replicates).

102

Figure 5. 10 A) Chromatograms for increasing concentrations (from 25 to  $800 \text{ pg L}^{-1}$ ) of the mercury species; a)  $\text{Hg}^{2+}$ ; b)  $\text{CH}_3\text{Hg}$ ; c)  $\text{CH}_3\text{CH}_2\text{Hg}$ ; d)  $\text{Hg}^0$  residual from the calibration standards. Analytical curves for B)  $\text{CH}_3\text{Hg}$ ; C)  $\text{CH}_3\text{CH}_2\text{Hg}$ ; D)  $\text{Hg}^{2+}$  using a) aqueous standards; b) matrix-matched standards using a petroleum sample (corrected by the original mercury species content) and c) matrix-matched standards using mineral oil. Matrix matching: oil ( $40 \text{ mg L}^{-1}$ ) and NaCl ( $30 \text{ g L}^{-1}$ ) (standard deviation for  $n = 3$ ).

105

Figure 5. 1 Graphical abstract

Figure 5. 2 A) Typical chromatograms obtained using the GC-CV-AFS system after derivatization of  $\text{Hg}^{2+}$  standard solutions with  $\text{NaBPr}_4$ , showing the formation of organic mercury artifacts. (B) Relative signals of  $\text{CH}_3\text{Hg}$  and  $\text{Hg}^{2+}$  with organic mercury (as  $\text{CH}_3\text{Hg}$ ) relative percent levels (artifact). The standard deviation for  $n = 3$ .

91

Figure 5. 3 Inorganic mercury ( $\text{Hg}^{2+}$ ) recovery and formation of  $\text{CH}_3\text{Hg}$  artifact measured in the presence of increasing quantities of (A)  $\text{NaCl}$ ; (B)  $\text{NaNO}_3$ ; (C) dispersed crude oil. Indicated values are the percentage ratio between the measured  $\text{CH}_3\text{Hg}$ , and  $\text{Hg}^{2+}$  and N.A. is no artifact formed. Measurements made by GC-CV-AFS after propylation.(standard deviation for  $n = 3$ ) 92

Figure 5. 4 Recoveries for inorganic mercury ( $\text{Hg}^{2+}$ ) and organomercury species ( $\text{CH}_3\text{Hg}$  and  $\text{CH}_3\text{CH}_2\text{Hg}$ ), at  $800 \text{ pg L}^{-1}$ , after distillation of solutions containing increasing quantities of (A)  $\text{NaCl}$ ; (B) dispersed crude oil. Measurements made by GC-CV-AFS after propylation (standard deviation for  $n = 3$ ). 94

Figure 5.5 Recoveries for inorganic mercury ( $\text{Hg}^{2+}$ ) and organomercury species ( $\text{CH}_3\text{Hg}$  and  $\text{CH}_3\text{CH}_2\text{Hg}$ ), at  $800 \text{ pg L}^{-1}$ , using extraction before distillation of aqueous solutions containing  $\text{NaCl}$  ( $40 \text{ g L}^{-1}$ ) and dispersed crude oil ( $60 \text{ mg L}^{-1}$ ): (A) using Triton X-114 and B using Triton X-100. Measurements made by GC-CV-AFS after propylation (standard deviation for  $n = 3$ ). 97

Figure 5. 6 Ultrasound effect on the recoveries for inorganic mercury ( $\text{Hg}^{2+}$ ) and organomercury species ( $\text{CH}_3\text{Hg}$  and  $\text{CH}_3\text{CH}_2\text{Hg}$ ), at  $800 \text{ pg L}^{-1}$ , obtained using extraction with Triton X-114 (0.5%) before distillation of aqueous solutions containing  $\text{NaCl}$  ( $40 \text{ g L}^{-1}$ ) and dispersed crude oil ( $80 \text{ mg L}^{-1}$ ). Measurements made by GC-CV-AFS after propylation (standard deviation for  $n = 3$ ) 98

Figure 5. 7 Effect of the pH on ultrasonic-assisted extraction (40 min), using Triton X-100 (0.5%), on the recoveries for inorganic mercury ( $\text{Hg}^{2+}$ ) and organomercury species ( $\text{CH}_3\text{Hg}$  and  $\text{CH}_3\text{CH}_2\text{Hg}$ ), at  $800 \text{ pg L}^{-1}$ , before distillation of simulated PW samples ( $40 \text{ g L}^{-1}$  of  $\text{NaCl}$  and  $80 \text{ mg L}^{-1}$

dispersed crude oil). Measurements made by GC-CV-AFS after propylation (standard deviation for  $n = 3$ ). 99

Figure 5.8 Effect of temperature during 40 min US assisted extraction on the recoveries of inorganic mercury ( $\text{Hg}^{2+}$ ) and organomercury species ( $\text{CH}_3\text{Hg}$  and  $\text{CH}_3\text{CH}_2\text{Hg}$ ), at  $800 \text{ pg L}^{-1}$ , before distillation of simulated PW samples ( $40 \text{ g L}^{-1}$  of  $\text{NaCl}$  and  $80 \text{ mg L}^{-1}$  dispersed crude oil). Extraction using Triton X-114 (0.5%) and  $\text{H}_2\text{SO}_4$  (pH 3) and measurements made by GC-CV-AFS, after propylation (standard deviation for  $n = 3$ ). 102

Figure 6.1 Graphical abstract 106

Figure 6.2 Absorption spectra of thiomersal ( $20 \text{ mg L}^{-1}$ ) with detail showing the effect of radiation exposure (a. 0 min, b. 15 min, c. 30 min, d. 60 min, e. 80 min) to A) visible light and B) UV. C) Absorption spectra of thiomersal ( $20 \text{ mg L}^{-1}$ ) in the presence of GQDs: (a) without Incidence of UV and (b) after 50 min irradiation with UV, with detail showing the effect of UV radiation exposure; D) Hg measured signal from the UV treated thiomersal solution ( $50 \text{ }\mu\text{L}$  aliquot) in the presence of GQDs along UV incidence (error bar is the standard deviation for  $n=3$ ). 107

Figure 6.3 Scanning transmission electron microscopic image of A) GQDs nanoparticle dispersion after 50 min visible radiation exposure; B) GQDs nanoparticle dispersion after 50 min UV radiation exposure. 108

Figure 6.4 A) Absorption spectra of thiomersal ( $20 \text{ mg L}^{-1}$ ) in the presence of GQDs under the exposure to visible light: (a) 0 min, (b) 15 min, (c) 30 min, (d) 60 min, (e) 80 min B) Hg measured signal from the UV treated thiomersal solution ( $50 \text{ }\mu\text{L}$  aliquot) in the presence of GQDs (after dilution)

along with visible radiation incidence (error bar is the standard deviation for  $n=3$ ). 108

Figure 6.5 A) Hg measured signal (using CV-AAS after fast reduction with  $\text{SnCl}_2$ ) from solutions of thiomersal containing different volumes of the synthesis dispersion of GQDs; B) Time profile of the measured Hg release during visible radiation exposure of thiomersal ( $20 \text{ mg L}^{-1}$ ) in the presence of different volumes of the synthesis dispersion of GQDs: a)  $50 \mu\text{L}$ , b)  $20 \mu\text{L}$ , c)  $17 \mu\text{L}$  and d)  $17 \mu\text{L}$  with  $\text{H}_2\text{O}_2$  (1%). 110

Figure 6.6 Hg measured from the photo-degraded thiomersal in the presence of  $17 \mu\text{L}$  aqueous dispersion of GQDs: A) in function of pH (25 min irradiation time); B) in function of time at pH 5.0; C) after 25 min irradiation time in the presence of either formic acid or hydrogen peroxide; D) in function of time at pH 5.0 in the presence of hydrogen peroxide 2% v/v. Error bars are the standard deviations for  $n=3$ . 111

Figure 6.7 A) Chromatogram (GC-CV-AAS) showing formation of  $\text{CH}_3\text{CH}_2\text{Hg}$  of a thiomersal solution along irradiation time: a) 0 min, b) 5 min, c) 10 min, d) 15 min, e) 20 min. B) Chromatogram (HPLC with detection at 222 nm) showing thiomersal and degradation products peak along time: a) 0 min, b) 5 min, c) 10 min, d) 15 min. Thiomersal solution containing  $17 \mu\text{L}$  of dispersion of GQDs, 2%  $\text{H}_2\text{O}_2$ , and at pH 5. 112

Figure 6.8 Hg measured signal by multipath-CV-AAS: A) in the function of the concentration of thiomersal. B) and C) in function of irradiation time of a thiomersal solution with  $C_0$  is the initial concentration ( $20 \text{ mg L}^{-1}$ ) and with  $C_t$  as concentration measured at different irradiation times. D) Effect of  $\text{CH}_3\text{CH}_2\text{Hg}$  on the thiomersal signal measured as Hg. Thiomersal solution containing  $17 \mu\text{L}$  of dispersion of GQDs, 2%  $\text{H}_2\text{O}_2$  and at pH 5. Error bars are the standard deviations for  $n=3$ . 116

Figure 7. 1 Graphical Abstracts

125

Figure 7. 2. (A) Photocatalytic production of  $Hg^0$  in function of UV exposure time: (a) reference signal (from  $1 \mu g L^{-1}$  of  $Hg^{2+}$ ) obtained through chemical reduction with  $SnCl_2$ ; (b) ( $1 \mu g L^{-1}$ )  $Hg^{2+}$  reduction value using GQDs-TiO<sub>2</sub>; (c) from  $Hg^{2+}$  ( $1 \mu g L^{-1}$ ) in the presence of P25-TiO<sub>2</sub>; (d) from  $Hg^{2+}$  ( $1 \mu g L^{-1}$ ) in the presence GQDs. (B) Temporal profiles for  $Hg^0$  (e) obtained from  $Hg^{2+}$  through chemical reduction with  $SnCl_2$ ; (f) obtained from  $Hg^{2+}$  ( $1 \mu g L^{-1}$ ) in the presence of GQDs-TiO<sub>2</sub> and (g) obtained from  $Hg^{2+}$  ( $1 \mu g L^{-1}$ ) in the presence of P<sub>25</sub>-TiO<sub>2</sub>; (h) obtained from  $Hg^{2+}$  ( $1 \mu g L^{-1}$ ) in the presence of GQDs.

127

Figure 7. 3 Instrumental conditions to measure mercury vapor produced by photo-catalysis performed using the quartz tube cell A); B) The traditional reduction procedure using bubbler cell.

128

Figure 7. 4 Comparison time profile of reduction ( $1 \mu g L^{-1}$   $Hg^{2+}$  standard solution) using: (a) chemical reduction by  $SnCl_2$  20% v/v; (b) Reduction promoted by GQDs-TiO<sub>2</sub>.

129

Figure 7. 5 (A) Photocatalytic production of  $Hg^0$  in function of UV exposure time: (a) reference signal (from  $1 \mu g L^{-1}$  of  $Hg^{2+}$ ) obtained through chemical reduction with  $SnCl_2$ ; (b) reference ( $1 \mu g L^{-1}$ )  $Hg^{2+}$  reduction value using GQDs-TiO<sub>2</sub>; (c) from  $CH_3Hg$  ( $1 \mu g L^{-1}$ ) in the presence of GQDs-TiO<sub>2</sub>; (d) from  $CH_3Hg$  ( $1 \mu g L^{-1}$ ) in the presence of P25-TiO<sub>2</sub>. (B) Temporal profiles for  $Hg^0$  (e) obtained from  $Hg^{2+}$  through chemical reduction with  $SnCl_2$ ; (f) obtained from  $CH_3Hg$  in the presence of GQDs-TiO<sub>2</sub> and (g) obtained from  $CH_3Hg$  in the presence of P<sub>25</sub>-TiO<sub>2</sub>.

130

Figure 7. 6 (A) Photocatalytic production of  $Hg^0$  in function of UV exposure time: (a) reference signal (from  $1 \mu g L^{-1}$  of  $Hg^{2+}$ )

obtained through chemical reduction with  $\text{SnCl}_2$ ; (b) reference ( $1 \mu\text{g L}^{-1}$ )  $\text{Hg}^{2+}$  reduction value using GQDs-TiO<sub>2</sub>; (c) from  $\text{CH}_3\text{CH}_2\text{Hg}$  ( $1 \mu\text{g L}^{-1}$ ) in the presence of GQDs-TiO<sub>2</sub>; (d) from  $\text{CH}_3\text{CH}_2\text{Hg}$  ( $1 \mu\text{g L}^{-1}$ ) in the presence of P<sub>25</sub>-TiO<sub>2</sub>. (B) Temporal profiles for  $\text{Hg}^0$  (e) obtained from  $\text{Hg}^{2+}$  through chemical reduction with  $\text{SnCl}_2$ ; (f) obtained from  $\text{CH}_3\text{CH}_2\text{Hg}$  in the presence of GQDs-TiO<sub>2</sub> and (g) obtained from  $\text{CH}_3\text{CH}_2\text{Hg}$  in the presence of P<sub>25</sub>-TiO<sub>2</sub>.

131

Figure 7. 7 (A) Typical chromatograms obtained using the GC-CV-AFS system after propylation (at pH 4.0) of an organic mercury species (150 and 300 pg): A) for  $\text{CH}_3\text{Hg}$  prior to UV exposition (solid line) and after 50 min of UV exposure in the presence of GQDs-TiO<sub>2</sub> (dashed line); B) for  $\text{CH}_3\text{CH}_2\text{Hg}$  prior to UV exposition (solid line) and after 50 min of UV exposure in the presence of GQDs-TiO<sub>2</sub> (dashed line). Organic species ( $\text{CH}_3\text{Hg}$  or  $\text{CH}_3\text{CH}_2\text{Hg}$ ) (a),  $\text{Hg}^{2+}$  (b) and  $\text{Hg}^0$  (c).

132

Figure 7. 8 Temporal profile of mercury produced from mercurial species under UV in the presence of GQDs-TiO<sub>2</sub>: (a) Reduction of standard solution ( $1 \mu\text{g L}^{-1}$ ) of  $\text{Hg}^{2+}$ ; b) Photochemical degradation of  $\text{CH}_3\text{CH}_2\text{Hg}$  ( $1 \mu\text{g L}^{-1}$ ); c) Photochemical degradation of  $\text{CH}_3\text{Hg}$  ( $1 \mu\text{g L}^{-1}$ ).

133

Figure 7. 9 Circumscribed experimental design for photocatalytic reduction of organic mercury species. A)  $\text{CH}_3\text{Hg}$ ; response surface to the released mercury value in pH, and the amount of GQDs-TiO<sub>2</sub> dispersion. B) Topographic plot for mercury signal referring to  $\text{CH}_3\text{Hg}$  reduction. C)  $\text{CH}_3\text{CH}_2\text{Hg}$ ; response surface to the released mercury value in pH, and the amount of GQDs-TiO<sub>2</sub> dispersion. D) Topographic plot for mercury signal referring to  $\text{CH}_3\text{CH}_2\text{Hg}$  reduction.

135

Figure 7. 10 Circumscribed experimental design for photocatalytic reduction of  $\text{Hg}^{2+}$ . A) surface response to the

mercury value released by pH, and the amount of GQDs-TiO<sub>2</sub> dispersion. B) Topographic plot for mercury signal referring to Hg<sup>2+</sup> reduction. 136

Figure 7. 11 Photocatalytic reactions for mercurial species using aqueous suspensions of GQDs-TiO<sub>2</sub> (0.6 mg) at around pH 3 adjusted using HCl and H<sub>2</sub>SO<sub>4</sub>. 137

Figure 7. 12 Effect of percent of formic acid on photocatalytic degradation of mercurial species mediated by GQDs-TiO<sub>2</sub>. Chemical reduction of Hg<sup>2+</sup> with SnCl<sub>2</sub> as a reference. 139

Figure 7. 13 Hg<sup>0</sup> absorbance measured in function of the UV exposition time for photocatalytic reactions using GQDs-TiO<sub>2</sub> nanocomposite (0.6 mg or 100 μL of the synthesis dispersion at 6 mg mL<sup>-1</sup>) in aqueous system at pH 3 and containing formic acid (2% v/v): a) Hg<sup>2+</sup> at 1 μg L<sup>-1</sup>; b) CH<sub>3</sub>CH<sub>2</sub>Hg at 1 μg L<sup>-1</sup>; c) CH<sub>3</sub>Hg at 1 μg L<sup>-1</sup>. 141

Figure 7. 14 Hg<sup>0</sup> signal temporal profile after measured in function of the UV exposition time for photocatalytic reactions using GQDs-TiO<sub>2</sub> nanocomposite (0.6 mg or 100 μL of the synthesis dispersion at 6 mg mL<sup>-1</sup>) in aqueous system at pH 3 and containing formic acid (2% v/v): a) Hg<sup>2+</sup> at 1 μg L<sup>-1</sup>; b) CH<sub>3</sub>CH<sub>2</sub>Hg at 1 μg L<sup>-1</sup>; c) CH<sub>3</sub>Hg at 1 μg L<sup>-1</sup>; d) mixture or organomercurial species (each one at 1 μg L<sup>-1</sup>). 138

Figure 7. 15 (A) Typical chromatograms obtained using the GC-CV-AFS system after derivatization of standard solutions of Hg<sup>2+</sup>, CH<sub>3</sub>Hg, CH<sub>3</sub>CH<sub>2</sub>Hg with NaBPr<sub>4</sub>, After photocatalytic degradation with UV-mediated GQDs-TiO<sub>2</sub> A) 0 min; B) 5 min; C) 8 min D) 12 min. 143

Figure 7. 16 Efficiency of GQD-TiO<sub>2</sub> nanocomposite (1.2 mg L<sup>-1</sup>) in promoting photoreaction to produce Hg<sup>0</sup> from different mercurial species at increasing concentrations:

A)  $\text{Hg}^{2+}$  after 5 min UV exposure; B)  $\text{CH}_3\text{Hg}$  after 13 min of UV exposure; C)  $\text{CH}_3\text{CH}_2\text{Hg}$  degradation after 9 min UV exposure. 145

Figure 7. 17 Hg measured signal by multipath-CV-AAS: A) in the function of the concentration of  $\text{Hg}^{2+}$ . D)  $\text{CH}_3\text{Hg}$ ; and E)  $\text{CH}_3\text{CH}_2\text{Hg}$ ; in function of irradiation time of a mercury species solution with  $C_0$  is the initial concentration (100; 300; 700  $\text{ng L}^{-1}$ ) and with  $C_t$  as concentration measured at different irradiation times. B; D; and F)  $\ln(C_0/C_t)$  mercury species solution. 147

Figure A. 1 Published paper: Chapter 4. 179

Figure A. 2 Published paper: Chapter 5. 177

Figure A. 3 Published paper: Chapter 6. 178

## List of tables

Table 3.1 Values of the refinement parameters obtained from XRD analysis by employing the Rietveld method.	57
Table 4. 1 Experimental conditions to perform quantitative analytical speciation of mercury CV-AAS with a multi-pass cell and UV-induced oxidation	80
Table 4. 2 Characteristics of the analyzed PW samples	80
Table 4. 3 Original concentrations of $\text{Hg}^{2+}$ e $\text{CH}_3\text{Hg}$ found in PW samples using the proposed method.	83
Table 4. 4 Quantification study after PW samples fortification with $\text{Hg}^{2+}$ for the estimation of the original analyte content.	84
Table 4.5 Quantification study after PW samples fortification with $\text{CH}_3\text{Hg}$ for the for the	84
Table 4.6 Comparison of results for the determination of $\text{Hg}^{2+}$ and $\text{CH}_3\text{Hg}$ in PW samples.	85
Table 4. 7 Comparison of the determination of $\text{Hg}^{2+}$ and $\text{CH}_3\text{Hg}$ in PW samples with the proposed method and using the method based on GC-CV-AFS.	85
Table 4. 8 Characteristics of different methods for the determination of total mercury in different samples using different analytical techniques.	86
Table 5. 1 Experimental conditions to perform quantitative analytical speciation of mercury GC-CV-AFS.	101
Table 5. 2 Characteristics of the PW samples.	103
Table 5. 3 Parameters of the analytical calibration curves obtained.	
Table 5.4 Average original recovered values of $\text{Hg}^{2+}$ and $\text{CH}_3\text{Hg}$ in PW samples using a fortification study.	106
Table 5. 5 Quantification study after PW samples fortification with $\text{Hg}^{2+}$ for the estimation of the original analyte content.	107

Table 5. 6 Quantification study after PW samples fortification with CH <sub>3</sub> Hg for the estimation of the original analyte content.	108
Table 6.1 Information on methods for the determination of thiomersal reported in the literature and the proposed method.	122
Table 7. 1 Parameters and data from the kinetic study of the photocatalytic degradation of mercury species using 0.12 mg mL <sup>-1</sup> GQDs-TiO <sub>2</sub> dispersion.	148
Table 7. 2 Chosen parameters for speciation analysis using CV-AAS after UV photocatalytic reaction mediated by GQDs-TiO <sub>2</sub> nanocomposite	149
Table 7. 3 Analytical figures of merit of the speciation method using CV-AAS after UV photocatalytic reaction mediated by GQDs-TiO <sub>2</sub> nanocomposite	149
Table 7. 4 Interference study concerning the effect of some transition metals on the photoreaction of mercurial species.	150
Table 7. 5 Study of recovery after fortification with CH <sub>3</sub> Hg and CH <sub>3</sub> CH <sub>2</sub> Hg of the SRM 2672a.	151
Table 7. 6 Comparison of determination CH <sub>3</sub> Hg and CH <sub>3</sub> CH <sub>2</sub> Hg fortification with the proposed method and using the GC-CV-AFS-based method.	152

## Lis of abbreviation

TM	Thiomersal
CV-AAS	Cold-vapor absorption spectrophotometry
CV-AFS	Cold vapour atomic fluorescence spectroscopy
STEM	Scanning transmission electron microscopy
TiO <sub>2</sub>	Titanium oxide
HPLC	High-performance liquid chromatography
LOD	Limit of detection
LOQ	Limit of quantification
UV-vis	Ultraviolet-visible
FTIR	Fourier-transform infrared spectroscopy
XPS	X-ray photo-electron spectroscopy
RFC	Relative Centrifugal Force
XRD	X-ray Diffraction
NaBPr <sub>4</sub>	Sodium tetra-n-propylborate
GQDs-TiO <sub>2</sub>	Graphene quantum dots (GQDs) doped titanium dioxide nanoparticles
SRM	Standard Reference Material
P <sub>25</sub> -TiO <sub>2</sub>	Titanium oxide Nanoparticles
Rwp	Weighted profile R-factor
Rp	Profile R-factor
CV-ICP-MS	Cold vapor inductively coupled plasma mass spectrometry
CV-AFS	Cold vapor generation coupled to atomic fluorescence spectrometry
ICP-OES	Inductively coupled plasma atomic emission spectroscopy
GC-CV-AFS	Gas chromatography coupled to cold vapour atomic fluorescence spectrometry
PVG-AFS	Photochemical vapor generation coupled with atomic fluorescence spectrometry

# 1 Introduction

## 1.1

### Contextualization of work

Polluted environmental compartments are one of the main concerns to society, in particular considering water bodies and atmosphere [1]. In this context, mercurial species are considered in the group of the most toxic global pollutants, yet released to the environment from natural and human activities [1]. Mercury, in the environment, mainly exists in the forms of elemental mercury ( $\text{Hg}^0$ ), inorganic mercury ( $\text{Hg}_2^{2+}$ ,  $\text{Hg}^{2+}$ ) and organic mercury (mainly  $\text{CH}_3\text{Hg}$ ,  $\text{CH}_3\text{CH}_2\text{Hg}$ ). When in organic form, in special as  $\text{CH}_3\text{Hg}$ , mercury is hazardous as it solubilizes in tissues then exercising its full neurotoxic potential affecting humans and superior animals through the food chain [2]. The Minamata Convention was established to phase out production and all of the technological use of mercury. The releasing of mercury from extractive activities, like oil drilling, also impose an environmental impact; thus, environmental agencies established severe limits for mercury concentration in residues. For instance, in petroleum industry, offshore operations are allowed to return the produced water back to the ocean only after checking levels of total mercury.

As mercury is a critical pollutant, there are several analytical methods in literature aiming its total determination or speciation. In this context, when dedicated mercury analysis is the goal, cold vapor (CV) based methods using atomic absorption spectrometry (AAS) and atomic fluorescence spectrometry (AFS) after chemical derivatization and gas chromatography (GC) are the indicated analytical tools. However, despite the vast literature on the topic, there still space to propose methods aiming specific complex matrices and also searching for innovative analytical approaches based on the use of nanomaterials to promote more efficiency in mercury detection and speciation. Those efforts may provide better accuracy using more straightforward and more robust analytical procedures

and reducing costs such as the ones related to the use of derivatization agents for chemical speciation.

## 1.2

### Thesis structure

This thesis is structured in seven chapters. In Chapter 2, a bibliographic review is made to present the theoretical foundations on mercury, sources of contamination, produced water, thiomersal, and the analytical method for the determination of mercury, carbon nanomaterials, called in this thesis graphene quantum dots (combined or not with nanoparticles of titanium dioxide) focusing on photocatalytic properties, also indicate other relevant information on these nanomaterials.

Chapter 3 contains detailed information on instrumentation and materials used in this work, and procedures for preparing solutions, production of graphene quantum dots dispersed in aqueous solutions. The detailed procedures involving the developed analytical methods are also presented.

The results are presented in four chapters (4, 5, 6 and 7), the first three have chapters had already been published, each one referring to the development of analytical methods for the determination of mercury species using different approaches. Results of chapter 7 will compose one manuscript aiming for publication. A brief summary of the work is presented at the beginning of each of these chapters before the full description of the results. A partial conclusion in each chapter is also presented.

Finally, in chapter 8 the overall conclusion of the thesis.

## 1.3

### The objective of this work

#### 1.3.1

##### General Objective

To develop analytical methods based on cold vapor generation of mercury aiming the analysis of challenging samples, in terms of matrix composition, also evaluating the use of nanomaterials as platforms to selectively photo-reduce inorganic mercury and photo-degrade organomercurial mercury species.

#### 1.3.2

##### Specific objectives

- ✓ Explore graphene quantum dots (GQDs) as photo-catalysts to enable efficient degradation of thiomersal into elemental mercury detected by CV-AAS.
- ✓ Associate chemical reduction of inorganic mercury and UV photochemical oxidation or organic mercurial species enabling indirect mercury speciation analysis using multipath cold vapor atomic absorption spectrometry (multipath-CV-AAS).
- ✓ Improve speciation analysis (ultra-trace levels) of mercury using ultrasonic extraction and distillation before chemical propylation in CV-GC-AFS.
- ✓ Adjust proper procedures for the analysis of PW samples aiming the improvement of accuracy in CV based spectrometric determinations.
- ✓ Produce nanocomposites consisting of TiO<sub>2</sub> and GQDs that mediate UV photoreaction of mercurial species.
- ✓ Study the kinetics of photo-degradation of mercurial species by TiO<sub>2</sub>-GQDs nanocomposites aiming speciation analysis using CV-AAS.

## 2 Theoretical fundamentals

### 2.1

#### Mercury

Mercury is a metal, presenting itself as a liquid at room temperature, that has no biological functions. It poses a high risk to the environment and humans due to its toxicity, persistence, long-distance transport potential and bio-accumulation [3]. The emissions and distributions of Hg to the environment occur from both human activity and natural processes [4]. Despite the efforts led by the United Nations (Minamata Convention) mercury release caused by human activity still accounts for 8.000 metric tons per year against 5.000 metric tons due to natural processes [5]. The Minamata Convention aims to ban new mercury mines, phasing-out the existing ones. It also intends to reduce and eventually eliminate mercury use in products and processes, control emissions to air and releases to land and water, and even regulate the informal sector of artisanal and small-scale gold mining. The Convention also addresses interim storage of mercury and its disposal once it becomes waste, sites contaminated by mercury as well as health issues [6].

Mercury is found in various chemical forms such as metallic mercury ( $\text{Hg}^0$ ), inorganic mercury ( $\text{Hg}^{2+}$ ), and organic mercury compounds such as methylmercury ( $\text{CH}_3\text{Hg}$ ), dimethylmercury ( $\text{CH}_3\text{HgCH}_3$ ), ethylmercury ( $\text{CH}_3\text{CH}_2\text{Hg}$ ), phenylmercury ( $\text{PhCH}_3\text{Hg}$ ). All forms of mercury are considered poisonous, but methylmercury is mainly the one that brings more concern due to its extreme toxicity, being able to accumulate in tissues. Methylmercury is easily absorbed by organisms at the bottom of the food chain, thus bio-accumulating in fish and seafood in general [7,8]. Therefore, the consumption of seafood is one of the primary sources of human contamination with mercury [9].

Mercury is also found in petroleum, which is still the most important source of energy for modern society. Petroleum is also the raw material for infinity industrial products such as chemical fertilizers and plastics. The concentration of

Hg in crude oil and natural gas varies from 0.01 ng g<sup>-1</sup> to 10 ng g<sup>-1</sup>, mainly depending upon its geological location [10].

Mercury in petroleum can be in its elemental form or present as a dissolved organic form (generally as R-Hg-R, R-Hg-X, where R is a methyl or ethyl group, and X = chloride and other anions), inorganic mercury salts and mercury compounds complexed with nitrogen and oxygen-containing ligands. One of the primary anthropogenic sources of mercury to the atmosphere is the burning of fuels, which contributes to the global cycle of methyl mercury in the aquatic food chain [5]. Total anthropogenic emissions of mercury in the United States of America, in 2014 were 50,068 kg with coal-fired pilot plants the largest source of anthropogenic mercury was coal-fired pilot plants [11].

Other relevant sources of mercury contamination related to the energy industry are discharges of water used in the production and processing of petroleum, which contains a variety of mercury species. In offshore operations, these waters, also known as produced water (PW) are discharged back into the oceans.

## 2.2

### Produced Waters

According to the Brazilian National Environment Council (CONAMA), produced water (PW) is water produced in conjunction with petroleum [12]. It comprises a mixture of endogenous water (formation), the one naturally present in geological reservoirs, and injected water, the one introduced into the reservoir to increase oil production [12]. Due to their complex composition, PW is considered harmful to the environment, and sometimes their volume exceeds oil/gas production [13,14].

PW is considered to be wastewater with a natural chemical composition that meets the geological characteristics of the source reservoir [13,14]. This may include toxic substances such as aromatic oil fractions (benzene, toluene, ethylbenzene, and xylene as well as polycyclic aromatic hydrocarbons), organic acids, phenols, and alkylated phenols. Besides, toxic elements (arsenic, lead, and mercury, among others) and radionuclides may be present [15] in a matrix of high salinity and temperature differing significantly from that of seawater [16]. A myriad of chemicals such as corrosion inhibitors, fouling inhibitors, biocides, oxygen

scavengers, emulsion breakers or boners, de-foamers, viscosifiers, hydrate inhibitors, and cleaners may also be present [17]. All of these compounds influence the composition of PW and its physicochemical properties. Water may also contain mercury in the form of suspended HgS, elemental Hg or its oxidized forms [2]. In Brazil, the maximum concentration of Hg in effluents, according to the CONAMA, is  $0.01 \text{ mg L}^{-1}$  [18].

Clearly, due to the environmental risk associated with it, and considering the fact that PW returns to the ocean, there is interest in developing analytical methods to characterize these wastes in order to monitor their characteristics before being discharged. Traces of metals and metalloids in PW are a health and environmental concern. To date, only some of these contaminants (Hg, Pb, V, Cr, and Mn) have been determined in PW in an attempts to regulate and control of this effluent [17].

In Brazil, the release of metal by human activities has doubled in the last 100 years, surpassing the natural release of metal, which led Government Authorities to regulate the use of mercury in the Brazilian industry. In the case of mercury, it is crucial to monitor not only the total mercury concentration related to these sources but also the variety of organic mercury species. In this context, PW is one of the most crucial mercury sources in the oil and gas industry, and its composition and salinity vary according to the geological source of water. Unfortunately, existing data on the presence of mercury in these waters is limited, especially when considering mercury speciation.

Determination of Hg in PW, as well as refinery water, is difficult because of the volatile and reactive nature of mercury and because of the matrix effects imposed by the high salinity and presence of oil residues. Therefore, it is not yet possible to assign a consistent range of mercury concentration in PW from offshore operations. In Brazil such data would be essential to evaluate the environmental impact of oil production operations.

## 2.3

### Hg determination methods

Several analytical methods have been reported for the determination of total mercury and its speciation in different matrices. As the toxicological, physical and

chemical properties of mercury are considerably dependent upon the degree of alkylation or its oxidation state, there is a growing need to develop analytical methods of speciation. The ideal procedure for speciation analysis should be based on maintaining the balance between the chemical forms of the element in the sample from collection to analyte determination. That is, the preparation and separation procedures should not affect the quantitative distribution of the species present. Proper sample collection and storage (and pre-treatment when required) are critical for mercury-containing sample analysis. In addition to the risk of contamination, the high volatility of some mercury species ( $\text{Hg}^0$  and  $(\text{CH}_3)_2\text{Hg}$ , for example) and the high chemical affinity of the Hg species, their surface adsorption capacity and their permeability through some plastics may lead losses at this critical stage of the analytical process.

Conversion between Hg species should be avoided during all analytical process. Polytetrafluoroethylene (PTFE), polyethylene terephthalate (PET) and glass have been proven to be suitable materials for collecting and storing samples. To preserve  $(\text{CH}_3)_2\text{Hg}$ , the water sample collection should be followed by acidification with HCl, and sample must be refrigerated. Also, care should be taken to avoid any residual oxidizing agents from the container during cleaning step to avoid decomposition of organic mercury species [19].

For mercury speciation, hyphenated techniques using coupling of a separation technique such as gas (GC) or liquid chromatography (HPLC) with atomic absorption or atomic fluorescence detection [8] are extensively used. In the use of GC it is necessary that all species are volatile, which implies, in many cases, a previous chemical derivatization step. By using reverse-phase liquid chromatography, as a separation technique, separation of the original water-soluble mercury species are easily achieved, and coupling with inductively coupled plasma mass spectrometry (ICP-MS) becomes feasible as column effluent can be introduced directly without the need for post-column derivatization. However, this approach is more costly in terms of acquisition and operation [20].

Non-chromatographic approaches such as the selective reduction reported in the Mago's method [21,22] are cost-effectively providing high analytical frequency and high sensitivity when using detection such as cold vapor atomic absorption spectrometry (CV-AAS) or cold vapor atomic fluorescence spectroscopy (CV-AFS). In Mago's method, mercury species respond differently to different reagents

in producing the detected  $\text{Hg}^0$ . For instance,  $\text{Hg}^0$  can be generated from the mercuric ion by its selective reduction by  $\text{SnCl}_2$  in acidic medium [22] while  $\text{CH}_3\text{Hg}$  can be reduced by  $\text{SnCl}_2$  in the presence of  $\text{Cd}^{2+}$  in acidic medium [23].

Extraction procedures (liquid-liquid extraction and solid-phase extraction) can be used for mercury speciation in liquid samples. Liquid-liquid extraction can be performed with an appropriate organic solvent or a mixture of solvents that easily extract ionized organic mercury compounds using a suitable solvent [24]. Solid-phase extraction methods are also reported for mercury extraction using resins based on 8-hydroxyquinoline [25]. All these treatments have some disadvantages such as incomplete extractions, unwanted chemical transformations and, in some cases, interferences in detection.

Undoubtedly the most popular analytical techniques employed to determine mercury at trace concentrations are based on the generation of cold vapor (CV) using chemical reducing agents such as  $\text{NaBH}_4$  [26,27],  $\text{SnCl}_2$  [28], sodium cyanotrihydroborate (III) [29] and sodium tetrahydroborate (THB) [30], or by electrolytic reduction [31]. The CV is generally coupled to different traditional spectrometric detection techniques such as atomic absorption spectrometry (CV-AAS) [31], atomic fluorescence spectrometry (CV-AFS) [30] and inductively coupled plasma optical emission (CV-ICP OES) [32] or mass spectrometry (CV ICP-MS) [28]. Some of these methods were employed along with flow injection systems to increase the degree of automation that improves analytical frequency [33].

Alternative approaches for mercury reduction of  $\text{Hg}^{2+}$  based on photochemical reactions under UV radiation have been proposed [34]. The presence of low molecular weight organic molecules, such as formic acid, acetic acid, and propanoic acid, generates electron donor species such as  $\cdot\text{CH}$  and  $\text{CCO}\cdot$  radicals that are very powerful reducing agents to produce  $\text{Hg}^0$  [35].

Atomic fluorescence spectrometry (AFS) enables speciation analysis with detection at  $\text{ng L}^{-1}$  levels, in most cases limited by background mercury levels, using instruments composed by a GC system (purge and retention systems) coupled to a dedicated AFS detection. GC-CV-AFS requires chemical derivatization, usually with sodium tetraethyl borate [36], sodium tetra(n-propyl) borate [37] or sodium tetraphenyl borate [38], providing fast reaction in producing highly volatile mercury species that are separated in the chromatographic column before detection [39-41].

Derivatization procedures such as ethylation can be sensitive not only to the pH but also to the ionic strength of solutions [42], which are critical in PW samples. Another drawback of ethylation is the fact that it is not possible to differentiate inorganic mercury from the ethylmercury originally present in sample [43,44]. In contrast, propylation converts  $\text{CH}_3\text{Hg}$  into methylpropylmercury,  $\text{Hg}^{2+}$  into dipropyl mercury and  $\text{CH}_3\text{CH}_2\text{Hg}$  into ethylpropylmercury, improving speciation and reliability of results since propylation tend to be efficient over a more extensive pH range and leads to more stable propylated derivatives[45]. The high content of organic matter and high ionic strength may interfere in propylation[42,46,47]. Therefore, mercury speciation analysis in PW samples requires efficient separation of the analytes before derivatization[48].

The widest procedures described in literature to separate organic mercury ( $\text{CH}_3\text{Hg}$  in most cases) from water samples, before derivatization, are solvent extraction [49,50] and inert gas purging assisted distillation [51,52]. Solvent extraction is time-consuming and labor-intensive, also requiring toxic organic solvents. Distillation of mercury species is being preferred since it is more effective in transferring mercury species to a less complex aqueous solution, not involving organic solvents. Distillation is adopted by the United States Environmental Protection Agency in the standard method for mercury speciation (EPA Method 1630, “*Methylmercury in water by distillation, aqueous ethylation, purge and trap, and cold vapor atomic fluorescence spectrometry*”) [46].

For complex samples, such as PW samples, the efficiency of the EPA standard method is affected by matrix components [51] due to interferences related to partial solubility of mercury species in the dispersed oil and because of the decreased mobility of mercury species due to the formation of  $\text{HgCl}_n^{(n-2)}$  complexes as the samples present very high chloride content (salt supersaturation is common). In this context, the use of ultrasonic (US) assisted extraction can be more efficient, reducing the time required for efficient extractions[53,54].

Ultrasound (US) assisted extraction efficiency depends on frequency, exposition time also upon the presence of additives that improve cavitation. Several authors have emphasized different applications of US for treatment of agricultural, biological and environmental samples for the determination of various elements and speciation purposes [53,55]. For instance, US was found to be useful for the

extraction of polycyclic aromatic hydrocarbons and polychlorinated biphenyls from soil samples [54].

US assisted extraction using hydrochloric acid solutions has also been used for total mercury [56] and also for mercury species in fish tissues before determination using flow injection and CV-AAS [57]. Recently, a microextraction assisted by US in a medium containing surfactant (Triton X-100) was used for the determination of residues of hormones in environmental waters using HPLC and spectrophotometric detection. Ultrasound aided emulsification and dispersion of the extraction solvent, improving extraction and pre-concentration of the hydrophobic analytes [58].

Currently, there are few works reported in the literature describing mercury determination and speciation in PW. However, many studies report the determination of mercury species in seawater.

Bloom and Crecelius, described an analytical method for the determination of total mercury in Pacific Northwest coastal waters using a refined two-stage gold amalgamation preconcentration technique in conjunction with CVAAS. Determinations were made on samples of unfiltered seawater, showing that mercury concentrations ranged from 0.1 to 1.0 ng L<sup>-1</sup> [59]. Chlba *et al.* reported the determination of alkyl mercury compounds in seawater by microwave-induced plasma emission spectrometry at atmospheric pressure combined with GC. The LOD for CH<sub>3</sub>HgCl, CH<sub>3</sub>CH<sub>2</sub>HgCl, and (CH<sub>3</sub>)<sub>2</sub>Hg were 0.09, 0.12 and 0.40 µg L<sup>-1</sup>, respectively. The method was applied for the determination of alkylmercury compounds in seawater, and pre-concentration was performed after extraction with benzene and cysteine [60]. Bloxham *et al.* described a method for speciation of alkylmercury compounds in seawater using HPLC coupled to ICP-MS. The three species were separated on a C<sub>18</sub> column at 260 s, 340 s, and 750 s, respectively, using a 1% v/v acetonitrile and 0.005% 2-mercaptoethanol mobile phase at 0.06 mol L<sup>-1</sup> ammonium acetate. The LOD in artificial seawater were 0.25 µg L<sup>-1</sup> for CH<sub>3</sub>HgCl, HgCl<sub>2</sub>, and 0.75 µg L<sup>-1</sup> for CH<sub>3</sub>CH<sub>2</sub>HgCl. Off-line pre-concentration using a dithiocarbamate resin allowed a 50-fold increase in detection [61].

Sanchez *et al.* reported mercury speciation analysis in seawater (from Gijon, Spain) by hyphenation of solid-phase microextraction to GC-ICP-MS. Blank values were the limiting factor in achieving lower detection limits of inorganic mercury. A laboratory synthesized sodium tetrapropylborate was better for derivatization

since the commercial one presented higher background levels of Hg. LOD were 0.17 and 0.35 ng L<sup>-1</sup> for Hg<sup>2+</sup> and CH<sub>3</sub>Hg respectively. The high salt content in samples was responsible for strong matrix effects, which were overcome by using analyte addition method [45]. Cairns *et al.* employed HPLC associated with ICP-MS and an on-line pre-concentration using micro-column for the analysis of Hg<sup>2+</sup> CH<sub>3</sub>Hg in the dissolved phase of natural waters. This method allowed the rapid pre-concentration and removal from sample matrix. The LOD of the method was 0.07 ng L<sup>-1</sup> for Hg<sup>2+</sup> and 0.02 ng L<sup>-1</sup> for CH<sub>3</sub>Hg, allowing the determination of these analytes in filtered Venetian lagoon seawater [62]. Chen *et al.* reported a method for speciation of mercury by cation exchange chromatography and detection by ICP-MS. Separation of Hg<sup>2+</sup>, CH<sub>3</sub>Hg, CH<sub>3</sub>CH<sub>2</sub>Hg, and phenylmercury (PhHg) was achieved within 2.0 - 2.5 min using two consecutive 12.5 mm cationic exchange columns and L-cysteine aqueous solution as mobile phase. The LOD for Hg<sup>2+</sup>, CH<sub>3</sub>Hg, CH<sub>3</sub>CH<sub>2</sub>Hg, and PhHg were 0.019, 0.027, 0.031 and 0.022 µg L<sup>-1</sup>. The method was applied in five seawater samples and five marine fish samples [63].

Saint'Pierre *et al.* developed an analytical method for inorganic mercury determination in PW using ICP-MS after electrothermal vaporization of samples. Analyte fortified samples were analyzed. The LOD and LOQ of the method were 0.12 µg L<sup>-1</sup> and 0.41 µg L<sup>-1</sup> respectively. The accuracy of the method was verified using the recovery tests by adding a certified urine sample to a PW sample achieving an average recovery of 106% [20]. Barbara *et al.* proposed an analytical method for the determination of inorganic mercury in PW in the presence of high salinity using a photochemical CV generation system coupled to ICP-OES. The LOD and LOQ achieved by the method were 1,2 e 4,0 µg L<sup>-1</sup> respectively. The recoveries in real samples showed recoveries ranging from 79 to 121 % [64]. Shigeta *et al.* determined CH<sub>3</sub>Hg, CH<sub>3</sub>CH<sub>2</sub>Hg in seawater and industrial wastewater by GC-MS. Alkyl mercury compounds were directly phenylated with sodium tetraphenylborate (NaBPh<sub>4</sub>) in water and extracted into toluene. The LOD values were 53.3 and 33.5 ng L<sup>-1</sup> for CH<sub>3</sub>Hg, CH<sub>3</sub>CH<sub>2</sub>Hg in pure water. The recoveries of alkylmercury compounds from seawater and four types of industrial wastewater were higher than 90 % [65]. Liu *et al.* developed a method for simultaneous determination of CH<sub>3</sub>Hg, CH<sub>3</sub>CH<sub>2</sub>Hg in water by GC-CV-AFS. Experimental conditions including derivatization, pH, distillation and complexing agents were optimized. The LOD (as Hg) of the method was 0.007 ng L<sup>-1</sup> for CH<sub>3</sub>Hg and 0.004

ng L<sup>-1</sup> for CH<sub>3</sub>CH<sub>2</sub>Hg. The method was applied to five different water samples including river water, effluent wastewater, seawater, industrial wastewater, groundwater, and recoveries higher than 87 % were achieved. Studies of CH<sub>3</sub>Hg and CH<sub>3</sub>CH<sub>2</sub>Hg artifact formation showed little influence in final results [66]. Yu *et al.* developed a method for the determination of CH<sub>3</sub>Hg in seawater by UV-induced methyl ethyl mercury (CH<sub>3</sub>HgCH<sub>2</sub>CH<sub>3</sub>) atomization based on derivatization using NaBEt<sub>4</sub> and GC-AFS. The UV atomizer has successfully converted CH<sub>3</sub>HgCH<sub>2</sub>CH<sub>3</sub> into Hg<sup>0</sup> below (<45 °C). The effects of UV lamp power, quartz tube length, GC carrier gas flow rate and NaBEt<sub>4</sub> concentration were optimized. The LOD of the method was 0.0002 ng L<sup>-1</sup> for CH<sub>3</sub>Hg. The method was applied to determine CH<sub>3</sub>Hg at sub-ng L<sup>-1</sup> level in different seawater samples [67].

## 2.4

### Thiomersal

Thiomersal (ethyl (2-mercaptobenzoate-(2-)-O, S) sodium (1-) mercurate (Figure 1) is an organomercury compound commonly used as a preservative agent [68,69]. TM is also known as thimerosal or mertiolate, and it is used to prevent bacteriological contamination and to ensure product stability. It was developed in 1927, and years later, it was employed as an antimicrobial agent in pharmaceuticals such as vaccines, eye care solutions, contact lens cleaning solutions, ointments [69].

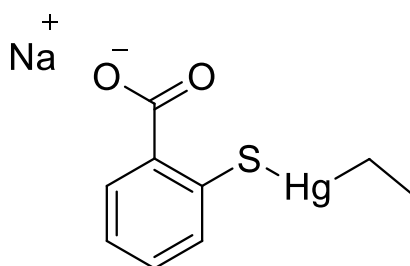


Figure 2. 1 Chemical structure of thiomersal

TM contains 49.55 % mercury in its composition, and it is metabolized and degraded, in the organism, to ethyl mercury and thiosalicylic acid [70]. The use of

TM in vaccines and pharmaceuticals is controversial as ethylmercury is toxic and seems to be related to severe neurological disorders [71,72]. Extensive use of thiomersal also raises environmental concerns due to the disposal of expired vaccines and medicines due to mercury-contaminated wastewater from pharmaceutical industries. The allowed limit of mercury in discharged aqueous effluents is  $5 \mu\text{g L}^{-1}$ , which is equivalent to  $10 \mu\text{g L}^{-1}$  of thiomersal [73]. Because of this, in recent decades, research efforts have focused on developing methods for the treatment of pharmaceutical effluent containing thiomersal [74,75].

## 2.5

### Analytical methods for thiomersal determination

Many analytical methods have been developed for the determination of low levels of thiomersal. Meyerx *et al.* determined thiomersal in water samples using HPLC, with a reversed-phase  $\text{C}_{18}$  column and ammonium carbonate solution (pH 7.9) as mobile phase. The method was applied in pharmaceutical formulations used for contact lens cleaning [76]. Bushee *et al.* developed a method for the determination of thiomersal in vaccines using HPLC coupled with the mass spectrometry (MS). The separation was made using a  $\text{C}_{18}$  column and mobile phase consisting of  $0.06 \text{ mol L}^{-1}$  ammonium acetate (pH 5.3), 3 % v/v acetonitrile and 0.005 % 2-mercaptoethanol. The TM concentration in samples was in the  $100 \mu\text{g mL}^{-1}$  range [77]. Silva *et al.* studied various liquid chromatography systems to determine thiomersal and its degradation products (thiosalicylic acid and dithiodibenzoic acid) using electrochemical detection (amperometry and coulometry) on a glassy carbon electrode. Separation systems included suppressed reverse phase chromatography, reverse phase ion pair chromatography and ion chromatography, this last one found to be the best for the determination of thiomersal in ophthalmic solutions in terms of selectivity and sensitivity (LOD of  $0.006 \mu\text{g mL}^{-1}$ ) [78]. Silva *et al.* also developed a method based on cyclic voltammetry-mediated electrochemical oxidation of thiomersal using a rotating vitreous carbon disc electrode. The best results were obtained using supporting electrolyte at pH 4.0 (acetate buffer) with measurements at  $40 \text{ mV s}^{-1}$ . The method LOD was from  $0.1 \mu\text{g mL}^{-1}$ , and the method was applied to the determination of thiomersal in contact lens cleaning solutions [79].

Shrivastaw and Singh developed a colorimetric method for the determination of thiomersal based on the formation of a complex with diphenyl thiocarbazon in the presence of dithizone in alkaline medium. The complex formed has a maximum absorbance at 538 nm, which differs from the one of dithizone (478 nm). The method was applied in the determination of thiomersal in hepatitis B vaccines. The authors report that this method only requires microliters of sample and can estimate thiomersal concentrations of 0.5  $\mu\text{g}$  [80]. Gil *et al.* developed a method for the determination of thiomersal in ophthalmic solutions by CV-AAS using UV/H<sub>2</sub>O<sub>2</sub> oxidation process. The conversion of TM to Hg<sup>2+</sup> was achieved under 10 min of UV exposure in the presence of 100  $\mu\text{L}$  of H<sub>2</sub>O<sub>2</sub>. The reduction of Hg<sup>2+</sup> to Hg<sup>0</sup> was carried out in a batch reactor coupled to a quartz furnace atomizer, kept at room temperature, used to measure the temporal absorption profile of Hg. This reduction/vaporization process was improved by the addition of formic acid to the sample solution before UV irradiation. The method was applied to the determination of thiomersal in seven commercial ophthalmic solutions with LOD of 0.04  $\mu\text{g mL}^{-1}$  in terms of thiomersal [81]. Dos Santos *et al.* developed a method for the quantification of thiomersal by photochemical mercury CV generation coupled to an ICP OES system. Mercury emission was detected at 253, and 652 nm and the LOD was 0.3  $\mu\text{g mL}^{-1}$  of Hg or 0.6  $\mu\text{g mL}^{-1}$  of thiomersal in solution. The procedure was applied to the analysis of rabies, diphtheria/ tetanus, hepatitis B and influenza vaccines from two producers [82]. He *et al.* also described a method for the direct determination of thiomersal in vaccines by photochemical CV generation coupled to ICP OES using dielectric barrier discharge (DBD) as the excitation/emission source. The method eliminated the need to use strong oxidizers and conventional chemical reducing agents. The LOD for Hg<sup>2+</sup> and thiomersal (as Hg) were calculated as 0.19  $\mu\text{g L}^{-1}$  and 0.17  $\mu\text{g L}^{-1}$ . The method was successfully applied in the analysis of commercial vaccines [68].

Fredj *et al.* developed a gas diffusion flow injection method for the determination of thiomersal in biological samples. The method was based on the generation of mercury CV from the thiomersal reaction with SnCl<sub>2</sub> in acidic medium. The evolved CV diffuses through a Teflon membrane into a flow of an acidic permanganate solution (40  $\mu\text{g mL}^{-1}$ ) where it was oxidized and converted to Hg<sup>2+</sup>. The resulting decrease in absorbance of the flowing solution was monitored at 528 nm and related to thiomersal. The method produced a linear response in the

concentration range of 1-30  $\mu\text{g mL}^{-1}$ . The LOD was 0.07  $\mu\text{g mL}^{-1}$ , and the method has been successfully applied for the determination of thiomersal in different types of vaccines [83]. Campanella *et al.* developed a flow injection method based on the photochemical oxidation of the thiomersal, which was quantitatively converted into  $\text{Hg}^{2+}$  by microwave (MW) and UV. Then,  $\text{Hg}^{2+}$  was reduced to Hg with a  $\text{NaBH}_4$  solution to be detected by CV-AFS in a miniature Ar/ $\text{H}_2$  flame. The method covered the concentration range of 0.01-2  $\mu\text{g mL}^{-1}$ , with a LOD of 0.003  $\mu\text{g mL}^{-1}$ . The method was applied in the determination of thiomersal in ophthalmic solutions, with recoveries between 97% and 101% [84]. Acosta *et al.* developed a method for the determination of thiomersal,  $\text{CH}_3\text{CH}_2\text{Hg}$ , and  $\text{Hg}^{2+}$  by HPLC coupled to AFS. The method consisted of the formation of mercury CV, generated by the post-column UV photo-reduction in a medium containing formic acid. The LOD was 0.09, 0.09 and 0.07  $\mu\text{g L}^{-1}$  for thiomersal,  $\text{CH}_3\text{CH}_2\text{Hg}$  and  $\text{Hg}^{2+}$  respectively. This method was applied in the analysis of effluents from the pharmaceutical industry and in the waters of the San Luis River in Argentina [75]. Zaręba *et al.* studied a simple HPLC method for simultaneous separation, identification, and quantification of thiomersal in vaccines and drugs by molecular absorption, after post-column derivatization with dithizone, enabling LOD of 0.3  $\mu\text{g}$  for thiomersal [85]. Piech *et al.* proposed the electrochemical determination of thiomersal using differential pulse redissolution voltammetry. The method was applied for determination of thiomersal in alkaline solution in the presence of EDTA, using a mercury film silver-based electrode by applying potential at -1500 mV. The LOD was 0.37  $\mu\text{g mL}^{-1}$ , after pre-concentration (90 s) and linear response covered two orders of magnitude. The proposed method was successfully applied in the determination of thiomersal in different vaccines [86]. Acosta *et al.* reported an HPLC method with fluorimetric detection to determine TM and degradation products. The analytes were subjected to UV irradiation using a home-made photoreactor (which served as the interface between the LC column and the fluorimeter) in order to promote molecular fluorescence sensitivity of the degradation organic products. This method was applied in the determination of thiomersal,  $\text{CH}_3\text{CH}_2\text{Hg}$  and thiosalicylic acid in pharmaceutical effluent samples and waters of the La Carolina and Jáchal rivers (Argentina). The LOD of the method was 0.73  $\mu\text{g mL}^{-1}$  [87].

## 2.6

### Graphene quantum dots (GQDs)

A quantum dot is a nanometer-sized particle (with semiconductor properties) with structure confined in all three spatial dimensions. Inorganic semiconductor quantum dots (QDs) have attracted a great deal of interest in the last two decades due to their peculiar optical and electronic properties [88]. The main disadvantages of inorganic QDs include their toxicity (in the case of the very popular CdSe or CdTe QDs and the ones containing Pb and As) and the fact that when dispersed (colloidal dispersion) they are susceptible to minute environmental changes such as pH and ionic force.

Graphene is a two-dimensional material and exhibits an infinite radius of Bohr [89]. In contrast, graphene quantum dots (GQDs) is a zero-dimensional material as three dimensions are in nanoscale range. GQDs are graphene fragments that are small enough to be under exciton confinement and quantum size effect. Typically, GQDs have diameters below 20 nm but size as large as 100 nm are commonly found in literature. Such a size limitation results in a quantum effect (differentiation of the once degenerated energy levels of both conduction band, or CB, and valence band, or VB), confinement effect (as crystalline structure limits the distribution of electrons resulting in a non-zero semiconductor bandgap) and edge effects. Because GQDs are more "molecule-like" they present spectroscopic features associated with the quantum confinement induced VB – CB transition. Compared the typical 7 eV HOMO-LUMO gap for benzene, density functional theory calculations showed that GQDs energy bandgap decreases to about 2 eV in cluster consisting of 20 rings [90]. Since GQDs is a carbon-based nanoparticle, it is more resilient to environmental conditions in aqueous dispersion and is significantly less toxic compared to most of the inorganic QDs.

GQDs were produced by Ponomarenko and Geim in 2008 [91] based on a procedure reported for carbon dots (CDs) [92]. GQDs differ from the CDs as they present graphene lattices, which are smaller than 100 nm in size and less than 10 layers thick [93], while CDs are usually nearly spherical nanoparticles, usually with less than 10 nm in size [93]. GQDs also exhibit different chemical and physical properties when compared to other carbon-based materials such as CDs, CNTs, fullerene and graphene as it is photoluminescent and can be quickly stabilized in

water [94] due to the broad edge effect of GQDs, which can be modified by functional groups, as opposed, for instance, to CNTs limited by their one-dimensional characteristics. In fact, modifications (doping) of GQDs have been proposed in order to achieve tuning of optical and electronic properties, such as the first attempts investigated by Zhao *et al.*, in 2012, involving the use of nitrogen rich organic compounds to produce GQDs [95].

In general, GQD extinction spectra present a prominent peak at about 230 nm, which is attributed to the excitation  $\pi \rightarrow \pi^*$  of the  $\pi$  bonds [96]. Functional groups in GQDs can introduce other absorption features and affect photoluminescence (the so-called edge effect) [97]. Photoluminescence quantum yields reported for GQDs vary significantly, but it is, in general below 30% [98]. Besides, contrary to inorganic QDs, photoluminescence from GQDs generally present a wider bandwidth and it is not uncommon that spectral emission shifts to red and decreases in intensity with the increasing excitation wavelength [98]. It should also be noted that the spectroscopic properties of GQDs may vary depending on the preparation method and the functional groups at the edges of the particles.

The preparation of GQDs, as for any nanomaterial, is classified in two main categories, top-down and bottom-up, according to the precursor material. The top-down method refers to the direct cutting of carbon or graphene-related materials (such as graphene [94], graphene oxide [99], carbon nanotubes [100], carbon fibers [101], carbon black [102], graphite powder [103] and coal [104] etc.) in nanometric size structures through various processes. In bottom-up approach, organic compounds (aromatic or non-aromatic) such as polycyclic aromatic hydrocarbons [105], benzene [106], hexaperi-hexabenzocoronene [107], glucose [108], fullerene [109], citric acid [110], among several others, are converted, through reactions, to GQDs.

One of the most attractive properties of GQDs is that they are carbon material with low intrinsic toxicity [111]. They are compatible with various solvents and can be modified with functional groups, at their edges, affecting electronic properties. The peculiar properties make GQDs much more desirable for many applications compared to inorganic semiconductor QDs including in application concerning photo-catalysis.

## 2.7

### Titanium dioxide

Titanium is one of the most abundant elements on earth, presenting mostly in the oxide form (most stable state). As  $\text{TiO}_2$ , it can be found in three different crystalline forms which are brookite, rutile, and anatase [112]. However, the anatase and rutile forms are the most common and studied, but important photocatalytic activity is a characteristic only in anatase.

$\text{TiO}_2$  has attracted attention since Fujishima and Honda, in 1972, discovered the photosensitizing effect of a  $\text{TiO}_2$  electrode for  $\text{H}_2\text{O}$  electrolysis when in combination with a Pt counter electrode and incidence of UV [113]. Since then,  $\text{TiO}_2$  has been used for photo-catalysis, wastewater purification, and solar energy conversion [114-116].  $\text{TiO}_2$  are considered wide band-gap semiconductors (3.0 eV to 3.2 eV) and a photo-catalyst with high hydrogen generation through UV [112]. Among several oxide semiconductor photo-catalysts,  $\text{TiO}_2$  presents biological and chemical inertness, strong oxidizing power, non-toxic character and long-term stability against photo and chemical corrosion, in addition to high photocatalytic efficiency [117,118]. The photocatalytic efficiency is attributed to oxygen species such as  $\text{O}_2^{\cdot-}$ ,  $\text{H}_2\text{O}_2$ , and  $\text{HO}^{\cdot}$  produced on the  $\text{TiO}_2$  surface when illuminated by photons with energy more significant than its bandgap. In this way, electrons will be excited to the CB, thus creating a pair of electron-hole [119]. Holes ( $\text{h}^+$ ) and hydroxyl radicals ( $\text{OH}^{\cdot}$ ) generated in the valence band and electrons and superoxide anions ( $\text{O}_2^{\cdot-}$ ) generated in the conduction band enable  $\text{TiO}_2$  to decompose and mineralize organic compounds by a series oxidation reactions that lead to carbon dioxide [119].

Literature reports many studies on the use of  $\text{TiO}_2$  for catalytic photo-oxidation of different substances such as dyes [120] and pollutants in domestic [121] and industrial effluents [122]. Most of these studies focus on industrial wastewater treatment, but some researchers have used the process of treating sewage [120,123].

$\text{TiO}_2$  has some disadvantages as photo-catalyst, such as a high energy bandgap (3.2 eV) that makes inefficient the visible light capture. In an attempt to increase the photoluminescent efficiency of  $\text{TiO}_2$ , two essential strategies have been explored: (i) narrowing the  $\text{TiO}_2$  gap by producing hybrid materials to expand the

UV absorption to the visible range [124] and (ii) introducing conductive channels for electron separation, resulting in delayed excitation recombination [125]. The association with hetero-structures improve capture of electrons and the separation of electron-hole pairs. In this context, GQDs are the most promising hetero-structure to be associated with TiO<sub>2</sub> due to their ability to trap electrons [125]. Combining TiO<sub>2</sub> nanoparticles with GQDs increases catalytic activity to various degrees depending on the intrinsic characteristics of the hybrid and can bring about analytically interesting optical reactivity and activity.

## 2.8

### **Photo-catalytic applications of GQDs and GQDs associated with TiO<sub>2</sub>.**

In recent years, GQDs have received increasing attention in the field of photocatalysis. Zero-dimension GQDs also consist of several layers of sp<sup>2</sup> hybridized honeycomb carbon structure, which benefits charge transport involved in photocatalytic processes. Besides, GQDs present finite bandgap within the energy scale of the visible light of the spectrum [126]. Roushani *et al.* investigated the catalytic behavior of GQDs (prepared by direct pyrolysis of citric acid) in the degradation of a cationic dye. The adjusted parameters showed that in the presence of 10 μL GQDs dispersion, at pH 5, was very efficient in dye photo-degradation [127]. Fan *et al.* reported the degradation of methylene blue using GQDs and polyethylenimine and polyethylene glycol-modified GQDs under visible radiation. It was observed that the degradation rate could be controlled by the use of different polymers [127].

Bottom-up methods allow the production of GQDs rich in functional groups such as carboxylic and hydroxyl groups, facilitating the combination of GQDs with other catalysts [128,129]. Gupta *et al.* incorporated GQDs into TiO<sub>2</sub> nanotube arrays and found that methylene blue could be more efficiently decomposed compared to pure TiO<sub>2</sub> under UV irradiation [130]. Pan *et al.* proved that amine-functionalized GQDs could extend TiO<sub>2</sub> absorption to a broader region, which gave the GQDs/TiO<sub>2</sub> hybrid (or GQDs/TiO<sub>2</sub> composite) good activity for methyl orange photo-degradation under visible radiation [131]. Yan *et al.* constructed GQDs/TiO<sub>2</sub> based photoelectric sensors to detect dopamine under visible light [132].

### 3. Experimental

#### 3.1.

#### Apparatus

Mercury (cold vapor) measurements were made on a dedicated mercury CV multipass atomic absorption spectrometer (multipass-CV-AAS), model RA-915 (LUMEX, Russia), equipped with Zeeman background correction and connected to an RP-92 accessory for chemical reduction in aqueous solution. An automated analytical system (GC-CV-AFS) was used for mercury speciation studies. The GC-CV-AFS system comprised a purge module and a retention/pre-concentration module, which functions are respectively to purge the volatile derivatized mercury species from the sample into the system where they are retained in pre-concentration traps to be later desorbed. A chromatographic module and a pyrolysis module performed respectively the separations of the mercury derivatized species and the thermic decomposition of these species to  $\text{Hg}^0$  before reaching the mercury dedicated fluorescence detection system. The GC column (provided by Brooks Rand Instruments) was a U-shaped glass column (4 mm internal diameter) packed with a 15 % OV-3 (phenylmethyl dimethyl silicone 10 %) on Chromasorb White. The GC column temperature was set to 36 °C and the Ar gas flow was 30 mL min<sup>-1</sup>.

Distillation of samples was performed on the temperature-controlled methylmercury distillation system (Brooks Rand Instruments), which consists of a 10 vial position aluminum heater block coupled to a temperature controller and an inert gas flow controller. The Teflon vials (70 mL volume) were stoppered with Teflon lids with two openings to allow a flow of carrier gas (argon) percolating into the solution and carrying the volatile propylated mercurial species. The heating block was closed with an insulated lid to prevent sample reflux. Distillates were collected in Teflon vials placed in another aluminum block containing ice.

UV-vis absorption spectra were acquired on a Perkin-Elmer, model Lambda 35, double beam spectrophotometer (Perkin-Elmer, UK) using 1000 nm min<sup>-1</sup> scan rate, 10 nm spectral bandpass and 1 cm optical path length quartz cuvettes.

Photoluminescence measurements were made on a model LS 55 luminescence spectrometer (Perkin-Elmer) using 1000 nm min<sup>-1</sup> scan rate, 10.0 nm spectral bandpass in 1 cm optical length quartz cuvettes. Chromatographic analysis performed on a high-performance liquid chromatography system (Model 1200, Agilent Technologies, Japan) equipped with a multiple wavelength fluorescence detector, a column oven, and an Agilent Eclipse column. XDB - C18 (250 × 4.6 mm and Average Particle Size 5 μm).

GQD images were taken using a field emission scanning electron microscope (JEOL, model JSM-6701F, Japan) operated in the 30 kV scanning transmission electron microscopy (STEM) mode. Raman spectroscopy and atomic force microscopy (AFM) for topology were performed using a micro-Raman spectrometer (NT-MDT, NTEGRA SPECTRA, Russia) equipped with a charge-coupled device detector and a solid-state laser. Raman measurements were obtained using a chilled coupled charge pair device and a 473 nm laser source, and AFM images were obtained using the touch mode diamond tip (7 × 7 microns). X-ray photoelectron spectroscopy (XPS) was performed using a spectrometer equipped with a commercial Alpha 110 hemispherical electronic energy analyzer with Mg radiation K $\alpha$  ( $h\nu = 1253.6$  eV). The high-resolution XPS spectra were obtained (passage energy of 20 eV) and the data were processed using the CasaXPS software. The reference energy was the C1s peak at 284.5 eV. The FT-IR spectra of the GQDs and the GQDs-TiO<sub>2</sub> hybrid were made with the Perkin Elmer Spectrum-Two Fourier Transform Infrared spectrophotometer.

Conductivity measurements were made using an mCA 150 model conductivity meter (Tecnopon, Brazil) with a double-platinum plate sensor. The pH meter was a model mPA 210 (Tecnopon, Brazil) with a glass membrane electrode combined with an Ag|AgCl(KCl<sub>sat</sub>). A 9-L ultrasonic bath with timer and heating control (Ultra Clean 800A, Unique, Brazil) were used for the treatment of samples. The laboratory-made photochemical reactor consisted of six commercial fluorescent lamps (6 W each, emitting in the visible spectral range) set on the internal wall of a PVC tube (20 cm diameter × 30 cm width) fixed onto a wood box, as a base that contain a mechanical rotor that kept the test-tube circular rack rotating (6 rotations min<sup>-1</sup>). A small fan was placed at the top of the reactor in order to keep its internal temperature below 30°C. The lamp set consisted either of fluorescent visible range lamps or bacteriological fluorescent lamps (main line at 253 nm and

secondary lines in the 296 to 313 nm range). Samples were accommodated inside 20 mL glass tubes, which were placed (vertically) inside the reactor in a circular test-tube rack. A centrifuge (Sorvall Biofuge Stratos model, Thermo Scientific, USA) was used for sample treatment. Total carbon measurements were made on a Carbon Analyzer model TOC-V<sub>CPN</sub> (Shimadzu, Japan).

### 3.2

#### Reagents and materials

Ultrapure water (18.2 MΩ cm) was obtained from the Milli-Q gradient A10 ultra-purifier (Millipore, USA). Thiomersal, L-cysteine, sodium acetate, titanium (IV) oxide (P25-TiO<sub>2</sub> nanopowder with 21 nm average particle size) were purchased from Sigma-Aldrich (USA). The derivatization agent sodium tetra-n-propyl borate (NaBPr<sub>4</sub>) was obtained from abcr GmbH Co (Germany). Tin chloride (SnCl<sub>2</sub>) was from Vetec (Brazil). Mercury speciation adequate acetate buffer solution (pH 4.9), potassium hydroxide solution (2 % v/v), standard solutions of methyl mercury (CH<sub>3</sub>HgCl) at (1 and 1000) mg L<sup>-1</sup>, ethyl mercury (CH<sub>3</sub>CH<sub>2</sub>HgCl) at (1 and 1000) mg L<sup>-1</sup>, standard solution (1 and 1000) mg L<sup>-1</sup> of HgCl<sub>2</sub>; and sodium tetraethyl borate, NaB(CH<sub>3</sub>CH<sub>2</sub>)<sub>4</sub>, were acquired from Brooks Rand Instruments (USA). Mercuric nitrate, sodium hydroxide, hydrochloric acid, phosphoric acid, methanol (HPLC grade), hydrogen peroxide (30% vol), formic acid, citric acid sodium chloride, sulfuric acid, ammonium hydroxide, dichloromethane, Triton X-114, and Triton X-100 were obtained from Merck (Germany). Standard reference material NIST (USA) SRM 1641c (*mercury in water*) and 2672a level (*mercury in urine*) were used for accuracy tests. Pharmaceutical solution (Tecnoquímicas S.A) contained 0.1 g of thiomersal per 100 mL was purchased in a local drugstore, and PW samples were provided by Petrobras (Brazil).

Syringe filters (0.45 μm) were from Whatman, UK. Dialysis membrane (retained molecular weight of 3.5 kDa) was from Spectrum Laboratories Inc. (USA). Nitrogen (99.99 %) and argon (99.999 %) were from Lynde gases (Brazil).

### 3.3.

#### Synthesis of nanomaterials

##### 3.3.1

##### Production of graphene quantum dots.

Graphene quantum dots (GQDs) used for the degradation of TM were obtained based on the procedure described in the literature [133], using 0.50 g of citric acid placed into a 5 mL beaker that was heated to about 240°C. As the mixture became molten (changing from colorless to brown in about 5 min) the hot liquid was added into 50 mL of NaOH 0.25 mol L<sup>-1</sup> aqueous solution at room temperature, in order to obtain (after filtering on a 0.45 µm syringe filter) a clear pale yellow aqueous sample that was further dialyzed (24 h). This was called the aqueous synthesis dispersion of GQDs. The GQDs used for the mercury speciation study was prepared similarly but using water, instead of NaOH solution, as the hydro-exfoliation medium.

##### 3.3.2

##### Preparation of the GQDs-TiO<sub>2</sub> nanoparticles

The composite of GQDs and P<sub>25</sub>-TiO<sub>2</sub> nanoparticles (P<sub>25</sub>-TiO<sub>2</sub> NPs) were produced by the pyrolysis of citric acid in the presence of P<sub>25</sub>-TiO<sub>2</sub> NPs based on a literature procedure used with minor modifications [133,134]. Briefly, 1.0 g citric acid was mixed 30 mg P<sub>25</sub>-TiO<sub>2</sub> NPs in a 5 mL beaker. The mixture was heated to about 240 °C in order to melt the citric acid. After about 2 min, the hot melted liquid mixture (pale yellow to brownish) was poured into 50 mL of water, at room temperature, to form the so-called synthesis dispersion. The dispersion was kept under stirring for 24 h. Then, the GQDs-TiO<sub>2</sub> NPs dispersion was centrifuged at

(11.200 RFC) for 20 min. The solid pellet was separated from the supernatant and dried, under vacuum, at 60 °C for 10 h.

### 3.4

#### Characterization of nanomaterials

##### 3.4.1

##### Graphene quantum dots

The GQDs obtained from the hydro-exfoliation of melting citric acid in NaOH solution were characterized after dilution in water in order to produce an extinction spectrum with maximum of about 0.5 according to work described by Toloza *et al.* The spectrum presented broad extinction spectrum, covering the violet-blue range, with a maximum peak at about 200 nm and first excitonic shoulder at 370 nm. The dispersion showed bright photoluminescence emission (maximum at 460 nm) under excitation at 370 nm. The quantum yield of these GQDs was about 8% at 25 °C. Characteristic Raman features of graphene (bands G and D) appeared respectively near 1586  $\text{cm}^{-1}$  and 1358  $\text{cm}^{-1}$ . The produced GQDs had a size distribution in the range from 3 to 8 nm, with an average diameter of 5.2 nm [133].

The GQDs dispersion to be mixed with P25-TiO<sub>2</sub> NPs, forming the nanocomposite used for speciation of mercury, was hydro-exfoliated in ultrapure water. The diluted GQDs dispersion (50 times dilution factor in water) produced a spectrum that covered the violet-blue range with a maximum peak at about 200 nm and first excitonic shoulder at 335 nm (Figure 3.1B). The diluted dispersion (100 times in water) showed bright photoluminescence emission (maximum at 473 nm) under excitation at 348 nm (Figure 3.1A). The quantum yield of these GQDs was about 21% at 25 °C. The size distribution of GQDs (Figure 3.2A) showed nanoparticles sizes ranging from a few nanometers up to about 50 nm but with an average diameter of about 25 nm (estimated from STEM image taking into consideration 100 elected GQDs).

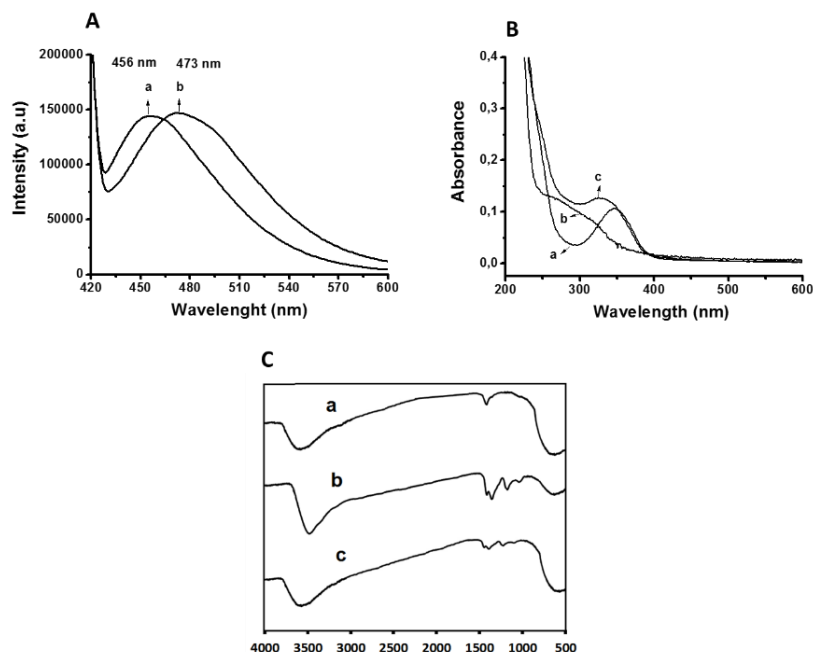


Figure 3.1 A) Photoluminescence spectra of aqueous dispersions of (a) GQDs and (b) GQDs/TiO<sub>2</sub> NPs; B) UV-visible spectra of aqueous dispersions of (a) GQDs, (b) P<sub>25</sub>-TiO<sub>2</sub> NPs and (c) nanomaterial prepared using GQDs and TiO<sub>2</sub> NPs; C) FTIR spectra of a dry film of (a) TiO<sub>2</sub> NPs, (b) GQDs and (c) nanomaterial prepared using GQDs and TiO<sub>2</sub> NPs.

### 3.4.2

#### Nanocomposite of graphene quantum dots and GQDs-TiO<sub>2</sub> NPs

The P<sub>25</sub>-TiO<sub>2</sub> NPs average particle size, also estimated from 100 nanoparticles in a solid sample, was 20.3 nm (STEM image in Figure 3.2B) but the distribution of sizes includes small fractions of nanoparticle sizes as small as a few nanometers and fractions up to 50 nm range. In the case of the mixture containing GQDs and TiO<sub>2</sub> NPs, STEM images were obtained from an aqueous dispersion. It was found nanomaterials with a distribution of diameters varying within a wide range of sizes (similar to the distribution observed for the pure TiO<sub>2</sub> NPs). Average size was 19.5 nm but from a STEM image with a small sampling of sizes (Figure 3.2C) shows nanoparticles up to 51.7 nm along other smaller ones (not marked but clearly in the range below 10 nm). In principle, no clear difference, in sizes, was

found considering the general profile pure solid P25-TiO<sub>2</sub> NPs and the mixture containing TiO<sub>2</sub> NPs and GQDs.

The extinction spectra of the diluted dispersion of nanoparticles were obtained (1 mL of dispersion filtered in a 0.22 μm and diluted in water to complete 10.00 mL). For the GQDs, the broad extinction spectrum was observed, with the characteristic maximum intensity in the 200 nm range, reaching a minimum just before 300 nm (Figure 3.1B, spectrum *a*). This spectral characteristics can be attributed to the  $\pi$ - $\pi^*$  transition of C=C carbon sp<sup>2</sup> [135]. The GQDs first excitonic band appeared at 345 nm. The typical extinction profile from TiO<sub>2</sub> NPs is found in spectrum *b* of Figure 3.1B, characteristic of the exciton transition arising from the transfer of an electron from oxygen to a titanium ion [136]. As the GQDs, the material prepared by mixing GQDs and TiO<sub>2</sub> NPs showed an extinction profile with high intensity in the 200 nm range that reached a minimum just before 300 nm. However, the first excitonic appeared at 335 nm (15 nm shorter than the one characteristic of GQDs), which is an indication of the formation of composite with characteristics that differentiate from the original materials.

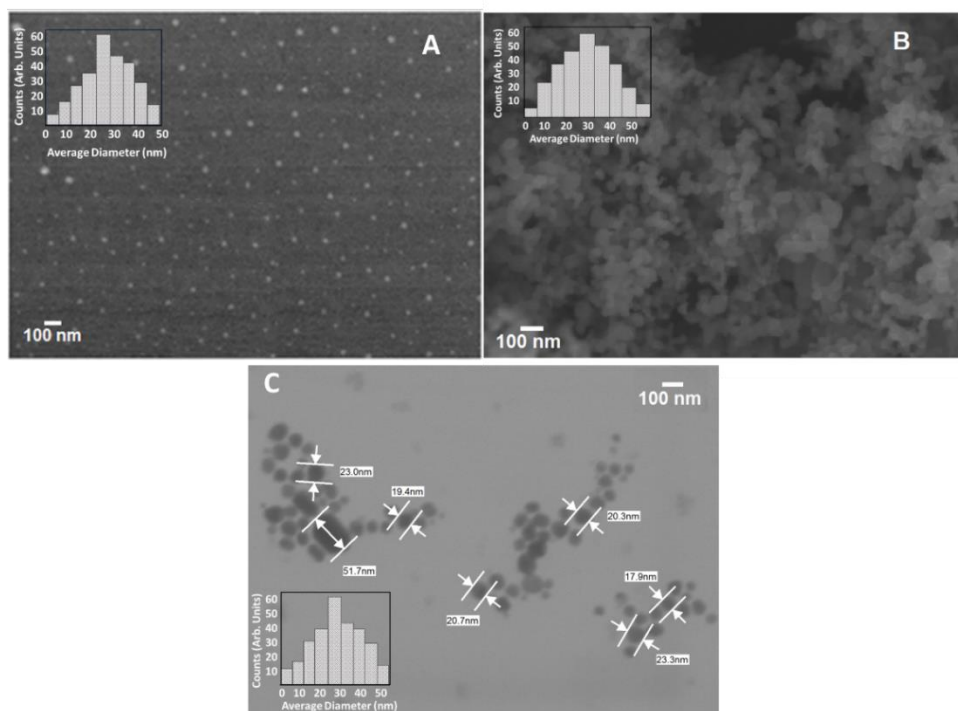


Figure 3.2 STEM images of A) GQDs in dispersion; B) solid P<sub>25</sub>-TiO<sub>2</sub> NPs and C) mixture of GQDs and TiO<sub>2</sub> dispersed in water.

The formation of a differentiated nanomaterial (a nanocomposite) is confirmed by comparing photoluminescent emission from GQDs and the nanomaterial produced by mixing GQDs and TiO<sub>2</sub> NPs (Figure 3.1A). In both cases, the nanomaterial aqueous dispersion produced bright blue-violet emission upon excitation at 345 nm. However, the maximum emission observed for the nanomaterial produced by mixing GQDs and TiO<sub>2</sub> NPs presents a hypsochromic effect, appearing at 456 nm or 17 nm shorter than the one of the GQDs (at 476 nm) confirming the formation of a nanocomposite. Even after six months of storage (under refrigeration) the dispersion presented a bright appearance, and the photoluminescence of the nanocomposite dispersion was stable and produced strong photoluminescence with maximum at 456 nm.

The infrared spectrum was obtained (using Fourier transform and attenuated total reflection) using films (from moist spots formed from partially dried dispersions) of P<sub>25</sub>-TiO<sub>2</sub> NPs GQDs and GQDs-TiO<sub>2</sub> NPs. In TiO<sub>2</sub> nanoparticles (spectrum *a* of Figure 3.2C), the band appearing in the region below than (500-700)

$\text{cm}^{-1}$  is attributed to the elongation vibration Ti–O and Ti–O–Ti [137]. The band at  $3500 \text{ cm}^{-1}$  and  $1500 \text{ cm}^{-1}$  is attributed to O–H bonding due to the interaction of  $\text{TiO}_2$  and water. For the GQDs (spectrum *b* of Figure 3.2C) exhibited free O–H binding, C–O stretch vibration, C–H vibration, C=O vibration, and C=C aromatic ring stretch respectively at  $3416 \text{ cm}^{-1}$ ,  $1079 \text{ cm}^{-1}$ ,  $1353 \text{ cm}^{-1}$ ,  $1724$  and  $1579 \text{ cm}^{-1}$ . It was noticed that the characteristic peaks from both  $\text{TiO}_2$  NPs and GQDs were found in the GQDs- $\text{TiO}_2$  NPs (spectrum *c* of Figure 3.2C), indicating that some association of GQDs- $\text{TiO}_2$  NPs was successfully obtained. Such association is probably composed by larger nanoparticles of  $\text{TiO}_2$  NPs (in the 30 to 50 nm range) decorated with small GQDs (the ones in the scale range below 10 nm), which explains why no significant differences in the size distribution of nanoparticles was found when comparing  $\text{TiO}_2$  and the nanomaterial produced by mixing GQDs and  $\text{TiO}_2$  NPs.

The XRD patterns of pure- $\text{TiO}_2$  and GQDs- $\text{TiO}_2$  NPs samples are depicted in Figure 3.3. A full profile refinement was performed to the diffraction patterns of the samples to determine the cell parameters, cell volume, and mean crystallite size. The well-refined pattern for GQDs- $\text{TiO}_2$  NPs is shown in Figure 3.4. The Rietveld analysis revealed that both samples are composed of 88 % (in weight) of anatase (JCPDS # 21-1272) and 12 % (in weight) of rutile (JCPDS # 21 -1276). No peak related to the carbonaceous component was detected. This may be due to the low concentration of the GQDs that could be below the XRD limit detection or due to their incorporation into the  $\text{TiO}_2$  lattice. In Table 3.1 it is displayed values of the refinement parameters obtained from the XRD analysis. It can be noticed that the GQDs deposition causes a reduction in the lattice parameters *a* and *c* of both anatase and rutile phases. This lattice contraction is related to the defects induced by the GQDs or the substitution due to its reduced size compared to titanium. Similar results were reported by Kim *et al.* [138].

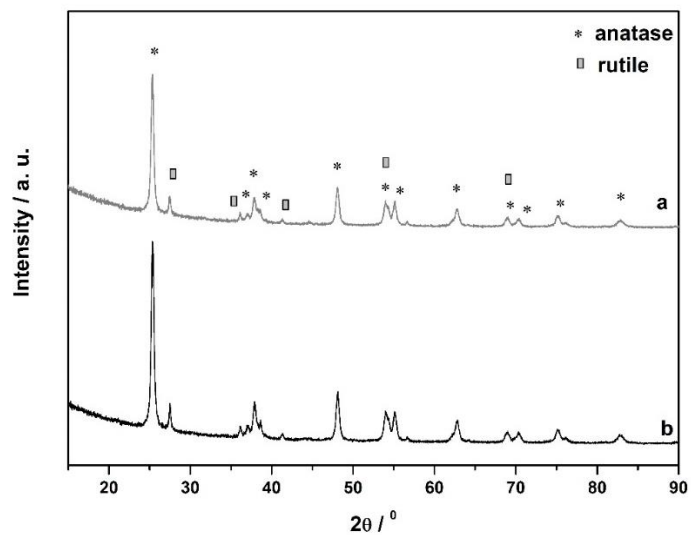


Figure 3.3 XRD patterns of the GQDs/TiO<sub>2</sub> (a) and (b) pure P25-TiO<sub>2</sub> NPs samples.

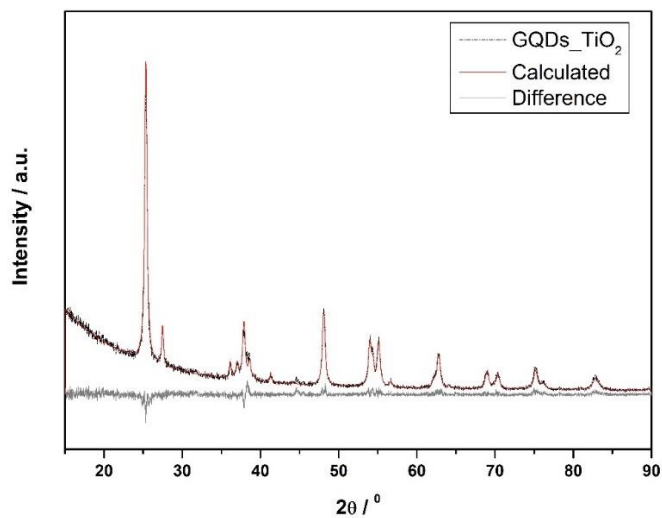


Figure 3.4 XRD pattern with Rietveld refined data for GQDs/TiO<sub>2</sub> NPs. The dotted line represents the experimental points, red line the Rietveld refined data, and the grey line is the difference between experimental data and refined data.

Table 3.1 Values of the refinement parameters obtained from XRD analysis by employing the Rietveld method.

Refinement Parameters	P <sub>25</sub> -TiO <sub>2</sub>	GQDs-TiO <sub>2</sub>
Anatase	a = 3.7860 Å*	a = 3.7852 Å*
	c = 9.5065 Å*	c = 9.5033 Å*
	Cell Volume = 136.27 Å <sup>3</sup>	Cell Volume = 136.16 Å <sup>3</sup>
	***LVolIB = 17 nm	***LVolIB = 17 nm
Rutile	a = 4.5947 Å	a = 4.5939 Å
	c = 2.9584 Å	c = 2.9576 Å
	Cell Volume = 62.45 Å <sup>3</sup>	Cell Volume = 62.42 Å <sup>3</sup>
	***LVolIB = 27 nm	***LVolIB = 25 nm
GOF**	1.17	1.23
R <sub>wp</sub> **	7.68	8.63
R <sub>p</sub> **	5.61	6.31

### 3.5

#### General procedures

##### 3.5.1

#### Cleaning and purification

Determination of mercury species at the ultra-trace level is a major challenge as contamination in the environment and from impurities in reagents can be usually found, making the results difficult to obtain. Because of this, cleaning materials in combination with the use of high purity reagents is essential when eliminating Hg contamination. In a clean room, all glass and Teflon apparatuses, previously soaked in HNO<sub>3</sub> (5% v/v), were washed with a detergent solution and then with distilled water before rinsing three times with ultrapure water and then placed in a oven at 45 °C for 1 h. The material used in the distillation was further washed using acetone, dichloromethane, and then hexane before drying in the oven. Occasionally, it was also necessary to place material in detergent solution inside an ultrasonic bath to clean glass materials containing oil residues and other organic residues.

### 3.5.2

#### Preparation of solutions

The  $\text{SnCl}_2$  solution (20 % w/v) was prepared by dissolving 20 g of the salt in 100 mL of concentrated HCl. The solution was heated to reduce the volume to about 50 mL in order to eliminate mercury contamination. After cooling, the final volume (100 mL) was adjusted with water. Before use, the solution was placed in a glass washing bottle to be purged with nitrogen (15 min).

An alkaline solution of the derivatization agent,  $\text{NaB}(\text{CH}_2\text{CH}_2\text{CH}_3)_4$  at 1 % m/v, was made by dissolving 0.05 g of the reagent in 2.5 mL of KOH (2 % v/v) solution, adjusting final volume to 5.0 mL with water, then stored at 5°C.

### 3.5.3

#### Verification of trace amounts of mercury

A prior verification of original traces of  $\text{Hg}^0$  in samples was made by selecting 10 mL of homogenized samples and placing them into the RP-92 chemical reduction accessory of the CV-AAS system (no reducing reagent was added) for determination. The purity of the reagents was verified by determining residual mercury using the CV-AAS system. For such evaluations, 1 mL aliquots of a reagent solution were 10-fold diluted and mixed with 3 mL of  $\text{SnCl}_2$  (20 % m/v) in the RP-92 chemical reduction accessory. The measured residual mercury of each reagent was considered in the final calculation of the mercury in PW samples.

### 3.5.4

#### Determination of sample conductance and turbidity in PW samples

Conductance and turbidity of samples were measured in order to respectively estimate concentrations of dispersed oil and salt. For conductance measurements,

PW samples were centrifuged (2,800 RCF for 30 min) to remove the excess of oil. Then, the supernatant was passed through a 0.2  $\mu\text{m}$  PTFE syringe filter before performing conductance measurements. Conductance values were compared to values obtained from NaCl standards. Oil concentrations in PW samples were measured by turbidimetry (light extinction at 650 nm using 10 nm spectral bandpass). Oil concentrations in the samples were estimated using a calibration curve made with either crude oil or mineral oil dispersed in water (0.5 to 300  $\text{mg L}^{-1}$ ).

### 3.6

#### **Specific procedures used in “Thiomersal photo-degradation with visible light-mediated by graphene quantum dots: indirect quantification using optical multipath mercury cold-vapor absorption spectrophotometry”**

##### 3.6.1

##### **Preparation of solutions**

Thiomersal (sodium salt) standard stock solution (20  $\text{mg L}^{-1}$ ) were prepared by dissolving appropriate amounts of standard in ultrapure water. Its aqueous intermediary solution (1000  $\text{ng L}^{-1}$ ) was prepared by diluting the stock solution in ultrapure water. Working solutions (100, 200, 300, 400  $\text{ng L}^{-1}$ ) of thiomersal were prepared by the dilution of the intermediary solution. The  $\text{CH}_3\text{Hg}$  and  $\text{CH}_3\text{CH}_2\text{Hg}$  intermediary solutions (at 1000  $\text{ng L}^{-1}$ ) were prepared by the direct dilution of a 1  $\text{mg L}^{-1}$  standard using ultrapure water. Working solutions (10 and 100  $\text{ng L}^{-1}$ ) were prepared by the direct dilution of the intermediary solution.

### 3.6.2

#### **Analytical procedure for the determination of Hg by multipass-CV-AAS.**

Sample solutions (200  $\mu\text{L}$ ) were transferred to glass test tubes containing 10.00 mL of a  $\text{H}_2\text{O}_2$  (1 %) solution with the pH adjusted to 4.5 (by the addition of 50 to 80  $\mu\text{L}$  of a 0.1 mol  $\text{L}^{-1}$  HCl solution) also containing 17  $\mu\text{L}$  of the synthesis dispersion of GQDs. Glass test tubes (made of quartz for some specific tests) were placed in a circular rack inside the photo-reactor, and they were kept rotating in order to be uniformly exposed to the visible radiation from all of the six lamps inside the reactor. Then, the test tube content was transferred to a glass reaction cell containing 2 mL of an  $\text{SnCl}_2$  aqueous solution (20 % v/v) in order to provide a rapid reduction to Hg, that was transferred, by an airflow passing through the solution, to the multipass-CV-AAS system operating in a continuous acquisition mode. The subsequent analysis was performed after removing the previous solution (though the bottom of the cell), washing with ultrapure water and  $\text{SnCl}_2$  solution until Hg signal reached baseline (this procedure took about 2 min to be performed).

### 3.6.3

#### **Analytical procedure for the determination of $\text{CH}_3\text{CH}_2\text{Hg}$ by GC-CV-AFS.**

The GC-CV-AFS analysis was made using an aliquot (50  $\mu\text{L}$ ) of a thiomersal solution, previously exposed to the visible range radiation in the presence of GQDs. This solution aliquot was transferred to a sample flask (amber with 40 mL volume and septum cap) containing 20 mL of ultrapure water, then mixed with 200  $\mu\text{L}$  of the acetate buffer solution and 100  $\mu\text{L}$  of the derivatization reagent solution (1 % v/v). After 15 min,  $\text{CH}_3\text{CH}_2\text{Hg}$  and  $\text{Hg}^{2+}$  were respectively converted in the volatile ethyl propyl mercury ( $\text{CH}_3\text{CH}_2\text{HgCH}_3\text{CH}_2\text{CH}_2$ ) and di-propylmercury ( $(\text{CH}_3\text{CH}_2\text{CH}_2)_2\text{Hg}$ ). The flask was placed in the automatic sampler of the GC-CV-AAS system to be transferred to a purge vessel, forcing the liberation of volatile Hg

species, that were carried, by a argon flow ( $312 \text{ mL min}^{-1}$ ) to a dried trap where they were adsorbed and then thermally desorbed to be carried, by an argon flow ( $34 \text{ mL min}^{-1}$ ), through the chromatographic column. After separation, the Hg species zones passed through a tube section heated by resistance to thermally decompose them to the Hg vapor detected by AFS. The signal was acquired as peak height and retention times for  $\text{CH}_3\text{CH}_2\text{Hg}$  and  $\text{Hg}^{2+}$  were respectively about 5 min and 8 min.

### 3.6.4

#### Liquid chromatographic analysis

High-performance liquid-chromatography was made under isocratic elution at a constant flow rate of  $1.0 \text{ mL min}^{-1}$  using a pH 2.5 mobile phase that consisted of a methanol/phosphoric acid solution ( $0.02 \text{ mol L}^{-1}$ ) in a 60/40 % v/v proportion. The separation was made on a  $4.6 \times 250 \text{ mm}$  Eclipse Plus  $\text{C}_{18}$  (Agilent, USA) with  $5 \mu\text{m}$  particle size keeping the oven temperature at  $25^\circ\text{C}$ .

### 3.6.5

#### Analysis of samples containing thiomersal

For the determination of thiomersal in a pharmaceutical formulation (Merthiolate topical solution), the sample was diluted 1000 times before placing  $200 \mu\text{L}$  into a test tube containing  $10 \text{ mL}$  of an  $\text{H}_2\text{O}_2$  solution (1 %) with the pH adjusted to 4.5 and containing  $17 \mu\text{L}$  of the synthesis dispersion of GQDs. This mixture was placed inside the reactor and irradiated for 20 min. Then the total volume was transferred to the chemical reduction cell (containing  $2 \text{ mL}$  of the  $\text{SnCl}_2$  20% v/v solution) connected to the multipass-CV-AAS system.

The aqueous effluents (acquired from a local pharmaceutical industry) was fortified with thiomersal followed by two-fold dilution. Then the mixture was vortex-mixed for 5 min and passed through a  $0.45 \mu\text{m}$  filter. The solution ( $10 \text{ mL}$ ) containing  $\text{H}_2\text{O}_2$  solution (1 %), the pH adjusted to 5.0 and containing  $17 \mu\text{L}$  of the synthesis dispersion of GQDs, were then placed into the photochemical reactor for 20 min.

Fresh urine samples, donated by a volunteer, aliquots (2 mL) were fortified with thiomersal, then mixed with 1.3 mL of an acetonitrile/methanol 50/50 % v/v solution. The mixture was vortex-mixed for 5 min and then centrifuged for 15 min at 500 RFC, in order to separate the protein content and other solids [139]. After this clean-up procedure, the supernatant was filtered through a 0.45  $\mu\text{m}$  syringe filter and brought to a final volume of 10 mL with ultrapure water. The solution was transferred to test tube and placed into the photochemical reactor for 20 min. Then the solution was transferred to the reduction cell connected to the multipass-CV-AAS system.

### 3.7

#### **Specific procedures in “Speciation and ultra-trace determination of mercury in produced waters from offshore drilling operations using portable instrumentation and matrix-matching calibration”**

##### 3.7.1.

##### **Solutions and standards**

$\text{CH}_3\text{Hg}$  and  $\text{Hg}^{2+}$  (1000  $\text{ng L}^{-1}$ ) standard solutions were prepared by diluting appropriate volumes of standard stock solutions in 10.00 mL volumetric flasks (stored in the refrigerator protected from light). The  $\text{SnCl}_2$  solution (20 % m/v) was prepared by dissolving 20 g of the salt in 100 mL of concentrated HCl. The solution was heated to reduce volume to about 50 mL aiming to eliminate mercury contamination. After cooling-down, final volume (100 mL) was adjusted with water. Before use, the solution was placed in a glass washer bottle to be purged with nitrogen (15 min). Utensils were soaked in 10 %  $\text{HNO}_3$  (v/v) for 24 h, cleaned with detergent and rinsed with water.

In order to prepare the 1000  $\text{mg L}^{-1}$  oil dispersions, crude oil sample (or mineral oil) was weighed in 25 mL volumetric flasks. Then, water was added until half of the total volume. This mixture was vigorously stirred (15 min) and placed

in an ultrasonic bath for 20 min. The final volume was adjusted with water. In order to evaluate matrix effects (imposed by dispersed oil and NaCl), standard solutions of 30 and 70 ng L<sup>-1</sup> of either Hg<sup>2+</sup> or CH<sub>3</sub>Hg were prepared in solutions containing different oil and NaCl contents.

### 3.7.2

#### Determination of mercury in PW samples by multipass-CV-AAS

For the determination of the mercury species in PW by multipass-CV-AAS, samples were collected in polyethylene tubes (15 mL) and centrifuged (2800 RFC for 20 min) to remove the excess of oil, forming a pellet at the bottom of the tube. Then samples (supernatant phase) were diluted with water to reach robust range of oil and salt contents to perform analysis. Sample dilution factor could be adjusted to proper concentration range for the analytical curve. The range of salt and oil content, that enabled robust conditions for mercury quantification (matrix-matched calibration), were respectively from 2 to 6 g L<sup>-1</sup> and from 2 to 6 mg L<sup>-1</sup>.

A prior verification was made in all PW samples by placing 10 mL of diluted samples in the CV-AAS system bubbler (no reducing reagent) to determine possible original traces of Hg<sup>0</sup>. In order to evaluate possible losses of mercury in the centrifugation process, the oil pellet, at the bottom of the tube, was subjected to a mineralization process. The whole PW samples were also submitted to the mineralization process to obtain total mercury content. This mineralization was based on the procedure described in the literature [140] briefly summarized as follows: In a 100 mL glass flask, 10 g of PW samples (alternatively the whole oil pellet) was mixed with 10 mL of a concentrated mineral acid solution (HNO<sub>3</sub>:H<sub>2</sub>SO<sub>4</sub>, 2.25:1, in volume). This mixture was heated for 1 h at 90° C, and then, the mixture was allowed to cool to room temperature. An aliquot of 1 mL of the digested sample was diluted to 10 mL and analyzed using the multipass-CV-AAS system after reduction with SnCl<sub>2</sub> (20 % w/v).

For the determination of the inorganic mercury, 10 mL of diluted PW sample supernatant were added to the glass reaction cell (instrument reduction accessory where a continuous airflow was passed through the solution) containing 3 mL of SnCl<sub>2</sub> (20% m/v) to enable fast Hg<sup>2+</sup> reduction and transferring of the formed Hg<sup>0</sup> to the multipass cell of the CV-AAS spectrometer (operating in a continuous

acquisition mode). For the determination of total mercury (for the indirect determination of  $\text{CH}_3\text{Hg}$ ), 1 mL of PW sample was transferred to 10 mL volumetric flasks followed by the addition of  $\text{H}_2\text{SO}_4$  ( $0.1 \text{ mol L}^{-1}$ ) and  $\text{H}_2\text{O}_2$  (30 %) before adjusting final volume with water so as to obtain pH 3 and  $\text{H}_2\text{O}_2$  of about 1%. The solution was placed into 15 mL volume quartz tube, stoppered and then exposed to UV (5 min). Then, solution was transferred to the glass reaction cell to perform reduction (using  $\text{SnCl}_2$ ) of both the original and the photo-produced  $\text{Hg}^{2+}$ , producing the detectable  $\text{Hg}^0$  vapor. Eventual fortifications of PW samples were made by adding appropriate volumes of standard solution ( $1 \text{ mg L}^{-1}$ ) of  $\text{Hg}^{2+}$  and  $\text{CH}_3\text{Hg}$ .

### 3.7.3

#### Determination of mercury by GC-CV-AFS

For the comparative study, experiments using GC-CV-AFS were performed following the procedure reported in the literature [141] using an extraction procedure (extraction of  $\text{CH}_3\text{Hg}$ ) based on a reported procedure [60] but using dichloromethane (instead of benzene) as an extraction solvent. The extraction was made by mixing 25 mL of the PW sample with 2 mL of concentrated HCl and with 2.5 mL of dichloromethane. The samples were then stirred vigorously for 10 min before collecting the organic phase (after separation of phases). The remaining aqueous phase was submitted to the extraction two more times (three extractions in total). These collected organic phases were mixed in a vial where 5 mL of aqueous solution containing L-cysteine (1 % w/v) and sodium acetate (0.8 %) was added to be then stirred for 10 min. After phase separation, the organic phase was collected, and the remaining aqueous phase was mixed with 0.8 mL of HCl and 1 mL of dichloromethane. After stirring (10 min), the organic phase was collected and mixed with the previously collected one. Next, 5 mL of ultrapure water was added and vortex mixed with the organic phase. After phase separation, the organic phase, at the top of the vial, was gently evaporated under a flow of argon in order to get the mercury species in the aqueous phase. Then, 1 mL of the extracted material was diluted to 10 mL with ultrapure water and transferred to amber glass flasks where 0.2 mL of acetate buffer solution and 0.1 mL of  $\text{NaB}(\text{CH}_3\text{CH}_2)_4$  derivatization agent were added. The final volume (45 mL) was adjusted with ultrapure water. The

samples were then placed into GC-CV-AFS system for speciation analysis of  $\text{Hg}^{2+}$  (as  $\text{Hg}(\text{CH}_3\text{CH}_2)_2$ ) and  $\text{CH}_3\text{Hg}$  (as  $\text{CH}_3\text{HgCH}_3\text{CH}_2$ ) detecting them as  $\text{Hg}^0$  after thermal decomposition [141].

### 3.8

#### **Specific procedures in “Mercury speciation in offshore petroleum produced waters by gas chromatography cold vapor atomic fluorescence spectrometry”**

##### 3.8.1

##### **Solutions, standards, and nanoparticle dispersions.**

Standard solutions of  $\text{CH}_3\text{Hg}$ ,  $\text{CH}_3\text{CH}_2\text{Hg}$ , and  $\text{Hg}^{2+}$  ( $1000 \text{ ng L}^{-1}$ ) were prepared by diluting appropriate volumes of standard stock solutions into 10.00 mL amber volumetric flasks (stored in the refrigerator protected from light). In order to prepare the  $1000 \text{ mg L}^{-1}$  oil dispersions, a crude oil sample (or mineral oil) was weighed into 25 mL volumetric flasks. Water was added (10 mL) followed by vigorous stirring (15 min) and placed in an ultrasonic bath for 20 min (before the experiments). The final volume was adjusted with water. NaCl stock solution (about  $300 \text{ g L}^{-1}$ ) was prepared by dissolving NaCl in water (about  $60^\circ\text{C}$ ) leaving the solution to slowly cooling down to room-temperature before adjusting final volume. The stock solutions of Triton X-114 and Triton X-100 (both at 5 % m/v) were prepared from the dissolution of surfactants in water with less concentrated solutions prepared from the dilution of stock solutions.

### 3.8.2

#### Extractions of mercurial species using Triton X-114.

For the extraction of analytes from the PW samples, turbidity and conductivity determinations were previously made to estimate oil and salt contents present in original samples. When necessary, samples were diluted to adjust salt and oil contents to the extraction conditions. These diluted PW samples (about 50.0 g) were placed into glass vials along with aliquots of a stock solution of Triton X-114 (5 % m/v) and of a stock solution of  $\text{H}_2\text{SO}_4$  ( $2 \text{ mol L}^{-1}$ ), adjusting the solution to about pH 3. These vials were placed in a water bath at  $40^\circ\text{C}$  inside an ultrasonic bath (40 min) to extract mercury species from oil.

### 3.8.3

#### Distillation of PW samples.

The distillation of simulated PW samples (containing  $40 \text{ mg L}^{-1}$  mineral oil and  $30 \text{ g L}^{-1}$  NaCl) and real PW samples were carried out on a distillation system for methylmercury, using a procedure based on the EPA-1630 method. The distillation was made at  $130^\circ\text{C}$  with argon flow adjusted to the range between 45 and  $80 \text{ mL min}^{-1}$ . The efficiency in distillations in PW samples was controlled by using reference solutions (standard solutions containing  $\text{CH}_3\text{HgCl}$ ,  $\text{CH}_3\text{CH}_2\text{HgCl}$ ,  $\text{HgCl}_2$ ). Teflon vials contained 50 mL of control solutions or extracted PW samples (real or simulated) or extracted matrix-matched standards and 0.5 mL  $\text{H}_2\text{SO}_4$  solution ( $8 \text{ mol L}^{-1}$ ). Distillation was performed until the collection of about 40 mL of final distillate (total distillation time was about 150 min). Then, the vials containing the collected solutions were capped and stored at  $4^\circ\text{C}$  in the dark. A  $50 \mu\text{L}$  solution of simethicone ( $75 \text{ g L}^{-1}$ ) was added as antifoaming agent.

### 3.8.4

#### Speciation and mercury determination using GC-CV-AFS.

Mercury speciation analysis in PW samples was made on a GC-CV-AFS system. Before the determinations, aiming to compensate interferences during

propylation, the distilled samples were subjected to conductance analysis in order to estimate the residual salt that was carried to the distillate. In the case of the simulated PW samples, 30 mL volumes of the distillate were used. For the real PW samples, volumes varying from 1.00 to 25.00 mL were used depending on the concentration of the mercury species. Samples (real or simulated) were transferred to 40 mL amber flasks to be mixed with 0.2 mL acetate buffer and 0.1 mL of the propylation agent. When required, the final volume (slightly under 40 mL) was adjusted with water. The samples were then placed into the sampler rack of the GC-CV-AFS system and the solutions purged with argon to transfer the derivatized volatile mercury species to be separated in a GC column with temperature adjusted to 36°C using argon as mobile phase (30 mL min<sup>-1</sup> gas flow). After passing through the separation column, the separated zones of the mercury species were thermally decomposed, in an on line furnace, to produce the measurable Hg<sup>0</sup>. The instrumental and experimental conditions for mercury speciation using GC-CV-AFS are shown in Table 2. The analytical curves of the method were constructed (in the presence of 40 mg L<sup>-1</sup> mineral oil and 30 g L<sup>-1</sup> NaCl) in the concentration range from 25 to 800 pg L<sup>-1</sup> of Hg<sup>2+</sup>, CH<sub>3</sub>Hg, and CH<sub>3</sub>CH<sub>2</sub>Hg.

### 3.9

#### **Specific procedures in “Photo-generation of cold mercury vapor mediated by GQDs-TiO<sub>2</sub> nanocomposite: on-line ultra-trace speciation of mercury and kinetic studies”**

##### 3.9.1

#### **Preparation of solutions and dispersions**

Standard solutions of CH<sub>3</sub>Hg, CH<sub>3</sub>CH<sub>2</sub>Hg, and Hg<sup>2+</sup> (at 1000 ng L<sup>-1</sup>) were prepared by diluting appropriate volumes of standard solutions in 10.00 mL amber volumetric flasks (stored in the refrigerator protected from light). When necessary, sequential dilution was made to achieve lower concentrations.

Aqueous dispersions of the GQDs-TiO<sub>2</sub> nanocomposite were prepared by dispersing 30 mg of the solid in 10 mL of water after a brief, vigorous vortex mixing followed by 10 min sonication. Prior to use, the solution was placed in a glass

washing bottle to be purged with nitrogen (15 min). All glass material was immersed in 10% (v/v) HNO<sub>3</sub> for 24 h, cleaned with detergent and rinsed with ultrapure water prior to use.

### 3.9.2.

#### **Mercury UV photochemical speciation analysis by CV-AAS UV using GQDs-TiO<sub>2</sub> nanocomposites**

Volumes of 100 µL of sample standard solutions (or sample solution) were transferred to the quartz tubes (attached to the CV-AAS system) containing 5.00 mL of a solution containing H<sub>2</sub>O<sub>2</sub> (1 % in volume), formic acid (1 % m/v) with pH adjusted to 3.0 (by adding small volumes of an HCl solution 0.1 mol L<sup>-1</sup>). To this solution, 100 µL of the GQDs/TiO<sub>2</sub> NPs dispersion (3 mg mL<sup>-1</sup>) was added. To the quartz tube, a small magnetic bar was inserted before placing it inside the photo-reactor, positioning it in the center of the device and on the top of the magnetic stirrer. After 5 min (Hg<sup>2+</sup>), 9 min (CH<sub>3</sub>Hg) and 13 min (CH<sub>3</sub>CH<sub>2</sub>Hg) of UV exposure the generated Hg<sup>0</sup>, from the photocatalytic degradations, was transferred, through a controlled airflow (3 mL min<sup>-1</sup>), to the CV-AAS system operating in continuous acquisition mode and conditions adjusted according to Table 1). Before the subsequent analysis, the system was flushed with air passing through a tube containing ultrapure water residual Hg signal reached the baseline level.

### 3.9.3

#### **Mercury speciation analysis by GC-CV-AFS**

Speciation studies were also made using the GC-CV-AFS system. Aliquots (0.10 mL) of standard solutions of the mercurial species were mixed with GQDs-TiO<sub>2</sub> NPs and exposed to UV in closed quartz tubes. Then they were transferred to 40 mL amber vials with septum caps containing 20 mL of ultrapure water, 0,2 mL of the acetate buffer solution and 0,10 mL of a NaB(CH<sub>2</sub>CH<sub>2</sub>CH<sub>3</sub>)<sub>4</sub> aqueous solution (1 % v/v). After 15 min, CH<sub>3</sub>Hg, CH<sub>3</sub>H<sub>2</sub>Hg and Hg<sup>2+</sup> were respectively converted into the volatile methyl(n-propyl)mercury, CH<sub>3</sub>HgCH<sub>2</sub>CH<sub>2</sub>CH<sub>3</sub>, ethyl(n-propyl)mercury, CH<sub>3</sub>H<sub>2</sub>HgCH<sub>2</sub>CH<sub>2</sub>CH<sub>3</sub>, and

di-n-propyl mercury,  $\text{Hg}(\text{CH}_2\text{CH}_2\text{CH}_3)_2$ . These flasks were placed into the automatic sampler of the GC-CV-AFS system from where solutions were transferred to a glass cell to be bubbled with an argon flow ( $312 \text{ mL min}^{-1}$ ) that carried the volatile to the chromatographic module. The GC column temperature was adjusted to  $36^\circ\text{C}$  with Ar mobile phase flow adjusted to  $30 \text{ mL min}^{-1}$ . As separation occurs in the chromatographic module, the separated zones of the propylated mercury species were thermally decomposed in  $\text{Hg}^0$  before reaching the dedicated fluorescence detection system.

#### 4.

### **Results and discussion I. Speciation and ultra-trace determination of mercury in produced waters from offshore drilling operations using portable instrumentation and matrix-matching calibration**

Paper published as: “*Speciation and ultra-trace determination of mercury in produced waters from offshore drilling operations using portable instrumentation and matrix matching calibration.*” (See Attachment A1).

It is important to remark that all information taken from Chapter 4 of this thesis, must be cited as J.R. Miranda-Andrades, S. Khan, C.A.T. Toloza, R.M. Maciel, R. Escalfoni, M.L.B. Tristão, R.Q. Aucelio, *Speciation and ultra-trace determination of mercury in produced waters from offshore drilling operations using portable instrumentation and matrix-matching calibration*, *Microchem. J.* 146 (2019). doi:10.1016/j.microc.2019.02.045.

#### 4.1

##### **Abstract**

Mercury speciation analysis in produced water (PW) was achieved by optical multipath cold vapor atomic absorption spectrometry. One sample aliquot was treated with  $\text{SnCl}_2$ , producing  $\text{Hg}^0$  that was carried out to the optical detection cell to be determined. Another aliquot was exposed to UV, promoting oxidation of  $\text{CH}_3\text{Hg}$  to  $\text{Hg}^{2+}$ , and then determined after chemical reduction with  $\text{SnCl}_2$ . The  $\text{CH}_3\text{Hg}$  content was the difference in the results achieved for both aliquots. Matrix effects imposed by oil and salt were studied, and although intensity of the mercury time profile was affected, quantification was successfully achieved by using matrix-matched standards containing adjusted NaCl and total oil content. Both conductivity (to estimate salt content) and turbidimetry (to estimate oil content) measurements were made for the PW samples in order to adjust sample to the

matrix-matched standards. Analyte addition was also used, and limit of quantification was  $12 \text{ ng L}^{-1}$  with satisfactory recoveries for both  $\text{Hg}^{2+}$  and  $\text{CH}_3\text{Hg}$ . A pictorial description of the work is presented in Figure 4.1.

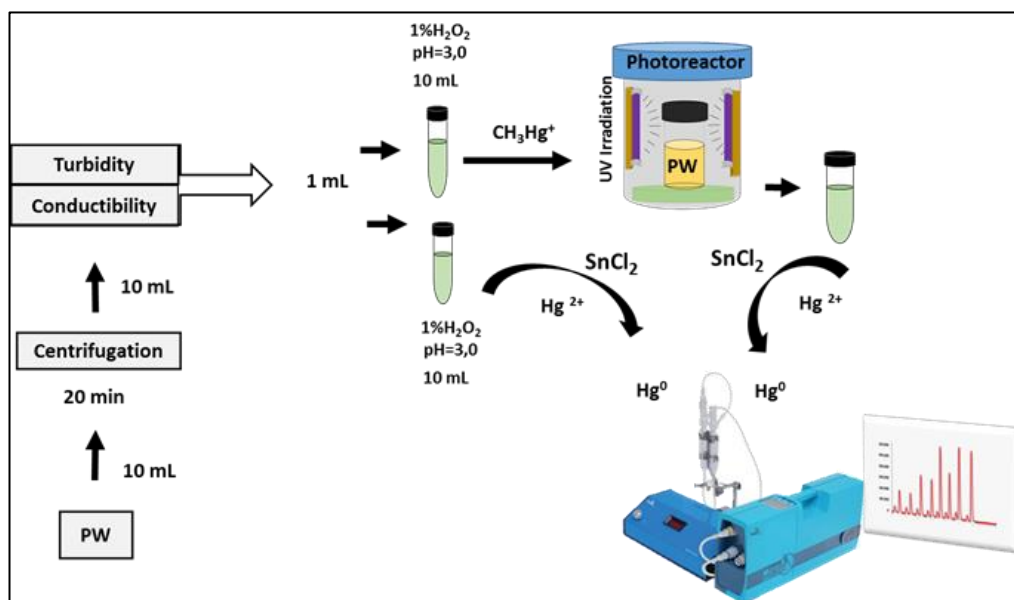


Figure 4.1 Graphical Abstract

## 4.2

### Results and discussion.

#### 4.2.1

##### Generation of Hg vapor from $\text{Hg}^{2+}$

For the generation of cold mercury vapor, for determinations using the CV-AAS system,  $\text{Hg}^{2+}$  (either the original in-sample or the photo-generated one) must be efficiently reduced to  $\text{Hg}^0$  and transferred to the multi-pass detection cell.  $\text{SnCl}_2$  solution (reducing agent) was added to the sample cell of the reduction accessory coupled to the CV-AAS system. In order to achieve the most full and

well-shaped mercury time profile, different  $\text{SnCl}_2$  concentrations were tested (a fixed 2 mL  $\text{SnCl}_2$  solution volume was chosen) to reduce the  $\text{Hg}^{2+}$  of a standard solution ( $50 \mu\text{g L}^{-1}$ ). Signal intensities were measured as the height of time profile. The maximum signal intensities (more efficient reduction) were achieved with  $\text{SnCl}_2$  concentrations higher than 20 % (m/v) enabling sharp profile and fast  $\text{Hg}$  vapor evolution (Figure 4.2A). The volume of the  $\text{SnCl}_2$  (20 % v/v) solution (0.5 to 4.0 mL), added to the sample cell, was adjusted. For all of the tested volumes, the profile shapes were similar in terms of evolution time of the  $\text{Hg}$  vapor, but the profile area was higher using volumes from 2.0 to 4.0 mL (Figure 4.2B). Therefore, a 3.0 mL volume of the  $\text{SnCl}_2$  (20 % v/v) was selected.

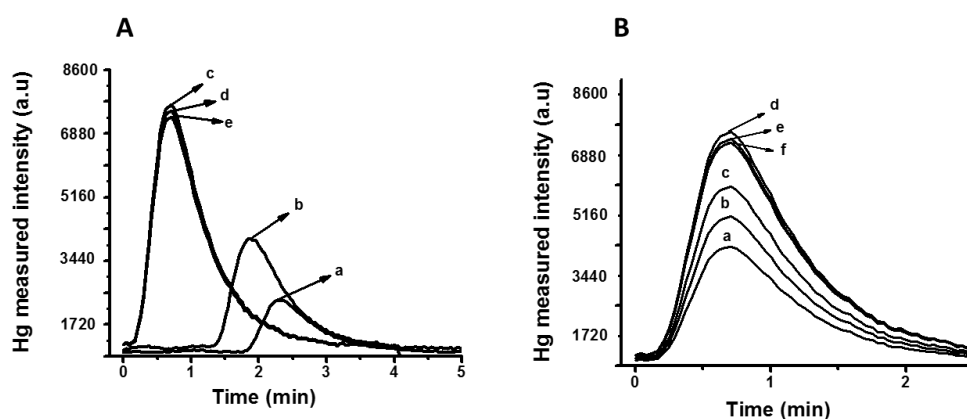


Figure 4.2 Time profiles after chemical reduction of a  $\text{Hg}^{2+}$  standard solution ( $50 \mu\text{g L}^{-1}$ ): A) using 2 mL of  $\text{SnCl}_2$  at a) 5 %; b) 10 %; c) 20 %; d) 30 %; e) 40 % (w/w); B) using different volumes of  $\text{SnCl}_2$  (20 % w/w) solution: a) 0.5 mL; b) 1.0 mL; c) 1.5 mL; d) 2.0 mL; e) 3.0 mL; f) 4.0 mL.

#### 4.2.2

##### Effect of oil and salt content in the generation of $\text{Hg}$ vapor from $\text{Hg}^{2+}$

Since the method aimed at the determination of  $\text{Hg}^{2+}$  and  $\text{CH}_3\text{Hg}$  in PW, the effects of oil and salt content on the generation of  $\text{Hg}$  vapor was studied. Sodium chloride is the main inorganic component in PW, being present at higher concentrations than in seawater (typically from 30 to  $400 \text{g L}^{-1}$ ) [48,142]. Because of the high formation constants, at high concentrations of chloride, it is possible that  $\text{Hg}^{2+}$  tend to form stable  $\text{HgCl}_n^{(2-n)}$  complex ions that may hinder the reduction of  $\text{Hg}^{2+}$  to  $\text{Hg}^0$  [143-145]. However, it is also true that the condition adjusted for

reduction of  $\text{Hg}^{2+}$  is rich in HCl. Besides, PW present oil dispersed as microdroplets that could solubilize part of the mercury species, affecting kinetics of reduction.

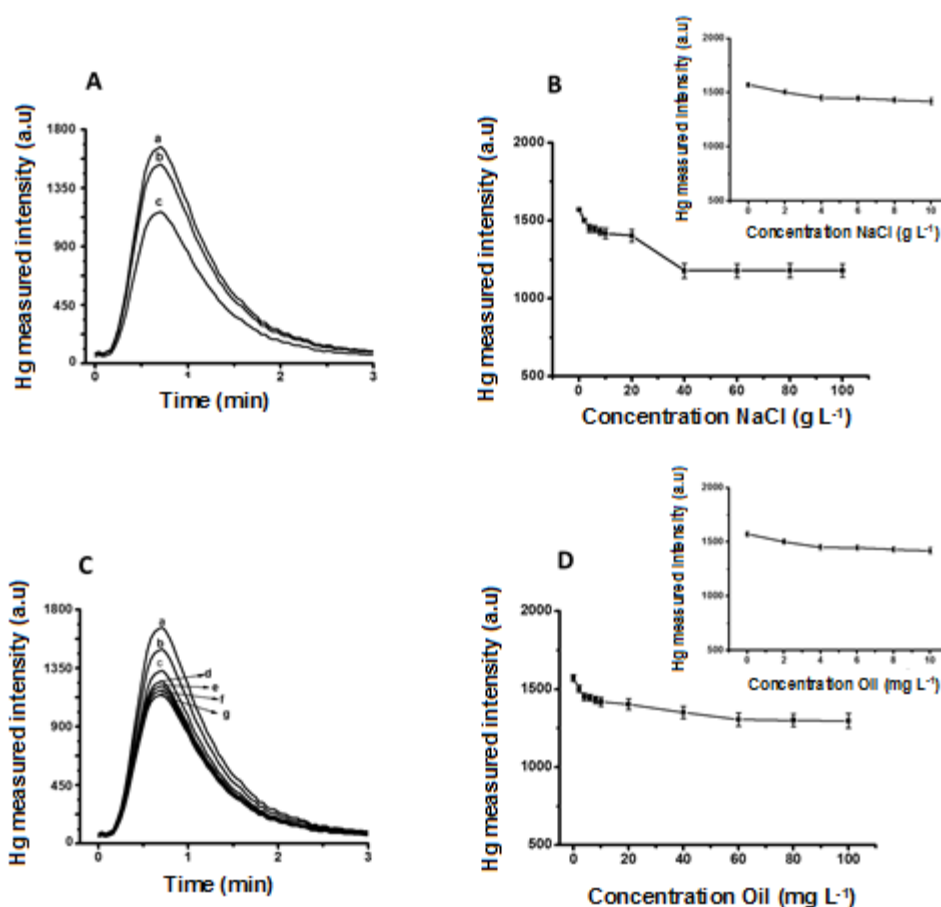


Figure 4.3 A) Effect of NaCl in the time profiles after chemical reduction of a  $\text{Hg}^{2+}$  standard solution ( $50 \mu\text{g L}^{-1}$ ) in the presence of NaCl at a) 0; b) 10; c)  $100 \text{ g L}^{-1}$ . B) Mercury signal intensities (from a  $50 \text{ ng L}^{-1}$   $\text{Hg}^{2+}$  standard solution) in function of the NaCl concentrations (0 -  $100 \text{ g L}^{-1}$ ). C) Effect of Oil in the time profiles after chemical reduction of a  $\text{Hg}^{2+}$  standard solution ( $50 \mu\text{g L}^{-1}$ ) in the presence of dispersed oil at: a) 0; b) 10; c) 20; d) 40; e) 60; f) 80; g)  $100 \text{ g L}^{-1}$  oil. D) Mercury signal intensities (from a  $50 \text{ ng L}^{-1}$   $\text{Hg}^{2+}$  standard solution) in function of the dispersed oil (0 -  $100 \text{ mg L}^{-1}$ ). See Table 4.1 for chemical reduction conditions.

The  $\text{Hg}^{2+}$  determinations were made using aqueous mixtures added into the reaction cell containing  $50 \text{ ng L}^{-1}$  of  $\text{Hg}^{2+}$ . A univariate study was made to evaluate the influence of NaCl content (from 0 to  $100 \text{ g L}^{-1}$ ) on the Hg vapor generation. The overall signal profile was not affected (Figure 4.3A) with no shift in peak maximum of time profiles as the concentration of NaCl increased, which indicated no drastic influence on the Hg vapor formation/release kinetics. However, intensity (peak height) decreased as the concentration of NaCl increased from  $2 \text{ g L}^{-1}$  (about 2 %)

to  $10 \text{ g L}^{-1}$  (about 5 % as seen in the insert of Figure 4.3), further decreasing (about 9.5% of the original signal) was observed at  $40 \text{ g L}^{-1}$ , then remaining constant up to  $100 \text{ g L}^{-1}$  of NaCl (Figure 4.3B).

The presence of oil, dispersed in the aqueous mixture containing  $50 \text{ ng L}^{-1}$  of  $\text{Hg}^{2+}$ , was evaluated. Oil affected the formation/release of Hg vapor (Figure 4.3C), but there was no significant change in the peak maximum of the time profile. In the presence of  $10 \text{ mg L}^{-1}$  of dispersed oil (crude oil), the Hg signal decreased 7 % (Figure 4.3D insert) and further decreasing of about 23 %, 27 % and 30 % of the original signal ( $\text{Hg}^{2+}$  standard without oil) occurred when oil contents were increased respectively to  $20 \text{ mg L}^{-1}$ ,  $40 \text{ mg L}^{-1}$ , and  $100 \text{ mg L}^{-1}$  (Figure 4.3D).

A further study was made to evaluate the simultaneous effect of these two major PW sample matrix components using a circumscribed Central Composite Design (CCD) with 10 mL aqueous mixtures, containing NaCl and oil contents (at specific concentrations) and a fixed 70 pg of  $\text{Hg}^{2+}$ , were directly introduced into the reaction cell of the reduction accessory of the CV-AAS system. The experimental design levels (codified values in parenthesis) for NaCl (in  $\text{g L}^{-1}$ ) were 20 ( $-\sqrt{2}$ ); 32 (-1); 60 (0); 88 (+1) and 100 ( $+\sqrt{2}$ ) while for dispersed oil content, the chosen levels, in  $\text{mg L}^{-1}$ , were 20 ( $-\sqrt{2}$ ); 32 (-1); 60 (0); 88 (+1) and 100 ( $+\sqrt{2}$ ). Authentic replicates ( $n = 8$ ) were only made at the central point (0,0).

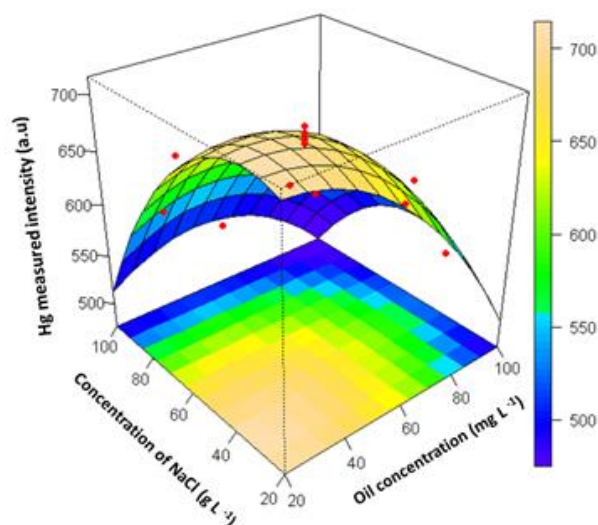


Figure 4.4 Circumscribed experimental planning for the chemical reduction of  $\text{Hg}^{2+}$ : A) Response surface for mercury vapor released in the presence of both NaCl and dispersed oil.

### 4.2.3

#### UV-mediated photo-oxidation of organic-mercury to $\text{Hg}^{2+}$

A fraction of the mercury in PW might be present as organic-Hg. Since  $\text{CH}_3\text{Hg}$  is stable in the presence of  $\text{SnCl}_2$ , the conversion of the organic-Hg into Hg vapor must be preceded by oxidation to produce  $\text{Hg}^{2+}$ , being UV-induced oxidation a practical and efficient way to achieve this [143]. In order to evaluate the photo-oxidation, the Hg measurements from aqueous solutions fortified with  $\text{CH}_3\text{Hg}$  were compared with results obtained from solutions fortified with  $\text{Hg}^{2+}$  at an equivalent concentration.

First, a study was carried out to evaluate the pH (from 1.5 to 5.0) that enabled the efficient formation of  $\text{Hg}^{2+}$  from organic-Hg. Aqueous samples were fortified at  $50 \text{ ng L}^{-1}$  of either  $\text{Hg}^{2+}$  or  $\text{CH}_3\text{Hg}$  in solutions with pH adjusted by the addition of appropriate volumes of  $0.10 \text{ mol L}^{-1}$  solutions of either  $\text{NH}_4\text{OH}$  or  $\text{H}_2\text{SO}_4$ . For  $\text{CH}_3\text{Hg}$ , standard solutions were exposed to UV (for 5 min) before transferring them to the reaction cell to reduce  $\text{Hg}^{2+}$  to Hg vapor (using  $\text{SnCl}_2$ ). For the  $\text{Hg}^{2+}$  standard solution, no exposure to UV was used, and solution was placed directly into the

reaction cell to produce Hg vapor. In Figure 4.5A, it can be seen that maximum response obtained from an  $\text{Hg}^{2+}$  standard solution was achieved at the pH from 2.5 and 3.0, decreasing at higher pH values due to hydrolysis of  $\text{Hg}^{2+}$ . Very acidic conditions (below pH 2.5) favored the  $\text{Hg}^{2+}$  reduction, promoting loss of Hg vapor during the transferring of the irradiated solution to the reaction cell where the reaction with  $\text{SnCl}_2$  occurs. In the case of the  $\text{Hg}^{2+}$  produced from  $\text{CH}_3\text{Hg}$ , a similar trend was observed in the pH range from 3.0 to 3.5, but the results were slightly less intense than the ones obtained from the  $\text{Hg}^{2+}$  standard due probably to a non-quantitative photo-oxidation of the organic mercury and/or loss of mercury, as Hg vapor, formed during irradiation. Therefore, pH 3.0 was chosen to perform the photo-oxidation of  $\text{CH}_3\text{Hg}$ .

The UV exposure time determines the extent of formation of free radicals responsible for the oxidation of organic-Hg. Aliquots of 10 mL of a  $\text{CH}_3\text{Hg}$  standard solution ( $70 \text{ ng L}^{-1}$ ) were placed in quartz tubes and exposed to UV from periods from 2 to 20 min. The most efficient production of  $\text{Hg}^{2+}$  from  $\text{CH}_3\text{Hg}$  was achieved with 15 min (Figure 4.5B curve a). At higher irradiation times, a signal decreasing was observed probably because of the photo-induced formation of Hg that promotes significant loss of analyte during the steps before the analytical Hg vapor generation in the CV-AAS system.

Aiming to decrease UV exposure time to achieve oxidation of organic-Hg,  $\text{H}_2\text{O}_2$  was tested (to in situ provide oxygenated free radicals) at a range between 1 % and 5%. Standard solutions of  $\text{CH}_3\text{Hg}$  containing  $\text{H}_2\text{O}_2$  were exposed to UV, for 3 min, before transferring them to the reaction cell of the CV-AAS system. It was observed (Figure 4.5C) that high efficiency in the oxidation of organic mercury was obtained already in the presence of 1 %  $\text{H}_2\text{O}_2$ , providing about 94% recovery (compared to signal measured from an  $\text{Hg}^{2+}$  aqueous standard). Based on these results, a study was carried out using  $\text{CH}_3\text{Hg}$  solution ( $70 \text{ ng L}^{-1}$  at pH 3.0) containing  $\text{H}_2\text{O}_2$  1 % and a significant decreasing of time (from 15 to 5 min) was achieved in obtaining the most efficient production of  $\text{Hg}^{2+}$  (Figure 4.5B curve b).

#### 4.2.4

### Effect of oil and salt content in the generation of Hg vapor from Hg<sup>2+</sup> in the photo-oxidation of organic-Hg

Oil dispersed in microdroplets may act as barrier to UV, decreasing organic-Hg oxidation efficiency. By exposing CH<sub>3</sub>Hg standard solutions (150 ng L<sup>-1</sup>), containing increasing amounts of dispersed mineral oil, indicating a decreasing in Hg<sup>2+</sup> formation efficiency, leading to about 10% less intense signal, compared to the signal measured from a reference Hg<sup>2+</sup> standard solution, when oil content was 10 and 20 mg L<sup>-1</sup>. Signal decreased about 15% (at 40 mg L<sup>-1</sup> of oil), 20 % (at 60 mg L<sup>-1</sup> of oil and 34 % (at 80 mg L<sup>-1</sup> of oil). This effect was caused by the decline in radiance due to radiation scattering and also by some partition of mercury species in oil phase.

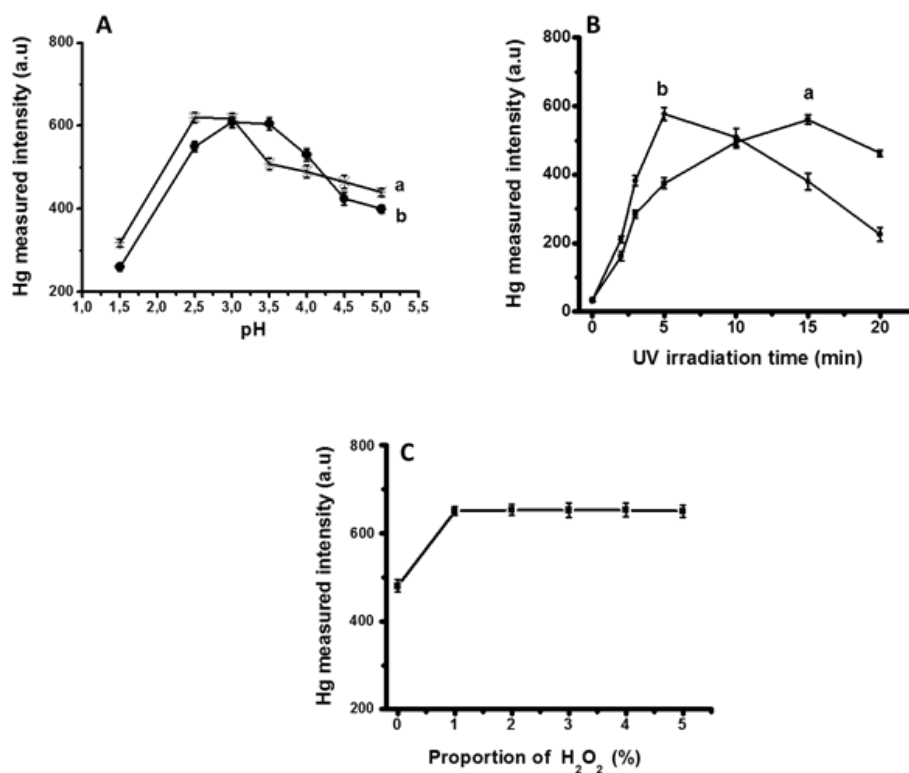


Figure 4.5 A) Effect of pH of the 50 ng L<sup>-1</sup> analyte solution on mercury signal intensities: a) Hg<sup>2+</sup>; b) CH<sub>3</sub>Hg. B) UV irradiation time for the quantitative conversion of CH<sub>3</sub>Hg (70 ng L<sup>-1</sup>) into Hg<sup>2+</sup> (to be measured as mercury vapor) Effect of UV irradiation time on the oxidation of 70 ng L<sup>-1</sup> solution of CH<sub>3</sub>Hg in the absence (a) and (b) in the presence of H<sub>2</sub>O<sub>2</sub>. C) Effect of H<sub>2</sub>O<sub>2</sub> on the photo-induced oxidation of CH<sub>3</sub>Hg (70 ng L<sup>-1</sup>). See Table 4.1 for photo-induced oxidation and chemical reduction conditions.

The effect of salt content was also studied, and a significant drop in  $\text{CH}_3\text{Hg}$  photo-oxidation efficiency occurred as the  $\text{NaCl}$  in solution was increased. Efficiency in formation of  $\text{Hg}^{2+}$  (evaluated as  $\text{Hg}$  vapor after reduction with  $\text{SnCl}_2$ ) decreased 9 % as  $\text{NaCl}$  increased to  $4 \text{ g L}^{-1}$  further decreasing to 31 % of the reference signal as  $\text{NaCl}$  reaches  $10 \text{ g L}^{-1}$ . The interference could be due to a shifting in equilibrium to form stable  $\text{CH}_3\text{Hg}^+\text{Cl}^-$  ion pair in the sample solution [145] that is less prone to photo-oxidation. A comparative interference effect of both salt and oil contents in the measured signal ( $\text{Hg}$  vapor) obtained from a  $\text{Hg}^{2+}$  standard solution and a  $\text{CH}_3\text{Hg}$  standard solution (the former requiring UV treatment previously to the final reduction) is in Figure 4.6, showing that interferences are more drastic during photochemical treatment.

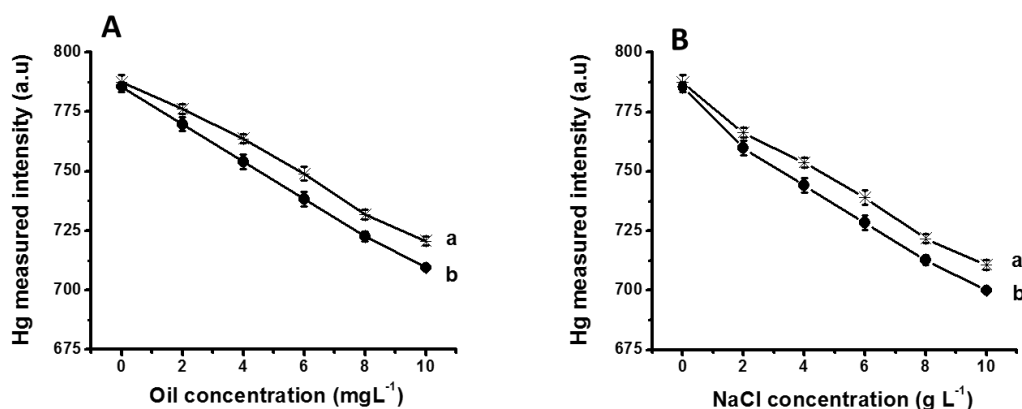


Figure 4.6 A) Comparative interference imposed by the dispersed oil content (2 - 10  $\text{mg L}^{-1}$ ) on the mercury signal: a) Solution of  $\text{Hg}^{2+}$  ( $75 \text{ ng L}^{-1}$ ); b) Solution of  $\text{CH}_3\text{Hg}$  ( $75 \text{ ng L}^{-1}$ ). B) Comparative interference imposed by the  $\text{NaCl}$  content (2 - 10  $\text{g L}^{-1}$ ) on the mercury signal: a) Solution of  $\text{Hg}^{2+}$  ( $75 \text{ ng L}^{-1}$ ); b) Solution of  $\text{CH}_3\text{Hg}$  ( $75 \text{ ng L}^{-1}$ ). See Table 4.1 for photo-induced oxidation and chemical reduction conditions.

A study to simultaneously evaluate the effect of salinity and dispersed oil was made using a circumscribed CCD measuring signal ( $\text{Hg}$  vapor) from solutions containing 700  $\text{pg}$  of  $\text{CH}_3\text{Hg}$  with chosen experimental design levels (and codified value in parenthesis) for  $\text{NaCl}$  (in  $\text{g L}^{-1}$ ) and dispersed oil content (in  $\text{mg L}^{-1}$ ) of 2 ( $-\sqrt{2}$ ); 3.2 (-1); 6 (0); 8.8 (+1) and 10 ( $+\sqrt{2}$ ). Replicates ( $n = 8$ ) were only made at (0,0).

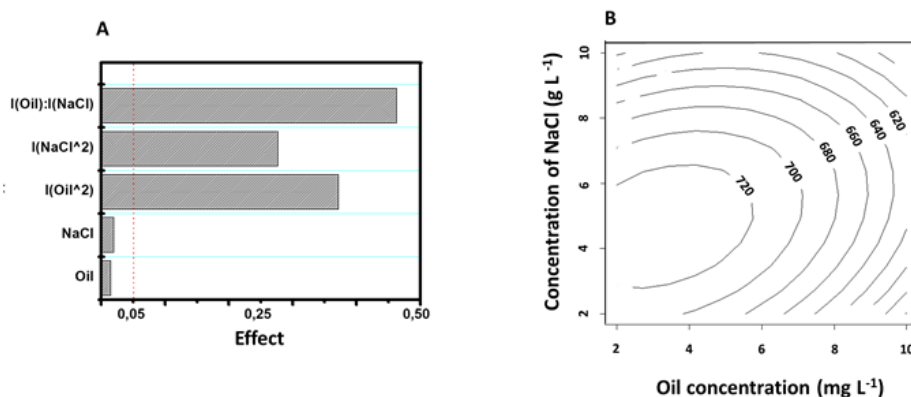


Figure 4.7 A) Graphic of effects; B) Topographic plot for mercury signal in the presence of both NaCl and dispersed oil. See Table 1 for photo-induced oxidation and chemical reduction conditions.

Response surface equation model was:  $y = 610 + 0.61 x_1 + 36.1 x_2 - 0.03 x_1^2 - 4.90 x_2^2 + 0.25 x_1 x_2$ . The graphic of effects (Figure 4.7A) indicated relevant interaction between factors, the relevance of the quadratic contributions and also for the linear effect for oil. The variability in replicate measurements was 2.1 %, and the topographic plot (Figure 4.7B) indicated a robust region that would lead to statistically similar results covering the mixture range containing 3 up to 6 g L<sup>-1</sup> of salt and from 2 up to 6 mg L<sup>-1</sup> of NaCl (salt content).

#### 4.2.5

#### Analysis strategy, analytical figures of merit, and method application.

The conditions for the quantitative speciation of mercury are indicated in Table 4.1. Method accuracy in the determination of inorganic mercury in a simple water matrix was evaluated by analyzing the SRM 1641c (Mercury in natural water with certified value for mercury of  $1.47 \pm 0.04$  mg L<sup>-1</sup>). The experimental value obtained was  $1.52 \pm 0.08$  mg L<sup>-1</sup> using the method (only the chemical reduction step with SnCl<sub>2</sub>) with quantification with analytical curve using fresh aqueous standards of Hg<sup>2+</sup> (in 2 % HNO<sub>3</sub> v/v). Although the average experimental value and standard deviation were higher, the statistical similarity was proven using a two-tailed *Student t*-test ( $\alpha = 0.05$  and  $n_1 = n_2 = 3$ ), which can be considered satisfactory

considering the significant dilution factor applied to the sample in order to perform analysis with the multipass-CV-AAS.

It is essential to point out that rotational type interferences are expected when  $\text{Hg}^{2+}$  (original or converted from organic-mercury) solution contains NaCl or dispersed oil as can be seen in Figure 5.8A (interference from NaCl) and Figure 4.8B (interference from oil), with decreasing in sensitivities, compared to a standard analyte curve in water, even at lower levels of PW matrix components. A straightforward way to compensate such interferences is the analyte addition method. However, this strategy becomes cumbersome when a large number of samples must be analyzed.

The analytical curve adjusted for PW samples becomes viable as interferences imposed (on the photochemical oxidation of  $\text{CH}_3\text{Hg}$  and the reduction of  $\text{Hg}^{2+}$ ) by the two primary components of PW samples have been modeled.

Besides, the interference model provided by the experimental design indicated robust conditions for the Hg measured (by CV-AAS) from mixtures containing both salt and oil in contents in the range around 3 to 6  $\text{g L}^{-1}$  and 2 to 6  $\text{mg L}^{-1}$  respectively. Therefore, if calibration standards are prepared in a matrix-matched solution containing adjusted quantities of NaCl and dispersed mineral oil within the range

of signal robustness, and samples are diluted to adjust salt content and centrifuged to adjust oil contents (within the robust response range), a matrix matching calibration can be used for determinations.

Following such strategy,  $\text{Hg}^{2+}$  analytical curve was constructed in the range from the quantification limit up to 200  $\text{ng L}^{-1}$  in aqueous mixtures containing 5  $\text{mg L}^{-1}$  of dispersed mineral oil, and 5  $\text{g L}^{-1}$  of NaCl. The instrumental limit of quantification (LOQ) was 12  $\text{ng L}^{-1}$ , calculated based on the amount of detected Hg that was 10 times the standard deviation of the 10 background Hg measurements using authentic replicate solutions containing dispersed mineral oil and NaCl. Background signal was equivalent to a concentration of  $\text{Hg}^{2+}$  of  $8.0 \pm 0.4 \text{ ng L}^{-1}$ . The analytical response in this range was linear ( $R^2 = 0.9995$ ), homoscedasticity of data was observed, and the equation was  $I = (9.713 \pm 0.011 \text{ L ng}^{-1}) \text{ CH}_3\text{Hg} (1.857 \pm 0.322)$ . The matrix-matched analytical curve (containing 5  $\text{g L}^{-1}$  NaCl and 5  $\text{mg L}^{-1}$  of mineral oil) was compared to the aqueous analytical curve for  $\text{Hg}^{2+}$  (Figure

4.8C) showing that the adjusted matrix imposes only 10 % decrease in sensitivity despite the high relativity content of interferents.

Table 4.1 Experimental conditions to perform quantitative analytical speciation of mercury CV-AAS with a multi-pass cell and UV-induced oxidation

Step	Inorganic mercury	Total mercury (inorganic + organic)
<b>I</b> Photochemical oxidation of sample in a quartz tube	-	Diluted sample: 10.00 mL a
	-	H <sub>2</sub> O <sub>2</sub> (30%): 0.4 mL
	-	UV exposure time: 5 min
	-	pH = 3
<b>II</b> Reduction in the reaction cell of the Bubbler accessory	Sample volume: 10.00 mL	Sample volume: total volume in step I
	SnCl <sub>2</sub> (20% w/v): 3 mL	SnCl <sub>2</sub> (20% w/v): 3 mL
	Air flow rate: 1 mL min <sup>-1</sup>	Air flow rate: 1 mL min <sup>-1</sup>
<b>III</b> Detection	$\lambda = 253.65 \text{ nm}$	$\lambda = 253.65 \text{ nm}$

Table 4.2 Characteristics of the analyzed PW samples

Sample	Salt content <sup>a</sup> (g L <sup>-1</sup> )	Original oil content <sup>b</sup> (mg L <sup>-1</sup> )	Salt content after dilution (g L <sup>-1</sup> )	Oil content after centrifugation <sup>b,c</sup> and dilution (mg L <sup>-1</sup> )
PW 1	45	125	4.5	3.6
PW 2	56	136	5.6	4.4
PW 3	70	225	7.0	6.0
PW 4	65	160	6.5	4.3

a. Measured by conductometry after sample dilution and using standards made with NaCl.

b. Measured by turbidimetry after dilution and using standards made with dispersed mineral oil samples.

c. Sample centrifuged at 2800 RFC for 20 min at 25 °C.

Accuracy was evaluated as instrumental precision (1.6 % considering the coefficient of variation from analysis of 10 aliquots of a matrix-matched standard solution of Hg<sup>2+</sup> of 50 ng L<sup>-1</sup>). Intermediate precision was 3.0 %, calculated as coefficient of variation from the analysis of 10 independent matrix-matched Hg<sup>2+</sup> (50 ng L<sup>-1</sup>) standard solutions.

The method was applied in the determination and speciation of mercury in four available PW samples. Before determination, samples were analyzed to estimate dispersed oil and salt (estimated as NaCl) contents (Table 4.2). Since high

oil and salt contents were found, PW samples were treated to adjust matrix for the analysis. Therefore, samples were centrifuged to force separation of part of the oil content forming an oil pellet on the bottom of the centrifugation tube. The average oil removing, in a replicate experiment ( $n = 4$ ), was  $71.3 \pm 2.4 \%$ . Then, an average volume of 1000  $\mu\text{L}$  of the aqueous supernatant (volume that can be adjusted depending upon sample matrix and expected Hg content) was collected, 10-fold diluted, transferred to the quartz tube and placed into the photochemical reactor.

The speciation analyses in real PW samples were made using the proposed method. The results (corrected for the dilution factor) are summarized in Table 4.3 and indicated the presence of total mercury at  $\mu\text{g L}^{-1}$  level (from 0.23 to  $0.82 \mu\text{g L}^{-1}$ ) from where organic mercury concentration (reported as  $\text{CH}_3\text{Hg}$ ) varied from 0.02 to  $0.07 \mu\text{g L}^{-1}$  and inorganic mercury ( $\text{Hg}^{2+}$ ) was in the range from 0.19 to  $0.80 \mu\text{g L}^{-1}$ . The total mercury obtained after complete mineralization of sample, (also indicated in Table 4.3) was found to be statistically similar to the ones obtained through the photo-oxidation method for total mercury.

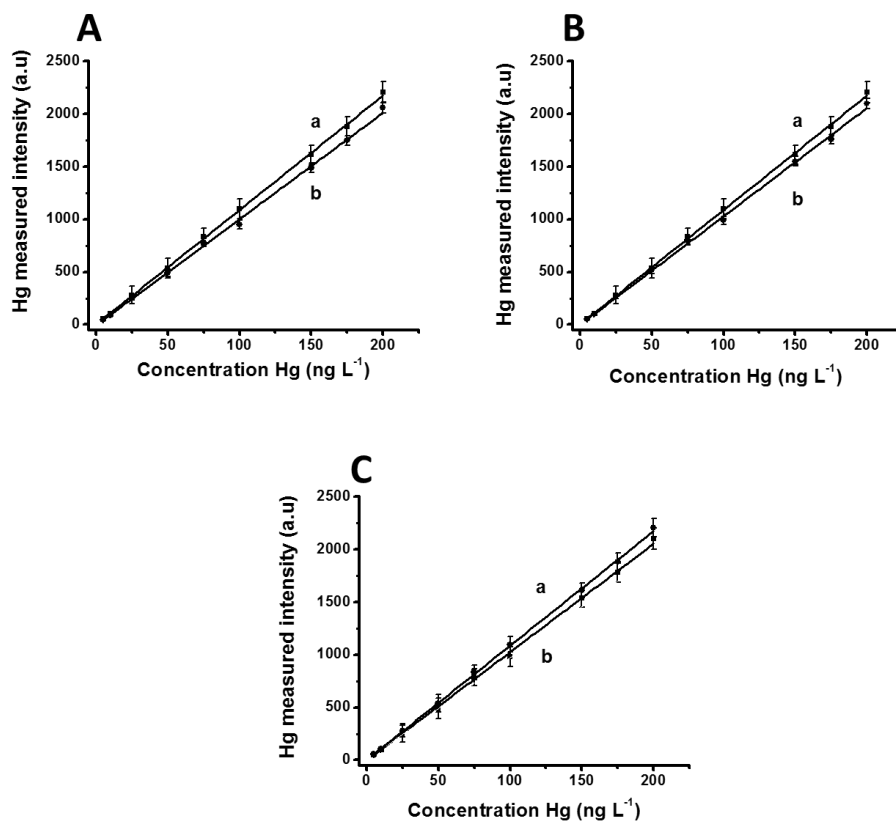


Figure 4.8 A) Analytical curves: a) using a standard solution of  $\text{Hg}^{2+}$  and b) using standard solution of  $\text{Hg}^{2+}$  in the presence of  $5 \text{ g L}^{-1}$  NaCl. B) Analytical curves: a) using standard solution of  $\text{Hg}^{2+}$  and b) using standard solution of  $\text{Hg}^{2+}$  in the presence of  $5 \text{ mg L}^{-1}$  of dispersed mineral oil; C) Analytical curves: a) using standard solution of  $\text{Hg}^{2+}$  and b) using standard solution of  $\text{Hg}^{2+}$  in a solution containing  $5 \text{ g L}^{-1}$  NaCl and  $5 \text{ mg L}^{-1}$  of dispersed mineral oil.

Table 4.3 Original concentrations of  $\text{Hg}^{2+}$  e  $\text{CH}_3\text{Hg}$  found in PW samples using the proposed method.

Sample	$\text{Hg}^{2+}$ ( $\mu\text{g L}^{-1}$ )	Total mercury ( $\mu\text{g L}^{-1}$ )	$\text{CH}_3\text{Hg}$ ( $\mu\text{g L}^{-1}$ )	Total mercury after mineralization ( $\mu\text{g L}^{-1}$ )
PW 1	$0.80 \pm 0.01$	$0.82 \pm 0.01$	$0.02 \pm 0.01$	$0.83 \pm 0.02$
PW 2	$0.49 \pm 0.01$	$0.52 \pm 0.02$	$0.03 \pm 0.02$	$0.54 \pm 0.03$
PW 3	$0.19 \pm 0.02$	$0.23 \pm 0.01$	$0.04 \pm 0.02$	$0.22 \pm 0.02$
PW 4	$0.38 \pm 0.01$	$0.45 \pm 0.01$	$0.07 \pm 0.01$	$0.46 \pm 0.03$

Table 4.4 Quantification study after PW samples fortification with  $\text{Hg}^{2+}$  for the estimation of the original analyte content.

Sample	$\text{Hg}^{2+}$ fortification level ( $\mu\text{g L}^{-1}$ )	Total $\text{Hg}^{2+}$ found ( $\mu\text{g L}^{-1}$ )	Original $\text{Hg}^{2+}$ recovered in the fortification experimenta ( $\mu\text{g L}^{-1}$ )	Average original $\text{Hg}^{2+}$ ( $\mu\text{g L}^{-1}$ )
PW 1	2.50	$3.32 \pm 0.01$	$0.82 \pm 0.01$	$0.81 \pm 0.05$
	5.00	$5.81 \pm 0.03$	$0.81 \pm 0.03$	
	10.00	$10.80 \pm 0.04$	$0.80 \pm 0.02$	
PW 2	2.50	$3.01 \pm 0.02$	$0.51 \pm 0.02$	$0.50 \pm 0.03$
	5.00	$5.52 \pm 0.01$	$0.52 \pm 0.01$	
	10.00	$10.51 \pm 0.02$	$0.49 \pm 0.02$	
PW 3	2.50	$2.31 \pm 0.03$	$0.19 \pm 0.03$	$0.20 \pm 0.04$
	5.00	$5.21 \pm 0.02$	$0.21 \pm 0.02$	
	10.00	$1.22 \pm 0.02$	$0.22 \pm 0.02$	
PW 4	2.50	$0.66 \pm 0.03$	$0.41 \pm 0.03$	$0.40 \pm 0.04$
	5.00	$0.89 \pm 0.02$	$0.39 \pm 0.02$	
	10.00	$10.22 \pm 0.03$	$0.40 \pm 0.03$	

<sup>a</sup> Discounting the  $\text{Hg}^{2+}$  fortified concentration.

Table 4.5 Quantification study after PW samples fortification with  $\text{CH}_3\text{Hg}$  for the for the estimation of the original analyte content.

Sample	$\text{CH}_3\text{Hg}$ fortification Level ( $\mu\text{g L}^{-1}$ )	Total $\text{CH}_3\text{Hg}$ found ( $\mu\text{g L}^{-1}$ )	Original $\text{CH}_3\text{Hg}$ recovered in the fortification experiment <sup>a</sup> ( $\mu\text{g L}^{-1}$ )	Average origin $\text{CH}_3\text{Hg}$ ( $\mu\text{g L}^{-1}$ )
PW 1	0.25	$0.28 \pm 0.03$	$0.03 \pm 0.01$	$0.03 \pm 0.01$
	0.50	$0.54 \pm 0.01$	$0.04 \pm 0.01$	
	1.00	$1.02 \pm 0.02$	$0.02 \pm 0.01$	
PW 2	0.25	$0.29 \pm 0.02$	$0.04 \pm 0.01$	$0.04 \pm 0.01$
	0.50	$0.55 \pm 0.04$	$0.05 \pm 0.01$	
	1.00	$1.03 \pm 0.05$	$0.03 \pm 0.01$	
PW 3	0.25	$0.29 \pm 0.01$	$0.04 \pm 0.01$	$0.05 \pm 0.01$
	0.50	$0.57 \pm 0.02$	$0.07 \pm 0.01$	
	1.00	$1.05 \pm 0.01$	$0.05 \pm 0.01$	
PW 4	0.25	$0.33 \pm 0.02$	$0.07 \pm 0.02$	$0.08 \pm 0.02$
	0.50	$0.58 \pm 0.02$	$0.08 \pm 0.01$	
	1.00	$1.09 \pm 0.04$	$0.09 \pm 0.01$	

<sup>a</sup> Discounting the  $\text{CH}_3\text{Hg}$  fortified concentration.

It is essential to point out that the oil pellets obtained after centrifugation of the samples were analyzed after mineralization and levels of mercury were below the background level. Besides, original reduced mercury levels in samples were found to be insignificant as aliquots of the samples were analyzed in the CV-AAS system without the addition of reducing agent.

Table 4.6 Comparison of results for the determination of  $\text{Hg}^{2+}$  and  $\text{CH}_3\text{Hg}$  in PW samples.

Samples	$\text{Hg}^{2+}$ found original sample ( $\mu\text{g L}^{-1}$ )	$\text{Hg}^{2+}$ recovered in the fortification experiment ( $\mu\text{g L}^{-1}$ )	$t_{\text{calculated}}^*$
PW 1	$0.80 \pm 0.01$	$0.84 \pm 0.03$	0.321
PW 2	$0.49 \pm 0.01$	$0.52 \pm 0.01$	0.840
PW 3	$0.19 \pm 0.02$	$0.22 \pm 0.03$	0.547
PW 4	$0.38 \pm 0.01$	$0.41 \pm 0.02$	0.321

Samples	$\text{CH}_3\text{Hg}$ found original sample ( $\mu\text{g L}^{-1}$ )	$\text{CH}_3\text{Hg}$ recovered in the fortification ( $\mu\text{g L}^{-1}$ )	$t_{\text{calculated}}^*$
PW 1	$0.02 \pm 0.01$	$0.025 \pm 0.005$	1.22
PW 2	$0.03 \pm 0.02$	$0.034 \pm 0.002$	0.547
PW 3	$0.04 \pm 0.02$	$0.046 \pm 0.004$	1.33
PW 4	$0.07 \pm 0.01$	$0.078 \pm 0.006$	0.824

\* $t_{\text{critical}}$  (two-tailed student-t test;  $\alpha=0.05$  (g.l. =  $n_1 + n_2 - 2 = 4$ ) = 2.77.

Table 4.7 Comparison of the determination of  $\text{Hg}^{2+}$  and  $\text{CH}_3\text{Hg}$  in PW samples with the proposed method and using the method based on GC-CV-AFS.

Samples	$\text{Hg}^{2+}$ found method CV-AAS ( $\mu\text{g L}^{-1}$ )	$\text{Hg}^{2+}$ found method GC-CV-AFS ( $\mu\text{g L}^{-1}$ )	$t_{\text{calculated}}^*$
PW 1	$0.80 \pm 0.01$	$0.84 \pm 0.03$	0.321
PW 2	$0.49 \pm 0.01$	$0.52 \pm 0.01$	0.840
PW 3	$0.19 \pm 0.02$	$0.22 \pm 0.03$	0.547
PW 4	$0.38 \pm 0.01$	$0.41 \pm 0.02$	0.321

Samples	$\text{CH}_3\text{Hg}$ found method CV-AAS ( $\mu\text{g L}^{-1}$ )	$\text{CH}_3\text{Hg}$ found Method GC-CV-AFS ( $\mu\text{g L}^{-1}$ )	$t_{\text{calculated}}^*$
PW 1	$0.02 \pm 0.01$	$0.025 \pm 0.005$	1.22
PW 2	$0.03 \pm 0.02$	$0.034 \pm 0.002$	0.547
PW 3	$0.04 \pm 0.02$	$0.046 \pm 0.004$	1.33
PW 4	$0.07 \pm 0.01$	$0.078 \pm 0.006$	0.824

\* $t_{\text{critical}}$  (two-tailed student-t test;  $\alpha=0.05$  (g.l. =  $n_1 + n_2 - 2 = 4$ ) = 2.77

PW samples were also fortified with analytes at three levels (see Table 4.4 for  $\text{Hg}^{2+}$  fortification levels and Table 4.5 for  $\text{CH}_3\text{Hg}$  fortification levels). The analyte fortification percent recoveries (discounted the original concentrations reported in Table 4.3) were close to 100 %. Total recovered concentrations at the

different fortification levels allowed the estimation of the original  $\text{Hg}^{2+}$  and  $\text{CH}_3\text{Hg}$  concentrations in samples which are close to the ones determined and displayed in Table 4.3 (according to two-tailed *Student t*-test at 95 % confidence limit indicated in Table 4.6). The results of this study were compared with those values for  $\text{CH}_3\text{Hg}$  and  $\text{Hg}^{2+}$  obtained by GC-CV-AFS and found to be statistically similar (Table 4.7). The results using GC-CV-AFS also have shown that original  $\text{Hg}^0$  in sample was insignificant.

Table 4.8 Characteristics of different methods for the determination of total mercury in different samples using different analytical techniques.

Method	Sample	LOD (ng L <sup>-1</sup> ) or LOQ (ng L <sup>-1</sup> )	Reference
CV-ICP-MS	Humic-rich natural waters	2.2 (LOQ)	[28]
FIA and pre-concentration system coupled with AFS	Standard reference material. (Peach Leaves NIST 1547)	10 (LOD)	[33]
Photo-CV-AFS	Certified reference water and geological samples	20 (LOD)	[146]
ICP-OES	Artificial produced water	1200 (LOD)	[64]
Photo-CV-AAS.	Biofuel	90 (LOD)	[35]
CV-AAS	Fish homogenate and horse kidney samples	41 (LOD)	[140]
GC-CV-AFS	Biological Materials	1.3 (ALOD)	[141]
GC-He-MIP	Seawater	9 (LOD)	[60]
PVG-AFS	Fish oil supplements.	500 (LOD)	[144]
CV-multipass-AAS	Produced water	12 (LOQ)	<b>This work</b>

LOD: Limit of detection; LOQ: Limit of quantification; ALOD: Absolute limit of detection.

CV: cold vapor; ICP-MS: inductively coupled plasma mass spectrometry; AFS: atomic fluorescence spectrometry; FIA: flow injection analysis; OES: optical emission spectrometer; He-MIP: atmospheric pressure helium microwave-induced plasma optical spectrometry; GC: Gas Chromatography; PVG: Photochemical vapor generation;

### 4.3

#### Partial Conclusion

The proposed method for the speciation of mercury in PW samples enabled ultra-trace capability (LOQ of  $12 \text{ ng L}^{-1}$ ) using the multipass-CV-AAS system with proper accuracy achieved by matrix-matched calibration to compensate interferences imposed by the major components of the PW samples. Efficiency in  $\text{CH}_3\text{Hg}$  oxidation to  $\text{Hg}^{2+}$  and the efficiency in converting  $\text{Hg}^{2+}$  to the detectable Hg vapor were achieved under adjusted experimental conditions. Recoveries from the analyses of real samples were similar to those from multiple fortification experiments and also similar to those found using a speciation method adapted from literature. Although there is no specific legislation for the disposal of PW in many oil-producing countries, for mercury there are specific international and national disposable limits (in Brazil, the National Council of the Environment 393/2007 resolution requires monitoring of PW metal concentrations before their disposal into the ocean). The CV-AAS method developed uses a laboratory-made photochemical reactor and a portable multipass-CV-AAS setup, which can be easily adapted for analysis in off-shore petroleum platforms. The developed method does not rely on tedious sample extraction procedures as it enables easy direct photochemical procedure for speciation in PW samples. When compared to the other reported methods for PW and seawater, the proposed method enabled better sensitivity. Besides, limits of quantification were similar to those achieved more sophisticated methods, based on ICP-MS and AFS techniques, that rely on the use of more complex procedures.

## 5.

### **Results and discussion II. Combination of ultrasonic extraction in a surfactant-rich medium and distillation for mercury speciation in offshore petroleum produced waters by gas chromatography cold vapor atomic fluorescence spectrometry**

Paper published as: “*Combination of ultrasonic extraction in a surfactant-rich medium and distillation for mercury speciation in offshore petroleum produced waters by gas chromatography cold vapor atomic fluorescence spectrometry*” (See Attachment A2).

It is important to remark that all information taken from Chapter 5 of this thesis, must be cited as: *Combination of ultrasonic extraction in a surfactant-rich medium and distillation for mercury speciation in offshore petroleum produced waters by gas chromatography cold vapor atomic fluorescence spectrometry* J.R. Miranda-Andrades, S. Khan, M.J. Pedrozo-Penãfiel, K. de C.B. Alexandre, R.M. Maciel, R. Escalfoni, M.L.B. Tristão, R.Q. Aucelio, Spectrochim. Acta - Part B At. Spectrosc. 158 (2019) 105641. doi:10.1016/j.sab.2019.105641.

#### 5.1

##### **Abstract**

A new analytical method for mercury speciation in offshore petroleum produced water samples (PW) was developed using the combination of extraction (assisted by ultrasound in the presence of surfactant) and distillation before propylation and determination by gas chromatography cold vapor atomic fluorescence spectrometry (GC-CV-AFS). Ultrasonic (US) treatment (40 min) and the use of Triton X-114 (at 0.5 % w/v at pH 3) improved recoveries during the distillation used to separate mercury species from the interfering PW matrix (rich in dispersed oil and salt). Recoveries as high as 92 % ( $\text{Hg}^{2+}$ ), 87 % ( $\text{CH}_3\text{Hg}$ ) and 86 % ( $\text{CH}_3\text{CH}_2\text{Hg}$ ) were achieved. Conditions were adjusted to minimize artifact formation during the samples treatment process in systems containing the major

PW matrix components. The method detection limits were 5.0, 8.0, and 11.0  $\mu\text{g L}^{-1}$  respectively for  $\text{Hg}^{2+}$ ,  $\text{CH}_3\text{Hg}$ , and  $\text{CH}_3\text{CH}_2\text{Hg}$ . The use of matrix-matched standards (containing mineral oil at 40  $\text{mg L}^{-1}$  and  $\text{NaCl}$  at 30  $\text{g L}^{-1}$ ) improved accuracy of the method that was successfully applied for the analysis of four different PW samples, obtained from off-shore operations, with  $\text{Hg}^{2+}$  and  $\text{CH}_3\text{Hg}$  detected at the  $\text{ng L}^{-1}$  level. A pictorial description of the work is in Figure 5.1.

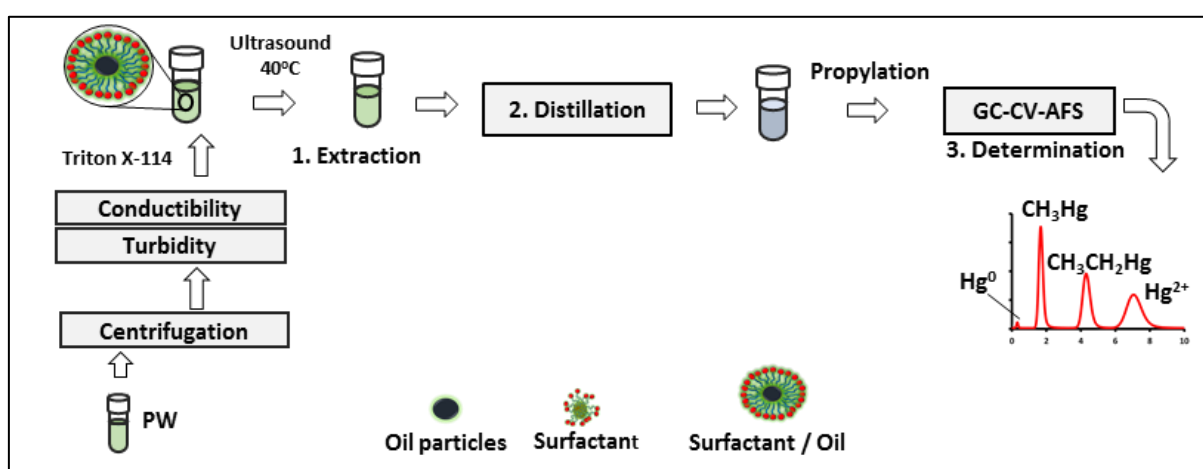


Figure 5.1 Graphical abstract

## 5.2.1

### Results and discussion

## 5.2.2

### Artifacts of organic mercury species during derivatization by $\text{NaBPr}_4$ .

Huang reported a study, using data collected by GC-ICP-MS, concerning the formation of organomercury artifacts during propylation (derivatization using  $\text{NaBPr}_4$ ) showing that the formation of methylmercury ( $\text{CH}_3\text{Hg}$ ) and ethylmercury ( $\text{CH}_3\text{CH}_2\text{Hg}$ ), as well as of other unidentified organomercury compounds, is dependent upon the concentration of  $\text{Hg}^{2+}$  and also on the quality of the propylation reagent [37]. Increased  $\text{CH}_3\text{Hg}$  artifacts were found as the amount of  $\text{Hg}^{2+}$  in the

sample became higher (0.28% or about 10 times higher at 1000 ng of  $\text{Hg}^{2+}$  than at 1 ng of  $\text{Hg}^{2+}$ ). In contrast,  $\text{CH}_3\text{CH}_2\text{Hg}$  artifact remained fairly stable (about 2 %) as the amount of  $\text{Hg}^{2+}$  increased from 100 ng to 1  $\mu\text{g}$  [37].

In order to obtain reliable results by speciation analysis using GC-CV-AFS, the formation of organomercury artifacts was evaluated during propylation using levels of  $\text{Hg}^{2+}$  varying from 200 to 10.000 times lower than the ones tested by Huang. The  $\text{Hg}^{2+}$  aqueous standard solutions (40 mL) were adjusted to concentrations (total amount in parenthesis) as follows: 25  $\text{pg L}^{-1}$  (1 pg); 50  $\text{pg L}^{-1}$  (2 pg); 250  $\text{pg L}^{-1}$  (11 pg); 500  $\text{pg L}^{-1}$  (23 pg) and 1000  $\text{pg L}^{-1}$  (45 pg) and the amount of propylation reagent used in this study was five times lower than the one used by Huang. As the detector is  $\text{Hg}^0$  dedicated, signals from different mercury species (measured as integrated peak area) can be directly compared.

In Figure 5.2A, typical chromatograms obtained from the experiments indicate, besides the increasing  $\text{Hg}^{2+}$  contents in standards, at the retention time ( $t_R$ )  $7.78 \pm 0.02$  min, the presence of different mercury species, as artifacts from the derivatization process, were found at  $t_R$  of  $1.86 \pm 0.01$  min for  $\text{CH}_3\text{Hg}$  and  $4.37 \pm 0.02$  min for  $\text{CH}_3\text{CH}_2\text{Hg}$ . The higher artifact levels have been found in the experiment made using the higher concentration of  $\text{Hg}^{2+}$  (1000  $\text{pg L}^{-1}$ ), representing about 0.30% (in terms of  $\text{CH}_3\text{Hg}$ ) and only about 0.20 % (in terms of  $\text{CH}_3\text{CH}_2\text{Hg}$ ) of the signal observed for  $\text{Hg}^{2+}$ . These values imposed a maximum baseline level expected for organic mercury (taking as reference the concentration of  $\text{Hg}^{2+}$ ) of about 3  $\text{pg L}^{-1}$  for  $\text{CH}_3\text{Hg}$  and 2  $\text{pg L}^{-1}$  for  $\text{CH}_3\text{CH}_2\text{Hg}$ . A relative evolution of the  $\text{CH}_3\text{Hg}$  generated as artifact can be seen in Figure 5.2B with indication of the ratio values between the  $\text{CH}_3\text{Hg}$  and the  $\text{Hg}^{2+}$  signals. Elemental mercury ( $t_R$  at  $0.38 \pm 0.02$  min) was detected during the analyzes of all of the standards but its relative value, related to the signal obtained for  $\text{Hg}^{2+}$ , remained almost constant and about 0.70 %. Probably source of  $\text{Hg}^0$  is the environmental impurity and also from natural degradation of the organic species and reduction of  $\text{Hg}^{2+}$  during the analytical process.

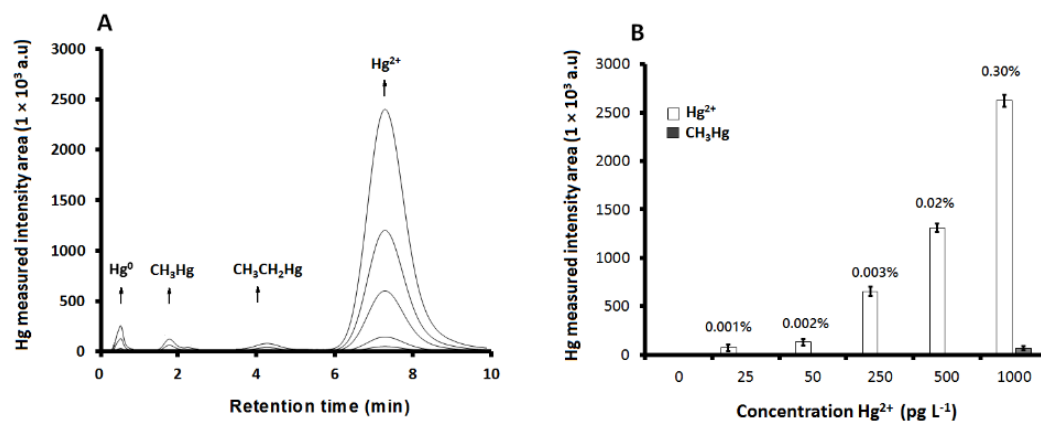


Figure 5.2 A) Typical chromatograms obtained using the GC-CV-AFS system after derivatization of  $\text{Hg}^{2+}$  standard solutions with  $\text{NaBPr}_4$ , showing the formation of organic mercury artifacts. (B) Relative signals of  $\text{CH}_3\text{Hg}$  and  $\text{Hg}^{2+}$  with organic mercury (as  $\text{CH}_3\text{Hg}$ ) relative percent levels (artifact). The standard deviation for  $n = 3$ .

### 5.2.3

#### Artifact of $\text{CH}_3\text{Hg}$ produced during distillation.

Distillation is one of the most used procedures, including in the EPA 1630 method, to separate mercury species present in samples previously to chemical derivatization. Several studies have reported  $\text{CH}_3\text{Hg}$  artifact in a process called artificial methylation [147]. For this reason, the formation of  $\text{CH}_3\text{Hg}$  and  $\text{CH}_3\text{CH}_2\text{Hg}$  were evaluated during distillation of solutions containing one of the significant components of PW samples (crude oil or NaCl). However, literature reports that artificial methylation does not occur when  $\text{Hg}^{2+}$  is in deionized water, suggesting that the artifact is not due to distillation, but a result of matrix components affecting the reaction of  $\text{Hg}^{2+}$  in samples [148]. Standard solutions containing  $800 \mu\text{g L}^{-1}$  of  $\text{Hg}^{2+}$  were distilled in the presence of increasing concentrations of dispersed crude oil (from 0 to  $300 \text{ mg L}^{-1}$ ) or NaCl (from 0 to  $100 \text{ g L}^{-1}$ ). Control aqueous systems were prepared without the addition of  $\text{Hg}^{2+}$  but containing either dispersed crude oil or dissolved NaCl. It is known that the formation of artifacts increases at the end of the distillation stage, when sample matrix components (in the case organic matter) and  $\text{Hg}^{2+}$  are concentrated in the distillation flask [41,44], therefore it was decided to distill no further than 80 % of the total sample solution volume. The distilled samples (about 40 mL) were buffered (0.2 mL standard acetate buffer solution) and mixed with the propylation

agent (0.1 mL of the NaBPr<sub>4</sub> solution) before placing them in the sampler of the CG-CV-AFS system. The results of this study are shown in Figure 5.3.

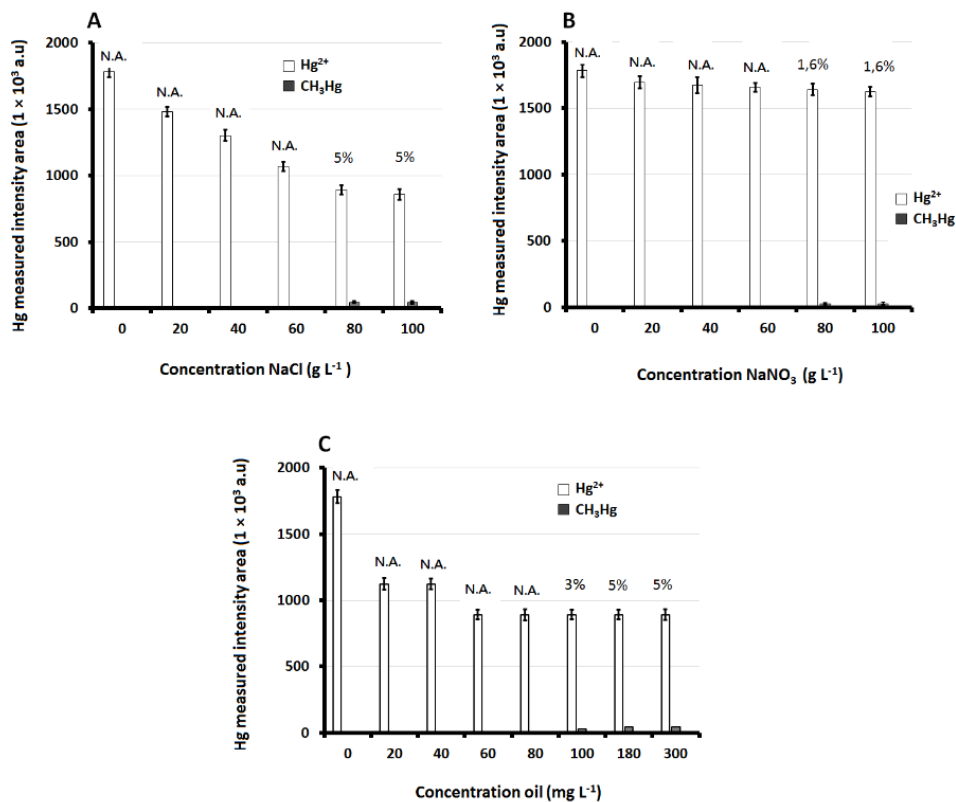


Figure 5.3 Inorganic mercury (Hg<sup>2+</sup>) recovery and formation of CH<sub>3</sub>Hg artifact measured in the presence of increasing quantities of (A) NaCl; (B) NaNO<sub>3</sub>; (C) dispersed crude oil. Indicated values are the percent ratio between the measured CH<sub>3</sub>Hg, and Hg<sup>2+</sup> and N.A. is no artifact formed. Measurements made by GC-CV-AFS after propylation. (standard deviation for n =3)

The results were corrected by the measured values in control mixtures (the ones containing either salt or oil without fortification of Hg<sup>2+</sup>) and CH<sub>3</sub>Hg percent values reported are the ones above the determined baseline level produced during propylation and measured by GC-CV-AFS (Figure 5.3A). As a reference, propylation of an Hg<sup>2+</sup> standard solution (800 pg L<sup>-1</sup>) generated about 0.10 % (0.80 pg L<sup>-1</sup>) of CH<sub>3</sub>Hg and about 0.05% (0.38 pg L<sup>-1</sup>) of CH<sub>3</sub>CH<sub>2</sub>Hg as an artifact. Distillation performed in the presence of NaCl only produced CH<sub>3</sub>Hg values above baseline levels at the highest concentrations of salt (80 and 100 g L<sup>-1</sup>) with formation of 40 pg L<sup>-1</sup> of CH<sub>3</sub>Hg (50 times higher the baseline level). It is known

that  $\text{NaBPr}_4$  undergoes alkyl cleavages and rearrangement [37] and it is possible that, at high levels of chlorine, the stability of the propylation reagent is somehow affected, thus explaining the decreasing in recovery of  $\text{Hg}^{2+}$  and the higher production of  $\text{CH}_3\text{Hg}$  as the formed methyl radical reacts with  $\text{Hg}^{2+}$ . However, no increase in  $\text{CH}_3\text{CH}_2\text{Hg}$  was observed, which seem to be counter-intuitive since ethyl mercury artifacts would be expected as propylation reagent degrades. In order to confirm the interference caused by chlorine, a similar experiment was made using  $\text{NaNO}_3$  instead of  $\text{NaCl}$  (Figure 5.3B). In this case, formation of  $\text{CH}_3\text{Hg}$  artifacts also occurred only at the higher concentrations of salt but in a significantly lesser extent of about  $13 \text{ pg L}^{-1}$  (30 times lower than the obtained in the presence of  $\text{NaCl}$ ). Similarly, there was no measurable contribution for  $\text{CH}_3\text{CH}_2\text{Hg}$  as artifact.

Increased levels of  $\text{CH}_3\text{Hg}$  artifact only occurred when dispersed oil was at the higher tested content: at  $100 \text{ mg L}^{-1}$  ( $24 \text{ pg L}^{-1}$  of  $\text{CH}_3\text{Hg}$ ) and at 180 and  $300 \text{ mg L}^{-1}$  ( $40 \text{ pg L}^{-1}$  of  $\text{CH}_3\text{Hg}$ ) as seen in Figure 5.3C. These values were corrected by original  $\text{CH}_3\text{Hg}$  values found in the crude oil used in the study (about  $14 \text{ pg L}^{-1}$ ). It is reported that  $\text{CH}_3\text{Hg}$  artifact increases as a result of the action of natural organic matter on the  $\text{Hg}^{2+}$  in the sample [146,147], which corroborates the results found in the experiment. The measured values of  $\text{CH}_3\text{CH}_2\text{Hg}$  remained at baseline levels as the dispersed crude oil increased.

#### 5.2.4

#### **Matrix effects imposed by oil and salt in the efficiency of the distillation of mercury species.**

The matrix effect imposed by the presence of oil and salt on the efficiency of the removal of the mercury species by distillation was also studied using standard solutions containing  $800 \text{ pg}$  of each of the mercury species ( $\text{Hg}^{2+}$ ,  $\text{CH}_3\text{Hg}$  and  $\text{CH}_3\text{CH}_2\text{Hg}$ ) prepared in the presence of increasing content of dispersed oil (from 0 to  $100 \text{ mg L}^{-1}$ ) or  $\text{NaCl}$  (from 0 to  $100 \text{ g L}^{-1}$ ).

For  $\text{Hg}^{2+}$ , compared to the result achieved in the reference solution (absence of  $\text{NaCl}$ ), the performed distillation has produced a continuous decreasing in recovered  $\text{Hg}^{2+}$  as the concentration of  $\text{NaCl}$  increased (Figure 5.4A) to the point that when salt concentration was  $80 \text{ g L}^{-1}$  and  $100 \text{ g L}^{-1}$  the recovered  $\text{Hg}^{2+}$  was 73 % of the one obtained from the reference solution. Chloride, at low concentrations,

is known to improve volatility of mercury species during distillation of water samples. However, Yamamoto has reported that  $\text{Hg}^{2+}$  tend to form stable and troublesome to distillate  $\text{Hg}(\text{Cl})_n^{(2-n)}$  complexes in solutions at high chloride concentrations [149].

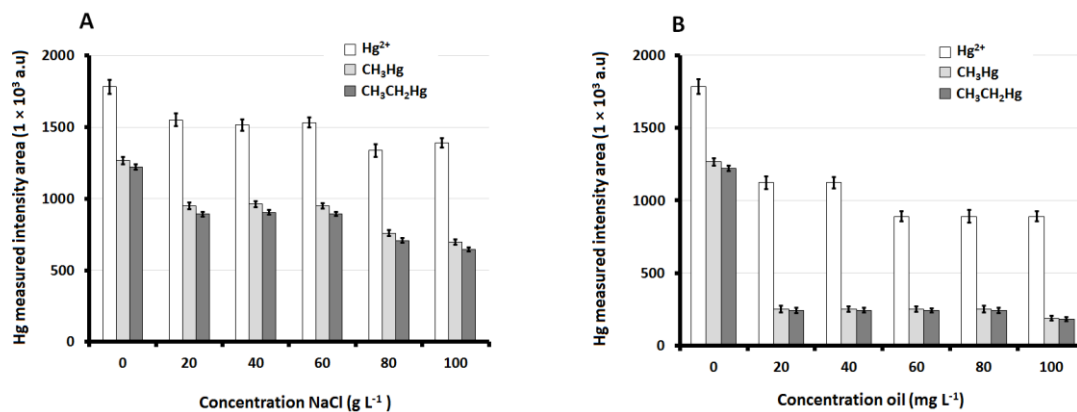


Figure 5.4 Recoveries for inorganic mercury ( $\text{Hg}^{2+}$ ) and organomercury species ( $\text{CH}_3\text{Hg}$  and  $\text{CH}_3\text{CH}_2\text{Hg}$ ), at  $800 \mu\text{g L}^{-1}$ , after distillation of solutions containing increasing quantities of (A) NaCl; (B) dispersed crude oil. Measurements made by GC-CV-AFS after propylation (standard deviation for  $n=3$ ).

Results from a similar study using  $\text{NaNO}_3$ , instead of NaCl, as the salt content of solutions corroborated the fact that chloride plays an important role in fixing  $\text{Hg}^{2+}$  in the distilled solution as nitrate<sup>2-</sup>, which does not tend to form complexes with mercury, had no such a significant influence on the recovery of  $\text{Hg}^{2+}$ . The presence of dispersed oil also reduced recoveries of  $\text{Hg}^{2+}$  during distillation but the loss of analyte varied from 38 % (at  $20 \text{ mg g}^{-1}$  of oil) to 50 % (at  $100 \text{ mg g}^{-1}$  of oil) as seen in Figure 5.4B. The 1-octanol/water partition coefficients (expressed as  $\log K_{\text{OW}}$ ) of 0.52 for Hg (II) (as  $\text{HgCl}_2$ ) and 4.2 for  $\text{Hg}^0$  [150,151] indicate partial solubility of inorganic mercury in oil. Therefore, a fraction of inorganic mercury (especially in reductive conditions) is probably fixing mercury in the dispersed oil micro-droplets (high surface area of contact) during distillation. Besides, as the typical sulfur content of the crude oil used in these tests (total mercury of 2.6 % measured by CHNS elemental analysis) and traces of some sulfur-containing compounds might also playing an important role in decreasing mobility as they form stable complexes with  $\text{Hg}^{2+}$ .

Recoveries of organomercury species after distillation are shown in Figure 5.4. A loss of analyte was already observed for the reference solution as the recovery of  $\text{CH}_3\text{Hg}$  and  $\text{CH}_3\text{CH}_2\text{Hg}$  was about 70 % of the one achieved for  $\text{Hg}^{2+}$ . In solutions containing  $\text{NaCl}$  at concentrations up to  $60 \text{ g L}^{-1}$ , recoveries of organomercury were about 75% of the ones achieved for these same analytes in the reference solution. The organomercury recovered values steadily decreased as the salt content increased to  $80 \text{ g L}^{-1}$  (about 60%) and  $100 \text{ g L}^{-1}$  (about 55 %) when compared to the one recovered during distillation of the reference solution as seen in Figure 5.4A. Somehow, high concentration of chloride is decreasing efficiency in distillation of organomercury species as chloride tend to interact, especially in solutions below pH 6, with the methylmercury cation in solution [152].

The presence of dispersed oil strongly affected distillation of organomercury species as recoveries were only about 20% (compared to the ones of the reference solution) over the tested range of dispersed oil (Figure 5.4B). The affinities of both  $\text{CH}_3\text{HgCl}$  and  $\text{CH}_3\text{CH}_2\text{HgCl}$  to the high surface area of the oily phase (microdroplets of oil) is favored by the partial solubility of these analytes in oil ( $\log K_{\text{OW}(\text{CH}_3\text{HgCl})} = 0.23$  [153]). Therefore, it would be expected a sharp decreasing in recoveries as the fraction of oil increased. However, as the concentration of dispersed oil increased, the number of micro-droplets increased, but their size also increases, probably keeping the overall water-oil surface area of contact reasonably constant over the experiment and explaining the relatively constant low recovery achieved in the presence of different oil contents. Besides, another contributing factor in solubility in oil is based on the fact that  $\text{CH}_3\text{Hg}$  tends to form strong complexes with compounds containing sulfhydryl groups that might be present in crude oil [153].

It is important to point out that a synergic effect in decreasing recoveries of mercurial species is probably occurring when both oil and chloride are present in the water sample, as the chloride complexes of mercury and organic mercury may favor partition of mercurial species in the oil phase. Studies using solutions containing both matrix components are presented in the context of other studies in the following sections of this work.

### 5.2.5

#### **Ultrasonic extraction of the organic species in PW samples using non-ionic surfactants.**

As the study showed that efficiency of distillation, especially in the case of organic mercury, is strongly affected by the major matrix components of PW samples, it was decided to use a method for extracting the mercury species before the distillation process. Considering that the oil content produces a higher impact in recovery, it was decided to use a method to improve extraction of the mercury species to the aqueous phase before the distillation process. Literature reports the use of non-ionic surfactant and mineral acids to improve extraction of mercury from oil samples, after the breaking of the oil-water emulsion before total mercury determination in diesel oil, biodiesel and mineral oil samples using CV-AAS [17]. It was also reported the extraction of mercury by the aid of ultrasound and mineral acid [57] before total mercury determination by CV-AAS. Therefore, for the speciation method in PW samples it was decided to evaluate the combination of these procedures found in literature for the extraction of total mercury, applying the use of non-ionic surfactants and US treatment to improve recoveries of mercurial species before GC-CV-AFS analysis.

### 5.2.6

#### **Ultrasonic extraction using Triton X-100 and Triton X-114**

It has already been reported that nitric acid mineralizes  $\text{CH}_3\text{Hg}$  during sample distillation [154], affecting the speciation capability. Therefore, extraction was attempted using sulfuric acid at low concentrations. A series of optimizations were made to adjust the extraction conditions. For the preliminary extraction studies, 50 mL of a simulated PW samples, fortified with  $\text{Hg}^{2+}$ ,  $\text{CH}_3\text{Hg}$ , and  $\text{CH}_3\text{CH}_2\text{Hg}$  (each at  $800 \text{ pg L}^{-1}$ ), containing dispersed crude oil ( $80 \text{ mg L}^{-1}$ ) and  $\text{NaCl}$  ( $40 \text{ g L}^{-1}$ ). It is important to mention that the interference impact of the presence of  $\text{NaCl}$  is more effective at concentrations higher than  $40 \text{ g L}^{-1}$  and simple dilution may be used to minimize its effect on recoveries. However, the association of oil and high concentrations of chlorine might produce stronger interference than the ones

observed in the preliminary tests using either oil or salt. The ultrasound-assisted extractions were made using either Triton X-100 or Triton X-114, at concentrations (above critical micelle concentrations) varying from 0.05 to 2.0 % m/v with 20 min of US treatment (immersion of sample in an ultrasound bath with no temperature control at this point). Following the vigorous stirring of samples, they were transferred to the distillation flasks and mixed with 0.5 mL of  $\text{H}_2\text{SO}_4$  ( $8 \text{ mol L}^{-1}$ ). As surfactants produced an excessive amount of foam during sample distillation, 50  $\mu\text{L}$  of a solution of simethicone ( $75 \text{ g L}^{-1}$ ) was added as antifoaming agent. After collecting about 40 mL of distilled material, it was transferred to Teflon vials where 0.2 mL of acetate buffer and 0.1 mL of propylation reagent were mixed before placing them to the auto-sampler of the GC-CV-AFS.

The results in Figure 5.5 showed that surfactants played an important role in improving recoveries of  $\text{CH}_3\text{Hg}$  and  $\text{CH}_3\text{CH}_2\text{Hg}$  in samples containing dispersed oil ( $60 \text{ mg L}^{-1}$ ) and  $\text{NaCl}$  ( $40 \text{ g L}^{-1}$ ). It was found that higher recoveries were achieved using a concentration of surfactants above 0.5 % were about 2.6 times for Triton-X 114 (Figure 5.5A) and 2 times for Triton-X 100 (Figure 5.5B), when compared with recovery, found using the procedure without surfactant. Results indicate that partition of  $\text{CH}_3\text{Hg}$  and  $\text{CH}_3\text{CH}_2\text{Hg}$  in water is improved by the formation of surfactant assemblies. Further optimization of the extraction procedure is needed, and because better results were achieved using Triton-X 114, this surfactant was the one used to continue this work.

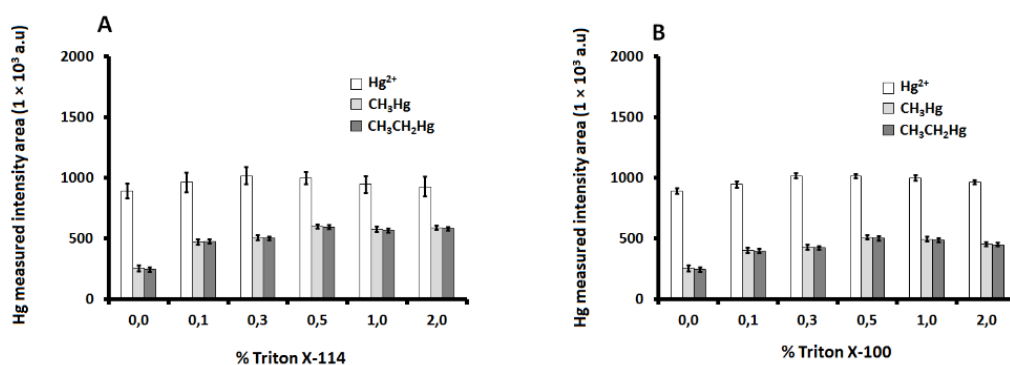


Figure 5.5 Recoveries for inorganic mercury ( $\text{Hg}^{2+}$ ) and organomercury species ( $\text{CH}_3\text{Hg}$  and  $\text{CH}_3\text{CH}_2\text{Hg}$ ), at  $800 \text{ pg L}^{-1}$ , using extraction before distillation of aqueous solutions containing  $\text{NaCl}$  ( $40 \text{ g L}^{-1}$ ) and dispersed crude oil ( $60 \text{ mg L}^{-1}$ ): (A) using Triton X-114 and B using Triton X-100. Measurements made by GC-CV-AFS after propylation (standard deviation for  $n = 3$ ).

### 5.2.7

#### Time of the ultrasonic treatment to extract mercury species from PW samples.

The time required for the ultrasonic agitation of the simulated PW samples in the presence of Triton X-114 (0.5 %) was evaluated under no temperature control.

A gradual increase in the recoveries of the mercury species occurred as the samples were placed under prolonged ultrasonic agitation (Figure 5.6) reaching maximum values after 40 min with recoveries of 61% for  $\text{Hg}^{2+}$  and about 50% for both  $\text{CH}_3\text{Hg}$  and  $\text{CH}_3\text{CH}_2\text{Hg}$  when compared to results achieved in from distillate standard solutions (without salt and oil).

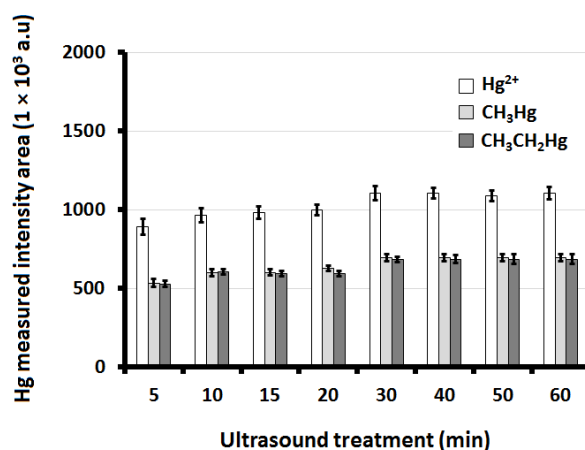


Figure 5.6 Ultrasound effect on the recoveries for inorganic mercury ( $\text{Hg}^{2+}$ ) and organomercury species ( $\text{CH}_3\text{Hg}$  and  $\text{CH}_3\text{CH}_2\text{Hg}$ ), at  $800 \text{ pg L}^{-1}$ , obtained using extraction with Triton X-114 (0.5 %) before distillation of aqueous solutions containing  $\text{NaCl}$  ( $40 \text{ g L}^{-1}$ ) and dispersed crude oil ( $80 \text{ mg L}^{-1}$ ). Measurements made by GC-CV-AFS after propylation (standard deviation for  $n=3$ )

### 5.2.8

#### Effect of pH and temperature on the extraction of mercury species in PW samples.

A study to evaluate the influence of the pH in the extraction efficiency was made by controlling the amount of the  $\text{H}_2\text{SO}_4$  ( $3 \text{ mol L}^{-1}$ ) added to the sample

solution. The pH range of the simulated PW samples (containing 80 mg L<sup>-1</sup> oil and 40 g L<sup>-1</sup> NaCl) was determined using universal pH strips and expressed in the range between 1 and 4 (Figure 5.7).

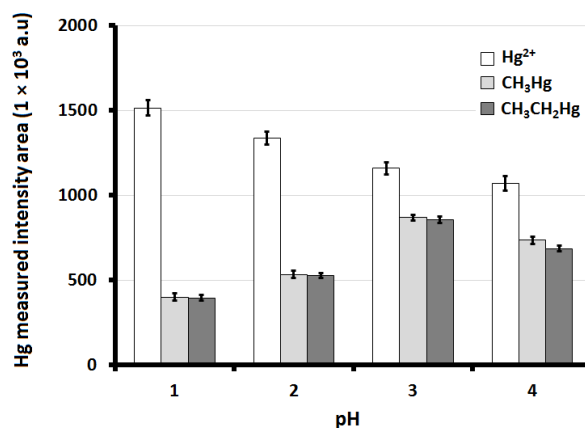


Figure 5.7 Effect of the pH on ultrasonic-assisted extraction (40 min), using Triton X-100 (0.5 %), on the recoveries for inorganic mercury (Hg<sup>2+</sup>) and organomercury species (CH<sub>3</sub>Hg and CH<sub>3</sub>CH<sub>2</sub>Hg), at 800 µg L<sup>-1</sup>, before distillation of simulated PW samples (40 g L<sup>-1</sup> of NaCl and 80 mg L<sup>-1</sup> dispersed crude oil). Measurements made by GC-CV-AFS after propylation (standard deviation for n =3).

After the addition and mixing of H<sub>2</sub>SO<sub>4</sub>, the mixtures were left to rest for 30 min before performing the ultrasonic treatment (40 min). It was observed that best recoveries for organic mercury had been achieved in mixtures with pH 3 while the Hg<sup>2+</sup> was better recovered at lower pH values (1 and 2), which can be attributed to either by mineralization of organomercury species (since recoveries of both CH<sub>3</sub>Hg and CH<sub>3</sub>CH<sub>2</sub>Hg was low at more acidic solutions) or by the minimization of the Hg<sup>2+</sup> hydrolysis. Extraction at the pH 3 was used because of the best compromise between recoveries of organomercury and inorganic mercury.

In an effort to achieve maximum efficiency in US assisted extractions of mercury species in the simulated PW samples (containing 80 mg L<sup>-1</sup> of dispersed oil and 40 mg L<sup>-1</sup> of NaCl), the temperature was evaluated (controlled during extraction in the range from 30°C to 70°C). The simulated PW matrix was fortified with the analytes (at 800 µg L<sup>-1</sup>) before addition of Triton X-114 (0.5 %) and pH adjusted to 3. Temperature control in the ultrasonic bath was adjusted to the desired value after transferring water, heated to a specific temperature, to the ultrasonic

bath. The samples were placed inside the ultrasonic bath to be sonicated for 40 min. The temperature of the water inside the bath was monitored with a thermocouple meter and controlled within  $\pm 5^\circ\text{C}$  range, adding, when necessary, small amounts of hot or cold water during the process.

After distillation, the results from the GC-CV-AFS showed that the maximum efficiencies for organomercury species were obtained with extractions performed at  $40^\circ\text{C}$  and, at higher temperatures, such efficiency decreased (Figure 5.8) probably due to the increase of organic mercury species solubility in the oil phase. In contrast, it was observed a continuous improvement in the extraction of  $\text{Hg}^{2+}$  with the increase in temperature (Figure 5.8), that probably improves solubility of the inorganic mercury into the aqueous phase. Therefore, extractions at  $40^\circ\text{C}$  were implemented as a compromise condition used for the method.

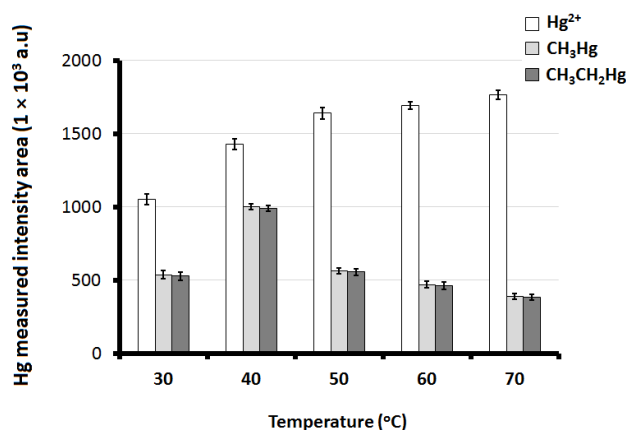


Figure 5. 8. Effect of temperature during 40 min US assisted extraction on the recoveries of inorganic mercury ( $\text{Hg}^{2+}$ ) and organomercury species ( $\text{CH}_3\text{Hg}$  and  $\text{CH}_3\text{CH}_2\text{Hg}$ ), at  $800 \text{ pg L}^{-1}$ , before distillation of simulated PW samples ( $40 \text{ g L}^{-1}$  of NaCl and  $80 \text{ mg L}^{-1}$  dispersed crude oil). Extraction using Triton X-114 (0.5 %) and  $\text{H}_2\text{SO}_4$  (pH 3) and measurements made by GC-CV-AFS, after propylation (standard deviation for  $n = 3$ ).

### 5.2.9

#### The efficiency of extraction in function of the oil content.

As oil was the PW matrix component that imposed the most severe interference, affecting recoveries especially for organomercury species, the robustness of the results using chosen extraction conditions (Table 5.1) was evaluated using different oil contents (from 20 to 100 mg L<sup>-1</sup>) and fixing the concentration of NaCl at 30 g L<sup>-1</sup>.

Table 5.1 Experimental conditions to perform quantitative analytical speciation of mercury GC-CV-AFS.

Step	Parameters of the method
<b>I</b> Extraction of mercury species	Sample: 50.00 mL <sup>a</sup> Triton X-114: 0.5 % m/v ultrasonic bath: 40 min pH 3 Temperature: 40 °C
<b>II</b> Distillation of the samples	Sample volume: 50 mL H <sub>2</sub> SO <sub>4</sub> (8 mol L <sup>-1</sup> ): 0.5 mL Ar flow rate: 1 mL min <sup>-1</sup>
<b>III</b> Detection GC-CV-AFS	1 to 10 mL of sample <sup>b</sup> , 0.2 mL acetate buffer, and 0.1 mL de NaBPr <sub>4</sub>

<sup>a</sup> PW samples 2-fold diluted.

<sup>b</sup> Dependent upon the concentration of mercury in samples.

It was found a consistency in recoveries for all of the mercury species (each one at 800 pg L<sup>-1</sup>) in samples containing oil in the range from 20 to 60 mg L<sup>-1</sup> (Figure 5.9A) with recoveries of 92 % for Hg<sup>2+</sup>, 87 % for CH<sub>3</sub>Hg and 86 % for CH<sub>3</sub>CH<sub>2</sub>Hg when compared to the results achieved by the direct analysis of an aqueous standard solution containing the same concentrations of analytes (Figure 5.9B).

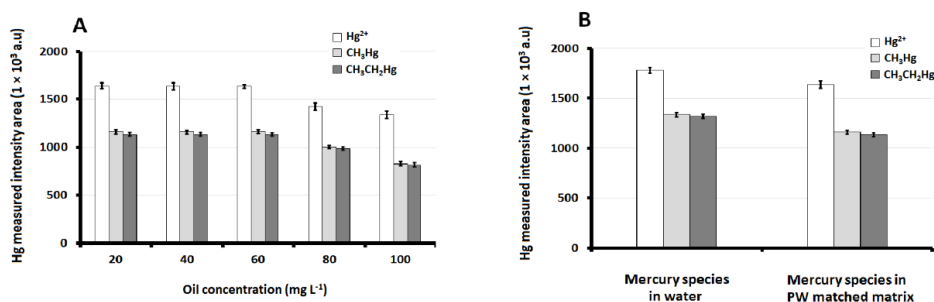


Figure 5.9. Determination of mercury species (at  $800 \text{ pg L}^{-1}$ ) using the chosen conditions for the US assisted extraction using Triton X114 (conditions in Table 2) in PW simulated samples containing dispersed oil in the range from 20 to  $100 \text{ mg L}^{-1}$  before distillation and GC-CV-AFS determination after propylation. Error bars (associated standard deviation of three replicates).

The experiment showed that oil content could be adjusted to the robust range (from 20 to  $60 \text{ mg L}^{-1}$ ) by simple centrifugation in order to achieve consistent recoveries. It is also important to point out that NaCl content can be adjusted within the robust range of 20 to 40 % as seen in Figure 5.4 by dilution before removing oil by centrifugation.

## 5.2.10

### Analytical characteristics of the method.

The analyzes of real PW samples were performed using the conditions to maximize analyte recovery and minimize the formation of artifact. The analytical procedure comprises an ultrasonic extraction using Triton X-114 in acidic conditions and distillation to remove mercury species (inorganic and organic) from sample matrix before the chromatographic separation of species to be measured by atomic fluorescence (as  $\text{Hg}^0$ ). Detailed conditions for each step of the analytical procedure are summarized in Table 5.1.

Table 5.2 Characteristics of the PW samples.

Sample	Salt content <sup>a</sup> (g L <sup>-1</sup> )	Original oil content <sup>b</sup> (mg L <sup>-1</sup> )	Salt content after dilution (g L <sup>-1</sup> )	Oil content after dilution <sup>b</sup> (mg L <sup>-1</sup> )
PW 5	37	87	18.5	43.5
PW 6	46	106	23.0	53.0
PW 7	65	114	32.5	57.0
PW 8	54	94	18.0	31.4

<sup>a</sup>Measured by conductometry after sample dilution and using standard solutions made with NaCl.

<sup>b</sup>Measured by turbidimetry after dilution and using standards made with dispersed mineral oil in water.

Due to the impact of the high contents of NaCl and dispersed oil in samples (see characteristics of the analyzed real PW samples in Table 5.2), the standards used for quantification were matrix-matched by adding known content of NaCl and mineral oil within the robust range of the analytical response for the speciation analysis. The original PW samples had its oil content adjusted to enable matrix components within the robust range for the recovery of analytes (20 and 60 mg L<sup>-1</sup> of dispersed oil) and, in general, adjusting of oil content was compromised with the dilution factor required to adjust the NaCl within the robust range (between 20 and 40 g L<sup>-1</sup>). When the compromise was not achievable, the salt content in standards was adjusted to the same range of the sample.

The analytical curves were constructed with the matrix-matched standard solutions containing Hg<sup>2+</sup>, CH<sub>3</sub>Hg, and CH<sub>3</sub>CH<sub>2</sub>Hg, each one in the concentration range from 25 to 800 pg L<sup>-1</sup>, after ultrasonic treatment and distillation. Matrix-matching of standards was made by adjusting the content of mineral oil to 40 mg L<sup>-1</sup> and NaCl to 30 g L<sup>-1</sup>. The limit of detection method (LOD) was 5 pg L<sup>-1</sup> for Hg<sup>2+</sup>, 8 pg L<sup>-1</sup> for CH<sub>3</sub>Hg and 11 pg L<sup>-1</sup> for CH<sub>3</sub>CH<sub>2</sub>Hg by calculating the amount of the measured mercury species (as Hg<sup>0</sup>) that was 3 times the standard deviation of baseline measurements (n = 10) using authentic replicates (extracted and distilled synthetic samples containing dispersed mineral oil at 40 mg L<sup>-1</sup> and NaCl at 30 g L<sup>-1</sup>). Limits of quantification (LOQ) were calculated using 10 times the baseline standard deviation with values shown in Table 5.3 along the equations of the analytical curves for each of the mercury species.

Table 5.3 Parameters of the analytical calibration curves obtained.

Mercury species	Equation	R <sup>2</sup>	LOD (pg L <sup>-1</sup> )	LOQ (pg L <sup>-1</sup> )
Hg <sup>2+</sup>	$Y = 2.03 \times 10^6 X + 973$	0.9994	5.0	12.0
CH <sub>3</sub> Hg	$Y = 1.47 \times 10^6 X - 2226$	0.9998	8.0	17.0
CH <sub>3</sub> CH <sub>2</sub> Hg	$Y = 1.37 \times 10^6 X - 7200$	0.9983	11.0	17.0

Typical chromatograms of increasing concentrations of mercury species are shown in Figure 5.10A. In terms of sensitivity, analytical curves prepared with mercury species in water, and PW matrix-matched medium is shown in Figure 5.10B-10D. It is important to notice that PW matrix imposes interference even after extraction and distillation. Thus, matrix-matched standards (within the robust analytical response range) provided accurate determinations. A comparison was made in order to evaluate if pure mineral oil could be used as matrix component to simulate crude oil and statistically similar results (sensitivities) were achieved when considering the curve constructed using crude oil corrected by the found original mercury species content (Hg<sup>2+</sup> and CH<sub>3</sub>Hg).

The difficulty in finding certified reference materials is a major problem when evaluating the reliability of methods applied to organic mercury. Therefore, the standard reference material SRM 1641c (Mercury in natural water with a Hg<sup>2+</sup> value of  $1.47 \pm 0.04$  mg L<sup>-1</sup>) was used to at least evaluate the accuracy of the method towards inorganic mercury in a simple water matrix that did not require ultrasonic extraction. The experimental result was  $1.50 \pm 0.04$  mg L<sup>-1</sup> using the proposed method by directly distilling the sample before determination by GC-CV-AFS.

Precision was evaluated using a PW matrix-matched standard (mineral oil at 40 mg L<sup>-1</sup> and NaCl at 30 g L<sup>-1</sup>). Instrumental precision of 1.4 % was observed considering the coefficient of variation of 10 aliquots of one single PW matrix-matched standard solution of Hg<sup>2+</sup> (75 pg L<sup>-1</sup>). The intermediate precision was 2.7 %, calculated as the coefficient of variation from the analysis of 10 independent PW matrix-matched standard solutions of Hg<sup>2+</sup> (75 pg L<sup>-1</sup>).

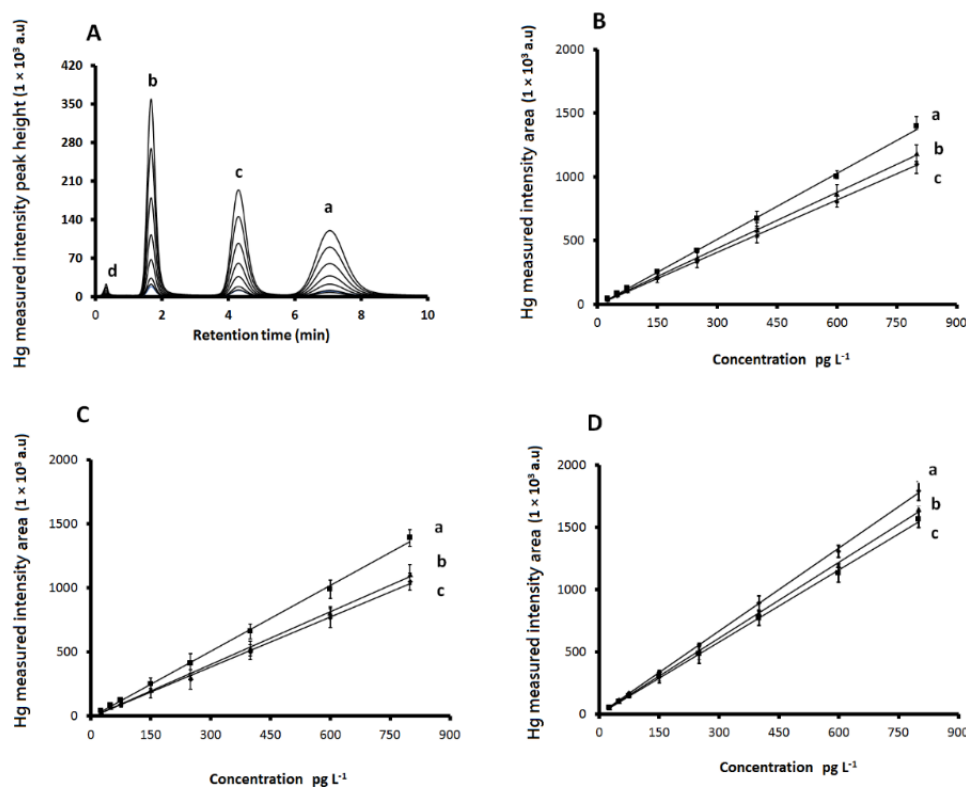


Figure 5.10. A) Chromatograms for increasing concentrations (from 25 to 800  $\text{pg L}^{-1}$ ) of the mercury species; a)  $\text{Hg}^{2+}$ ; b)  $\text{CH}_3\text{Hg}$ ; c)  $\text{CH}_3\text{CH}_2\text{Hg}$ ; d)  $\text{Hg}^0$  residual from the calibration standards. Analytical curves for B)  $\text{CH}_3\text{Hg}$ ; C)  $\text{CH}_3\text{CH}_2\text{Hg}$ ; D)  $\text{Hg}^{2+}$  using a) aqueous standards; b) matrix-matched standards using a petroleum sample (corrected by the original mercury species content) and c) matrix-matched standards using mineral oil. Matrix matching: oil ( $40 \text{ mg L}^{-1}$ ) and  $\text{NaCl}$  ( $30 \text{ g L}^{-1}$ ) (standard deviation for  $n = 3$ ).

### 5.2.11

#### Application of the mercury method in real PW samples.

The method was applied in the determination and speciation of mercury in four available PW samples (referred to as PW1, PW2, PW3, and PW4) obtained from offshore petroleum drilling platforms. Before determination, the samples were analyzed to estimate the dispersed oil and salt contents (estimated as  $\text{NaCl}$ ) in order to evaluate the procedure (centrifuging and dilution) required to adjust matrix to the robust response condition of the method. Such characteristics, before and after adjustments, are shown in Table 5.2. Standards of the mercury species (50.00 mL volume) were prepared in aqueous systems containing mineral oil ( $40 \text{ mg L}^{-1}$ ) and  $\text{NaCl}$  ( $30 \text{ g L}^{-1}$ ). Both sample and standards were submitted to the extraction and distillation. For standards, all 50.00 mL was used, but for samples, depending upon

the original mercury concentrations, 1.00 to 10.00 mL of sample was used with final volume (50.00 mL) adjusted with ultrapure water. Proper blank solutions were prepared for samples and standards.

The results (corrected for the dilution factor) are summarized in Table 5.4, indicating the presence of  $\text{Hg}^{2+}$  from 0.35 to 0.64  $\mu\text{g L}^{-1}$  and  $\text{CH}_3\text{Hg}$  from 0.022 to 0.053  $\mu\text{g L}^{-1}$ . No  $\text{CH}_3\text{CH}_2\text{Hg}$  above baseline levels were found in PW samples.

Table 5.4 Average original recovered values of  $\text{Hg}^{2+}$  and  $\text{CH}_3\text{Hg}$  in PW samples using a fortification study.

Sample	Average original $\text{Hg}^{2+}$ <sup>a,c</sup> ( $\mu\text{g L}^{-1}$ )	Average original $\text{CH}_3\text{Hg}$ <sup>b,c</sup> ( $\mu\text{g L}^{-1}$ )
PW 5	0.34 ± 0.03	0.042 ± 0.002
PW 6	0.63 ± 0.02	0.021 ± 0.001
PW 7	0.57 ± 0.03	0.032 ± 0.002
PW 8	0.38 ± 0.03	0.054 ± 0.002

<sup>a</sup>Average values discounting the  $\text{Hg}^{2+}$  fortified concentration at 3.00  $\mu\text{g L}^{-1}$ ; 6.00  $\mu\text{g L}^{-1}$ ; 12.00  $\mu\text{g L}^{-1}$ .

<sup>b</sup>Average values discounting the  $\text{CH}_3\text{Hg}$  fortified concentration with fortification at 0.100  $\mu\text{g L}^{-1}$ ; 0.200  $\mu\text{g L}^{-1}$ ; 0.400  $\mu\text{g L}^{-1}$ .

<sup>c</sup>Associated standard deviation for n = 3.

The PW samples were also fortified with analytes at three levels: 3.0, 6.0, and 12.0  $\mu\text{g L}^{-1}$  for  $\text{Hg}^{2+}$  and 0.100, 0.200, and 0.400  $\mu\text{g L}^{-1}$  for  $\text{CH}_3\text{Hg}$ . The average analyte original contents, calculated by the average recovery achieved using the fortification values are indicated in Table 5.4 with detailed results in Table 5.5 for  $\text{Hg}^{2+}$  and in Table 5.6 for  $\text{CH}_3\text{Hg}$ . The percent recoveries obtained from the analyte fortification procedure enabled estimation of the contents of  $\text{Hg}^{2+}$  and  $\text{CH}_3\text{Hg}$  that agreed with the original values quantified in samples (two-tailed *Student's t*-test at 95% of the confidence limit). For  $\text{CH}_3\text{CH}_2\text{Hg}$ , fortifications at three concentration levels (0.100, 0.200 and 0.400  $\mu\text{g L}^{-1}$ ) were made in one PW sample (PW-1) and recoveries varied between 85 and 88 %.

Table 5.5 Quantification study after PW samples fortification with  $\text{Hg}^{2+}$  for the estimation of the original analyte content.

Sample	$\text{Hg}^{2+}$ fortification level ( $\mu\text{g L}^{-1}$ )	$\text{Hg}^{2+}$ found <sup>a</sup> ( $\mu\text{g L}^{-1}$ )	Original $\text{Hg}^{2+}$ recovered in the fortification experiment <sup>b</sup> ( $\mu\text{g L}^{-1}$ )	Average original $\text{Hg}^{2+}$ <sup>c</sup> ( $\mu\text{g L}^{-1}$ )
PW 5	3.00	$3.35 \pm 0.01$	$0.35 \pm 0.01$	$0.34 \pm 0.03$
	6.00	$6.33 \pm 0.03$	$0.33 \pm 0.02$	
	12.00	$12.34 \pm 0.04$	$0.34 \pm 0.02$	
PW 6	3.00	$3.63 \pm 0.02$	$0.63 \pm 0.02$	$0.63 \pm 0.02$
	6.00	$6.64 \pm 0.01$	$0.64 \pm 0.01$	
	12.00	$12.63 \pm 0.02$	$0.63 \pm 0.01$	
PW 7	3.00	$3.58 \pm 0.03$	$0.58 \pm 0.01$	$0.57 \pm 0.03$
	6.00	$6.57 \pm 0.02$	$0.57 \pm 0.02$	
	12.00	$12.58 \pm 0.02$	$0.58 \pm 0.02$	
PW 8	3.00	$3.39 \pm 0.03$	$0.39 \pm 0.02$	$0.38 \pm 0.03$
	6.00	$6.38 \pm 0.02$	$0.38 \pm 0.02$	
	12.00	$12.37 \pm 0.03$	$0.37 \pm 0.01$	

<sup>a</sup> Standard deviation based on the three total  $\text{Hg}^{2+}$  values found per sample.

<sup>b</sup> Values discounting the  $\text{Hg}^{2+}$  fortification concentration and the found concentration in the fortified sample (standard deviation for  $n = 3$ ).

<sup>c</sup> Average values were computing all fortification levels.

The results achieved for  $\text{Hg}^{2+}$  in PW-1 using the proposed method was  $0.35 \pm 0.02 \mu\text{g L}^{-1}$  being similar to  $0.33 \pm 0.01 \mu\text{g L}^{-1}$  obtained using the CV-AAS method, according to the two-tailed *Student t*-test ( $\alpha = 0.05$  and  $n = 3$ ). Results achieved using both methods were also statistically similar for the other ones as indicated as sample (result using GC-CV-AFS/result using CV-AAS): PW-2 ( $0.64 \pm 0.03 \mu\text{g L}^{-1} / 0.62 \pm 0.01 \mu\text{g L}^{-1}$ ), PW-3 ( $0.56 \pm 0.01 \mu\text{g L}^{-1} / 0.54 \pm 0.02 \mu\text{g L}^{-1}$ ) and PW-4 ( $0.39 \pm 0.01 \mu\text{g L}^{-1} / 0.37 \pm 0.01 \mu\text{g L}^{-1}$ ).

Table 5.6 Quantification study after PW samples fortification with CH<sub>3</sub>Hg for the estimation of the original analyte content.

Sample	CH <sub>3</sub> Hg fortification level (µg L <sup>-1</sup> )	CH <sub>3</sub> Hg found <sup>a</sup> (µg L <sup>-1</sup> )	Original CH <sub>3</sub> Hg recovered in the fortification experiment <sup>b</sup> (µg L <sup>-1</sup> )	Average original CH <sub>3</sub> Hg <sup>c</sup> (µg L <sup>-1</sup> )
PW 5	0.100	0.143 ± 0.003	0.043	0.042 ± 0.002
	0.200	0.240 ± 0.001	0.040	
	0.400	0.442 ± 0.002	0.042	
PW 6	0.100	0.122 ± 0.003	0.022	0.021 ± 0.001
	0.200	0.221 ± 0.001	0.021	
	0.400	0.421 ± 0.002	0.021	
PW 7	0.100	0.132 ± 0.002	0.032	0.032 ± 0.002
	0.200	0.234 ± 0.001	0.034	
	0.400	0.430 ± 0.001	0.030	
PW 8	0.100	0.154 ± 0.002	0.054	0.054 ± 0.002
	0.200	0.055 ± 0.002	0.055	
	0.400	0.053 ± 0.002	0.054	

<sup>a</sup> Standard deviation based on the three total CH<sub>3</sub>Hg values found per sample

<sup>b</sup> Values discounting the CH<sub>3</sub>Hg fortification concentration and the found concentration in the fortified sample (standard deviation for n = 3)

<sup>c</sup> Average values were computing all fortification levels.

### 5.3

#### Partial conclusion

An analytical method for the speciation of mercury in PW samples was developed using GC-CV-AFS after US extraction, aided by Triton X-114 (above the critical micelle concentration). Improved recovery of mercury species in oily and salty water samples was achieved during sample distillation, also improving efficiency in derivatization with sodium tetra(n-propyl)borate with reduced artifact formation. Conditions were adjusted to enable high recoveries in samples containing dispersed oil in the range from 20 to 60 mg L<sup>-1</sup> and salt in the range from 20 to 40 g L<sup>-1</sup>. Proper accuracy was achieved by matrix-matched calibration to compensate interferences imposed by major components of the PW samples. Studies in real PW samples enabled accurate results, and limits of detection were in the pg L<sup>-1</sup> level. The proposed method is an advance in the EPA Method 1630, allowing accurate mercury determinations in water samples from offshore petroleum operations since mercury in PW must attend specific limits before their disposal into the ocean. There are no reports of mercury speciation in PW samples

using the GC-CV-AFS. In this sense, the combination of procedures to improve analyte recovery in sample treatment and the use of calibration by matrix-matched analyte standards, to improve accuracy, are original contributions in ultra-trace determination of mercury.

## 6. Results and discussion III. Thiomersal photo-degradation with visible light-mediated by graphene quantum dots: indirect quantification using optical multipath mercury cold-vapor absorption spectrophotometry

A paper published as “*Thiomersal photo-degradation with visible light-mediated by graphene quantum dots: indirect quantification using optical multipath mercury cold-vapor absorption spectrophotometry.*” (Attachment A3).

It is important that all information taken from Chapter 4 of this thesis must be cited as J.R. Miranda-Andrades, S. Khan, C.A.T. Toloza, E.C. Romani, F.L. Freire Júnior, R.Q. Aucelio, *Thiomersal photo-degradation with visible light-mediated by graphene quantum dots: Indirect quantification using optical multipath mercury cold-vapor absorption spectrophotometry*, Spectrochim. Acta Part B At. Spectrosc. 138 (2017). doi:10.1016/j.sab.2017.10.011.

### 6.1

#### Abstract

Thiomersal is employed as a preservative in vaccines, cosmetics and pharmaceutical products due to its capacity to inhibit bacterial growth. Thiomersal contains 49.55 % of mercury in its composition, and its highly toxic ethylmercury degradation product has been linked to neurological disorders. The photo-degradation of thiomersal has been achieved by visible light using graphene quantum dots as catalysts. The generated mercury cold vapor (using adjusted experimental conditions) was detected by multipath atomic absorption spectrometry allowing the quantification of thiomersal at values as low as  $20 \text{ ng L}^{-1}$  even in complex samples as aqueous effluents of pharmaceutical industry and urine. A kinetic study (pseudo-first-order with  $k = 0.11 \text{ min}^{-1}$ ) and insights on the photo-degradation process are presented. The pictorial description of the work is presented in Figure 6.1.

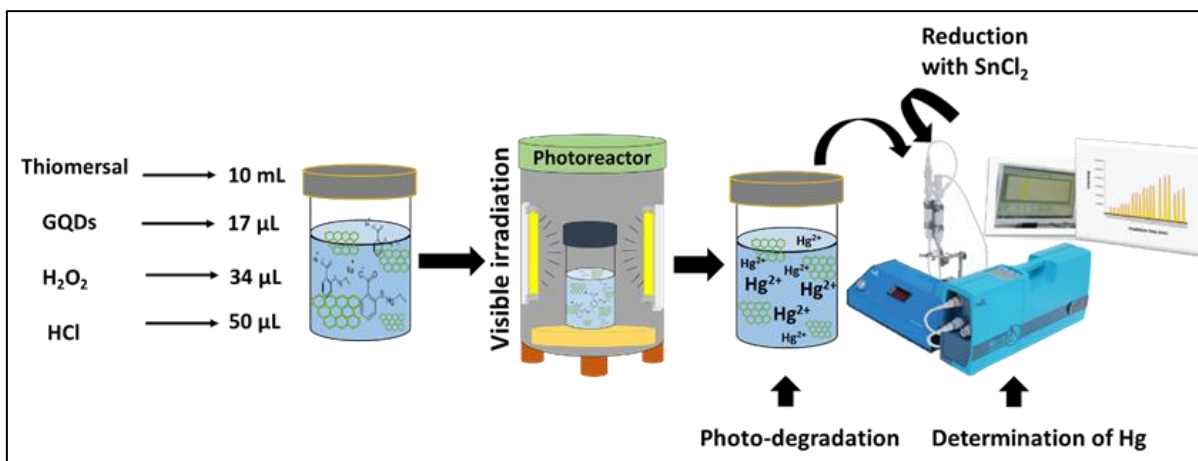


Figure 6.1 Graphical abstract

## 6.2

### Results and Discussion

#### 6.2.1

##### Preliminary studies

An aqueous solution of thiomersal ( $20 \text{ mg L}^{-1}$ ), placed into glass test tubes, was first exposed to visible radiation in the photochemical reactor. Periodically (every 10 min) an aliquot was collected, diluted and monitored by molecular absorption spectrophotometry. No changes in the typical absorption spectrum (Figure 6.2A) was found (intensities measured at 205 and 233 nm) over 140 min experiment. Residual mercury concentration (about  $10 \text{ ng L}^{-1}$ ), detected at the original solution, did not increase over the UV irradiation exposure time as thiomersal does not react with the reducing agent ( $\text{SnCl}_2$ ) thus no additional  $\text{Hg}^{2+}$  was formed to produce the Hg that was quantified by multipath-CV-AAS. In contrast, when the thiomersal solution (placed in quartz test tubes) was exposed to UV radiation, the degradation of thiomersal was observed over time (Figure 6.2B) but even after 80 min of UV exposure, a fraction of thiomersal (about 15 to 20%) could be still detected, indicating a relatively inefficient photo-degradation process. The previous addition of  $50 \text{ μL}$  of the GQDs synthesis dispersion into the solution irradiated with UV resulted in an initial decrease of the absorption band of thiomersal that ceased up after 50 min UV exposure (Figure 6.2C). The formation

of increased quantities of  $\text{Hg}^{2+}$  (latter converted into Hg for CV-AAS detection) was also observed during this period, stabilizing after 50 min (Figure 6.2D). As the solution of thiomersal in the presence of GQDs was exposed to UV, the opacity of the liquid increased indicating the aggregation of the carbon nanostructures (Figure 6.3), thus decreasing the catalytic properties of the carbon structures until thiomersal degradation was no longer observed.

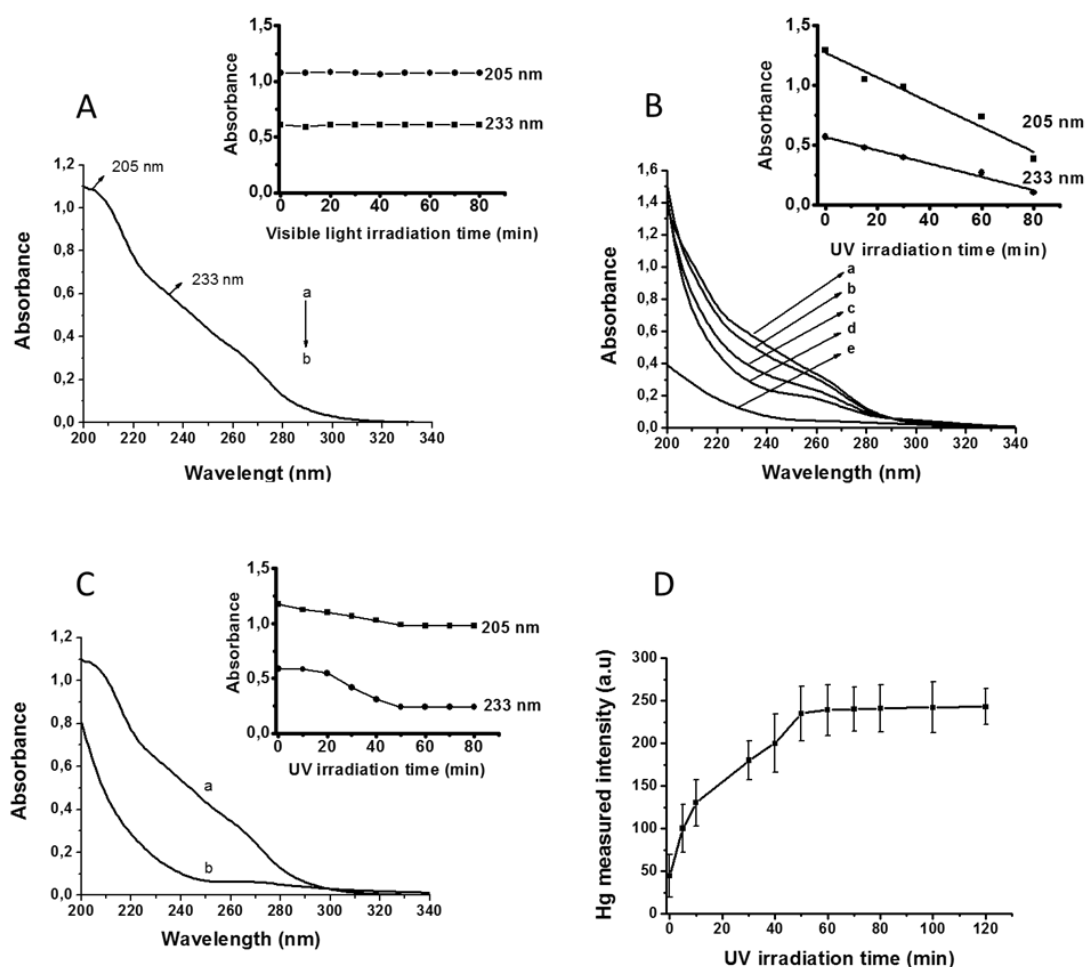


Figure 6.2 Absorption spectra of thiomersal (20 mg L<sup>-1</sup>) with detail showing the effect of radiation exposure (a. 0 min, b. 15 min, c. 30 min, d. 60 min, e. 80 min) to A) visible light and B) UV. C) Absorption spectra of thiomersal (20 mg L<sup>-1</sup>) in the presence of GQDs: (a) without incidence of UV and (b) after 50 min irradiation with UV, with detail showing the effect of UV radiation exposure; D) Hg measured signal from the UV treated thiomersal solution (50  $\mu\text{L}$  aliquot) in the presence of GQDs along UV incidence (error bar is the standard deviation for  $n=3$ ).

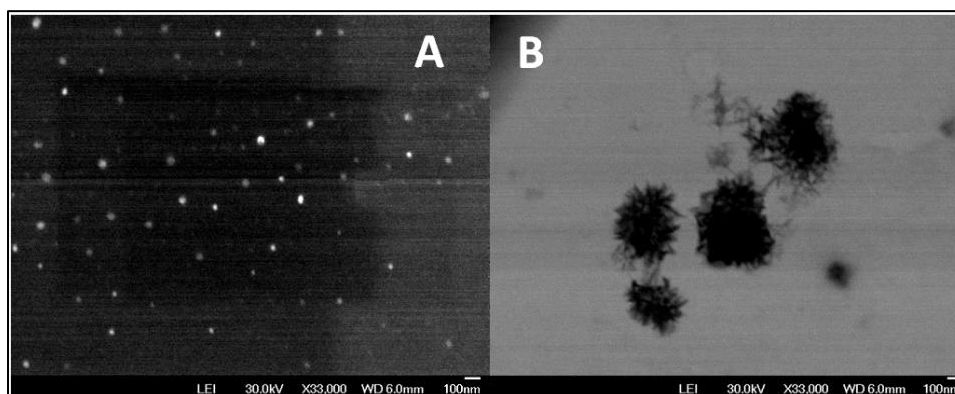


Figure 6.3 Scanning transmission electron microscopic image of A) GQDs nanoparticle dispersion after 50 min visible radiation exposure; B) GQDs nanoparticle dispersion after 50 min UV radiation exposure.

The experiment using dispersed GQDs (50  $\mu\text{L}$  of the synthesis dispersion) was repeated by irradiating the solution with visible radiation. In this case, the degradation of thiomersal further continued up to the point that its absorbance spectrum almost reached baseline (Figure 6.4A) at 80 min. In the graphic inserted (Figure 6.4A) it can be seen the thiomersal degradation monitored at two wavelengths (205 nm, and 233 nm) in the function of visible irradiation time (up to 80 min). The Hg measured (by CV-AAS) from aliquots of the solution along the experiment also increased up to 60 min visible radiation exposure (Figure 6.4B), indicating that a more effective degradation occurred.

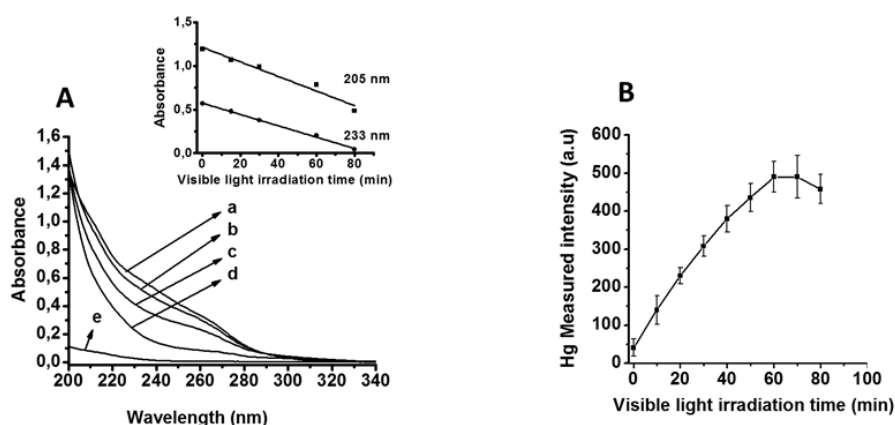


Figure 6.4 A) Absorption spectra of thiomersal ( $20 \text{ mg L}^{-1}$ ) in the presence of GQDs under the exposure to visible light: (a) 0 min, (b) 15 min, (c) 30 min, (d) 60 min, (e) 80 min. B) Hg measured signal from the UV treated thiomersal solution (50  $\mu\text{L}$  aliquot) in the presence of GQDs (after dilution) along with visible radiation incidence (error bar is the standard deviation for  $n=3$ ).

### 6.2.2

#### **Study of the conditions to improve the efficiency of the visible radiation photo-degradation of thiomersal mediated by GQDs**

The study of experimental conditions was made aiming to reduce time to achieve quantitative degradation of thiomersal. First, the experiment was performed using thiomersal solutions ( $100 \text{ ng L}^{-1}$ ) where different volumes of the GQDs synthesis dispersion (from 5 to 100  $\mu\text{L}$ , which corresponds to total carbon values from 1.8 to 35.2 mg) were added. The experiment was repeated three times by irradiation of samples during 15 min with aliquots of the irradiated samples transferred to the chemical reactor (to perform a final fast reduction of the formed  $\text{Hg}^{2+}$  with  $\text{SnCl}_2$ ) connected to the CV-AAS system. The result was quite interesting since the measured Hg increased up to 17  $\mu\text{L}$ , sharply decreasing to lower measured values as seen in Figure 6.5A. Such decreasing of the detected Hg at higher quantities of GQDs can be explained by repeating the experiments with the chemical reactor (still connected to the CV-AAS system) placed inside the photochemical reactor. The experiment indicated that GQDs itself not only converts thiomersal into  $\text{Hg}^{2+}$  but also can convert the formed  $\text{Hg}^{2+}$  into elemental Hg. Thus the release of Hg was continuous along the irradiation time (time profile an of Figure 6.5B) and increased as the added GQDs dispersion volume was higher than 17  $\mu\text{L}$  (time profiles b and c of Figure 6.5B), corroborating results shown in Figure 6.5A.

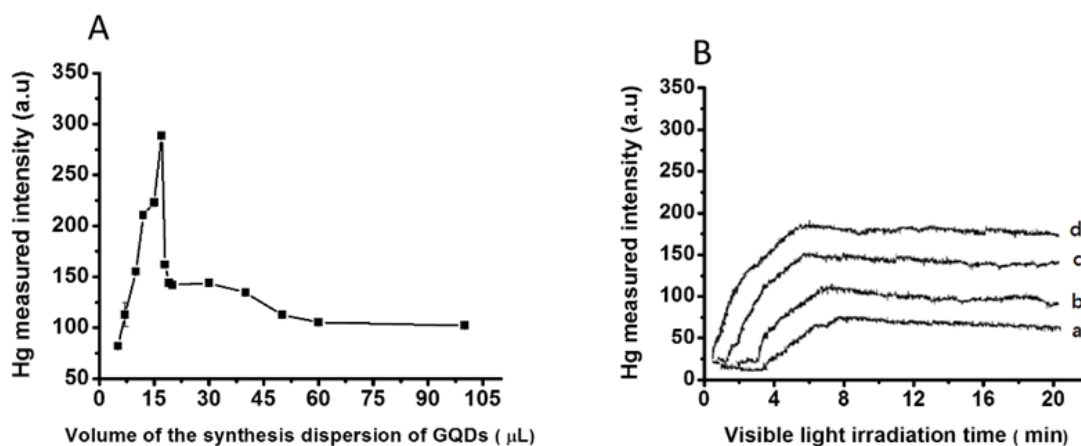


Figure 6.5. A) Hg measured signal (using CV-AAS after fast reduction with  $\text{SnCl}_2$ ) from solutions of thiomersal containing different volumes of the synthesis dispersion of GQDs; B) Time profile of the measured Hg release during visible radiation exposure of thiomersal ( $20 \text{ mg L}^{-1}$ ) in the presence of different volumes of the synthesis dispersion of GQDs: a)  $50 \text{ }\mu\text{L}$ , b)  $20 \text{ }\mu\text{L}$ , c)  $17 \text{ }\mu\text{L}$  and d)  $17 \text{ }\mu\text{L}$  with  $\text{H}_2\text{O}_2$  (1%).

Despite this fact, the option in this work was to perform a discontinued procedure to form Hg from  $\text{Hg}^{2+}$  by using  $\text{SnCl}_2$  in the chemical reactor rather than try to perform the slower formation of Hg using GQDs. Therefore, the chosen condition was the use of  $17 \text{ }\mu\text{L}$  of synthesis GQDs dispersion (equivalent to  $6 \text{ mg}$  total carbon) that seemed to produce the best efficient formation of  $\text{Hg}^{2+}$  with a lower further reduction to Hg.

The pH of the irradiated solution was adjusted (by adding small volumes of a  $0.1 \text{ mol L}^{-1}$  HCl solution), and the best pH range for the photo-degradation of thiomersal was between 4.5 and 5.5 (Figure 6.6A). At lower pH environment, it is reported that  $\text{H}^+$  compete with thiomersal to the sites on the surface of the GQDs, reducing its catalytic capability [127]. Alternatively, as the pH values become higher than 6.0, the negatively charged GQDs repulses the thiomersal anion, preventing them to make contact.

The light exposure time was studied using thiomersal solutions at pH 5.0 containing  $17 \text{ }\mu\text{L}$  of the synthesis dispersion of GQDs. Different test tubes were placed in the reactor, and one of them was taken out (every 5 min) to select an aliquot to be placed in the reduction reaction cell and measure Hg using CV-AAS. It was found that the maximum Hg signal was achieved after 25 min of light exposure (Figure 6.6B).

The addition of either formic acid or hydrogen peroxide is reported to improve degradation of thiomersal [81,82]. Therefore, amounts of either of these compounds were added into the visible irradiated solution containing GQDs in order to cover the range from 1 to 12 % v/v. The presence of formic acid did not increase the mercury signal measured by CV-AAS. In contrast, the presence of H<sub>2</sub>O<sub>2</sub> at 1 or 2 % improved the Hg signal measured by almost 70 % (Figure 6. 6C). The addition of H<sub>2</sub>O<sub>2</sub> also reduced the light exposure time to 20 min (Figure 6. 6D). An additional study was made to evaluate the effect of H<sub>2</sub>O<sub>2</sub> in the photo-degradation of thiomersal but in absence of GQDs. The study demonstrated that only H<sub>2</sub>O<sub>2</sub> is not enough to promote degradation of thiomersal by visible radiation.

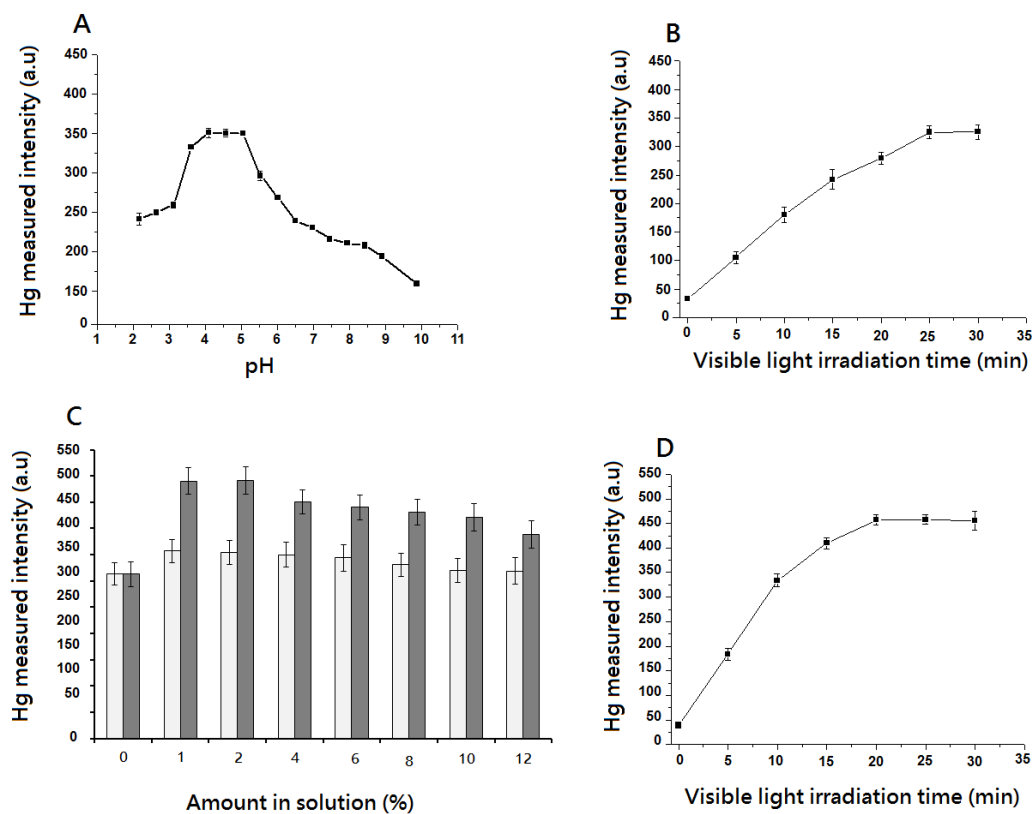


Figure 6.6. Hg measured from the photo-degraded thiomersal in the presence of 17  $\mu$ L aqueous dispersion of GQDs: A) in function of pH (25 min irradiation time); B) in function of time at pH 5.0; C) after 25 min irradiation time in the presence of either formic acid or hydrogen peroxide; D) in function of time at pH 5.0 in the presence of hydrogen peroxide 2 % v/v. Error bars are the standard deviations for n=3.

A Hg speciation study was made (using GC-CV-AAS) in order to monitor the formation of  $\text{CH}_3\text{CH}_2\text{Hg}$  previous to the formation of  $\text{Hg}^{2+}$ , under light exposure (mediated by GQDs) at the selected conditions. It was observed (Figure 6.7A) that the amounts formed of  $\text{CH}_3\text{CH}_2\text{Hg}$  (at retention time,  $t_R$ , about 5 min) increased from 5 to 15 min of visible light exposure time but they are shallow (at pg level in 50  $\mu\text{L}$  sampled volume), which indicates a fast conversion to  $\text{Hg}^{2+}$ . After 20 min light irradiation, the concentration of  $\text{CH}_3\text{CH}_2\text{Hg}$  drastically reduced, indicating that the photochemical reaction approaches the end. The signal from  $\text{CH}_3\text{CH}_2\text{Hg}$  measured at 0 min is due to the degradation of thiomersal, mediated by GQDs, under environmental light. Therefore, photo-reaction already occurs when GQDs is mixed to the thiomersal and solution is not protected from ambient light before placing into the reactor.

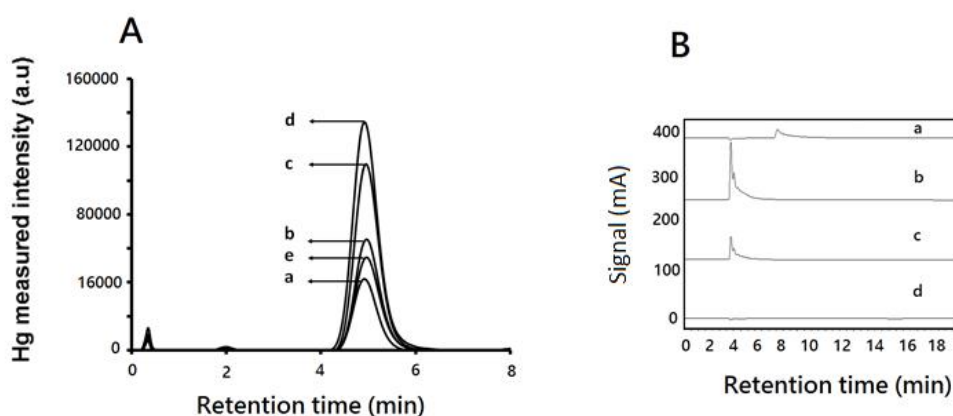


Figure 6.7 A) Chromatogram (GC-CV-AAS) showing the formation of  $\text{CH}_3\text{CH}_2\text{Hg}$  of a thiomersal solution along irradiation time: a) 0 min, b) 5 min, c) 10 min, d) 15 min, e) 20 min. B) Chromatogram (HPLC with detection at 222 nm) showing thiomersal and degradation products peak along time: a) 0 min, b) 5 min, c) 10 min, d) 15 min. Thiomersal solution containing 17  $\mu\text{L}$  of dispersion of GQDs, 2 %  $\text{H}_2\text{O}_2$ , and at pH 5.

### 6.2.3

#### Photo-catalytic oxidation efficiency

The interaction of the photon-excited GQDs with dissolved molecular oxygen, forming the very reactive superoxide radical, and with water, forming peroxide and hydroxyl radicals, produce a proper environment to degrade the nearby thiomersal, besides the possible direct interaction of thiomersal with the

photo-excited GQDs, in a possible similar mechanisms proposed by Roushani *et al.* [127]. Degradation due to the thiomersal self-photosensitization (in the presence of GQDs) pathway is not expected since it does not absorb significantly in the visible range.

These photocatalytic processes degrade thiomersal forming  $\text{CH}_3\text{CH}_2\text{Hg}$  that is then converted into  $\text{Hg}^{2+}$ , which in turn, in a reducing environment, is slowly reduced to Hg, as indicated in Figure 6.5B. In the presence of  $\text{H}_2\text{O}_2$ , the conversion of  $\text{Hg}^{2+}$  to Hg becomes more effective due to the presence of a larger quantity of free radicals formed from  $\text{H}_2\text{O}_2$  due to the incidence of light and the interaction with GQDs (profile of Figure 6.5B) but not fast enough to allow proper quantification by CV-AAS. That is the reason that a two-step procedure, using fast reduction made in a reduction cell with  $\text{SnCl}_2$ , was chosen for analytical purposes. Besides, the use of  $\text{SnCl}_2$  as a reducing agent is very selective in reducing  $\text{Hg}^{2+}$ , not producing foams or bubbles and not reducing organomercury species into Hg.

RP-HPLC with absorption photometric detection was performed in the thiomersal solutions submitted to the photochemical procedure mediated by GQDs (Figure 6.7B). The conditions used were the ones that enable resolved peaks from degradation products thiosalicylic (TSA) acid and dithiobenzoic acid (DTBA) [78]. Before light exposure, a sole peak of thiomersal is observed at  $t_R = 6.5$  min. As sample was exposed to light, the thiomersal peak rapidly disappeared (within 5 min) and a group of non-resolved peaks appeared in the 3 to 5 min  $t_R$  range (that include feature characteristic of TSA), which also decrease over time, forming non-absorbing degraded species, after 10 min of light exposure in acidic conditions. The appearing of a group of non-resolved peaks and their disappearance over time indicated the formation of a myriad of products, under the photochemical reaction conditions, that is further degraded to more simple non-absorbing species.

In order to evaluate the photocatalytic effect of a fixed amount of GQDs on thiomersal, an experiment was done by measuring the Hg formed by varying the amount of the analyte from  $10 \text{ ng L}^{-1}$  up to  $500 \text{ ng L}^{-1}$ . It was found that the magnitude of the measured Hg was directly proportional to the thiomersal content in the whole tested concentration range (Figure 6.8A). Thus this defined amount of GQDs is enough to three orders of magnitude of thiomersal.

A kinetic study has shown that a pseudo-first-order model holds for the photo-degradation of thiomersal as the GQDs concentration is kept at the fixed value that

enabled best catalytic performance. The relationships between the initial concentration of thiomersal ( $C_0$ ) and the concentration of this analyte over time ( $C_t$ ) in function of irradiation time with visible light, shown in Figure 6.8B and Figure 6.8C, corroborate such kinetic model. The experiment was made using three different initial concentrations of thiomersal (100, 200 and 300 ng L<sup>-1</sup>) and the obtained pseudo-first model kinetic constants were very close (respectively 0.1103; 0.1159 and 0.1154 min<sup>-1</sup>).

Finally, the effect of the presence of CH<sub>3</sub>Hg and CH<sub>3</sub>CH<sub>2</sub>Hg was evaluated in the photo-degradation of thiomersal mediated by GQDs. It was found that the presence of CH<sub>3</sub>Hg does not affect the expected Hg signal produced by thiomersal (at 100 ng L<sup>-1</sup>) even when CH<sub>3</sub>Hg was at the same concentration of thiomersal in the irradiated mixture. It is also important to point out that CH<sub>3</sub>Hg alone did not produce any signal above the expected baseline Hg signal. The selectivity towards CH<sub>3</sub>Hg is exciting and should be further studied in future work. In contrast, the presence of CH<sub>3</sub>CH<sub>2</sub>Hg produced an almost equivalent Hg signal that thiomersal produces. This can be observed in Figure 6.8D showing the signal ratios achieved by the thiomersal alone and the mixture containing the thiomersal in the presence of CH<sub>3</sub>CH<sub>2</sub>Hg (at concentrations of 1, 10 and 100 ng L<sup>-1</sup>). In samples containing thiomersal and CH<sub>3</sub>CH<sub>2</sub>Hg (as a degradation product) the Hg signal computed is related to the original non-degraded thiomersal.

#### 6.2.4

##### Analytical characteristics of the method

A sequence of standards covering concentrations of thiomersal from 10 ng L<sup>-1</sup> up to 500 ng L<sup>-1</sup> was used to construct three analytical curves (each one in a different day). A typical linear model is represented by the equation  $Y = (4.90 \pm 0.02 \text{ L ng}^{-1})X + (12.5 \pm 4.6)$  with  $R^2 = 0.9984$ . The limit of detection (6 ng L<sup>-1</sup>) and limit of quantification (20 ng L<sup>-1</sup>) were respectively achieved as the concentrations of thiomersal that enabled the Hg measured signal equivalent to 3  $s$  and 10  $s$ , where  $s$  was the standard deviation of the first measurable concentration of the analytical curve. The LOD value achieved in the present work is compared to the ones reported in literature in Table 6.1.

Precision was evaluated as instrumental precision (1.3 %), using the coefficient of variation of the signal produced by the analysis of 10 aliquots of the same thiomersal standard solution (at  $100 \text{ ng L}^{-1}$ ). The intermediary precision (2.0%) was evaluated as the coefficient of variation of the analyte recovery achieved by the analysis of ten independent thiomersal standard solutions (at  $100 \text{ ng L}^{-1}$ ).

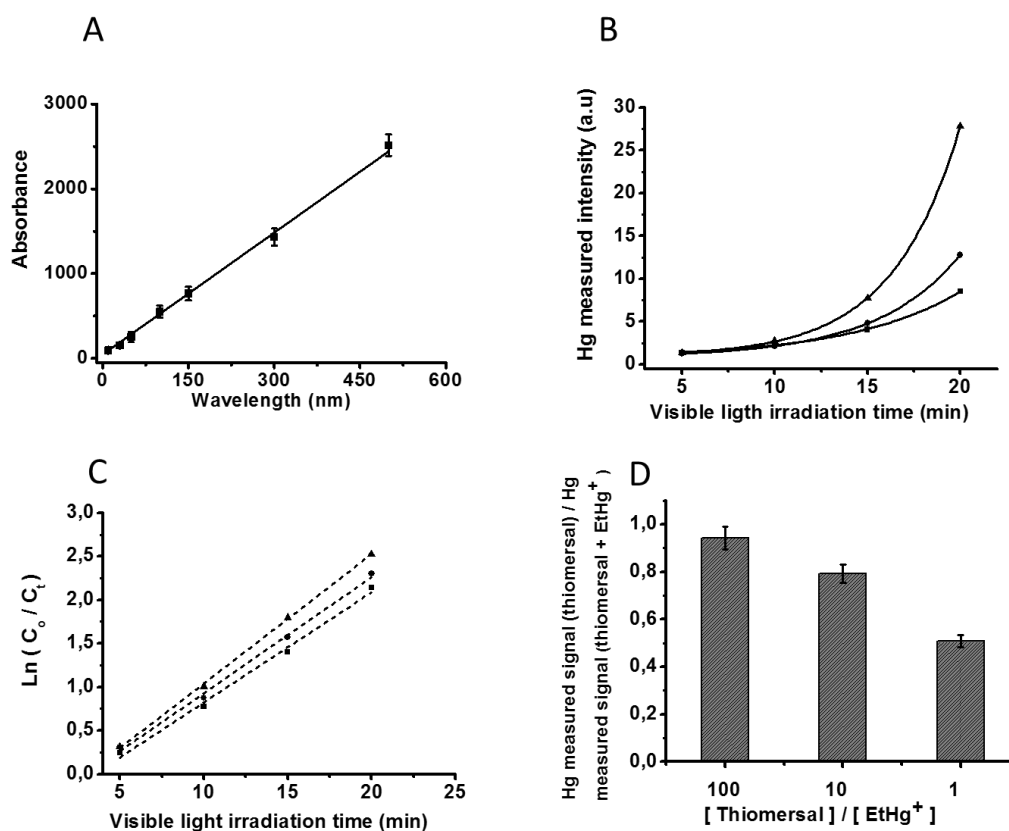


Figure 6.8 Hg measured signal by multipath-CV-AAS: A) in the function of the concentration of thiomersal. B) and C) in function of irradiation time of a thiomersal solution with  $C_0$  is the initial concentration ( $20 \text{ mg L}^{-1}$ ) and with  $C_t$  as concentration measured at different irradiation times. D) Effect of  $\text{CH}_3\text{CH}_2\text{Hg}$  on the thiomersal signal measured as Hg. Thiomersal solution containing  $17 \mu\text{L}$  of dispersion of GQDs, 2%  $\text{H}_2\text{O}_2$  and at pH 5. Error bars are the standard deviations for  $n=3$ .

Samples were analyzed to test the proposed method. One was a thiomersal based pharmaceutical formulation ( $9 \text{ mg L}^{-1}$ ) that was diluted 1000 times before analysis. The others were urine sample and a pharmaceutical industry effluent that was fortified with thiomersal (at, 100, 200 and  $300 \text{ ng L}^{-1}$ ). Analyzes of non-

fortified urine and pharmaceutical effluent samples showed  $\text{Hg}^{2+}$  mercury residues at the concentration of 7 and 11  $\text{ng L}^{-1}$  respectively.

In terms of analytical frequency, the photo-reaction could be made in ten different tubes at the same time (20 min treatment). Then, while the second load of tubes is inserted and irradiated, the first set of samples can be analyzed. Each solution can be determined in 2 min requiring the additional 1 min to perform cleaning before the next analysis (30 min total for the determination step for 10 samples).

Analyses were made in triplicate (in three different days) and the recovered results were 8.3  $\text{mg L}^{-1}$  ( $92.2 \pm 0.1 \%$ ) for the pharmaceutical formulation (already corrected for dilution), For urine the results were  $97.2 \pm 2 \text{ ng L}^{-1}$  (recovery of  $97.2 \pm 1.0\%$ ),  $193.4 \pm 1.0 \text{ ng L}^{-1}$  (recovery of  $96.7 \pm 1.0 \%$ ) and  $294.5 \pm 3 \text{ ng L}^{-1}$  (recovery of  $98.1 \pm 1.0\%$ ). For the pharmaceutical industry effluent samples the results were  $95.6 \pm 2 \text{ ng L}^{-1}$  (recovery of  $95.6 \pm 1.0 \%$ ),  $188 \pm 2.0 \text{ ng L}^{-1}$  (recovery of  $94.0 \pm 1.1 \%$ ) and  $292.8 \pm 3 \text{ ng L}^{-1}$  (recovery of  $97.6 \pm 1.0 \%$ ).

Table 6.1 Information on methods for the determination of thiomersal reported in the literature and the proposed method.

Method	Sample	LOD ( $\mu\text{g L}^{-1}$ )	Reference
RP-HPLC-UV	ophthalmic solution and vaccines	500	[76]
RP-HPLC-UV chemical derivatization	pharmaceutical solution and vaccines	300	[155]
RP-HPLC coulometric detection	ophthalmic solution	2000	[78]
RP-HPLC indirect fluorimetric detection and UV derivatization	pharmaceutical industry aqueous effluent	729	[87]
Colorimetry after chemical derivatization	vaccine	200	[80]
FIA with colorimetric detection	vaccine	70	[83]
Differential-pulse voltammetry with mercury-film electrode	vaccine	0.81	[86]
CV-AAS derivatization using UV	ophthalmic solution	40	[81]
CV-ICP-OES with UV derivatization	vaccines	0.6	[82]
CV-AFS	vaccines	0.06	[68]
FIA coupled with MW-assisted photochemical	Ophthalmic solution	3	[84]
RP-HPLC coupled AFS	pharmaceutical industry aqueous effluent	0.09	[75]
CV-AAS	pharmaceutical industry aqueous effluent	0.006	This work

RP-HPLC-UV: reversed-phase high-performance liquid chromatography with absorption detection in the UV; FIA: flow-injection analysis; MW: microwave; CV: cold vapour technique; AAS: atomic absorption spectrometry; AFS: atomic fluorescence detection.

### 6.3

#### Partial conclusion

Cold vapor atomic absorption spectrometry, using a multipass cell, provided the indirect determination of thiomersal, which was degraded in a photochemical reactor (using graphene quantum dots and visible radiation), then rapidly reduced to Hg with  $\text{SnCl}_2$ . Degradation with graphene quantum dots was very useful (following a pseudo-first-order kinetic) and made under adjusted conditions to maximize formation of  $\text{Hg}^{2+}$  and minimize formation of Hg in the photochemical

reaction step. The method was tested in samples with satisfactory recoveries at the ng L<sup>-1</sup> range, which is at least one order of magnitude lower than the most sensitive method reported in the literature for thiomersal.

## 7. Results and discussion IV. Photo-generation of mercury cold vapor mediated by a graphene quantum dots/TiO<sub>2</sub> nanocomposite: on-line ultra-trace speciation of mercury and kinetic studies.

The present chapter is presented in the format required to be submitted as an article in a scientific journal.

### 7.1

#### Abstract

This work presents a method for the speciation of mercury using a nanocomposite, consisting of GQDs and TiO<sub>2</sub> nanoparticles (GQDs-TiO<sub>2</sub> NPs), to mediate the photolytic degradation of mercurial species forming efficiently Hg<sup>0</sup> (without the need for chemical agents) that was detected by CV-AAS. For the determination, a sample solution (containing Hg<sup>2+</sup>, CH<sub>3</sub>CH<sub>2</sub>Hg, and CH<sub>3</sub>Hg at hundreds of ng L<sup>-1</sup>) were placed in quartz tubes, inside a photochemical reactor, and directly adapted to the mercury-dedicated spectrometer. For photocatalytic degradation, a microliter aliquot of GQDs-TiO<sub>2</sub> dispersion (0.6 mg of GQDs-TiO<sub>2</sub> nanocomposite) was added to the sample solution under adjusted conditions (pH 3, and containing formic acid 2 % v/v). Under these conditions, quantitative speciation was successfully achieved taking advantage of the differences in UV photodegradation kinetics: Hg<sup>2+</sup> (5 min), CH<sub>3</sub>CH<sub>2</sub>Hg (9 min) and 13 min for CH<sub>3</sub>Hg. The evaluation of the photodegradation kinetics was also made by GC-CV-AFS, which confirmed the differentiated decreasing in concentrations of Hg<sup>2+</sup>, CH<sub>3</sub>CH<sub>2</sub>Hg and CH<sub>3</sub>Hg during photo-degradation. The LOD of the method was 7

ng L<sup>-1</sup> for Hg<sup>2+</sup> and CH<sub>3</sub>Hg and 10 ng L<sup>-1</sup> for CH<sub>3</sub>CH<sub>2</sub>Hg. Figure 7.1 presents a illustration that represent the proposed method.

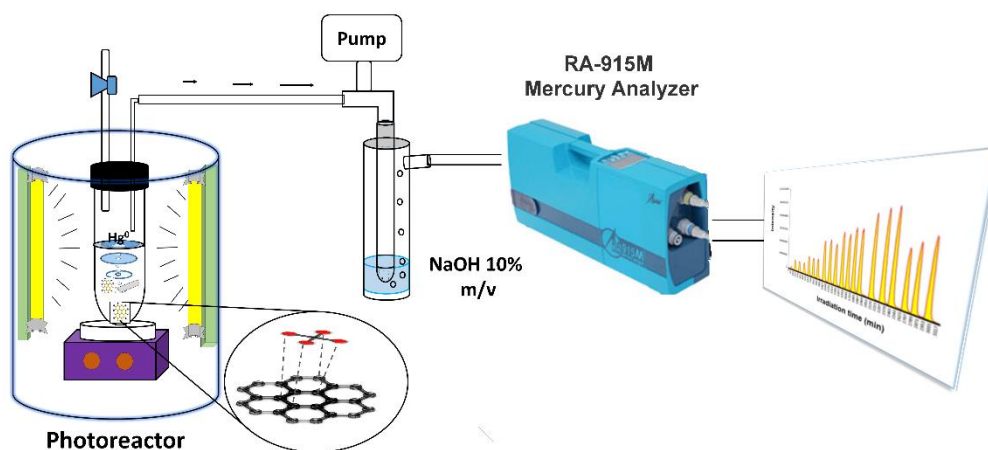


Figure 7.1 Graphical Abstracts

## 7.2

### Results and discussion

#### 7.2.1

##### Preliminary studies concerning the photo-reduction of Hg<sup>2+</sup>

Preliminary studies were performed to evaluate photocatalytic activity of the nanocomposite made of GQDs and P<sub>25</sub>-TiO<sub>2</sub> nanoparticles (GQDs-TiO<sub>2</sub> NPs) in reducing Hg<sup>2+</sup>, compared to the photocatalytic activities promoted by either P<sub>25</sub>-TiO<sub>2</sub> nanoparticles or GQDs (made from citric acid). Photocatalytic activities were compared as a rate of degradation of a standard aqueous solution of Hg<sup>2+</sup> (1 µg L<sup>-1</sup>) under the exposure to UV in acidic condition (about pH 4). For these studies, 5 mL aliquots of the standard Hg<sup>2+</sup> solution (containing 5 ng of mercury) were transferred to quartz tubes, placed inside a photo-reactor, on the top of a magnetic stirrer plate. The tube was stoppered with a rubber stopper (foiled with a Teflon tape) containing two openings, one for a glass tube connected to the CV-AAS system (by means of a silicone tube) and the other for an L-shaped glass tube,

connected to a glass stopcock, that was used to open or close the system to the air. The end of the L-shaped glass tube inside the quartz tube was kept about 2 cm above the solution in order not to promote bubbling. The solution was stirred and exposed to the UV, during specific times, before turning on the pump of the CV-AAS system and opening the system to the air to promote a continuous forced airflow to carry the mercury cold vapor to the spectrometer. Aliquots of 200  $\mu\text{L}$  of a nanomaterial dispersion (GQDs-TiO<sub>2</sub> or P<sub>25</sub>-TiO<sub>2</sub>) were added to the Hg<sup>2+</sup> standard solution under continuous stirring. The dispersions were prepared by adding 30 mg of nanomaterial in 5 mL water and sampling the 200  $\mu\text{L}$  under continuous stirring. Taking into consideration both the TC value of the GQDs-TiO<sub>2</sub> nanocomposite dispersion (18 mg L<sup>-1</sup>) and the aliquot volume, around 3  $\mu\text{g}$  of carbon was added to the Hg<sup>2+</sup> solutions. The efficiency of the photocatalytic reaction was evaluated by measuring the Hg<sup>0</sup> vapor generated as result of the photocatalytic degradation of Hg<sup>2+</sup> within the time interval of 70 min. As a quantitative reference, the mercury vapor produced by chemical reduction (using SnCl<sub>2</sub> with no addition of nanomaterial and no UV exposure) was also measured.

It is relevant to mention that the exposure of the solutions to radiation in the visible range, in the presence of the nanomaterials, does not promote the reduction of Hg<sup>2+</sup> as the mercury vapor measured was similar to the background levels (obtained from the standard solution exposed to visible radiation in the absence of nanomaterial). The measured values (in terms of relative signal) observed after exposure to the UV are shown in Figure 7.2 along with the reference value obtained by the chemical reduction using SnCl<sub>2</sub>. It is also important to point out that when GQDs dispersions are exposed to the UV, the nanomaterials tend to aggregate, forming bulk carbon particles with no quantum confinement properties [156] and, therefore, hindering its ability to catalyze the reduction of Hg<sup>2+</sup>. This is demonstrated in Figure 7.2 (line *d*) for an experiment made with a GQDs dispersion aliquot of about 3  $\mu\text{g}$  total carbon. A significant difference in photocatalytic efficiency was found for GQDs-TiO<sub>2</sub> when compared to P<sub>25</sub>-TiO<sub>2</sub>. The estimated rate of mercury reduction obtained using GQDs-TiO<sub>2</sub> (0.072 ng min<sup>-1</sup>, calculated from line *b* of Figure 7.2) was about 2.9 times the one observed using P<sub>25</sub>-TiO<sub>2</sub> (0.025 ng min<sup>-1</sup>, calculated from line *c* of Figure 7.2A). It was also found that maximum reduction using GQDs-TiO<sub>2</sub> was obtained after 50 min of UV exposure while P<sub>25</sub>-TiO<sub>2</sub> took 60 min to produce maximum reduction.

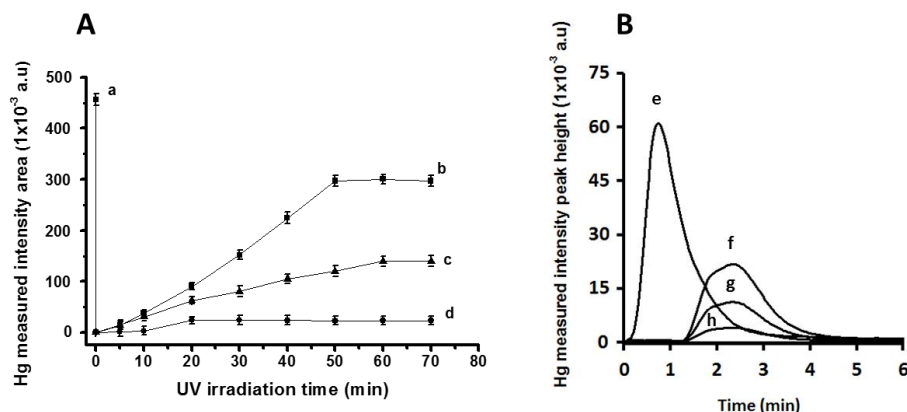


Figure 7.2. (A) Photocatalytic production of  $\text{Hg}^0$  in function of UV exposure time: (a) reference signal (from  $1 \mu\text{g L}^{-1}$  of  $\text{Hg}^{2+}$ ) obtained through chemical reduction with  $\text{SnCl}_2$ ; (b) ( $1 \mu\text{g L}^{-1}$ )  $\text{Hg}^{2+}$  reduction value using GQDs- $\text{TiO}_2$ ; (c) from  $\text{Hg}^{2+}$  ( $1 \mu\text{g L}^{-1}$ ) in the presence of  $\text{P25-TiO}_2$ ; (d) from  $\text{Hg}^{2+}$  ( $1 \mu\text{g L}^{-1}$ ) in the presence GQDs. (B) Temporal profiles for  $\text{Hg}^0$  (e) obtained from  $\text{Hg}^{2+}$  through chemical reduction with  $\text{SnCl}_2$ ; (f) obtained from  $\text{Hg}^{2+}$  ( $1 \mu\text{g L}^{-1}$ ) in the presence of GQDs- $\text{TiO}_2$  and (g) obtained from  $\text{Hg}^{2+}$  ( $1 \mu\text{g L}^{-1}$ ) in the presence of  $\text{P25-TiO}_2$ ; (h) obtained from  $\text{Hg}^{2+}$  ( $1 \mu\text{g L}^{-1}$ ) in the presence of GQDs.

Taking into consideration the total mercury content in solution and the reference signal obtained using chemical reduction (point *a* in Figure 7.2A), the maximum efficiency in reduction was 67 % for GQDs- $\text{TiO}_2$  and 31 % for  $\text{P25-TiO}_2$ . Such a result indicate that the GQDs modified  $\text{TiO}_2$  nanoparticles (nanocomposite) present differentiated catalytic properties, and the association of GQDs and  $\text{TiO}_2$  (probably decorating the surface of  $\text{TiO}_2$ ) minimized aggregation of the carbon nanoparticles under UV. Temporal profiles for  $\text{Hg}^0$  achieved by using GQDs- $\text{TiO}_2$  is compared to the one observed using chemical reduction by  $\text{SnCl}_2$  in Figure 7.2B.

## 7.2.2

### Adjustment of instrumental conditions to measure mercury vapor produced by photo-catalysis using GQDs- $\text{TiO}_2$ nanocomposite

In order to promote the photocatalytic reaction of  $\text{Hg}^{2+}$ , nanomaterials were kept evenly dispersed by magnetic stirring rather than by the bubbling of the solution with the forced air since stirring was found better to control reproducibility

of the process. Aiming to maximize the efficiency of the CV-AAS spectrometer (attached to the reaction cell) in collecting the formed mercury cold vapor, chemical reduction of  $\text{Hg}^{2+}$  ( $1 \mu\text{g L}^{-1}$  standard solution) by  $\text{SnCl}_2$  20 % v/v (no nanomaterial added) were performed using the quartz tube cell (Figure 7.3A) under stirring and compared to the traditional reduction procedure using bubbler cell (Figure 7.3B). Before addition of standard solution (5 mL), the reducing reagent (2 mL) was placed into the quartz tube then stirred (during 1 min), with the magnetic bar, to remove any residual mercury. The same was made when using the bubbler cell (with bubbling the reducing reagent for 1 min) after addition of the standard  $\text{Hg}^{2+}$  solution

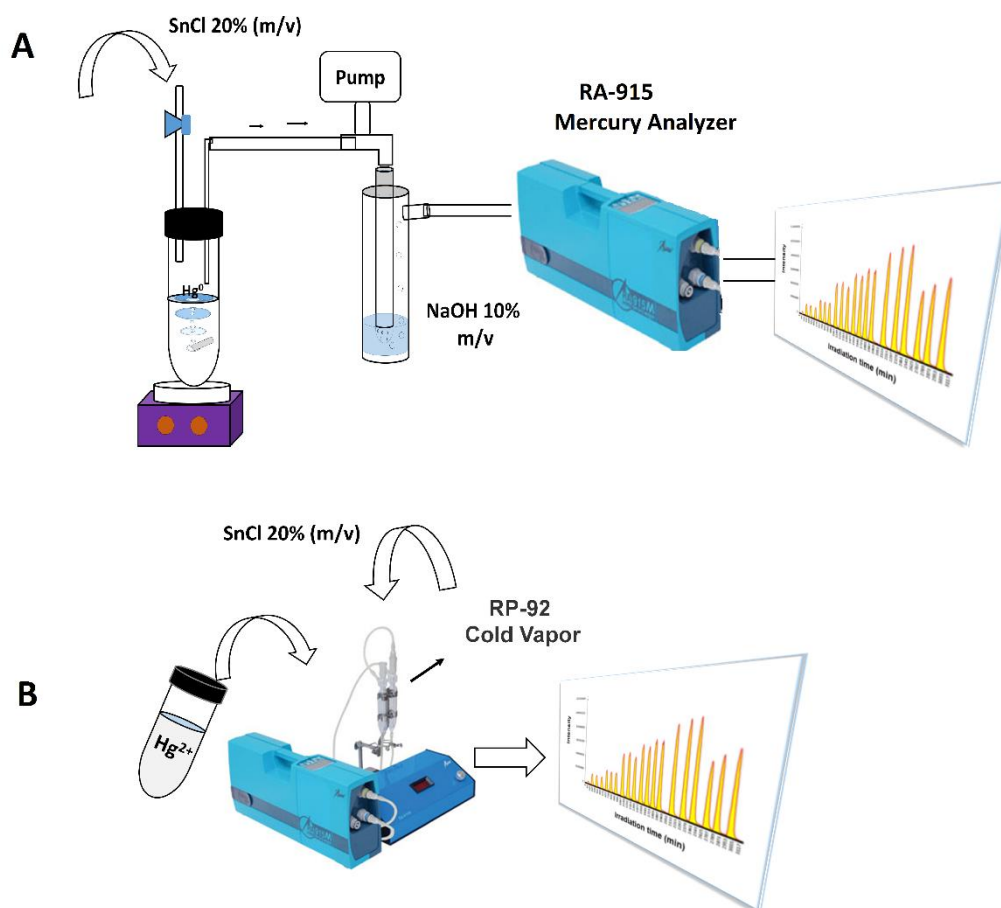


Figure 7.3 Instrumental conditions to measure mercury vapor produced by photo-catalysis performed using the quartz tube cell (A) and The traditional reduction procedure using bubbler cell (B).

The transport of  $\text{Hg}^0$  formed in the quartz tube cell was optimized by adjusting the airflow of the CV-AAS system (system pump flow rate) aiming to achieve the typical mercury time profile obtained with the bubbler cell with an air flow rate of  $1 \text{ mL min}^{-1}$  (Figure 7.4, time profile a). A similar profile (about 94 % in area) was achieved using the quartz tube cell with a flow rate of  $3 \text{ mL min}^{-1}$  as seen in Figure 7.4 (time profile b). The release of mercury from solution under stirring was slower when compared with the bubbler; therefore, a higher suction flow rate was required and a delayed time profile was obtained.

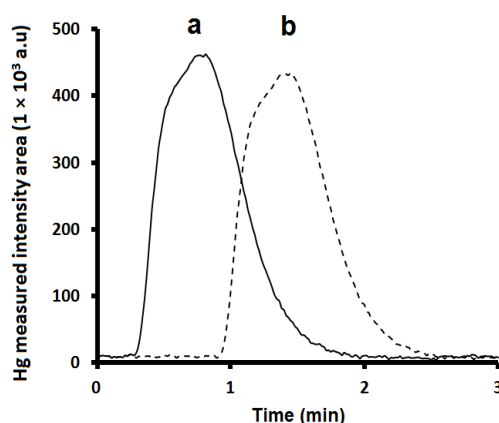


Figure 7.4 Comparison time profile of reduction ( $1 \mu\text{g L}^{-1} \text{Hg}^{2+}$  standard solution) using: (a) chemical reduction by  $\text{SnCl}_2$  20 % v/v; (b) Reduction promoted by GQDs- $\text{TiO}_2$ .

### 7.2.3

#### Photo-degradation of $\text{CH}_3\text{Hg}$ and $\text{CH}_3\text{CH}_2\text{Hg}$ .

As GQDs- $\text{TiO}_2$  NPs was efficient in promoting photo-reduction of  $\text{Hg}^{2+}$  under UV, the photocatalytic effect of GQDs- $\text{TiO}_2$  NPs upon organic mercurial species ( $\text{CH}_3\text{Hg}$  and  $\text{CH}_3\text{CH}_2\text{Hg}$ ) was also studied. The photocatalytic activities were evaluated as a degradation rate of standard aqueous solutions of  $\text{CH}_3\text{Hg}$  and  $\text{CH}_3\text{CH}_2\text{Hg}$  (at  $1 \mu\text{g L}^{-1}$ ) under UV at the original pH of the solutions (around pH 6). The efficiency of reaction was assessed by measuring the  $\text{Hg}^0$  vapor generated upon UV exposure (solutions exposed within the time interval from 5 to 70 min

before opening the quartz tube to the system for signal acquisition). These studies were performed following the same experimental conditions and procedure used during studies concerning  $\text{Hg}^{2+}$  with 5 mL of organomercury standard solutions ( $1 \mu\text{g L}^{-1}$ ) transferred to quartz tubes (equivalent to 5 ng of organomercury) along with 200  $\mu\text{L}$  aliquots of nanomaterial dispersions (GQDs-TiO<sub>2</sub> NPs or P<sub>25</sub>-TiO<sub>2</sub> NPs) kept under continuous magnetic stirring, inside a photoreactor. Mercury vapor detected after chemical reduction (using  $\text{SnCl}_2$  without addition of nanomaterials and no UV exposure) and through photo-reduction of  $\text{Hg}^{2+}$  (achieved in the presence of GQDs-TiO<sub>2</sub> nanocomposite) were used as quantitative reference.

The exposure of organic mercurial species, in the presence of either P<sub>25</sub>-TiO<sub>2</sub> NPs or GQDs-TiO<sub>2</sub> NPs, produced  $\text{Hg}^0$  similar to the background levels obtained from standard solutions exposed to visible radiation in the absence of nanomaterial. However, under UV radiation, nanomaterials promoted the formation of  $\text{Hg}^0$  from both the mercurial species as seen in Figures 7.5 for  $\text{CH}_3\text{Hg}$  and Figure 7.6 for  $\text{CH}_3\text{CH}_2\text{Hg}$  showing the recovered mercury (in relative signal) in function of UV exposure time and the temporal profiles of the generated mercury vapor during signal acquisition.

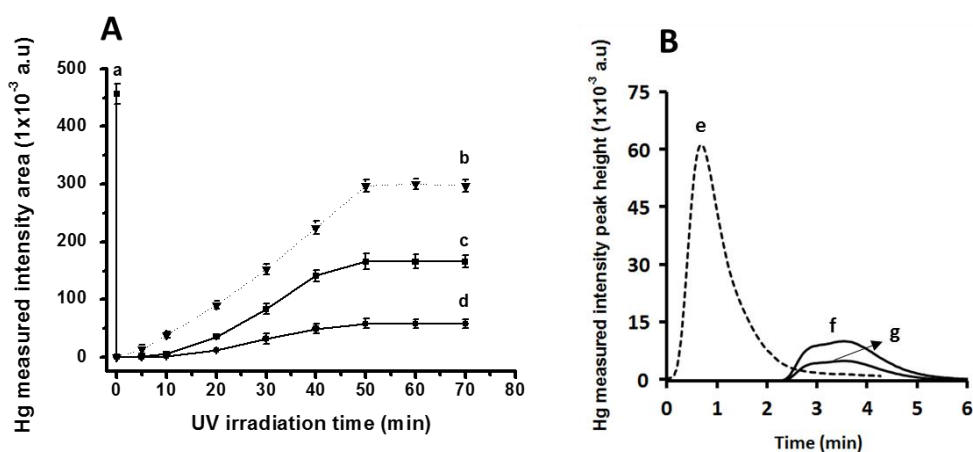


Figure 7.5. (A) Photocatalytic production of  $\text{Hg}^0$  in function of UV exposure time: (a) reference signal (from  $1 \mu\text{g L}^{-1}$  of  $\text{Hg}^{2+}$ ) obtained through chemical reduction with  $\text{SnCl}_2$ ; (b) reference ( $1 \mu\text{g L}^{-1}$ )  $\text{Hg}^{2+}$  reduction value using GQDs-TiO<sub>2</sub>; (c) from  $\text{CH}_3\text{Hg}$  ( $1 \mu\text{g L}^{-1}$ ) in the presence of GQDs-TiO<sub>2</sub>; (d) from  $\text{CH}_3\text{Hg}$  ( $1 \mu\text{g L}^{-1}$ ) in the presence of P<sub>25</sub>-TiO<sub>2</sub>. (B) Temporal profiles for  $\text{Hg}^0$  (e) obtained from  $\text{Hg}^{2+}$  through chemical reduction with  $\text{SnCl}_2$ ; (f) obtained from  $\text{CH}_3\text{Hg}$  in the presence of GQDs-TiO<sub>2</sub> and (g) obtained from  $\text{CH}_3\text{Hg}$  in the presence of P<sub>25</sub>-TiO<sub>2</sub>.

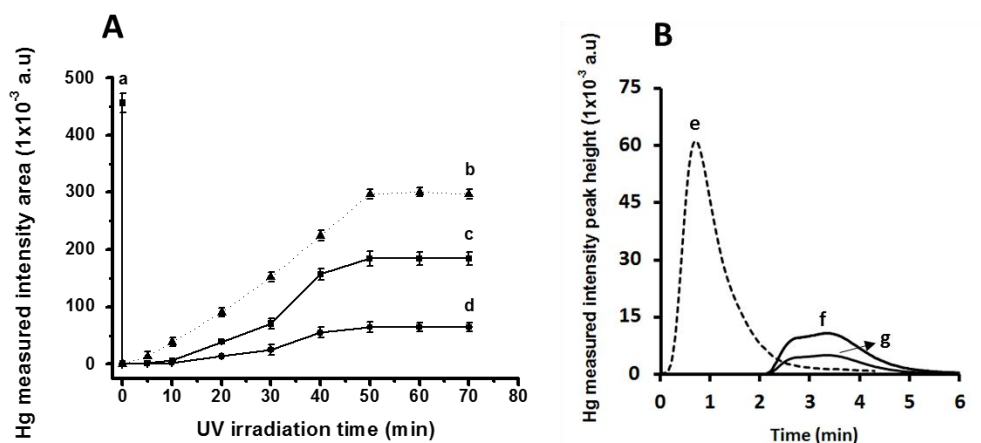


Figure 7.6. (A) Photocatalytic production of  $\text{Hg}^0$  in function of UV exposure time: (a) reference signal (from  $1 \mu\text{g L}^{-1}$  of  $\text{Hg}^{2+}$ ) obtained through chemical reduction with  $\text{SnCl}_2$ ; (b) reference ( $1 \mu\text{g L}^{-1}$ )  $\text{Hg}^{2+}$  reduction value using GQDs-TiO<sub>2</sub>; (c) from  $\text{CH}_3\text{CH}_2\text{Hg}$  ( $1 \mu\text{g L}^{-1}$ ) in the presence of GQDs-TiO<sub>2</sub>; (d) from  $\text{CH}_3\text{CH}_2\text{Hg}$  ( $1 \mu\text{g L}^{-1}$ ) in the presence of P<sub>25</sub>-TiO<sub>2</sub>. (B) Temporal profiles for  $\text{Hg}^0$  (e) obtained from  $\text{Hg}^{2+}$  through chemical reduction with  $\text{SnCl}_2$ ; (f) obtained from  $\text{CH}_3\text{CH}_2\text{Hg}$  in the presence of GQDs-TiO<sub>2</sub> and (g) obtained from  $\text{CH}_3\text{CH}_2\text{Hg}$  in the presence of P<sub>25</sub>-TiO<sub>2</sub>.

In terms of photocatalytic efficiency in degrading the organic mercurial species, the GQDs-TiO<sub>2</sub> NPs was more efficient when compared to P<sub>25</sub>-TiO<sub>2</sub> NPs, in both cases producing maximum intensity in measured  $\text{Hg}^0$  after 50 min of UV exposure. The  $\text{CH}_3\text{Hg}$  photo-degradation rate (estimated by the sensitivity of the best linear fit between the mercury amounts recovered between 10 and 50 min of UV exposure) was 2.7 times higher in the presence of GQDs-TiO<sub>2</sub> ( $19 \text{ ng min}^{-1}$ ) than in the presence of P<sub>25</sub>-TiO<sub>2</sub> NPs ( $7 \text{ ng min}^{-1}$ ). In terms of the recovered  $\text{Hg}^0$  (taking as a reference the recovered value using chemical reduction) the use of GQDs-TiO<sub>2</sub> NPs produced 39.1 % and P<sub>25</sub>-TiO<sub>2</sub> NPs only 15.1 % of the total mercury content in solution (percent values corrected taking into consideration the mercury content in  $\text{CH}_3\text{Hg}$ ). For  $\text{CH}_3\text{CH}_2\text{Hg}$ , the photo-degradation rate observed using GQDs-TiO<sub>2</sub> NPs ( $20 \text{ ng min}^{-1}$ ) was 3.3 times higher in the presence of P<sub>25</sub>-TiO<sub>2</sub> NPs ( $6 \text{ ng min}^{-1}$ ). Recovered  $\text{Hg}^0$  achieved from  $\text{CH}_3\text{CH}_2\text{Hg}$  were 49.7 % and 16.3% of the  $\text{Hg}^0$  measured from the mercury content (percent values corrected, taking into consideration the mercury content in  $\text{CH}_3\text{CH}_2\text{Hg}$ ).

In order to understand the UV induced photocatalytic reactions promoted by GQDs-TiO<sub>2</sub> NPs, a speciation study was performed using a gas-chromatographic system coupled with mercury cold vapor dedicated atomic spectrometry

fluorescence (GC-CV-AFS). For the experiments made using either  $\text{CH}_3\text{Hg}$  or  $\text{CH}_3\text{CH}_2\text{Hg}$ , an aliquot of mercurial standard (equivalent to 150 pg and 300 pg for  $\text{CH}_3\text{Hg}$  and  $\text{CH}_3\text{CH}_2\text{Hg}$  respectively) was introduced into the system to be derivatized with the propylation agent in order to obtain a chromatographic reference as seen in Figure 7.7A and Figure 7.7B (as solid lines). The reference chromatogram show typical peaks for  $\text{CH}_3\text{Hg}$  (at  $1.86 \pm 0.01$  min) and  $\text{CH}_3\text{CH}_2\text{Hg}$  ( $4.37 \pm 0.02$  min) and residual reduced mercury (consisting mostly of background Hg and artifact Hg) at ( $0.38 \pm 0.02$  min). As these standard solutions have been exposed to UV (25 min for  $\text{CH}_3\text{Hg}$  and 15 min for  $\text{CH}_3\text{CH}_2\text{Hg}$ ), in the presence of GQDs-TiO<sub>2</sub> NPs, before transferring to the GC-CV-AFS (to be propylated, separated and detected as  $\text{Hg}^0$ ), the profile (as dotted line) showed significant decreasing of organic mercurial content, appearance of the typical peak of  $\text{Hg}^{2+}$  and significant increasing of the  $\text{Hg}^0$  peak magnitude. The overall result indicated that mediation of GQDs-TiO<sub>2</sub> NPs promotes the photo-degradation of organic mercury into  $\text{Hg}^{2+}$  due to the formation of  $\cdot\text{OH}$  free radicals. Besides, upon UV, the formed GQDs excitonic becomes a source of electrons to improve TiO<sub>2</sub> NPs efficiency in promoting the reduction of  $\text{Hg}^{2+}$ .

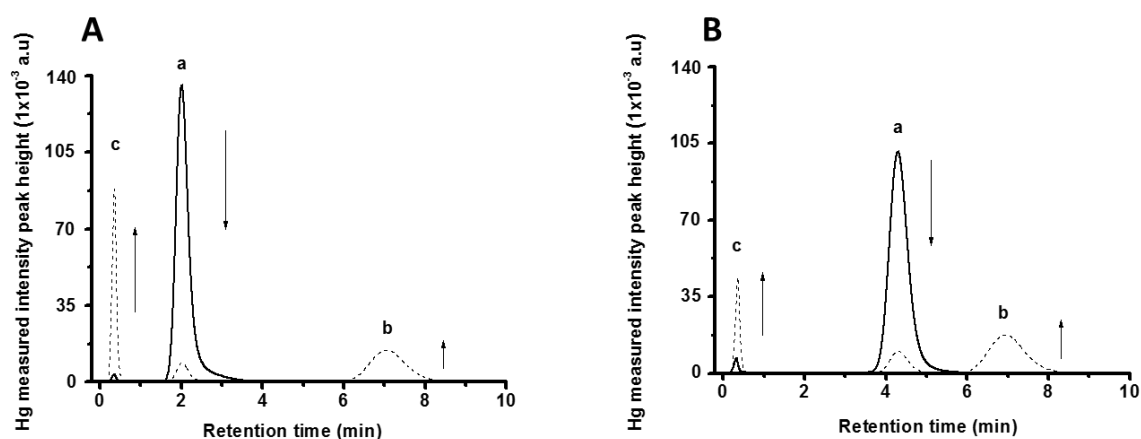


Figure 7.7. (A) Typical chromatograms obtained using the GC-CV-AFS system after propylation (at pH 4.0) of an organic mercury species (150 and 300 pg): A) for  $\text{CH}_3\text{Hg}$  prior to UV exposition (solid line) and after 50 min of UV exposure in the presence of GQDs-TiO<sub>2</sub> (dashed line); B) for  $\text{CH}_3\text{CH}_2\text{Hg}$  prior to UV exposition (solid line) and after 50 min of UV exposure in the presence of GQDs-TiO<sub>2</sub> (dashed line). Organic species ( $\text{CH}_3\text{Hg}$  or  $\text{CH}_3\text{CH}_2\text{Hg}$ ) (a),  $\text{Hg}^{2+}$  (b) and  $\text{Hg}^0$  (c).

Finally, as the temporal profiles of the photo-generation of  $\text{Hg}^0$  (under UV in the presence of GQDs-TiO<sub>2</sub>) were compared, it is clearly seen a difference in the

initial release of  $\text{Hg}^0$  starting at 1.67 min from  $\text{Hg}^{2+}$ , 2.12 min from  $\text{CH}_3\text{CH}_2\text{Hg}$  and 2.33 min from  $\text{CH}_3\text{Hg}$ , which indicated that upon further optimizations, a potential speciation through temporal separation (Figure 7.8).

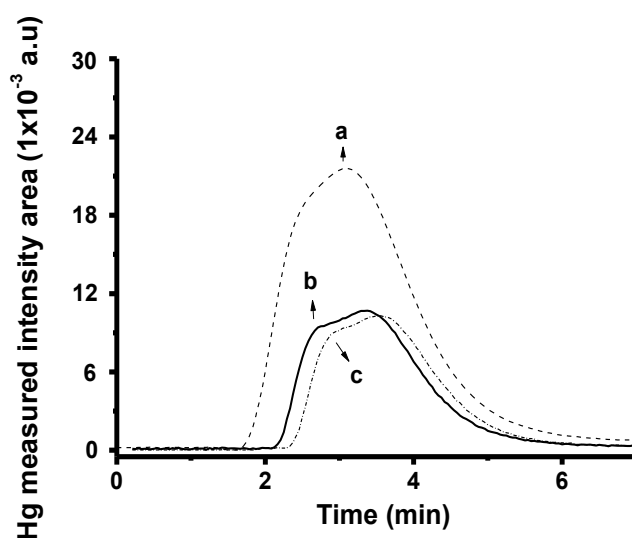


Figure 7.8. Temporal profile of mercury produced from mercurial species under UV in the presence of GQDs-TiO<sub>2</sub>: (a) Reduction of standard solution (1  $\mu\text{g L}^{-1}$ ) of  $\text{Hg}^{2+}$ ; b) Photochemical degradation of  $\text{CH}_3\text{CH}_2\text{Hg}$  (1  $\mu\text{g L}^{-1}$ ); c) Photochemical degradation of  $\text{CH}_3\text{Hg}$  (1  $\mu\text{g L}^{-1}$ ).

## 7.2.4

### Optimization of photo-reaction conditions

#### 7.2.4.1

#### Photocatalytic conditions in function of pH and GQDs-TiO<sub>2</sub> NPs content

Aiming to maximize efficiency in the photo-degradation of the organic mercurial species also enabling speciation through selective time-delay in the releasing of  $\text{Hg}^0$ , it was used a circumscribed central composite design (CCD) concerning the role of the GQDs-TiO<sub>2</sub> NPs in the photocatalytic processes. In this study, the simultaneous alteration of the pH and the amount of GQDs-TiO<sub>2</sub> NPs dispersed in the system was made in order to identify the best condition for the efficient photo-degradation of  $\text{CH}_3\text{Hg}$  and  $\text{CH}_3\text{CH}_2\text{Hg}$  by performing a limited number of experiments.

The study was performed by exposing samples to UV during 50 min over a wide range of pH (from 2 to 12, adjusted by adding NaOH or HCl solutions) and using amounts of GQDs-TiO<sub>2</sub> NPs from 0.15 mg and 1.2 mg, adjusted by the addition of volumes from 25 to 200 μL of the 6 mg mL<sup>-1</sup> GQDs-TiO<sub>2</sub> NPs dispersion and keeping the mercury species concentration at 1 μg L<sup>-1</sup>. Experimental design levels (coded values in parentheses) for GQDs-TiO<sub>2</sub> NPs ( $V_{NP}$  as added volume in μL<sup>-1</sup>) were 20 ( $-\sqrt{2}$ ); 43 (-1); 100 (0); 157 (+1) and 180 ( $+\sqrt{2}$ ) whereas for pH values, the chosen pH levels were 2.0 ( $-\sqrt{2}$ ); 3.5 (-1); 7 (0); 10.5 (+1) and 12 ( $+\sqrt{2}$ ). Authentic replicates (n = 8) were made only at the central point (0,0) to estimate variance. The response surface equation for CH<sub>3</sub>Hg was  $y = 25 V_{NP} - 301.8 \text{ pH} - 0.101 V_{NP}^2 - 1.5 \text{ pH}^2 + 0.1 V_{NP} \text{ pH}$ , which indicated a strong influence of pH, small influence for the quadratic factors despite the slight curvature in response surface, and no significant interaction between factors. For CH<sub>3</sub>CH<sub>2</sub>Hg the equation was  $y = 27 V_{NP} - 132.3 \text{ pH} - 0.1 V_{NP}^2 - 9.7 \text{ pH}^2 - 0.4 V_{NP} \text{ pH}$  that also pointed out to main influence of pH, some relevance of pH<sup>2</sup>, no relevance of  $V_{NP}^2$  and no relevant interaction. Through the surface response and the respective contour plot, the best degradation for both CH<sub>3</sub>Hg (Figure 7.9A and Figure 7.9B) and CH<sub>3</sub>CH<sub>2</sub>Hg (Figure 7.9C and Figure 7.9D) was achieved in the acid range below pH 4.0 using 100 μL of the GQDs-TiO<sub>2</sub> NPs original dispersion (equivalent to 0.6 mg of GQDs-TiO<sub>2</sub> NPs). The observed variability of replicate measurements, like coefficient of variation (CV) at the central point (0,0) was below 0.5 %.

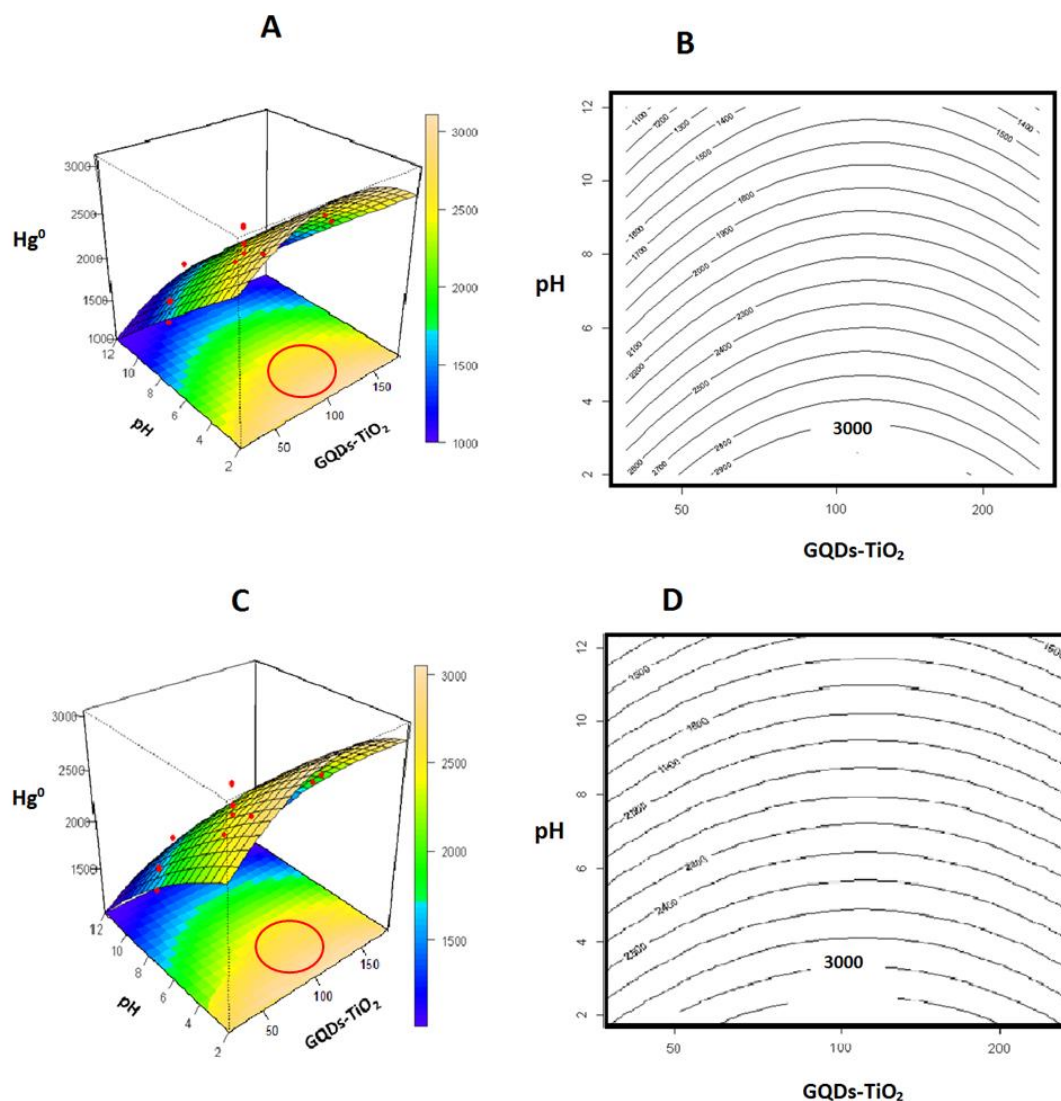


Figure 7.9. Circumscribed experimental design for photocatalytic reduction of organic mercury species. A)  $\text{CH}_3\text{Hg}^+$ ; response surface to the released mercury value in pH, and the amount of GQDs- $\text{TiO}_2$  dispersion. B) Contour plot for mercury signal referring to  $\text{CH}_3\text{Hg}^+$  reduction. C)  $\text{CH}_3\text{CH}_2\text{Hg}^+$ ; response surface to the released mercury value in pH, and the amount of GQDs- $\text{TiO}_2$  dispersion. D) Topographic plot for mercury signal referring to  $\text{CH}_3\text{CH}_2\text{Hg}^+$  reduction.

The same experimental design was applied for  $\text{Hg}^{2+}$  even in the solutions in pH condition (pH above 5) when it is expected the analyte to form  $\text{Hg}(\text{OH})_{2(s)}$  and, at higher concentrations of  $\text{OH}^-$ , soluble ion complexes in the form of  $\text{Hg}(\text{OH})_n^{(2-n)(\text{aq})}$ . As the sample containing  $\text{Hg}^{2+}$  is added into the GQDs- $\text{TiO}_2$  NPs dispersion, with previously adjusted pH, any formed solid could nucleate into the

surface of nanoparticles being prone to chemical transformations that lead to the formation of  $\text{Hg}^{2+}$  or  $\text{Hg}^0$ . However, experimental results indicated unfavorable photo-reduction of  $\text{Hg}^{2+}$  in pH below 8.0 and more efficiency in photo-catalytic reduction in pH values from pH around 4.0 down to pH 2.0. The model equation was  $y = 3.4 V_{\text{NP}} - 286.5 \text{ pH} - 0.05 V_{\text{NP}}^2 - 1.9 \text{ pH}^2 - 0.9 V_{\text{NP}} \text{ pH}$  and signal variability of replicate measurements (at 0,0) was 0.2 %. As for the organomercurial species, results indicated a strong dependence upon pH (best results at the acid range), a small influence of linear and quadratic contributions for nanocomposite content, that point out for the use of 100  $\mu\text{L}$  of nanoparticle dispersion, and no relevant interaction.

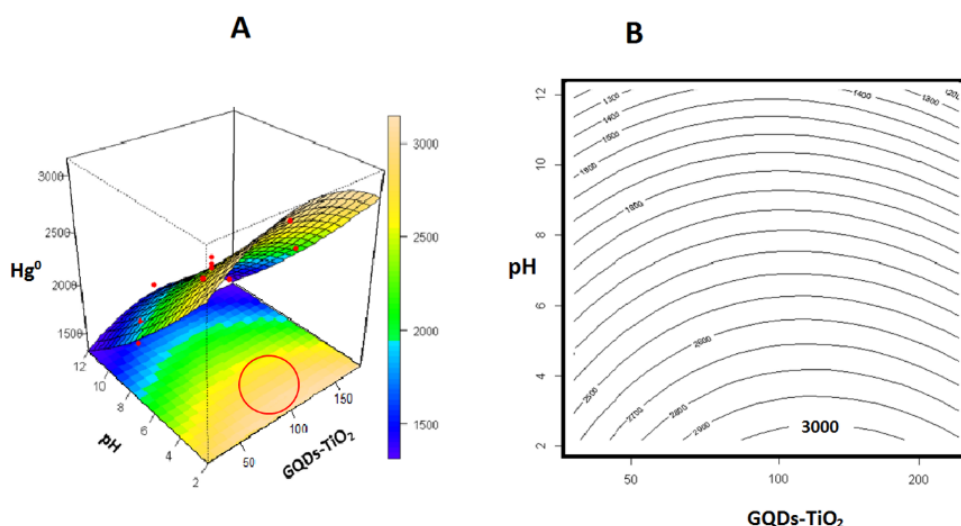


Figure 7.10. Circumscribed experimental design for photocatalytic reduction of  $\text{Hg}^{2+}$ . A) surface response to the mercury value released by pH, and the amount of GQDs- $\text{TiO}_2$  dispersion. B) Contour plot for mercury signal referring to  $\text{Hg}^{2+}$  reduction.

Since pH was controlled by the addition of hydrochloric acid, it was chosen to continue the study with aqueous systems adjusted to around pH 3 rather than a more acidic condition. This pH 3 is within the robust condition circulated in red in the response surfaces in Figure 7.10A and it is best viewed in the contour plot in Figure 7.10B. It is known that the presence of chloride may interfere in the  $\text{Hg}^{2+}$

reduction step due to the formation of  $\text{HgCl}_2^{(2-n)+}$  ion complexes. Besides, studies using suspensions composed only by  $\text{TiO}_2$  mention possible blocking of active surface sites on  $\text{TiO}_2$  due to the  $\text{Cl}^-$  adsorption present at concentration levels of  $10^{-2} \text{ mol L}^{-1}$  [157]. In order to check if interferences from chloride (from  $\text{HCl}$ ) would affect the formation of  $\text{Hg}^0$ , a comparison was made using aqueous systems with pH adjusted by the addition of aliquots of aqueous solutions of sulphuric acid. As a result no difference in  $\text{Hg}^0$  signal intensities was observed in photocatalytic degradation of organomercurial species and also in the photo-reduction of  $\text{Hg}^{2+}$  (Figure 7.11).

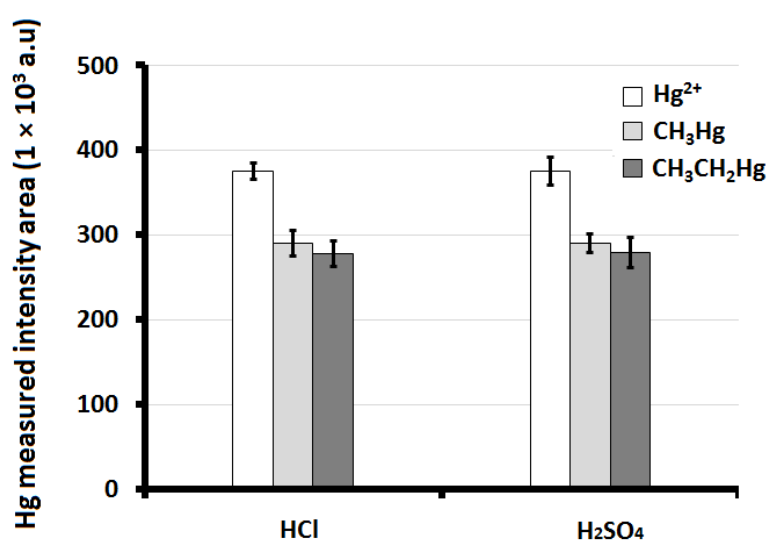


Figure 7.11. Photocatalytic reactions for mercurial species using aqueous suspensions of GQDs- $\text{TiO}_2$  (0.6 mg) at around pH 3 adjusted using  $\text{HCl}$  and  $\text{H}_2\text{SO}_4$ .

## 7.2.5

### UV irradiation studies

#### 7.2.5.1

##### pH and amount of GQDs- $\text{TiO}_2$ NPs

The influence of the UV irradiation time was studied using standard solutions of the mercury species ( $\text{Hg}^{2+}$ ,  $\text{CH}_3\text{Hg}$ ,  $\text{CH}_3\text{CH}_2\text{Hg}$ ) were added in aqueous systems at pH 3.0 and containing 100  $\mu\text{L}$  of GQDs- $\text{TiO}_2$  synthesis dispersion. The final concentration of each mercury species was  $1 \mu\text{g L}^{-1}$  in a 5 mL aqueous system

placed in the quartz tubes (connected directly to the CV-AAS system) inside the photochemical reactor. Each tube, containing the aqueous system, was UV irradiated in increasing time intervals (5 min intervals) under stirring and then, the air pump was turned on to transport the  $\text{Hg}^0$  generated during the photocatalytic reaction to the CV-AAS system. The maximum  $\text{Hg}^0$  signal was found to be reached after 10 min for  $\text{Hg}^{2+}$ , 20 for  $\text{CH}_3\text{CH}_2\text{Hg}$  and 30 min for  $\text{CH}_3\text{Hg}$ , which indicated a temporal separation in production of  $\text{Hg}^0$  from these different organic species in solution. Under these conditions, taking as reference the measured  $\text{Hg}^0$  obtained by chemical reduction using  $\text{SnCl}_2$ , the  $\text{Hg}^0$  produced by the photocatalytic reaction of  $\text{Hg}^{2+}$  was 78 %. For  $\text{CH}_3\text{Hg}$  and  $\text{CH}_3\text{CH}_2\text{Hg}$ , the efficiencies in the catalytic production of  $\text{Hg}^0$  were, respectively, 63 % and 72 % (percent values corrected taking into consideration the mercury content in the organomercurial species).

### 7.2.5.2

#### The effect of hydrogen peroxide and formic acid

It is known that the addition of hydrogen peroxide and formic acid, in the presence of dispersed semiconductors nanoparticles, generates free radicals in solution under UV. When aqueous  $\text{TiO}_2$  or  $\text{ZrO}_2$  suspension are irradiated with photons (of energy greater than semiconductors band gap) a charge carrier pair ( $e^-/h^+$ ) is formed also improving the production of strong oxidants (such as  $\bullet\text{OH}$  or  $\text{O}_2^{\bullet-}$ ) from water, especially when low weight organic molecules or hydrogen peroxide is present. It is possible that organic mercury is chemically degraded due to radicals attack and direct hole oxidation [158], while inorganic mercury is produced by reduction via conduction band electrons. However, UV-generated conduction band electrons ( $e^-$ ) and valence band holes ( $h^+$ ) tend to undergo recombination, decreasing the available number of  $e^-$  to promote photocatalytic reactions of mercury species. Low molecular organic compounds act as  $h^+$  scavengers [158] affecting the spontaneous excitonic recombination, thus increasing lifetime of conduction band electrons and their chance to participate in photocatalytic reactions.

The presence of hydrogen peroxide and formic acid in the aqueous system used to promote photocatalysis of the mercurial species was evaluated by adding

quantities of either substance as amounts between 1 and 10 % in volume. The presence of  $\text{H}_2\text{O}_2$  did not produce any improvement in the efficiency in the formation of  $\text{Hg}^0$  from  $\text{Hg}^{2+}$  also from the organomercury species. Contrary to studies that pointed out the importance of  $\text{H}_2\text{O}_2$  in promoting photochemical oxidation of  $\text{CH}_3\text{Hg}$  into  $\text{Hg}^{2+}$ , because of the production of free radicals [158], it is probable that QDs-TiO<sub>2</sub> nanocomposite is already producing enough free radicals, directly from the acidic aqueous system, to promote oxidation of the analytes without the need for  $\text{H}_2\text{O}_2$ .

Formic acid promoted a significant increase in the conversion of mercurial species in solution in the measurable  $\text{Hg}^0$ , as seen in Figure 7.12. It was found that the maximum improvement in photocatalytic efficiency is achieved already with 2% v/v of HCOOH, improving to about 30% the  $\text{Hg}^0$  detected by the CV-AAS system. The detected  $\text{Hg}^0$  measured using the photocatalytic reaction reached similar levels to the one achieved by using chemical reduction of  $\text{Hg}^{2+}$  (reference values included in the graphic in Figure 7.12).

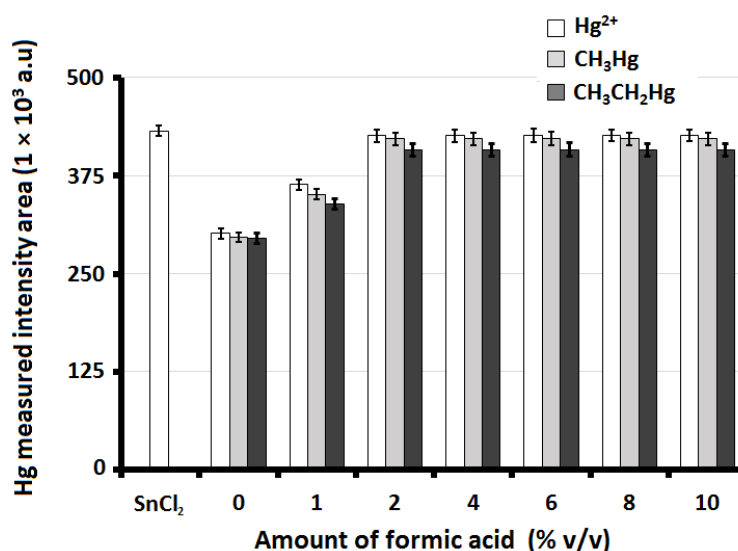


Figure 7.12 Effect of percent of formic acid on photocatalytic degradation of mercurial species mediated by QDs-TiO<sub>2</sub>. Chemical reduction of  $\text{Hg}^{2+}$  with SnCl<sub>2</sub> as a reference.

### 7.2.5.3

#### Temporal profiles of the UV induced photo-catalytic processes mediated by GQDs-TiO<sub>2</sub> NPs.

Under the adjusted conditions for the aqueous suspension (pH 3, formic acid at 2 % v/v and 0.6 mg of GQDs-TiO<sub>2</sub> NPs), the influence of the UV exposition time was studied using standard solutions of the mercurial species (Hg<sup>2+</sup>, CH<sub>3</sub>Hg, CH<sub>3</sub>CH<sub>2</sub>Hg) at 1 µg L<sup>-1</sup>. The study was made as indicated in the procedure described in section 3.5.1 but evaluating UV exposition of the aqueous suspension in time intervals of 1 min (under stirring), followed by transporting the Hg<sup>0</sup>, generated during the photocatalytic reaction, to the CV-AAS system. Results (Figure 7.13) showed a significant delay in the releasing of Hg<sup>0</sup> for the organic mercury species when compared to the inorganic mercury. The Hg<sup>0</sup> is measured above background levels and reached maximum value in the following intervals: from 1 to 4 min for Hg<sup>2+</sup>, from 6 to 8 min for CH<sub>3</sub>CH<sub>2</sub>Hg and from 10 to 12 min for CH<sub>3</sub>Hg. These results indicated a significant improvement in reaction kinetics promoted by the addition of formic acid as the Hg<sup>0</sup> evolution started at shorter times than the ones estimated in the experiment made by measurements made every 5 min without formic acid.

The differentiated delay in the evolution of Hg<sup>0</sup> may allow the chemical speciation analysis of these three organomercurial species in solution as Hg<sup>2+</sup> is firstly reduced reaching maximum before CH<sub>3</sub>CH<sub>2</sub>Hg photo-degradation process leads to the release of Hg<sup>0</sup> which, in turn, reaches the maximum before releasing of Hg<sup>0</sup> from CH<sub>3</sub>Hg.

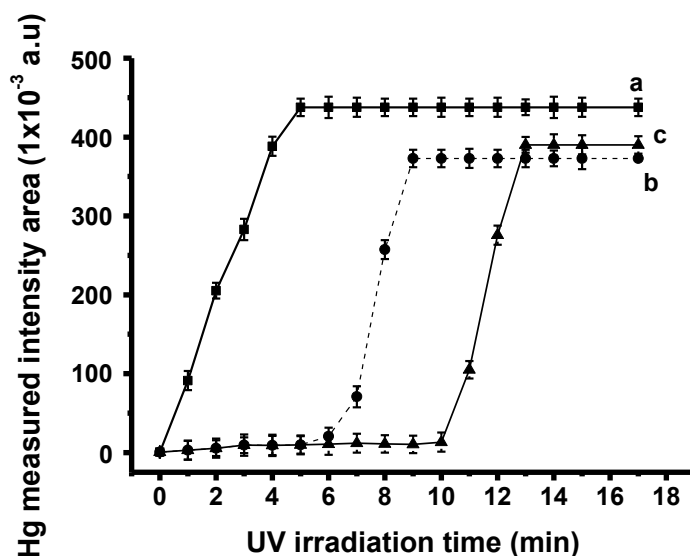


Figure 7.13.  $\text{Hg}^0$  absorbance measured in function of the UV exposition time for photocatalytic reactions using GQDs-TiO<sub>2</sub> nanocomposite (0.6 mg or 100  $\mu\text{L}$  of the synthesis dispersion at 6  $\text{mg mL}^{-1}$ ) in aqueous system at pH 3 and containing formic acid (2 % v/v): a)  $\text{Hg}^{2+}$  at  $1\mu\text{g L}^{-1}$ ; b)  $\text{CH}_3\text{CH}_2\text{Hg}$  at  $1\mu\text{g L}^{-1}$ ; c)  $\text{CH}_3\text{Hg}$  at  $1\mu\text{g L}^{-1}$ .

The temporal profiles for  $\text{Hg}^0$  were also obtained under the adjusted conditions, shown in Figure 7.14, for each of the mercurial species at  $1\mu\text{g L}^{-1}$ . The experiment was done under continuous UV irradiation of the aqueous suspensions inside the quartz tube and open to the CV-AAS system (with pump tuned on) in order to measure the  $\text{Hg}$  as it was formed during photocatalytic reaction. Figure 7.14 also shows temporal profile obtained from a mixture of the organomercurial species (each one at  $1\mu\text{g L}^{-1}$ ) reinforcing the expected capability for chemical speciation analysis.

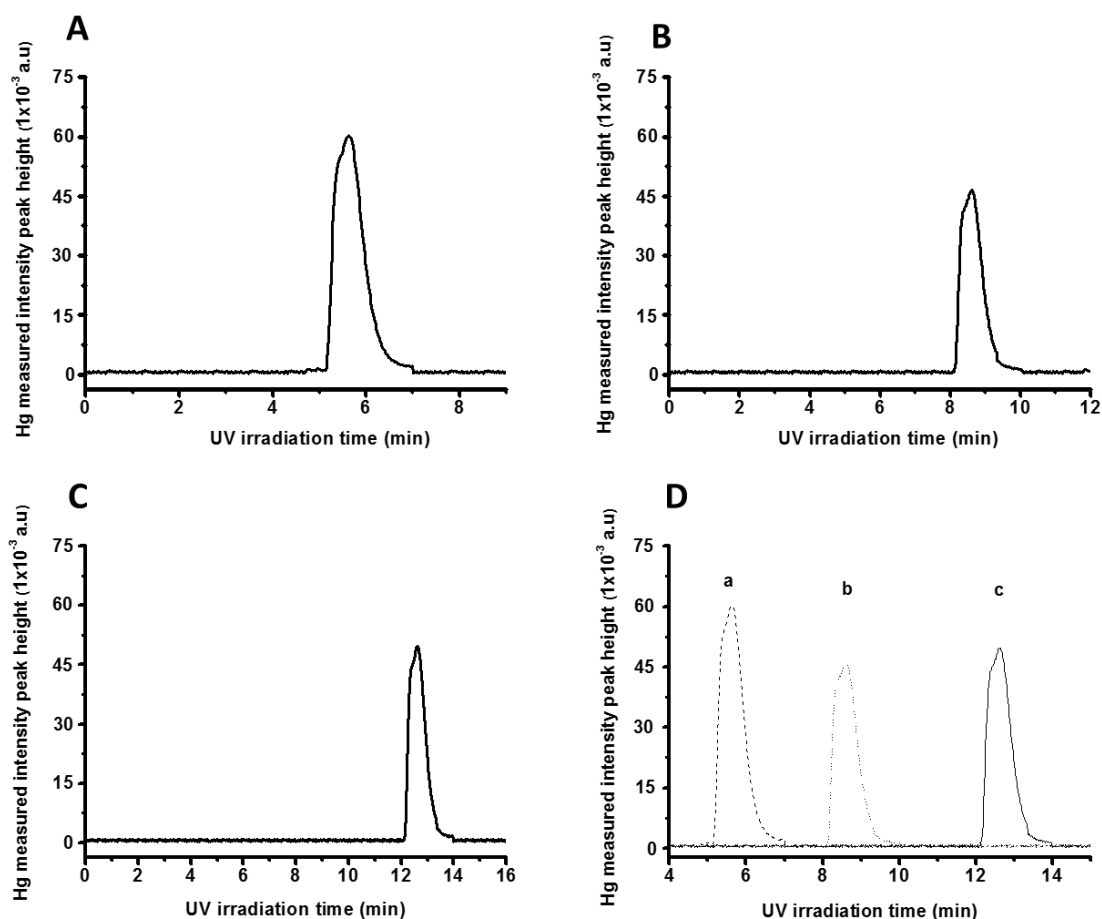


Figure 7.14  $\text{Hg}^0$  signal temporal profile after measured in function of the UV exposition time for photocatalytic reactions using GQDs-TiO<sub>2</sub> nanocomposite (0.6 mg or 100  $\mu\text{L}$  of the synthesis dispersion at 6  $\text{mg mL}^{-1}$ ) in aqueous system at pH 3 and containing formic acid (2 % v/v): a)  $\text{Hg}^{2+}$  at 1  $\mu\text{g L}^{-1}$ ; b)  $\text{CH}_3\text{CH}_2\text{Hg}$  at 1  $\mu\text{g L}^{-1}$ ; c)  $\text{CH}_3\text{Hg}$  at 1  $\mu\text{g L}^{-1}$ ; d) mixture of organomercurial species (each one at 1  $\mu\text{g L}^{-1}$ ).

An additional study was made using the GC-CV-AFS system in order to understand the evolution of the photocatalytic reaction. Aliquots (25  $\mu\text{L}$ ) of the irradiated suspensions (at the adjusted conditions) containing analytes (at 400  $\text{ng L}^{-1}$ ) were diluted (40 mL) in an aqueous solution containing acetate buffer (pH 4.0) and then propylated. The typical chromatogram is shown in Figure 7.15 (chromatogram A) obtained from the experiments. It is possible to observe the spectral profile (250  $\text{pg L}^{-1}$ ) of each mercury species at retention times ( $1.68 \pm 0.01$ ) min for  $\text{CH}_3\text{Hg}$ , ( $4.39 \pm 0.02$ ) min for  $\text{CH}_3\text{CH}_2\text{Hg}$  and ( $7.26 \pm 0.02$ ) min for  $\text{Hg}^{2+}$  before being subjected to the photocatalytic process. After 4 min of irradiation,  $\text{CH}_3\text{Hg}$  and  $\text{CH}_3\text{CH}_2\text{Hg}$  remain in solution, but the peak characteristic of  $\text{Hg}^{2+}$  disappeared as it was completely reduced to  $\text{Hg}^0$  (that appears at retention time peak

at  $(0.38 \pm 0.02)$  min (Figure 7.15, chromatogram B). The characteristic  $\text{CH}_3\text{CH}_2\text{Hg}$  peak vanished after 10 min of UV irradiation with about 30% reduction in the peak characteristic of the  $\text{CH}_3\text{Hg}$  species. In this same chromatogram, it was also observed the appearance of the  $\text{Hg}^{2+}$  species, which indicated the oxidation of organic mercury before final formation of  $\text{Hg}^0$  (Figure 7.15, chromatogram C). After 13 min of UV exposition, only the  $\text{Hg}^0$  peak is found in the chromatogram D as photocatalysis is completed.

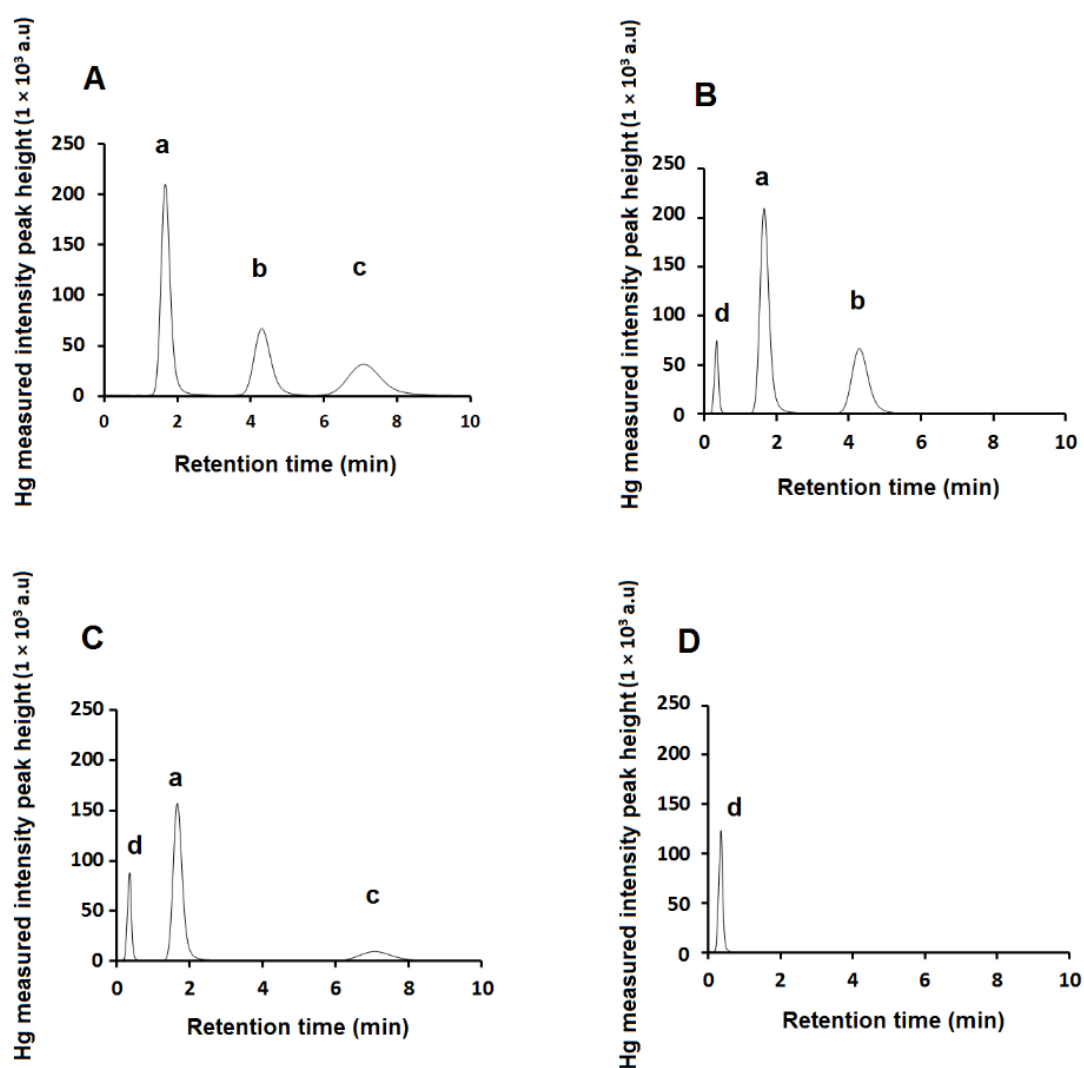


Figure 7.15. (A) Typical chromatograms obtained using the GC-CV-AFS system after derivatization of standard solutions of  $\text{Hg}^{2+}$ ,  $\text{CH}_3\text{Hg}$ ,  $\text{CH}_3\text{CH}_2\text{Hg}$  with  $\text{NaBPr}_4$ . After photocatalytic degradation with UV-mediated GQDs- $\text{TiO}_2$  A) 0 min; B) 5 min; C) 8 min D) 12 min.

## 7.2.6.

### Photo-reaction studies.

#### 7.2.6.1.

#### The photocatalytic efficiency of GQDs-TiO<sub>2</sub> NPs.

The photocatalytic efficiency of the dispersed GQDs-TiO<sub>2</sub> NPs was evaluated in function of the formation of Hg<sup>0</sup> from the mercurial species present at different proportions. Aqueous dispersions containing a fixed amount of GQDs-TiO<sub>2</sub> NPs (100 µL of the synthesis dispersion or 0.12 mg L<sup>-1</sup> of nanocomposite) was used as the concentration of mercurial species was varied from 0.01 to 5 µg L<sup>-1</sup> (Figure 7.16). It was found that the magnitude of the measured Hg<sup>0</sup> was directly proportional to the concentration of the mercurial species up to 3 µg L<sup>-1</sup> then stabilizing as the GQDs-TiO<sub>2</sub> NPs reaches the limit in efficiency to promote photo-reaction. The result is an indication of some saturation of the nanomaterial active sites occur as they become occupied by organic molecules, causing a decrease in degradation efficiency [159].

In order to improve efficiency to promote photoreaction of mercurial species at concentrations higher than 3 µg L<sup>-1</sup>, it could be used more of the dispersed nanocomposite. However, in the case, there is a risk to increase the turbidity of the medium decreasing the exposure of the nanomaterial to the UV. As the typical concentrations determined using the multipass CV-AAS spectrometer is in the ng L<sup>-1</sup> range, it was found that photocatalytic efficiency of the 0.12 mg L<sup>-1</sup> of dispersed nanomaterial is adequate for the intended quantitative applications where sample dilution is used to minimize potential interferences.

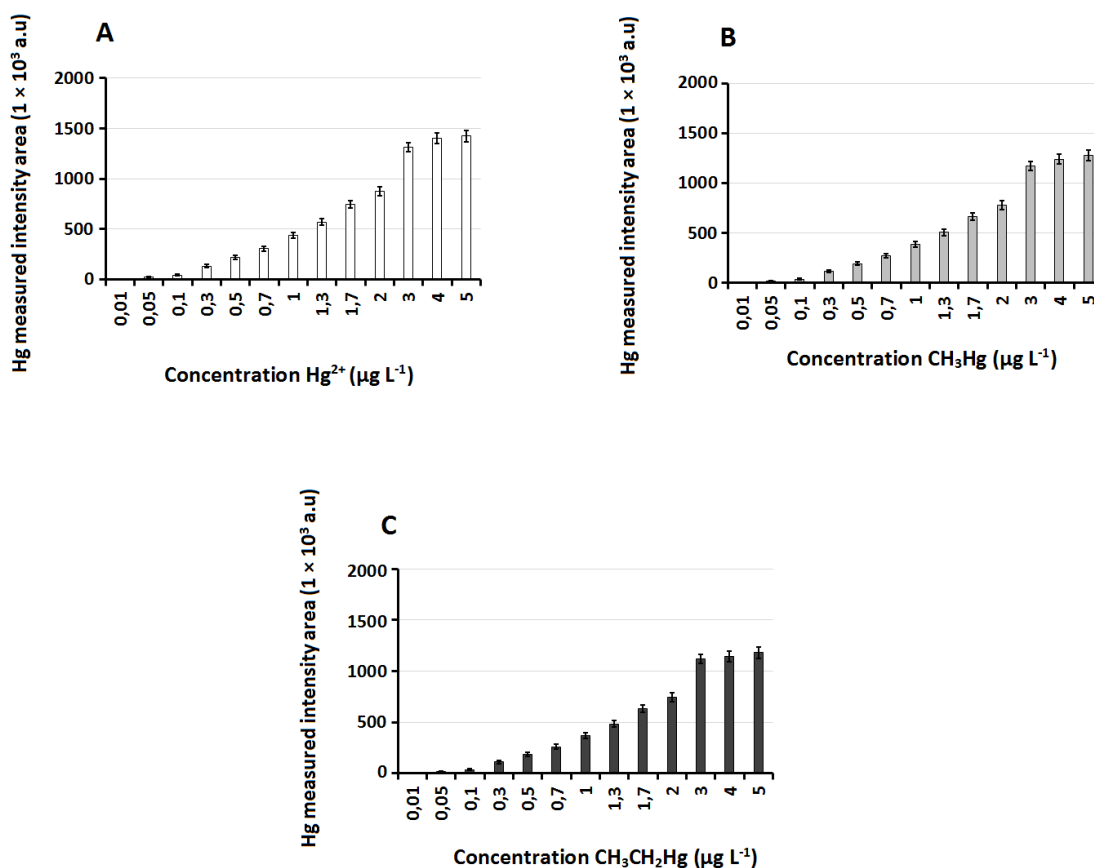


Figure 7.16. Efficiency of GQD-TiO<sub>2</sub> nanocomposite (1.2 mg L<sup>-1</sup>) in promoting photoreaction to produce Hg<sup>0</sup> from different mercurial species at increasing concentrations: A) Hg<sup>2+</sup> after 5 min UV exposure; B) CH<sub>3</sub>Hg after 13 min of UV exposure; C) CH<sub>3</sub>CH<sub>2</sub>Hg degradation after 9 min UV exposure.

### 7.2.6.2.

#### Photo-reaction kinetic study

Under the chosen conditions to perform GQDs-TiO<sub>2</sub> NPs mediated UV-induced photoreactions (Table 7.1) the kinetics of the photocatalytic degradation on mercurial species (Hg<sup>2+</sup>, CH<sub>3</sub>Hg, CH<sub>3</sub>CH<sub>2</sub>Hg) were performed using the Langmuir-Hinshelwood kinetic model [160], which seems to be the proper one as the premises of heterogeneous catalysis, under the influence of solvent (formic acid aqueous solution), are observed.

The experiments were performed with three different initial concentrations (C<sub>0</sub>) of the mercury species (100, 300 and 700 ng L<sup>-1</sup>) and monitoring the temporal profiles (area) of the produced Hg<sup>0</sup>. The result fits appropriately in the pseudo-first-

order modeled by Equation 1 for the rate of the unimolecular surface reaction ( $r$ ) and the integrated Equation 2.

$$r = -\frac{dc}{dt} = \frac{k_r k_{Hg} c_0}{1 + k_{Hg} c_0} \quad (1)$$

$$\ln\left(\frac{C_0}{C_t}\right) = k_r k_{Hg} t = k_{app} t \quad (2)$$

Where  $-(dc/dt)$  is the degradation rate of mercury species ( $\text{ng L}^{-1} \text{ min}$ ),  $c_0$  and  $c_t$  are respectively the initial concentrations of mercury species (in  $\text{ng L}^{-1}$ ) at a specific time ( $t$ ). Besides,  $k_r$  is the reaction rate constant (pseudo-first-order reaction),  $k_{Hg}$  is the adsorption coefficient of mercury species on the nanocomposite surface ( $\text{L/ng}$ ). The apparent rate constant ( $k_{app}$ ) is the apparent velocity constant of the degradation of mercurial species (approximation due to the minute concentrations of the mercurial species) determined from the sensitivity of the  $\ln(C_0 / C_t)$  versus time plots (Figure 7. 17B;D; F). The kinetic data obtained by the pseudo-first-order model including rate constants, linearity parameters of the model and maximum degradation of mercury species in the presence of GQDs-TiO<sub>2</sub> are presented in Table 7.1.

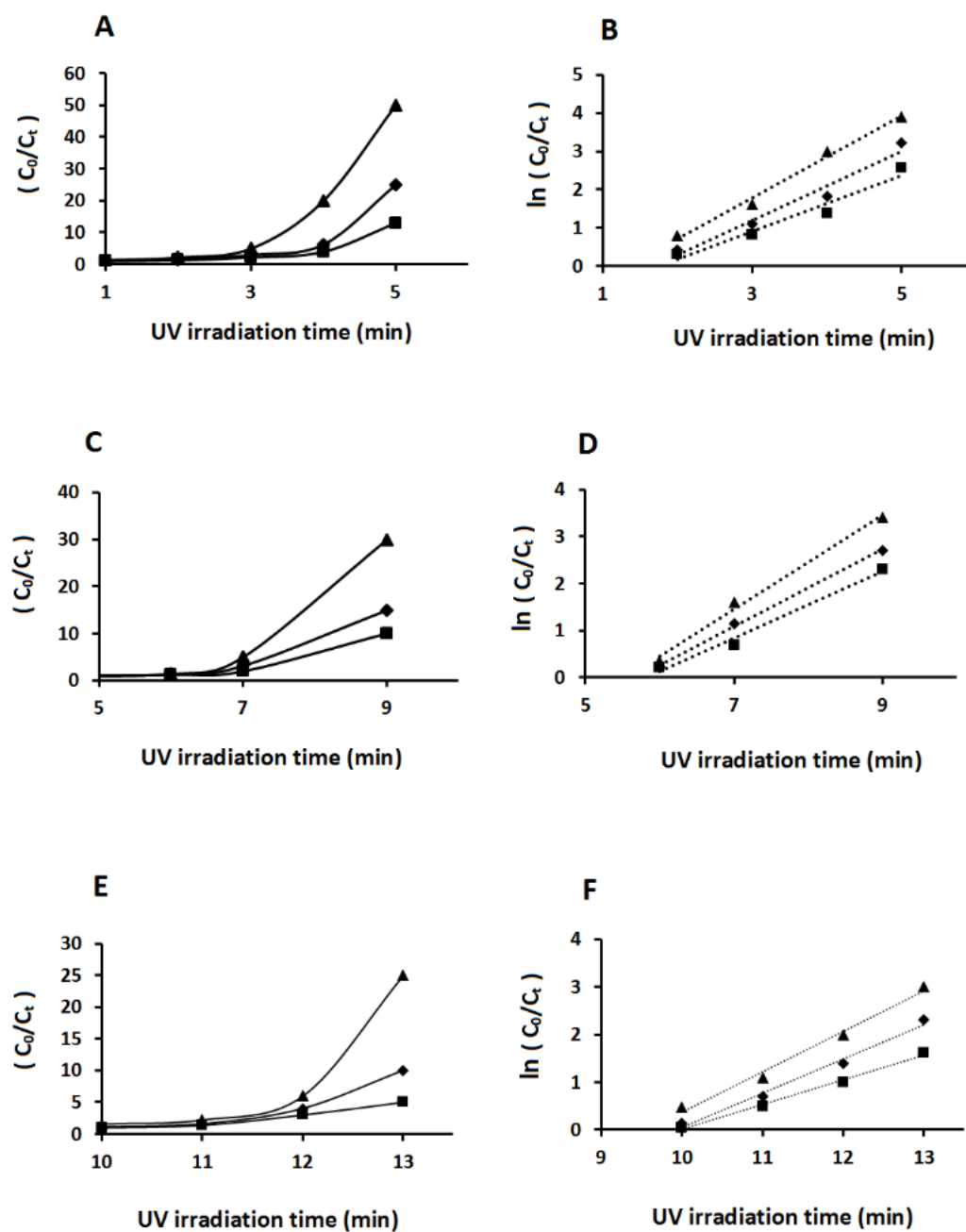


Figure 7.17. Hg measured signal by multipath-CV-AAS: A) in the function of the concentration of  $\text{Hg}^{2+}$ , D)  $\text{CH}_3\text{Hg}$ ; and E)  $\text{CH}_3\text{CH}_2\text{Hg}$ ; in function of irradiation time of a mercury species solution with  $C_0$  is the initial concentration (100; 300; 700  $\text{ng L}^{-1}$ ) and with  $C_t$  as concentration measured at different irradiation times. B; D; and F)  $\ln(C_0/C_t)$  mercury species solution.

Table 7.1 Parameters and data from the kinetic study of the photocatalytic degradation of mercury species using 0.12 mg mL<sup>-1</sup> GQDs-TiO<sub>2</sub> dispersion.

<b>Hg<sup>2+</sup> concentration (ng L<sup>-1</sup>)</b>	<b>Maximum degradation (%)</b>	<b><i>k</i><sub>app</sub> (min<sup>-1</sup>)</b>	<b>Linear model equation</b>	<b>Determination coefficient (<i>R</i><sup>2</sup>)</b>
100	95.6	0.0563	Y = 1.072X - 1.425	0.992
300	95.6	0.0511	Y = 0.968X - 1.531	0.988
700	95.4	0.0497	Y = 0.934X - 1.289	0.994
<b>CH<sub>3</sub>Hg concentration (ng L<sup>-1</sup>)</b>	<b>Maximum degradation (%)</b>	<b><i>k</i><sub>app</sub> (min<sup>-1</sup>)</b>	<b>Linear model equation</b>	<b>Correlation coefficients (<i>R</i><sup>2</sup>)</b>
100	92.4	0.0398	Y = 0.998X - 5.53	0.990
300	92.5	0.0355	Y = 0.903X - 0.467	0.998
700	92.4	0.0342	Y = 0.829X - 0.445	0.979
<b>CH<sub>3</sub>CH<sub>2</sub>Hg concentration (ng L<sup>-1</sup>)</b>	<b>Maximum degradation (%)</b>	<b><i>k</i><sub>app</sub> (min<sup>-1</sup>)</b>	<b>Linear model equation</b>	<b>Correlation coefficients (<i>R</i><sup>2</sup>)</b>
100	94.2	0.0433	Y = 0.849X - 8.121	0.978
300	94.3	0.0426	Y = 0.796X - 0.716	0.983
700	94.1	0.0419	Y = 0.691X - 0.619	0.986

In order to improve efficiency to promote photoreaction of mercurial species at concentrations higher than 3 μg L<sup>-1</sup>, it could be used more of the dispersed nanocomposite. However, there is a risk to increase the turbidity of the medium decreasing the exposure of the nanomaterial to the UV. As the typical concentrations determined using the multipass CV-AAS spectrometer is in the ng L<sup>-1</sup> range, it was found that photocatalytic efficiency of the 1.2 mg L<sup>-1</sup> of dispersed nanomaterial is adequate for the intended quantitative applications where sample dilution is used to minimize potential interferences.

## 7.2.7

### Analytical characteristics

#### 7.2.7.1

##### Analytical figures of merit

The conditions used for the quantitative mercury speciation, using photocatalytic reaction using GQDs-TiO<sub>2</sub> NPs, are presented in Table 7.2. The photocatalytic reaction was applied in aqueous standards (Hg<sup>2+</sup>, CH<sub>3</sub>Hg, CH<sub>3</sub>CH<sub>2</sub>Hg) covering concentrations from 10 ng L<sup>-1</sup> to 1000 ng L<sup>-1</sup> (in three

replicates) in order to construct analytical curves. The linear responses were modeled by the equations in Table 7.3, along with limits of detection (LOD) and limits of quantification (LOQ) values. LOD was calculated as the concentration equivalent to the signal  $y_{sp} + 3s_{sp}$ , where  $y_{sp}$  is the smallest possible integrated peak added to three times the standard deviation of the peak itself (10 replicates). For LOQ, the used criterion was the concentration that produced a signal of  $y_{sp} + 10s_{sp}$ .

Table 7.2 Chosen parameters for speciation analysis using CV-AAS after UV photocatalytic reaction mediated by GQDs-TiO<sub>2</sub> nanocomposite

Step	Parameters of the method
Photocatalytic reduction	
UV (6 lamps)	Main line at 253 nm and secondary lines in the range of 296 to 313 nm) and 24 W
Sample solution final volume	5.0 mL
Amount of GQDs-TiO <sub>2</sub> nanocomposite	0.12 mg L <sup>-1</sup> (from a 100 μL of a GQDs-TiO <sub>2</sub> nanocomposite dispersion at 6 mg mL <sup>-1</sup> )
Ar flow rate	3 mL min <sup>-1</sup>
pH	3
Formic acid final concentration	2% (v/v)
UV irradiation times	Hg <sup>2+</sup> (5 min); CH <sub>3</sub> CH <sub>2</sub> Hg (9 min); CH <sub>3</sub> Hg (13 min)

Table 7.3 Analytical figures of merit of the speciation method using CV-AAS after UV photocatalytic reaction mediated by GQDs-TiO<sub>2</sub> nanocomposite

Analyte	Linear equation	R <sup>2</sup>	LOD (ng L <sup>-1</sup> ) <sup>a</sup>	LOQ (ng L <sup>-1</sup> ) <sup>b</sup>
Hg <sup>2+</sup>	$Y = 429 \times 10^3 X - 668$	0.999	7.0	13.0
CH <sub>3</sub> Hg	$Y = 366 \times 10^3 X - 919$	0.998	7.0	14.0
CH <sub>3</sub> CH <sub>2</sub> Hg	$Y = 327 \times 10^3 X - 2364$	0.997	10.0	15.0

<sup>a</sup>Calculated as the concentration that produced a signal of  $y_{sp} + 3s_{sp}$  (n = 8).

<sup>b</sup>Calculated as the concentration that produced a signal of  $y_{sp} + 10s_{sp}$  (n = 8).

Instrumental precision was obtained using the coefficient of variation of the signal produced by the analysis of eight aliquots of the same standard solution of the mercury species (Hg<sup>2+</sup>, CH<sub>3</sub>Hg, CH<sub>3</sub>CH<sub>2</sub>Hg) at either 250 ng L<sup>-1</sup> (1.9 %) and 500 ng L<sup>-1</sup> (1.7 %). Intermediate precision was evaluated as the coefficient of variation of analyte percent recoveries obtained from eight independently prepared analyte standard solutions of the mercury species at either 250 ng L<sup>-1</sup> (2.1 %) and 500 ng L<sup>-1</sup> (2.3 %).

### 7.2.7.2

#### Evaluation of interferences on mercury cold vapor generation

As transition metal ions, especially  $\text{Cu}^{2+}$ ,  $\text{Co}^{2+}$ ,  $\text{Ni}^{2+}$ ,  $\text{Fe}^{2+}$ ,  $\text{Fe}^{3+}$ , are known to affect the efficiency in generating mercury cold vapor in traditional chemical reduction processes [161], the influence of the presence of some metal ions in the efficiency of the photocatalytic reaction, mediated by GQDs-TiO<sub>2</sub> nanocomposite, was evaluated. For these studies, photocatalytic reactions of the mercurial species were performed in the presence of 10, 50 and 100  $\mu\text{g L}^{-1}$  of a potential interferent ion, keeping constant the concentration of  $\text{Hg}^{2+}$ ,  $\text{CH}_3\text{Hg}$ , or  $\text{CH}_3\text{CH}_2\text{Hg}$  at 1  $\mu\text{g L}^{-1}$ . The results showed that even if the concentration of a transition metal ion was 100 times higher than the one of the mercurial species, percent recoveries were higher than 90 % as shown in Table 7.4.

Table 7.4 Interference study concerning the effect of some transition metals on the photoreaction of mercurial species.

Transition metal ion	Concentration of transition metal ion ( $\mu\text{g L}^{-1}$ )	Mercurial species percent recoveries (%)		
		$\text{Hg}^{2+}$	$\text{CH}_3\text{Hg}$	$\text{CH}_3\text{CH}_2\text{Hg}$
$\text{Cu}^{2+}$	10	95.3	95.3	94.4
	50	94.4	92.6	94.6
	100	92.6	94.4	92.5
$\text{Ni}^{2+}$	10	96.1	93.8	93.6
	50	94.7	92.7	92.7
	100	93.3	91.7	91.3
$\text{Co}^{2+}$	10	95.6	93.2	93.2
	50	93.2	92.4	92.8
	100	92.4	91.3	91.6
$\text{Fe}^{2+}$	10	93.6	93.6	93.8
	50	92.2	92.2	93.4
	100	91.8	91.8	92.2
$\text{Fe}^{3+}$	10	95.1	92.2	94.1
	50	93.5	91.7	92.2
	100	92.5	91.6	92.1

### 7.2.7.3

#### Analysis of urine sample

The accuracy of the method in determining mercury  $\text{Hg}^{2+}$  in urine was assessed by the analysis of the NIST SRM 2672a (*Toxic substances in urine* - at elevated levels) with a certified mercury value of  $(105 \pm 8) \mu\text{g L}^{-1}$ . The experimental value obtained was  $(107 \pm 4) \mu\text{g L}^{-1}$  using analytical curve using aqueous  $\text{Hg}^{2+}$  standards. The statistical similarity of the recovered value and the certified value was confirmed by a two-tailed Student t-test ( $\alpha = 0.05$  and  $n_1 = n_2 = 3$ ).

The certified urine sample was also fortified with organic mercury standards at two concentration levels (see Table 7.5). The recovered values for the fortified analyte, after photocatalytic reactions using GQDs-TiO<sub>2</sub>, for  $\text{CH}_3\text{Hg}$  and  $\text{CH}_3\text{CH}_2\text{Hg}$  (discounted the  $\text{Hg}^0$  from the original  $\text{Hg}^{2+}$  concentrations in urine) were satisfactory.

Table 7.5 Study of recovery after fortification with  $\text{CH}_3\text{Hg}$  and  $\text{CH}_3\text{CH}_2\text{Hg}$  of the SRM 2672a.

Analyte	$\text{CH}_3\text{Hg}$ fortification level ( $\mu\text{g L}^{-1}$ )	Hg Total found <sup>a</sup> ( $\mu\text{g L}^{-1}$ )	$\text{CH}_3\text{Hg}$ recovered in the fortification experiment <sup>c</sup> ( $\mu\text{g L}^{-1}$ )	Average <sup>a</sup> original Hg ( $\mu\text{g L}^{-1}$ )
$\text{CH}_3\text{Hg}$	5.0	$111.8 \pm 1.2$	$4.8 \pm 1.2$	$96.0 \pm 1.3$
	10.0	$116.7 \pm 0.6$	$9.7 \pm 0.6$	$97.0 \pm 1.6$
Analyte	$\text{CH}_3\text{CH}_2\text{Hg}$ fortification level ( $\mu\text{g L}^{-1}$ )	Hg Total found <sup>b</sup> ( $\mu\text{g L}^{-1}$ )	$\text{CH}_3\text{CH}_2\text{Hg}$ recovered in the fortification experiment <sup>c</sup> ( $\mu\text{g L}^{-1}$ )	Average <sup>b</sup> original Hg ( $\mu\text{g L}^{-1}$ )
$\text{CH}_3\text{CH}_2\text{Hg}$	5.0	$111.9 \pm 1.5$	$4.9 \pm 0.4$	$98.0 \pm 0.6$
	10.0	$116.6 \pm 1.3$	$9.6 \pm 0.7$	$96.0 \pm 0.4$

<sup>a</sup> After 13 min of UV irradiation

<sup>b</sup> After 9 min of UV irradiation

<sup>c</sup> Discounting the original  $\text{Hg}^{2+}$  concentration of the urine sample.

The recovered values of the organic species were obtained after discounting the concentration of inorganic mercury (from the original sample) of the total mercury concentrations recovered after photochemical reduction. The  $\text{CH}_3\text{Hg}$ ,  $\text{CH}_3\text{CH}_2\text{Hg}$  concentrations statistically similar to those obtained by GC-CV-AFS (Table 7.6)

Table 7.6 Comparison of determination  $\text{CH}_3\text{Hg}$  and  $\text{CH}_3\text{CH}_2\text{Hg}$  fortification with the proposed method and using the GC-CV-AFS-based method.

Analyte	Found method CV-AAS ( $\mu\text{g L}^{-1}$ )	Found method GC-CV-AFS ( $\mu\text{g L}^{-1}$ )	$t_{\text{calculated}}^{\text{a}}$
$\text{CH}_3\text{Hg}^{\text{b}}$	$4.8 \pm 1.3$	$4.9 \pm 2.1$	1.44
$\text{CH}_3\text{CH}_2\text{Hg}^{\text{b}}$	$4.8 \pm 0.6$	$4.9 \pm 1.6$	1.53

<sup>a</sup>  $t_{\text{critical}}$  (two-tailed student-t-test;  $\alpha = 0.05 = 2.77$  with g.l. =  $n_1 + n_2 - 2 = 4$ ).

## 7.2.8

### Partial conclusion

It was developed a simple and efficient method for mercury speciation analysis based on the photocatalytic reaction of mercury species using a dispersed nanomaterial (GQDs-TiO<sub>2</sub> NPs) as catalysts. The UV photocatalytic reactions, made in the adjusted pH and using formic acid as source of free radicals, enabled different kinetic allowing temporal separation of the Hg released from the different mercurial species detected by CV-AAS. The method was evaluated by the analysis of a standard reference urine sample with speciation after fortification with organic mercury species. The method can potentially replace tedious procedures based on chemical derivatization of the mercurial species that use toxic and expensive reagents being a cost-effective alternative for the ultra-trace determination and speciation of mercury.

## 8 General Conclusion

In this work, analytical methods were developed based on the generation of cold mercury vapor for the determination and speciation of mercury in produced waters. In addition, graphene quantum dots were used as catalytic agents to promote photo-reaction in order to determine organic and inorganic mercury species.

- ✓ The combination of extraction (ultrasound-assisted in the presence of surfactant) and distillation before propylation and determination by cold atomic fluorescence spectrometry by gas chromatography (GC-CV- AFS) allowed recoveries of up to 92 % ( $\text{Hg}^{2+}$ ), 87 % ( $\text{CH}_3\text{Hg}$ ) and 86 % ( $\text{CH}_3\text{CH}_2\text{Hg}$ ) in the fortification studies of original PW samples. Likewise, the conditions were adjusted to minimize the formation of artifacts during the sample treatment process in systems containing the main components of PW matrix.
- ✓ The photocatalytic degradation of the thiomersal in the presence of GQDs was studied, it was demonstrated that these nanomaterials promote the oxidation of thiomersal to inorganic mercury and soon after chemical reduction using  $\text{SnCl}_2$  were quantified in the CV-AAS system. Degradation with graphene quantum dots was very efficient (following pseudo-first-order kinetics) and was performed under adjusted conditions to maximize  $\text{Hg}^{2+}$  formation and minimize losses as Hg during the photochemical reaction step.
- ✓ This work also presented a new method for mercury speciation using nanocomposites of GQDs  $\text{P}_{25}$ - $\text{TiO}_2$  nanoparticles (GQDs- $\text{TiO}_2$  NPs) to mediate the photocatalytic degradation of mercury species at  $\text{Hg}^0$  efficiently (without the need for chemical reduction agents) was detected by CV-AAS. For photocatalytic degradation, microlitre aliquots of GQDs- $\text{TiO}_2$  dispersion were added to the sample solution under adjusted conditions (pH 3; 2% v/v formic acid). Under these conditions, quantitative speciation was successfully achieved, taking advantage of the differences in UV photodegradation kinetics:  $\text{Hg}^{2+}$  (4 min),  $\text{CH}_3\text{CH}_2\text{Hg}$  (8 min) and  $\text{CH}_3\text{Hg}$

(12 min). The evaluation of photodegradation kinetics was also performed by GC-CV-AFS, which confirmed that the photocatalytic reaction followed pseudo-first-order kinetics.

- ✓ The overall performance achieved in this work indicated that they are very competitive assays compared to the ones already reported in literature.

## 9. References

- [1] L. Wollenberger, B. Halling-sørensen, K.O. Kusk, Acute and chronic toxicity of veterinary antibiotics to *Daphnia magna*, *Chemosphere*. 40 (2000) 723–730. doi:10.1016/S0045-6535(99)00443-9.
- [2] K. Leopold, M. Foulkes, P. Worsfold, Methods for the determination and speciation of mercury in natural waters-A review, *Anal. Chim. Acta*. 663 (2010) 127–138. doi:10.1016/j.aca.2010.01.048.
- [3] G.-B. Jiang, J.-B. Shi, X.-B. Feng, Mercury Pollution in China, *Environ. Sci. Technol.* 40 (2006) 3672–3678. doi:10.1021/es062707c.
- [4] Z. Salehi, A. Esmaili-Sari, Hair mercury levels in pregnant women in Mahshahr, Iran: Fish consumption as a determinant of exposure, *Sci. Total Environ.* 408 (2010) 4848–4854. doi:10.1016/j.scitotenv.2010.06.027.
- [5] United Nations Environment Programme Global Mercury Assessment 2013 Sources, Emissions, Releases and Environmental Transport, n.d. <http://www.unep.org/hazardoussubstances/Mercury/Informationmaterials/ReportsandPublications/>.
- [6] The United Nations, Minamata convention on mercury, Kumamoto, Japan, on 10 October 2013, 2013. <https://treaties.un.org/doc/Treaties/2013/10/2013101011-16AM/CTC-XXVII-17.pdf>.
- [7] L. Trip, Methylmercury: a new look at the risks, *Public Health Rep.* 114 (1999) 397–415. doi:10.1093/phr/114.5.397.
- [8] C.M. Tseng, C.R. Hammerschmidt, W.F. Fitzgerald, Determination of methylmercury in environmental matrixes by on-line flow injection and atomic

fluorescence spectrometry, *Anal. Chem.* 76 (2005) 7131–7136. doi:10.1021/ac049118e.

[9] M. Mania, M. Wojciechowska-Mazurek, K. Starska, M. Rebeniak, J. Postupolski, [Fish and seafood as a source of human exposure to methylmercury], *Rocz. Państwowego Zakładu Hig.* 63 (2012) 257–264.

[10] S.M. Wilhelm, N. Bloom, Mercury in petroleum, *Fuel Process. Technol.* 63 (2000) 1–27. doi:10.1016/S0378-3820(99)00068-5.

[11] Y. Bolate, Inventory of U.S. sources of mercury emissions to the atmosphere, (2017) 1–29.

[12] C.N. do M.A. CONAMA, Resolução nº 393, 8 de agosto de 2007, Ministério do Meio Ambiente (2007) 72–73.

[13] G.T. Tellez, N. Nirmalakhandan, J.L. Gardea-Torresdey, Evaluation of biokinetic coefficients in degradation of oilfield produced water under varying salt concentrations, *Water Res.* 29 (1995) 1711–1718. doi:10.1016/0043-1354(94)00328-5.

[14] R. Shpiner, S. Vathi, D.C. Stuckey, Treatment of oil well “produced water” by waste stabilization ponds: Removal of heavy metals, *Water Res.* 43 (2009) 4258–4268. doi:10.1016/j.watres.2009.06.004.

[15] H.S. Dórea, J.R.L. Bispo, K.A.S. Aragão, B.B. Cunha, S. Navickiene, J.P.H. Alves, L.P.C. Romão, C.A.B. Garcia, Analysis of BTEX, PAHs and metals in the oilfield produced water in the State of Sergipe, Brazil, *Microchem. J.* 85 (2007) 234–238. doi:10.1016/j.microc.2006.06.002.

[16] C.W. Yeung, B.A. Law, T.G. Milligan, K. Lee, L.G. Whyte, C.W. Greer, Analysis of bacterial diversity and metals in produced water, seawater and sediments from an offshore oil and gas production platform, *Mar. Pollut. Bull.* 62 (2011) 2095–2105. doi:10.1016/j.marpolbul.2011.07.018.

- [17] P. De O Vicentino, D.M. Brum, R.J. Cassella, Development of a method for total Hg determination in oil samples by cold vapor atomic absorption spectrometry after its extraction induced by emulsion breaking, *Talanta*. 132 (2015) 733–738. doi:10.1016/j.talanta.2014.10.019.
- [18] Brasil, Ministério do Meio Ambiente. Resolução n. 357 (2005) 23p.
- [19] M.H. Martine Leermakers, Willy Baeyens, Philippe Quevauviller, Mercury in environmental samples: Speciation, artifacts and validation, *Trends Anal. Chem.* 24 (2005) 383–393. doi:10.1016/j.trac.2004.01.001.
- [20] T.D. Saint’Pierre, R.C.C. Rocha, C.B. Duyck, Determination of Hg in water associate to crude oil production by electrothermal vaporization inductively coupled plasma mass spectrometry, *Microchem. J.* 109 (2013) 41–45. doi:10.1016/j.microc.2012.05.005.
- [21] L. Magos, Selective atomic-absorption determination of inorganic mercury and methylmercury in undigested biological samples, *Analyst*. 96 (1971) 847–853. doi:10.1039/AN9719600847.
- [22] A.M. Limaverde Filho, R.C. de Campos, Redução seletiva aplicada à especiação de mercúrio em peixes: uma adaptação do método de Magos, *Quim. Nova*. 22 (1999) 477–482. doi:10.1590/S0100-40421999000400002.
- [23] A.M. Limaverde Filho, R.C. De Campos, Selective reduction for the determination of mercury in fish: An adaptation of the magos method, *Quim. Nova*. 22 (1999) 477–482. doi:10.1590/S0100-40421999000400002.
- [24] Z. Gao, X. Ma, Speciation analysis of mercury in water samples using dispersive liquid-liquid microextraction combined with high-performance liquid chromatography, *Anal. Chim. Acta*. 702 (2011) 50–55. doi:10.1016/j.aca.2011.06.019.

- [25] M. Daye, B. Ouddane, J. Halwani, M. Hamzeh, Solid phase extraction of inorganic mercury using 5-phenylazo-8- hydroxyquinoline and determination by cold vapor atomic fluorescence spectroscopy in natural water samples, *Sci. World J.* 2013 (2013). doi:10.1155/2013/134565.
- [26] I.L.S. Almeida, N.M.M. Coelho, Direct determination of inorganic mercury in ethanol fuel by cold vapor atomic absorption spectrometry, *Energy & Fuels.* 26 (2012) 6003–6007. doi:Doi 10.1021/Ef3010042.
- [27] P.S. Agustín Londonio, Fabián Fujiwara, Raúl Jiménez Rebagliati, Darío Gómez, Determination of mercury in size fractionated road dust samples by flow injection-cold vapor-atomic absorption spectrometry, *Microchem. J.* 105 (2012) 77–82. doi:10.1016/j.microc.2012.03.014.
- [28] H. Pyhtilä, P. Perämäki, J. Piispanen, M. Niemelä, T. Suoranta, M. Starr, T. Nieminen, M. Kantola, L. Ukonmaanaho, Development and optimization of a method for detecting low mercury concentrations in humic-rich natural water samples using a CV-ICP-MS technique, *Microchem. J.* 103 (2012) 165–169. doi:10.1016/j.microc.2012.02.010.
- [29] A. D’Ulivo, V. Loreti, M. Onor, E. Pitzalis, R. Zamboni, Chemical vapor generation atomic spectrometry using amineboranes and cyanotrihydroborate(III) reagents, *Anal. Chem.* 75 (2003) 2591–2600. doi:10.1021/ac020694p.
- [30] C.L. Chakrabarti, *Progress in analytical atomic spectroscopy*, Pergamon Press, 1983. [https://books.google.es/books?id=Q-p3DAAAQBAJ&pg=PP4&lr=&hl=pt-BR&source=gbs\\_selected\\_pages&cad=2#v=onepage&q&f=false](https://books.google.es/books?id=Q-p3DAAAQBAJ&pg=PP4&lr=&hl=pt-BR&source=gbs_selected_pages&cad=2#v=onepage&q&f=false) (accessed January 23, 2019).
- [31] M.H. Arbab-Zavar, G.H. Rounaghi, M. Chamsaz, M. Masrournia, Determination of mercury(II) ion by electrochemical cold vapor generation atomic absorption spectrometry., *Anal. Sci.* 19 (2003) 743–746. doi:10.2116/analsci.19.743.

- [32] E.J. Dos Santos, A.B. Herrmann, V.L.A. Frescura, R.E. Sturgeon, A.J. Curtius, A novel approach to cold vapor generation for the determination of mercury in biological samples, *J. Braz. Chem. Soc.* 19 (2008) 929–934.
- [33] E.H. N, V.uket Tirtom, S, ahande Goulding, Application of a wool column for flow injection online preconcentration of inorganic mercury(II) and methyl mercury species prior to atomic fluorescence measurement, *Talanta.* 76 (2008) 1212–1217. doi:10.1016/j.talanta.2008.05.038.
- [34] X. Guo, R.E. Sturgeon, Z. Mester, G.J. Gardner, Vapor generation by UV irradiation for sample introduction with atomic spectrometry, *Anal. Chem.* 76 (2004) 2401–2405. doi:10.1021/ac0353536.
- [35] C. Santos, Q. Oreste, A.M. Nunes, M.A. Vieira, A.S. Ribeiro, Determination of mercury in ethanol biofuel by photochemical vapor generation, *J. Anal. At. Spectrom.* 27 (2012) 689–694. doi:10.1039/c2ja10281a.
- [36] Q. He, X. Yu, Y. Li, H. He, J. Zhang, Dielectric barrier discharge induced atomization of gaseous methylethylmercury after NaBEt<sub>4</sub> derivatization with purge and trap preconcentration for methylmercury determination in seawater by GC-AFS, *Microchem. J.* 141 (2018) 148–154. doi:10.1016/j.microc.2018.05.028.
- [37] J.-H. Huang, Artifact formation of methyl- and ethyl-mercury compounds from inorganic mercury during derivatization using sodium tetra(n-propyl)borate, *Anal. Chim. Acta.* 532 (2005) 113–120. doi:10.1016/J.ACA.2004.10.057.
- [38] Y. Cai, S. Monsalud, K.G. Furton, Determination of methyl- and ethylmercury compounds using gas chromatography atomic fluorescence spectrometry following aqueous derivatization with sodium tetraphenylborate, *Chromatographia.* 52 (2000) 82–86. doi:10.1007/BF02490797.
- [39] P. Grinberg, R.C. Campos, Z. Mester, R.E. Sturgeon, A comparison of alkyl derivatization methods for speciation of mercury based on solid phase microextraction gas chromatography with furnace atomization plasma emission

spectrometry detection, *J. Anal. At. Spectrom.* 18 (2003) 902–909. doi:10.1039/b212545e.

[40] S. Rapsomanikis, Derivatization by ethylation with sodium tetraethylborate for the speciation of metals and organometallics in environmental samples. A review, *Analyst*. 119 (1994) 1429–1439. doi:10.1039/AN9941901429.

[41] V. Luckow, H.A. Rüssel, gas chromatographic determination of trace amounts of inorganic mercury, *J. Chromatogr. A*. 150 (1978) 187–194. doi:10.1016/S0021-9673(01)92111-9.

[42] N. Demuth, K.G. Heumann, Validation of methylmercury determinations in aquatic systems by alkyl derivatization methods for GC analysis using ICP-IDMS, *Anal. Chem.* 73 (2001) 4020–4027. doi:10.1021/ac010366+.

[43] Y. Mao, G. Liu, G. Meichel, Y. Cai, G. Jiang, Simultaneous speciation of monomethylmercury and monoethylmercury by aqueous phenylation and purge-and-trap preconcentration followed by atomic spectrometry detection, *Anal. Chem.* 80 (2008) 7163–7168. doi:10.1021/ac800908b.

[44] M.K. Donais, P.C. Uden, M.M. Schantz, S.A. Wise, Development, validation, and application of a method for quantification of methylmercury in biological marine Materials using gas chromatography atomic emission detection, *Anal. Chem.* 68 (1996) 3859–3866. doi:10.1021/ac960438a.

[45] L.R. Bravo-Sánchez, J.R. Encinar, J.I. Fidalgo Martínez, A. Sanz-Medel, Mercury speciation analysis in sea water by solid phase microextraction-gas chromatography-inductively coupled plasma mass spectrometry using ethyl and propyl derivatization. Matrix effects evaluation, *Spectrochim. Acta - Part B At. Spectrosc.* 59 (2004) 59–66. doi:10.1016/j.sab.2003.10.001.

[46] W.A. Telliard, Method 1630: Methylmercury in water by distillation, aqueous ethylation, purge and trap, and cold vapor atomic fluorescence spectrometry, *Sci. Technol.* (2001) 55.

- [47] R.G. Fernández, M.M. Bayón, J.I.G. Alonso, A. Sanz-Medel, Comparison of different derivatization approaches for mercury speciation in biological tissues by gas chromatography/inductively coupled plasma mass spectrometry, *J. Mass Spectrom.* 35 (2000) 639–646. doi:10.1002/(SICI)1096-9888(200005)35:5<639::AID-JMS990>3.0.CO;2-G.
- [48] Z. Khatib, J.M. Walsh, Extending the Life of Mature Assets: How integrating subsurface & surface knowledge and best practices can increase production and maintain integrity, *SPE Annu. Tech. Conf. Exhib.* (2014) 1–21. doi:10.2118/170804-MS.
- [49] M. Abuín, A.M. Carro, R.A. Lorenzo, Experimental design of a microwave-assisted extraction-derivatization method for the analysis of methylmercury, *J. Chromatogr. A.* 889 (2000) 185–193. doi:10.1016/S0021-9673(00)00210-7.
- [50] L. Liang, M. Horvat, E. Cernichiari, B. Gelein, S. Balogh, Simple solvent extraction technique for elimination of matrix interferences in the determination of methylmercury in environmental and biological samples by ethylation-gas chromatography-cold vapor atomic fluorescence spectrometry, *Talanta.* 43 (1996) 1883–1888. doi:10.1016/0039-9140(96)01964-9.
- [51] M. Horvat, N.S. Bloom, L. Liang, Comparison of distillation with other current isolation methods for the determination of methyl mercury compounds in low level environmental samples: Part I. Sediments, *Anal. Chim. Acta.* 281 (1993) 135–152. doi:10.1016/0003-2670(93)85348-N.
- [52] M. Horvat, L. Liang, N.S. Bloom, Comparison of distillation with other current isolation methods for the determination of methyl mercury compounds in low level environmental samples: Part II. Water, *Anal. Chim. Acta.* 282 (1993) 153–168. doi:10.1016/0003-2670(93)80364-Q.
- [53] J.L. Capelo, C. Maduro, C. Vilhena, Discussion of parameters associated with the ultrasonic solid-liquid extraction for elemental analysis (total content) by

electrothermal atomic absorption spectrometry. An overview, *Ultrason. Sonochem.* 12 (2005) 225–232. doi:10.1016/j.ultsonch.2003.10.010.

[54] M.N. Kayali-Sayadi, S. Rubio-Barroso, C.A. Díaz-Díaz, L.M. Polo-Díez, Rapid determination of PAHs in soil samples by HPLC with fluorimetric detection following sonication extraction, *Fresenius. J. Anal. Chem.* 368 (2000) 689–696. doi:10.1007/s002160000544.

[55] J.L. Luque-garcía, M.D.L. De Castro, Ultrasound: a powerful tool for leaching, *Trends Anal. Chem.* 22 (2003) 41–47. doi:10.1016/S0165-9936(03)00102-X.

[56] A.Q. Shah, T.G. Kazi, J.A. Baig, H.I. Afridi, G.A. Kandhro, S. Khan, N.F. Kolachi, S.K. Wadhwa, Determination of total mercury in muscle tissues of marine fish species by ultrasonic assisted extraction followed by cold vapor atomic absorption spectrometry, *J. Anal. Environ. Chem.* 11 (2010) 12–17.

[57] S. Río-Segade, C. Bendicho, Ultrasound-assisted extraction for mercury speciation by the flow injection-cold vapor technique, *J. Anal. At. Spectrom.* 14 (1999) 263–268. doi:10.1039/A806154H.

[58] J. Regueiro, M. Llompart, C. Garcia-Jares, J.C. Garcia-Monteagudo, R. Cela, Ultrasound-assisted emulsification-microextraction of emergent contaminants and pesticides in environmental waters, *J. Chromatogr. A.* 1190 (2008) 27–38. doi:10.1016/j.chroma.2008.02.091.

[59] N.S. Bloom, E.A. Crecelius, Determination of mercury in seawater at sub-nanogram per liter levels, *Marine Chemistry*, 14 (1983) 49-59. 10.1016/0304-4203(83)90069-5.

[60] and K.F. Koichi Chlba, Kazuo Yoshida, Klyoshi Tanabe, Hiroki Haraguchi, Determination of alkylmercury in seawater at the nanogram per liter level by gas chromatography/atmospheric pressure helium microwave-induced plasma emission spectrometry, *Anal. Chem.* (1983) 450–453. doi:10.1021 / ac00254a010.

[61] Martin J. Bloxham, Anthony Gachanja, Steve J. Hill And Paul J. Worsfold, Determination of mercury species in sea-water by liquid chromatography with inductively coupled plasma mass spectrometric selection, *J. Anal. At. Spectrom.* 11 (1996) 145–148. doi:10.1039 / JA9961100145.

[62] W.R.L. Cairns, M. Ranaldo, R. Hennebelle, C. Turetta, G. Capodaglio, C.F. Ferrari, A. Dommergue, P. Cescon, C. Barbante, Speciation analysis of mercury in seawater from the lagoon of Venice by on-line pre-concentration HPLC-ICP-MS, *Anal. Chim. Acta.* 622 (2008) 62–69. doi:10.1016/j.aca.2008.05.048.

[63] X. Chen, C. Han, H. Cheng, Y. Wang, J. Liu, Z. Xu, L. Hu, Rapid speciation analysis of mercury in seawater and marine fish by cation exchange chromatography hyphenated with inductively coupled plasma mass spectrometry, *J. Chromatogr. A.* 1314 (2013) 86–93. doi:10.1016/j.chroma.2013.08.104.

[64] B.B.A. Francisco, A.A. Rocha, P. Grinberg, R.E. Sturgeon, R.J. Cassella, Determination of inorganic mercury in petroleum production water by inductively coupled plasma optical emission spectrometry following photochemical vapor generation, *J. Anal. At. Spectrom.* 31 (2016) 751–758. doi:10.1039/C5JA00444F.

[65] K. Shigeta, H. Tao, K. Nakagawa, T. Kondo, T. Nakazato, A simple and robust method for determination of alkylmercury in seawater and industrial wastewater by phenylation pretreatment combined with GC-MS, *Anal. Sci.* 34 (2018) 227–233. doi:10.2116/analsci.34.227.

[66] M. Liu, Z. Gao, L. Chen, W. Zhao, Q. Lu, J. Yang, L. Ren, Z. Xu, A Reliable Method to Determine Monomethylmercury and Monoethylmercury Simultaneously in Aqueous Samples by GC–CVAFS After Distillation, *Arch. Environ. Contam. Toxicol.* 75 (2018) 495–501. doi:10.1007/s00244-018-0550-x.

[67] X. Yu, Q. He, Y. Li, H. He, J. Zhang, Atomic fluorescence spectrometric detection of methylmercury in seawater at sub ng L<sup>-1</sup> level by UV-induced atomization of gaseous methylethylmercury after NaBEt<sub>4</sub> derivatization with purge

and trap preconcentration and gas chromatography separation, *Spectrochim. Acta - Part B At. Spectrosc.* 152 (2019) 1–5. doi:10.1016/j.sab.2018.12.003.

[68] H. He, Z. Zhu, H. Zheng, Q. Xiao, L. Jin, S. Hu, Dielectric barrier discharge micro-plasma emission source for the determination of thimerosal in vaccines by photochemical vapor generation, *Microchem. J.* 104 (2012) 7–11. doi:10.1016/j.microc.2012.03.022.

[69] D.A. Geier, L.K. Sykes, M.R. Geier, A Review of Thimerosal (Merthiolate) and its Ethylmercury Breakdown Product: Specific Historical Considerations Regarding Safety and Effectiveness, *J. Toxicol. Environ. Heal. Part B.* 10 (2007) 575–596. doi:10.1080/10937400701389875.

[70] S. Trümpler, W. Lohmann, B. Meermann, W. Buscher, M. Sperling, U. Karst, Interaction of thimerosal with proteins—ethylmercury adduct formation of human serum albumin and  $\beta$ -lactoglobulin A, *Metallomics.* 1 (2009) 87–91. doi:10.1039/B815978E.

[71] José G. Dórea, Marcelo Farina and João B. T. Rochac, Toxicity of ethylmercury (and Thimerosal): A comparison with methylmercury, *J. Appl. Toxicol.* 33 (2013) 700–711. doi:10.1002/jat.2855.

[72] D.A. Geier, M.R. Geier, Neurodevelopmental disorders following Thimerosal-containing Childhood immunizations: A follow-up analysis, *Int. J. Toxicol.* 23 (2004) 369–376. doi:10.1080/10915810490902038.

[73] M. Velicu, H. Fu, R.P.S. Suri, K. Woods, Use of adsorption process to remove organic mercury thimerosal from industrial process wastewater, *J. Hazard. Mater.* 148 (2007) 599–605. doi:10.1016/j.jhazmat.2007.03.015.

[74] B. Pauwels, W. Verstraete, The treatment of hospital wastewater: An appraisal, *J. Water Health.* 4 (2006) 405–416. doi:10.2166/wh.2006.025.

- [75] G. Acosta, A. Spisso, L.P. Fernández, L.D. Martínez, P.H. Pacheco, R.A. Gil, Determination of thimerosal in pharmaceutical industry effluents and river waters by HPLC coupled to atomic fluorescence spectrometry through post-column UV-assisted vapor generation, *J. Pharm. Biomed. Anal.* (2014) 7–12. doi:10.1016/j.jpba.2014.09.011.
- [76] R.C. Meyerx, L.B. Cohn, Thimerosal Determination by High-pressure Liquid Chromatography, *J. Pharm. Sci.* (1978) 1636–1638. doi:10.1002/jps.2600671138.
- [77] D.S. Bushee, J.R. Moody, J.C. May, Determination of Thimerosal in Biological Products by Liquid Chromatography With Inductively Coupled Plasma Mass Spectrometric Detection, *J. Anal. At. Spectrom* 4 (1989), 773-775. doi: 10.1039 / JA989040077.
- [78] M. Pilar, J.R. Procopio, L. Hernhdez, Evaluation of the capability of different chromatographic systems for the monitoring of thimerosal and its degradation products by high- performance liquid chromatography with amperometric detection, *J. of Chromatography A.* 653 (1993), 267–273. doi:10.1016/0021-9673(93)83184-T.
- [79] M.P. Silva, J. Rodriguez, L. Hernaindez, Electrochemical Oxidative Determination of Thimerosal in Soft Contact Lens Care Solutions by Cyclic Voltammetry, *Analyst.* 11 (1994) 1971–1974. doi: 10.1039/AN9941901971
- [80] K.P. Shrivastaw, S. Singh, A New Method for Spectrophotometric Determination of Thiomersal in Biologicals, *Biologicals.* 1 (1995) 65–69. doi: 10.1016/1045-1056(95)90014-4.
- [81] S. Gil, I. Lavilla, C. Bendicho, Greener analytical method for determination of thiomersal (sodium ethylmercurithiosalicylate) in ophthalmic solutions using sono-induced cold vapour generation-atomic absorption spectrometry after UV/H<sub>2</sub>O<sub>2</sub> advanced oxidation, *J. Anal. At. Spectrom.* 22 (2007) 569. doi:10.1039/b615601k.

- [82] E. Jos, B. Herrmann, M. Baika, C.S. Sato, L. Tormen, E. Sturgeon, A. Jos, Determination of thimerosal in human and veterinarian vaccines by photochemical vapor generation coupled to ICP OES, (2010) 1627–1632. doi:10.1039/c0ja00029a.
- [83] A. Fredj, H. Okbi, N. Adhoum, L. Monser, Gas diffusion flow injection determination of thiomersal in vaccines, *Talanta*. 91 (2012) 47–51. doi:10.1016/j.talanta.2012.01.005.
- [84] B. Campanella, M. Onor, M. Carlo, A.D. Ulivo, C. Ferrari, E. Bramanti, Determination of thiomersal by flow injection coupled with microwave-assisted photochemical online oxidative decomposition of organic mercury and cold vapor atomic fluorescence spectroscopy, *Anal. Chim. Acta*. 804 (2013) 66–69. doi:10.1016/j.aca.2013.10.018.
- [85] Simultaneous Determination of Thimerosal and Aluminum in Vaccines and Pharmaceuticals with the Use of HPLC Method, *Acta Chromatographica*. 28 (2016) 299–311. doi:10.1556/1326.2016.28.3.2.
- [86] R. Piech, J. Wymazała, J. Smajdor, B. Paczosa-Bator, Thiomersal determination on a renewable mercury film silver-based electrode using adsorptive stripping voltammetry, *Anal. Methods*. 8 (2016) 1187–1193. doi:10.1039/C5AY02706C.
- [87] G. Acosta, S. Torres, M. Kaplan, L.P. Fernández, P.H. Pacheco, R.A. Gil, Liquid chromatography coupled to molecular fluorescence with postcolumn UV sensitization for thimerosal and derivative compounds monitoring in environmental samples, *Electrophoresis*. 37 (2016) 2531–2537. doi:10.1002/elps.201600147.
- [88] L. Li, P. Reiss, M. Protie, Core / shell semiconductor nanocrystals, *Small*. 5 (2009) 154–168. doi:10.1002/sml.200800841.

- [89] X. Yan, X. Cui, L. Li, Synthesis of Large , Stable Colloidal Graphene Quantum Dots with Tunable Size, *J. Am. Chem. Soc.* 132 (2010) 5944–5945. doi: 10.1021/ja1009376
- [90] B.G. Eda, Y. Lin, C. Mattevi, H. Yamaguchi, H. Chen, I. Chen, C. Chen, M. Chhowalla, Blue Photoluminescence from Chemically Derived Graphene Oxide, *Adv. Mater.* 22 (2010) 505–509. doi:10.1002/adma.200901996.
- [91] L.A. Ponomarenko, F. Schedin, M.I. Katsnelson, R. Yang, E.W. Hill, K.S. Novoselov, A.K. Geim, Chaotic Dirac Billiard in Graphene Quantum Dots, *Science*. 320 (2008) 356–358. doi: 10.1126/science.1154663.
- [92] X. Xu, R. Ray, Y. Gu, H.J. Ploehn, L. Gearheart, K. Raker, W.A. Scrivens, Electrophoretic Analysis and Purification of Fluorescent Single-Walled Carbon Nanotube Fragments, *J. Am. Chem. Soc.* 126 (2004) 12736–12737. doi: 10.1002/adma.200902825.
- [93] D. Wang, J. Chen, L. Dai, Recent Advances in Graphene Quantum Dots for Fluorescence Bioimaging from Cells through Tissues to Animals, *Part. Part. Syst. Charact.* 32 (2015) 515–523. doi:10.1002/ppsc.201400219.
- [94] B.D. Pan, J. Zhang, Z. Li, M. Wu, Hydrothermal Route for Cutting Graphene Sheets into Blue-Luminescent Graphene Quantum Dots, *Adv. Mater.* 22 (2010) 734–738. doi:10.1002/adma.200902825.
- [95] Y. Zhao, C. Hu, Y. Hu, H. Cheng, G. Shi, L. Qu, A Versatile , Ultralight, Nitrogen-Doped Graphene Framework, *Angew. Chem. Int.* 51 (2012) 11371–11375. doi:10.1002/anie.201206554.
- [96] L. Tang, R. Ji, X. Cao, J. Lin, H. Jiang, X. Li, K.S. Teng, Deep Ultraviolet Photoluminescence of Water-Soluble Self-Passivated Graphene Quantum Dots, *ASC Nano*. 6 (2012) 5102–5110. doi:10.1021/nn300760g.

- [97] S.H. Jin, G.H. Jun, S.H. Hong, S. Jeon, M. Science, I. Technology, Tuning the Photoluminescence of Graphene Quantum Dots through the Charge Transfer Effect of Functional Groups, *ACS Nano*. 72 (2013) 1239-1245. doi: 10.1021/nn304675g.
- [98] J. Shen, Y. Zhu, X. Yang, J. Zong, J. Zhang, One-pot hydrothermal synthesis of graphene quantum dots surface-passivated by polyethylene glycol and their photoelectric conversion under near-infrared light, *New J. Chem.* 36 (2012) 97–101. doi:10.1039/c1nj20658c.
- [99] S. C. Kim, S. B. Yang, J. H. Park, E. H. wang, S. Choi, G. Ko, S. Sim, C. Sone, H. J. Choi, S. Bae, and B. Hong. Anomalous Behaviors of Visible Luminescence from Graphene Quantum Dots : Interplay between Size and Shape, *ACS Nano*. 69 (2012) 8203-8208. doi: 10.1021/nn302878r
- [100] Y. Dong, H. Pang, S. Ren, C. Chen, Etching single-wall carbon nanotubes into green and yellow single-layer graphene quantum dots, *Carbon* 64 (2013) 245–251. doi:10.1016/j.carbon.2013.07.059.
- [101] J. Peng, W. Gao, B.K. Gupta, Z. Liu, R. Romero-aburto, L. Ge, L. Song, L.B. Alemany, X. Zhan, G. Gao, S.A. Vithayathil, B.A. Kaiparettu, A.A. Marti, T. Hayashi, J. Zhu, P.M. Ajayan, Graphene Quantum Dots Derived from Carbon Fibers, *J. Am. Chem. Soc.* 12 (2012) 844–849. doi: 10.1021/nl2038979.
- [102] Y. Dong, C. Chen, X. Zheng, L. Gao, Z. Cui, H. Yang, C. Guo, Y. Chi and C. M. Li, One-step and high yield simultaneous preparation of single- and multi-layer graphene quantum dots from CX-72 carbon black, *J. Mater. Chem.* 22 (2012) 8764–8766. doi:10.1039/c2jm30658a.
- [103] Y. Sun, S. Wang, C. Li, P. Luo, L. Tao, Y. Wei and G. Shi, Large scale preparation of graphene quantum dots from graphite with tunable fluorescence properties, *Phys. Chem. Chem. Phys.* 15 (2013) 9907–9913. doi:10.1039/c3cp50691f.

- [104] R. Ye, C. Xiang, J. Lin, Z. Peng, K. Huang, Z. Yan, N.P. Cook, E.L.G. Samuel, C. Hwang, G. Ruan, G. Ceriotti, A.O. Raji, J.M. Tour, A.A. Marti, Coal as an abundant source of graphene quantum dots, *Nature Communications*. (2013) 1–7. doi:10.1038/ncomms3943.
- [105] L. Zhou, J. Geng, B. Liu, Graphene quantum dots from polycyclic aromatic hydrocarbon for bioimaging and sensing of Fe<sup>3+</sup> and hydrogen peroxide, *Part. Part. Syst. Charact.* 30 (2013) 1086–1092. doi:10.1002/ppsc.201300170.
- [106] K. Habiba, V.I. Makarov, B.R. Weiner, G. Morell, J. Avalos, M.J.F. Guinel, Luminescent graphene quantum dots fabricated by pulsed laser synthesis, *Carbon N. Y.* 64 (2013) 341–350. doi:10.1016/j.carbon.2013.07.084.
- [107] R. Liu, D. Wu, X. Feng, Bottom-Up Fabrication of Photoluminescent graphene quantum dots with uniform morphology, (2011) 15221–15223. doi:10.1021/ja204953k.
- [108] L. Tang, R. Ji, X. Li, G. Bai, C.P. Liu, J. Hao, J. Lin, Deep Ultraviolet to near-infrared emission and photoresponse in layered N-doped graphene quantum dots, (2014) 6312–6320.
- [109] J. Lu, P. Shan, E. Yeo, C.K. Gan, P. Wu, K.P. Loh, Transforming C60 molecules into graphene quantum dots, 6 (2011) 247–252. doi:10.1038/nnano.2011.30.
- [110] J.P. Naik, P. Sutradhar, M. Saha, Molecular scale rapid synthesis of graphene quantum dots (GQDs), *J. Nanostructure Chem.* 7 (2017) 85–89. doi:10.1007/s40097-017-0222-9.
- [111] S. Zhu, J. Zhang, C. Qiao, S. Tang, Y. Li, W. Yuan, Strongly green-photoluminescent graphene quantum dots for bioimaging applications, *Chem. Commun.* 47 (2011) 6858–6860. doi:10.1039/c1cc11122a.

- [112] P.F. IBÁÑEZ, Propiedades coloidales de partículas de TiO<sub>2</sub>: aplicación al tratamiento fotocatalítico solar de aguas, Tesis doctoral. 2003.
- [113] L. Finegold, J.L. Cude, Electrochemical photolysis of water at a semiconductor electrode, *Nature*. 238 (1972) 37–38. doi:10.1038/238038a0.
- [114] J. Yu, H. Yu, B. Cheng, C. Trapalis, Effects of calcination temperature on the microstructures and photocatalytic activity of titanate nanotubes, *J. Mol. Catal. A Chem.* 249 (2006) 135–142. doi:10.1016/j.molcata.2006.01.003.
- [115] Y. Yang, H. Zhong, C. Tian, Photocatalytic mechanisms of modified titania under visible light, *Res. Chem. Intermed.* 37 (2011) 91–102. doi:10.1007/s11164-010-0232-4.
- [116] N. Phonthammachai, T. Chairassameewong, E. Gulari, A.M. Jamieson, S. Wongkasemjit, Structural and rheological aspect of mesoporous nanocrystalline TiO<sub>2</sub> synthesized via sol-gel process, *Microporous Mesoporous Mater.* 66 (2003) 261–271. doi:10.1016/j.micromeso.2003.09.017.
- [117] J.G. Yu, H.G. Yu, B. Cheng, X.J. Zhao, J.C. Yu, W.K. Ho, The Effect of calcination temperature on the surface microstructure and photocatalytic activity of TiO<sub>2</sub> thin films prepared by liquid phase deposition, *J. Phys. Chem. B.* 107 (2003) 13871–13879.
- [118] M.A. Fox, M.T. Dulay, Heterogeneous photocatalysis, 93 (2002) 341–357. doi:10.1021/cr00017a016.
- [119] R.L. Ziolli, W.F. Jardim, Photocatalytic decomposition of seawater-soluble crude-oil fractions using high surface area colloid nanoparticles of TiO<sub>2</sub>, *J. Photochem. Photobiol. A Chem.* 147 (2002) 205–212. doi:10.1016/S1010-6030(01)00600-1.

- [120] W.L.W. Lee, C.S. Lu, H.P. Lin, J.Y. Chen, C.C. Chen, Photocatalytic degradation of ethyl violet dye mediated by TiO<sub>2</sub> under an anaerobic condition, *J. Taiwan Inst. Chem. Eng.* 45 (2014) 2469–2479. doi:10.1016/j.jtice.2014.04.025.
- [121] R.J. Watts, S. Kong, M.P. Orr, G.C. Miller, B.E. Henry, Photocatalytic inactivation of coliform bacteria and viruses in secondary wastewater effluent, *Water Res.* 29 (1995) 95–100. doi:10.1016/0043-1354(94)E0122-M.
- [122] X. Zhang, D.K. Wang, D.R.S. Lopez, J.C. Diniz da Costa, Fabrication of nanostructured TiO<sub>2</sub> hollow fiber photocatalytic membrane and application for wastewater treatment, *Chem. Eng. J.* 236 (2014) 314–322. doi:10.1016/j.cej.2013.09.059.
- [123] I.V.L. Ferreira, L.A. Daniel, Fotocatálise heterogênea com TiO<sub>2</sub> no tratamento de esgoto, *Eng. Sanitária e Ambient.* 9 (2004) 335–342.
- [124] J. Tian, Y. Leng, Z. Zhao, Y. Xia, Y. Sang, P. Hao, J. Zhan, M. Li, H. Liu, Carbon quantum dots/hydrogenated TiO<sub>2</sub> nanobelt heterostructures and their broad spectrum photocatalytic properties under UV, visible, and near-infrared irradiation, *Nano Energy.* 11 (2015) 419–427. doi:10.1016/j.nanoen.2014.10.025.
- [125] H. Razmi, R. Mohammad-Rezaei, Graphene quantum dots as a new substrate for immobilization and direct electrochemistry of glucose oxidase: Application to sensitive glucose determination, *Biosens. Bioelectron.* 41 (2013) 498–504. doi:10.1016/j.bios.2012.09.009.
- [126] V.A. Online, L. Li, J. Peng, J. Zhao, J. Zhu, Focusing on luminescent graphene quantum dots: current status and future perspectives, (2013) 4015–4039. doi:10.1039/c3nr33849e.
- [127] M. Roushani, M. Mavaei, H.R. Rajabi, Graphene quantum dots as novel and green nano-materials for the visible-light-driven photocatalytic degradation of cationic dye, *J. Mol. Catal. A Chem.* 409 (2015) 102–109. doi:10.1016/j.molcata.2015.08.011.

[128] T. Yeh, S. Chen, H. Teng, Synergistic effect of oxygen and nitrogen functionalities for graphene-based quantum dots used in photocatalytic H<sub>2</sub> production from water decomposition, *Nano Energy*. 12 (2015) 476–485. doi:10.1016/j.nanoen.2015.01.021.

[129] H. Safardoust-hojaghan, M. Salavati-niasari, Degradation of methylene blue as a pollutant with N-doped graphene quantum dot / titanium dioxide nanocomposite, *J. Clean. Prod.* 148 (2017) 31–36. doi:10.1016/j.jclepro.2017.01.169.

[130] B.K. Gupta, G. Kedawat, Y. Agrawal, P. Kumar, J. Dwivedi, S.K. Dhawan, A novel strategy to enhance ultraviolet light driven photocatalysis from graphene quantum dots infilled TiO<sub>2</sub> nanotube arrays, (2015) 10623–10631. doi:10.1039/c4ra14039g.

[131] D. Pan, J. Jiao, Z. Li, Y. Guo, C. Feng, Y. Liu, L. Wang, M. Wu, Efficient Separation of Electron–Hole Pairs in Graphene Quantum Dots by TiO<sub>2</sub> Heterojunctions for Dye Degradation, (2015). doi:10.1021/acssuschemeng.5b00771.

[132] Y. Yan, Q. Liu, X. Du, J. Qian, H. Mao, K. Wang, Visible light photoelectrochemical sensor for ultrasensitive determination of dopamine based on synergistic effect of graphene quantum dots and TiO<sub>2</sub> nanoparticles, *ACA*. 853 (2015) 258–264. doi:10.1016/j.aca.2014.10.021.

[133] E.C. Romani, F.L. Freire, S. Khan, R.Q. Aucélio, R.L.D. Silva, C.A.T. Toloza, Different approaches for sensing captopril based on functionalized graphene quantum dots as photoluminescent probe, *J. Lumin.* 179 (2016) 83–92. doi:10.1016/j.jlumin.2016.06.055.

[134] D. Qu, M. Zheng, P. Du, Y. Zhou, L. Zhang, D. Li, H. Tan, Z. Zhao, Z. Xie, Z. Sun, Highly luminescent S, N co-doped graphene quantum dots with broad

visible absorption bands for visible light photocatalysts, *Nanoscale*. 5 (2013) 12272. doi:10.1039/c3nr04402e.

[135] T. Fan, W. Zeng, W. Tang, C. Yuan, S. Tong, K. Cai, Y. Liu, W. Huang, Y. Min, A.J. Epstein, Controllable size-selective method to prepare graphene quantum dots from graphene oxide, (2015). doi:10.1186/s11671-015-0783-9.

[136] H. Bevan, V. Dawes, R. a Ford, The electronic spectra of titanium dioxide, *Spectrochimica Acta*. 13 (1958) 43–49. doi: 10.1016/0371-1951(58)80005-3.

[137] P.F. Lim, K.H. Leong, L.C. Sim, A. Abd Aziz, P. Saravanan, Amalgamation of N-graphene quantum dots with nanocubic like TiO<sub>2</sub> : an insight study of sunlight sensitive photocatalysis, *Environ. Sci. Pollut. Res.* 26 (2019) 3455–3464. doi:10.1007/s11356-018-3821-1.

[138] J.-C. Lee, A.-I. Gopalan, G. Sai-Anand, K.-P. Lee, W.-J. Kim, Preparation of visible light photocatalytic graphene embedded rutile titanium(IV) oxide composite nanowires and enhanced NO<sub>x</sub> removal, *Catalysts*. 9 (2019) 170. doi:10.3390/catal9020170.

[139] J.M. Llabot, D.A. Allemandi, R.H. Manzo, M.R. Longhi, HPLC method for the determination of nystatin in saliva for application in clinical studies, *J. Pharm. Biomed. Anal.* 45 (2007) 526–530. doi:10.1016/j.jpba.2007.06.014.

[140] S.B. Adeloju, H.S. Dhindsa, R.K. Tandon, Evaluation of some wet decomposition methods for mercury determination in biological and environmental materials by cold vapour atomic absorption spectroscopy, *Anal. Chim. Acta*. 285 (1994) 359–364. doi:10.1016/0003-2670(94)80076-6.

[141] L. Liang, N. S. Bloom, and M. Horvat, Simultaneous determination of mercury speciation in biological materials by GC / CVAFS After Ethylation and Room Temperature Pre-collection, *Clin. Chem.* 40 (1994) 602–607.

- [142] J.K. Otton, T. Mercier, Produced water brine and stream salinity, n.d. <https://water.usgs.gov/orh/nrwww/Otten.pdf> (accessed January 13, 2019).
- [143] Y. Ma, H. Xu, Z. Qu, N. Yan, W. Wang, Absorption characteristics of elemental mercury in mercury chloride solutions, *J. Environ. Sci. (China)*. 26 (2014) 2257–2265. doi:10.1016/j.jes.2014.09.011.
- [144] G. Chen, B. Lai, N. Mei, J. Liu, X. Mao, Mercury speciation by differential photochemical vapor generation at UV-B vs. UV-C wavelength, *Spectrochim. Acta Part B At. Spectrosc.* 137 (2017) 1–7. doi:10.1016/j.sab.2017.09.007.
- [145] J.K. Kim, Ji Hyang; Yoon, Yong Dal; Kim, Comparison of damage induced by mercury chloride and ionizing radiation in the susceptible rat model (Conference) | ETDEWEB, Conference. (2003) 8. <https://www.osti.gov/etdeweb/biblio/20492007> (accessed January 8, 2019).
- [146] C. Zheng, Y. Li, Y. He, Q. Ma, X. Hou, Photo-induced chemical vapor generation with formic acid for ultrasensitive atomic fluorescence spectrometric determination of mercury: Potential application to mercury speciation in water, *J. Anal. At. Spectrom.* 20 (2005) 746–750. doi:10.1039/b503727a.
- [147] N.S. Bloom, J.A. Colman, L. Barber, Artifact formation of methyl mercury during aqueous distillation and alternative techniques for the extraction of methyl mercury from environmental samples, *Fresenius. J. Anal. Chem.* 358 (1997) 371–377. doi:10.1007/s002160050432.
- [148] J.R. Miranda-Andrades, S. Khan, C.A.T. Toloza, R.M. Maciel, R. Escalfoni, M.L.B. Tristão, R.Q. Aucelio, Speciation and ultra trace determination of mercury in produced waters from offshore drilling operations using portable instrumentation and matrix-matching calibration, *Microchem. J.* 146 (2019). doi:10.1016/j.microc.2019.02.045.

- [149] M. Yamamoto, Stimulation of elemental mercury oxidation in the presence of chloride ion in aquatic environments, *Chemosphere*. 32 (1996) 1217–1224. doi:10.1016/0045-6535(96)00008-2.
- [150] S. Okouchi, S. Sasaki, The 1-octanol/water partition coefficient of mercury, *Bull. Chem. Soc. Jpn.* 58 (1985) 3401–3402. doi:10.1246/bcsj.58.3401.
- [151] A. Turner, G.E. Millward, S.M. Le Roux, Sediment-water partitioning of inorganic mercury in estuaries, *Environ. Sci. Technol.* 35 (2001) 4648–4654. doi:10.1021/es010933a.
- [152] F. Detrick, Environmental Chemistry Short Communication, *Environ. Toxicol.* 10 (1991) 5–8.
- [153] B.C. Faust, The octanol/water distribution coefficients of methylmercuric species: The role of aqueous-phase chemical speciation, *Environ. Toxicol. Chem.* 11 (1992) 1373–1376. doi:10.1002/etc.5620111003.
- [154] U.S.E.P. Agency, Method 1630 Methyl Mercury in Water by Distillation , Aqueous Ethylation , Purge and Trap , and Cold Vapor Atomic Fluorescence Spectrometry Engineering and Analysis Division ( 4303 ), (1998).
- [155] M. Zaręba, P.T. Sanecki, R. Rawski, Simultaneous determination of thimerosal and aluminum in vaccines and pharmaceuticals with the use of HPLC method, *Acta Chromatogr.* 28 (2015) 1–13. doi:10.1556/1326.2016.28.3.2.
- [156] J.R. Miranda-Andrades, S. Khan, C.A.T. Toloza, E.C. Romani, F.L. Freire Júnior, R.Q. Aucelio, Thiomersal photo-degradation with visible light mediated by graphene quantum dots: Indirect quantification using optical multipath mercury cold-vapor absorption spectrophotometry, *Spectrochim. Acta - Part B At. Spectrosc.* 138 (2017) 81–89. doi:10.1016/j.sab.2017.10.011.

- [157] X. Wang, S.O. Pehkonen, A.K. Ray, Photocatalytic reduction of Hg(II) on two commercial TiO<sub>2</sub> catalysts, *Electrochim. Acta.* 49 (2004) 1435–1444. doi:10.1016/S0013-4686(03)00907-1.
- [158] H. Li, Z. Xu, L. Yang, Q. Wang, Determination and speciation of Hg using HPLC-AFS by atomization of this metal on a UV/nano-ZrO<sub>2</sub>/HCOOH photocatalytic reduction unit, *J. Anal. At. Spectrom.* 30 (2015) 916–921. doi:10.1039/c4ja00455h.
- [159] H.R. Rajabi, M. Farsi, Effect of transition metal ion doping on the photocatalytic activity of ZnS quantum dots: Synthesis, characterization, and application for dye decolorization, *J. Mol. Catal. A Chem.* 399 (2015) 53–61. doi:10.1016/j.molcata.2015.01.029.
- [160] N. Serpone, Photocatalytic Degradation of Chlorinated Phenols, *J. Phys. Chem.* 92 (1988) 5726–5731. doi:10.1021/j100331a036.
- [161] B. Welz, M. Melcher, Transition Metal Interferences in Hydride Generation Atomic-absorption Spectrometry Part 1. Influence of Cobalt, Copper, Iron and Nickel on Selenium Determination, 109 (1984) 2–5.

# 10 Attachment

## A

### Published papers



### Speciation and ultra trace determination of mercury in produced waters from offshore drilling operations using portable instrumentation and matrix-matching calibration



Jarol R. Miranda-Andrades<sup>a</sup>, Sarzamin Khan<sup>a,b</sup>, Carlos A.T. Toloza<sup>a,c</sup>, Roberta M. Maciel<sup>d</sup>, Rainério Escalfoni Jr<sup>d</sup>, Maria Luiza Bragança Tristão<sup>d</sup>, Ricardo Q. Aucelio<sup>a,\*</sup>

<sup>a</sup> Department of Chemistry, Pontifical Catholic University of Rio de Janeiro (PUC-Rio), Rio de Janeiro 22451-900, Brazil

<sup>b</sup> Department of Chemistry, University of Swabi, Khyber Pakhtunkhwa, Anbar 23561, Pakistan

<sup>c</sup> Chemistry Program, Universidad del Atlántico, Puerto Colombia, Atlántico, Colombia

<sup>d</sup> Leopoldo Américo Miguez de Mello Research Center - Petrobras (CENPES), Cidade Universitária, Quadra 7, Ilha do Fundão, Rio de Janeiro 21949-900, Brazil

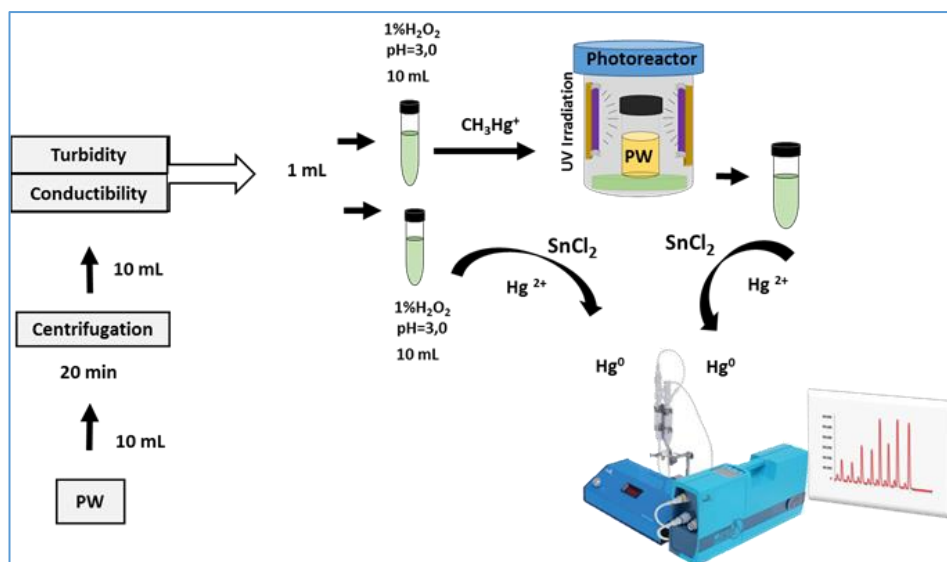


Figure A. 1 Published paper: Chapter 4.



## Combination of ultrasonic extraction in a surfactant-rich medium and distillation for mercury speciation in offshore petroleum produced waters by gas chromatography cold vapor atomic fluorescence spectrometry



Jarol R. Miranda-Andrades<sup>a</sup>, Sarzamin Khan<sup>b</sup>, Marlin J. Pedrozo-Penãfiel<sup>a</sup>,  
Kátia de Cassia B. Alexandre<sup>a</sup>, Roberta M. Maciel<sup>c</sup>, Rainério Escalfoni Jr<sup>c</sup>, Maria Luiza B. Tristão<sup>c</sup>,  
Ricardo Q. Aucelio<sup>a,\*</sup>

<sup>a</sup> Department of Chemistry, Pontifical Catholic University of Rio de Janeiro (PUC-Rio), Rio de Janeiro 22451-900, Brazil

<sup>b</sup> Department of Chemistry, University of Swabi, Khyber Pakhtunkhwa, Anbar-23561, Pakistan

<sup>c</sup> Leopoldo América Miguez de Mello Research Center - Petrobras (CENPES), Rio de Janeiro 21949-900, Brazil

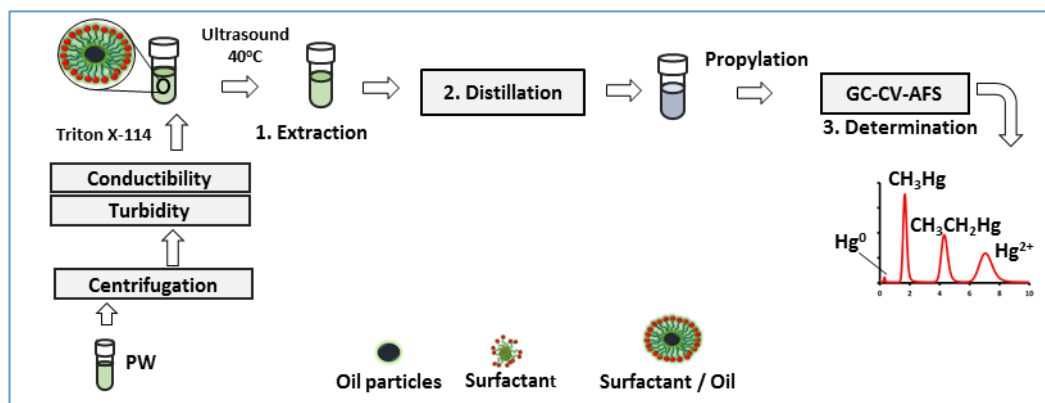


Figure A. 2 Published paper: Chapter 5



## Thiomersal photo-degradation with visible light mediated by graphene quantum dots: Indirect quantification using optical multipath mercury cold-vapor absorption spectrophotometry☆



Jarol R. Miranda-Andrades <sup>a</sup>, Sarzamin Khan <sup>a,b</sup>, Carlos A.T. Toloza <sup>a</sup>, Eric C. Romani <sup>c</sup>,  
Fernando L. Freire Júnior <sup>c</sup>, Ricardo Q. Aucelio <sup>a,\*</sup>

<sup>a</sup> Department of Chemistry, Pontifical Catholic University of Rio de Janeiro (PUC-Rio), Rio de Janeiro 22451-900, Brazil

<sup>b</sup> Department of Chemistry, University of Swabi, Khyber Pakhtunkhwa, Anbar 23561, Pakistan

<sup>c</sup> Department of Physics, Pontifical Catholic University of Rio de Janeiro (PUC-Rio), Rio de Janeiro 22451-900, Brazil

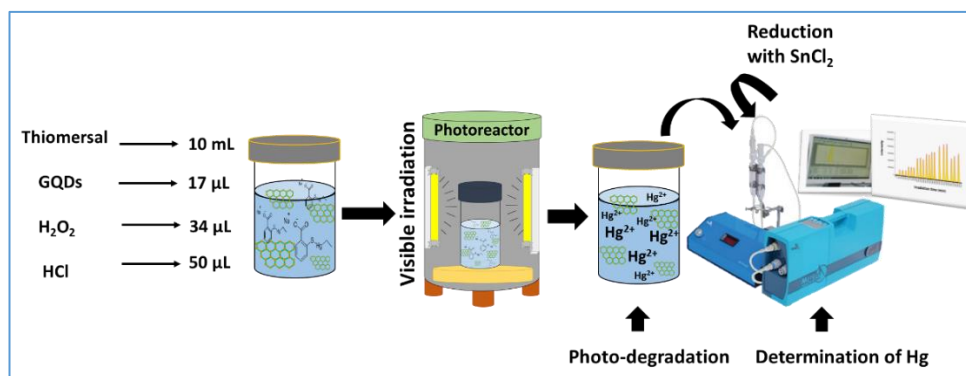


Figure A. 3 Published paper: Chapter 6.

**B****Participation in Congress****Oral presentation**

Indirect determination of thimerosal after graphene quantum dots assisted visible-light degradation and subsequent trace level determination of mercury by multipath optical spectrophotometry. **In 14th Rio Symposium on Atomic spectrometry. Vitoria, Espirito Santo 2017.**

Especiação fotoquímica e determinação do nível ultra-traço de mercúrio em águas de produção usando calibração por assemelhamento de matriz e espectrometria de absorção atômica de vapor frio com célula multipasso. **5to Congreso Uruguayo de Química Analítica (CUQA). Montevideo, Uruguai 2018.**

**Posters**

Indirect determination of thimerosal after graphene quantum dots assisted visible-light degradation and subsequent trace level determination of mercury by multipath optical spectrophotometry. **In 14th Rio Symposium on Atomic spectrometry. Vitoria, Espirito Santo 2017.**

Especiação fotoquímica e determinação do nível ultra-traço de mercúrio em águas de produção usando calibração por assemelhamento de matriz e espectrometria de absorção atômica de vapor frio com célula multipasso. **5to Congreso Uruguayo de Química Analítica (CUQA). Montevideo, Uruguai 2018.**

Ultra-Trace mercury speciation in produced water samples after extraction in ultrasound assisted organized medium, distillation and determination by CG-CV-AFS. **19° Encontro Nacional de Química Analítica e 7° Congresso iberoamericano de Química Analítica. 2018** (*Prêmio melhor painel da área de espectrometria atômica*).

Determinação indireta do timerosal após degradação assistida por pontos quânticos de grafeno e quantificação da determinação do nível de traços de mercúrio por espectrofotometria de absorção óptica multipass. **In: XVI Encontro Regional da Sociedade Brasileira de Química, 2017, Rio de Janeiro.**